Stefan Posch, Dipl.-Ing.

Thermodynamic Influence of the Lubrication Oil in Hermetic Reciprocating Compressors

DISSERTATION

in fulfillment of the requirements for the academic degree

Doktor der technischen Wissenschaften

submitted to

Graz University of Technology

Supervisor and 1st Reviewer

Ao.Univ.-Prof. Dipl.-Ing. Dr.techn. Raimund Almbauer

2nd Reviewer

Prof. Ing. Miroslav Jícha, CSc.

Graz, October 2017

Institut for Internal Combustion Engines and Thermodynamics
Head: Univ.-Prof. Dipl.-Ing. Dr.techn. Helmut Eichlseder

Statutory Declaration
Eidesstattliche Erklärung

I declare that I have authored this thesis independently, that I have not used other than the declared sources/resources, and that I have explicitly indicated all material which has been quoted either literally or by content from the sources used. The text document uploaded to TUGRAZonline is identical to the present doctoral dissertation.

Ich erkläre an Eides statt, dass ich die vorliegende Arbeit selbstständig verfasst, andere als die angegebenen Quellen/Hilfsmittel nicht benutzt, und die den benutzten Quellen wörtlich und inhaltlich entnommenen Stellen als solche kenntlich gemacht habe. Das in TUGRAZonline hochgeladene Textdokument ist mit der vorliegenden Dissertation identisch.

Graz, 24.10.2017

Stefan Posch

"What we know is a drop, what we don't know is an ocean."

- Sir Isaac Newton (1643-1727)

Foreword

The present thesis was written during my work as a university assistant at the Institute of Internal Combustion Engines and Thermodynamics at Graz University of Technology. It covers the main topics of my research in the field of hermetic reciprocating compressors. The thesis should give the reader an insight into the lubrication system of these kind of compressors and its influence on the compressor's thermodynamic behavior. Furthermore, the simulation tools to model the physical effects in the lubrication system are described.

At this point of the thesis I want to thank some persons who enabled the thesis, gave me a helping hand or supported me through the last four years.

Prof. Helmut Eichlseder, head of the Institute of Internal Combustion Engines and Thermodynamics, for giving me the opportunity to work as a university assistant at the institute which helped me not only to improve my knowledge in the field of thermodynamics but also to improve my didactic skills.

My supervisor Prof. Raimund Almbauer for creating the perfect environment to work independently on topics I am interested in. Thank you for sharing your knowledge with me and helping me when I got stuck. I appreciate the daily coffee (and sometimes cookie) breaks when we had time to talk not only about technical topics.

Prof. Miroslav Jícha for acting as a reviewer of this thesis. Thank you for finding the time to read through my work.

My colleagues from the research group and here especially Johann (Hansi) Hopfgartner. Hansi shared parts of his work with me which served as input data for my research. Furthermore, he helped me to develop the exergy loss model and he implemented the entropy generation rate methodology into the gas path simulation. He is one of my best friends since our time in Steyr and I hope that he still will be in the future.

My parents, my grandparents, my sister, my niece and all other members of my family for spending a lot of effort to make it possible for me to accomplish my studies. Thank you for being there for me when I needed you even though my time for you was sometimes limited.

All of my friends for providing welcome diversion from work whether on the bike, in the water or at breakfast at Kern.

And finally, my girlfriend Babsi for making me laugh when I was down and for helping me to see things from different perspectives. Life is so easy since I have met you.

To the reader of this thesis I also want to say thank you for your interest on my work. If you have any comments, questions or you just want to talk about this very interesting topic, do not hesitate to contact me.

Abstract

Simulation is an advisable tool for a wide range of engineering tasks. In the last two decades the use of simulation tools has become common in the traditional experimental driven development of refrigeration appliances. Especially compressor research and development without simulation is indispensable. The aim of the present work is the further development of numerical simulation in the field of hermetic compressors for refrigeration application. Special focus is laid on the influence of the lubrication oil on the thermal compressor behavior. Therefore, oil related sub systems are investigated using numerical simulation like the oil pump performance, for which an innovative modeling approach was developed, the oil distribution inside the compressor shell and the mechanical losses in the compressor crank mechanism. The results of these calculations are implemented in a holistic thermal compressor model. Experimental studies are carried out to validate the sub system simulations and the thermal model. Furthermore, a loss analysis approach based on the second law of thermodynamics is presented. Finally, the models are used to investigate the thermodynamics of an artificially cooled compressor.

Kurzfassung

Simulation ist ein zweckmäßiges Werkzeug für die Anwendung in einem weiten Bereich technischer Fragestellungen. Selbst in der traditionell weitestgehend experimentellen Entwicklung von Kühlgeräten stieg der Simulationsanteil in den letzten beiden Jahrzehnten stetig an. Speziell Forschung und Entwicklung von Kompressoren ist ohne die Verwendung von Simulation heutzutage undenkbar. Diese Arbeit beschäftigt sich mit der Weiterentwicklung von numerischen Simulationsmethoden für die Anwendung im Bereich hermetischer Hubkolbenkältemittelkompressoren. Der Fokus liegt dabei im Speziellen in der Untersuchung des Einflusses des Schmieröls auf das thermische Verhalten des Kompressors. Dazu werden die relevanten Teilsysteme mit Hilfe numerischer Simulation abgebildet. Dazu gehören die Ölpumpe, für die eine innovative Berechnungsmethode entwickelt wurde, die Verteilung des Öls im Inneren des Kompressors und die mechanischen Verluste im Kurbeltrieb. Die Ergebnisse aus diesen Berechnungen werden in ein umfassendes thermisches Modell des Kompressors implementiert. Mit Hilfe experimenteller Untersuchungen werden die Teilmodelle und das thermische Modell validiert. Weiters wird eine Verlustanalyse auf Basis des zweiten Hauptsatzes der Thermodynamik präsentiert. Abschließend werden die Modelle für die Untersuchung des thermischen Verhaltens eines künstlich gekühlten Kompressors verwendet.

Figures

1.1 Ideal working process of a reciprocating compressor 4
1.2 Real working process of a reciprocating compressor 4
1.3 Example of a refrigeration circuit 5
1.4 Compressor and capillary boundary conditions during on On/Off cylce [Hei15] 6
1.5 Schematic illustration of a hermetic reciprocating compressor 6
1.6 HXD55 compressor 7
1.7 Suction line of the HXD55 compressor 8
1.8 Discharge line of the HXD55 compressor 8
1.9 Valve plate of the HXD55 compressor 9
1.10 Crank drive of the HXD55 compressor 9
1.11 Schematic illustration of a calorimeter 10
1.12 American Society of Heating, Refrigerating and Air-Conditioning Engineers (ASHRAE) standard conditions for isobutane (R600a) 11
1.13 Density and kinematic viscosity of RENISO WF 5A as a function of temperature and dissolved R600a [DS06] 12
1.14 Modified compressor for the cooling experiment 13
1.15 Results of the cooling experiment 13

2.1 Thermodynamic system [Eic10] 19
2.2 Velocity and temperature of a fluid flow as a function of the distance to the wall [BS04] 22
2.3 Schematic pressure curve using non conservative cavitation models [LS78] 25
2.4 Shaft position of a static loaded bearing depending on the Sommerfeld number [GNP05] 26
2.5 Entropy balance [Kle12] 28

3.1 Cross section of the HXD55 compressor 30
3.2 Simulation domain and boundary conditions for the conventional method 33
3.3 Oil mass flow rate at the pump outlet 34
3.4 Relative static pressure at the pump inlet 34
3.5 Volumetric oil volume fraction gained by conventional simulation method (red = oil, blue = gas) 35
3.6 Individual oil pump parts 36

3.7 Simulation domain and boundary conditions for the lower centrifugal pump . . . 37
3.8 Volumetric oil volume fraction gained in the lower centrifugal pump . . 37
3.9 Geometry of the helical groove and the applied boundary conditions . . 38
3.10 Velocity in channel cross-section . . . 39
3.11 Velocity in channel direction . . . 39
3.12 Combination of the performance curves . . . 40
3.13 Flow chart of the split-up solution algorithm . . . 41
3.14 Oil pump test rig . . . 42
3.15 Modified oil pump . . . 42
3.16 Comparison of the computational time . . . 43
3.17 Application of the split-up method on the standard oil pump . . . 46
3.18 Application of the split-up method on the modified oil pump . . . 47

4.1 Visualization of the oil flow . . . 50
4.2 Mesh of the oil distribution simulation . . . 50
4.3 Boundary conditions of the oil distribution simulation . . . 51
4.4 Oil distribution inside the compressor shell at several time steps . . . 52
4.5 Oil film (a) and oil film thickness (b) . . . 53
4.6 Heat transfer coefficient distribution on the inner surface of the compressor shell before (a) and after (b) the interpolation . . . 54

5.1 Compressor crank drive with coordinate systems . . . 57
5.2 Cylinder pressure from CFD results . . . 58
5.3 Reaction forces at the cylinder liner . . . 58
5.4 Reaction forces at the conrod big end . . . 59
5.5 Reaction forces at the conrod small end . . . 59
5.6 Reaction forces at the crankshaft journal bearing 1 . . . 60
5.7 Reaction forces at the crankshaft journal bearing 2 . . . 60
5.8 Discretization of the simulation domain . . . 60
5.9 Bearing and piston meshes . . . 62
5.10 Determination of the bearing fluid film thickness . . . 62
5.11 Determination of the piston fluid film thickness . . . 63
5.12 Flow chart of the solution algorithm . . . 65
5.13 Test case for the code validation . . . 66
5.14 Static eccentricity by force variation (n =1000 rpm) . . . 66
5.15 Static eccentricity by speed variation (F =100 N) . . . 66
5.16 So-relative eccentricity relationship . . . 67
5.17 Static eccentricity and dynamic trajectory . . . 67
5.18 Piston eccentricity and tilting angle . . . 68
5.19 Orbital paths of the crankshaft bearings . . . 68
5.20 Mechanical power losses gained by the friction loss code . . . 68

5.21 Condensation process of the conrod 69
5.22 Mechanical power losses gained by AVL EXCITE Power Unit 70
5.23 Hydrodynamic pressure in the considered contacts 71

6.1 Velocity field inside the cylinder 76
6.2 Gas path wall heat flux values 76
6.3 Flow chart of the thermal model solution algorithm 78
6.4 Schematic overview of the sensor positions 79
6.5 Comparison between measured and simulated temperatures 80
6.6 Temperature field of the solid parts inside the compressor (a) and on the compressor shell (b) 81

7.1 Electrical exergy losses 84
7.2 Mechanical exergy losses 85
7.3 Entropy generation in the area of the suction valve 87
7.4 Exergy losses in the gas path 88
7.5 Thermal exergy losses 89
7.6 Schematic compressor process at ASHRAE -23.3/45 test conditions . . 89
7.7 Exergy losses of the entire compressor 90

8.1 Estimated temperatures for the artificial cooling example 91
8.2 Lumped volume temperatures of the artificial cooling example 92
8.3 Results of the artificial cooling example 93

Tables

1.1 Compressor Parameter HXD55 5

3.1 Input data for the oil pump simulations 31
3.2 Results of the validation of the oil pump simulation ($\dot{m}$ in [g s^{-1}]) . . . 44

5.1 Geometry data and oil viscosity for the code test 64

6.1 Thermocouple measuring points 79

Contents

Nomenclature and Abbreviations **xxi**

1 Introduction **1**
- 1.1 Reciprocating compressor basics . . . 2
  - 1.1.1 Working principle . . . 2
  - 1.1.2 Compressor as part of the refrigerator . . . 3
  - 1.1.3 Design aspects . . . 4
  - 1.1.4 Experimental investigation . . . 8
  - 1.1.5 Compressor oil . . . 10
- 1.2 Compressor cooling - a fundamental experiment . . . 12
- 1.3 Motivation . . . 14
- 1.4 Problem definition and realization . . . 15

2 Theoretical basics **17**
- 2.1 Conservation equations . . . 17
  - 2.1.1 Conservation of mass . . . 18
  - 2.1.2 Conservation of momentum . . . 18
  - 2.1.3 Conservation of energy . . . 18
  - 2.1.4 General conservation equation . . . 19
  - 2.1.5 Dimensionless numbers . . . 19
- 2.2 Heat transfer . . . 21
  - 2.2.1 Heat conduction . . . 21
  - 2.2.2 Convective heat transfer . . . 22
  - 2.2.3 Radiation . . . 23
- 2.3 Lubrication theory . . . 24
- 2.4 Second law of thermodynamics . . . 27

3 Oil pump **29**
- 3.1 Literature review . . . 30
- 3.2 Oil pump simulation . . . 31
- 3.3 Conventional oil pump simulation . . . 32
- 3.4 Split-up approach . . . 34
  - 3.4.1 Lower centrifugal pump . . . 36
  - 3.4.2 Helical groove . . . 37
  - 3.4.3 Upper centrifugal pump . . . 39

3.4.4 Combination of the sub models . . . 39
3.5 Experimental work . . . 40
3.6 Application of the split-up approach . . . 41

4 Oil distribution **49**
4.1 Literature review . . . 49
4.2 Simulation model . . . 49
4.3 Results . . . 51
4.3.1 Oil jet . . . 52
4.3.2 Oil film thickness . . . 53
4.3.3 Heat transfer . . . 53

5 Friction loss analysis **55**
5.1 Literature review . . . 55
5.2 Compressor friction loss code . . . 56
5.2.1 Multi-body system . . . 56
5.2.2 Numerical treatment of the Reynolds equation . . . 58
5.2.3 Gap kinematics . . . 62
5.2.4 Solution algorithm . . . 63
5.2.5 Code testing . . . 64
5.2.6 Results . . . 67
5.3 AVL EXCITE Power Unit . . . 67
5.3.1 Model layout . . . 69
5.3.2 Results . . . 70

6 Thermal Compressor Model **73**
6.1 Literature review . . . 74
6.2 Modeling . . . 74
6.2.1 Solid parts . . . 74
6.2.2 Refrigerant gas path . . . 75
6.2.3 Lumped volumes . . . 76
6.2.4 Solution algorithm . . . 77
6.3 Experimental work . . . 77
6.4 Results . . . 77

7 Exergy loss analysis **83**
7.1 Literature review . . . 83
7.2 Loss mechanism . . . 83
7.2.1 Electrical losses . . . 84
7.2.2 Mechanical losses . . . 84
7.2.3 Thermodynamic losses . . . 85
7.2.4 Outlet temperature . . . 88

7.3 Entire compressor losses 89

8 Application example **91**

9 Summary and conclusions **95**

10 Future work **97**

Bibliography **99**

Appendix **105**
A Paper 1 105
B Paper 2 115
C Paper 3 125
D Paper 4 135
E Paper 5 145

Nomenclature and Abbreviations

Roman letters

a	$m^2\ s^{-1}$	thermal diffusivity
A	m^2	area
B	m	width
c_v	$J\ kg^{-1}\ K^{-1}$	specific heat capacity
c_p	$J\ kg^{-1}\ K^{-1}$	specific heat capacity at p =const.
c_v	$J\ kg^{-1}\ K^{-1}$	specific heat capacity at v =const.
D	m	diameter
e_e	$J\ kg^{-1}$	specific external energy
e_x	m	eccentricity
E	J	Exergy
Ec	-	Eckert number
E_e	J	external energy
F	N	force
Gr	-	Grashof number
h	$J\ kg^{-1}$	specific enthalpy
h	m	fluid film thickness
L	m	characteristic length
m	kg	mass
$\dot{m}$	$kg\ s^{-1}$	mass flow
Nu	-	Nusselt number
p	$N\ m^{-2}$	pressure
P	W	power
Pr	-	Prandtl number
$\dot{Q}$	W	heat flux
Q	J	heat
$\dot{q}_\mathrm{V}$	$W\ m^{-3}$	rate of heat per volume
$\dot{Q}_0$	W	cooling capacity
r	m	coordinate
Ra	-	Rayleigh number
Re	-	Reynolds number
s	$J\ kg^{-1}\ K^{-1}$	specific entropy
S	$J\ K^{-1}$	entropy
So	-	Sommerfeld number
t	s	time
T	K	temperature

u	m	coordinate
u	m s^{-1}	velocity component in x-direction
U	J	inner energy
U	m s^{-1}	velocity
v	m s^{-1}	velocity component in y-direction
V	m^3	volume
V	m s^{-1}	velocity
v	m s^{-1}	velocity component in w-direction
W	J	work
x	m	coordinate
y	m	coordinate
z	m	coordinate

Greek letters

α	W m^{-2} K^{-1}	heat transfer coefficient
β	K^{-1}	volume expansion coefficient
Γ^{ϕ}	kg m^{-1} s^{-1}	diffusion coefficient of ϕ
δ	m	boundary layer thickness
ε	-	emissivity
ε	-	relative eccentricity
ε	W kg^{-1}	turbulent dissipation rate
Θ	K	difference to characteristic temperature
Θ	kg m^2	moment of inertia
λ	W m^{-1} K^{-1}	thermal conductivity
μ	N s m^{-2}	dynamic viscosity
ν	m^2 s^{-1}	kinematic viscosity
ξ	rad	angle to minimum fluid film thickness
ρ	kg m^{-3}	density
σ_{δ}	m	standard deviation of the combined roughness
ϕ	-	scalar
ϕ	rad	tilting angle
φ	rad	angular control variable
$\phi_{\mathrm{s}}, \phi_{\mathrm{x}}, \phi_{\mathrm{y}}$	-	flow factors
Φ	s^{-1}	dissipation term
χ	-	volume fraction
ψ	-	relative bearing clearance
ω	rad^{-1}	angular velocity
Ω	rad^{-1}	angular velocity

Vectors and matrices

$\mathbf{a}$	m s^{-2}	acceleration

$\mathbf{f}_b$	N m^{-3}	body force
$\mathbf{F}$	N	force
$\mathbf{n}$	-	area normal vector
$\mathbf{q}$	W m^{-2}	heat flux density
$\mathbf{r}$	m	distance
$\mathbf{T}$	N m	torsional moment
$\mathbf{u}$	m s^{-1}	velocity
τ	J m^{-3}	stress tensor

Constants

g	9.8067	m s^{-2}	gravity
σ	$5.670367 \cdot 10^{-8}$	W m^{-2} K^{-4}	Stefan-Boltzmann constant

Indices and abbreviations

I	shaft
II	case
3D	three-dimensional
amb	ambient
ASHRAE	American Society of Heating, Refrigerating and Air-Conditioning Engineers
BDC	Bottom Dead Center
cond	condenser
cyl	cylinder
CA	Crankangle
CAD	Computer Aided Design
CFD	Computational Fluid Dynamics
COP	Coefficient of Performance
Cr	conrod
Cs	crankshaft
Cyl	cylinder
d	discharge
e	external
e	east
el	electric
EHL	Elastohydrodynamic Lubrication
f	fluid
fluc	fluctuating
FDM	Finite Difference Method
FEA	Finite Element Analysis
FEM	Finite Element Method
FSI	Fluid Structure Interaction
FVM	Finite Volume Method
g	gaseous
g	generation
GITT	Generalized Integral Transform Technique
HTF	Heat Transfer Factor
i	inner, control variable
I	inertial system
irr	irreversible
l	liquid
LCP	lower centrifugal pump
LV	lumped volume
m	mean
M	midpoint
MBS	multi body system
n	north
oil	oil
out	outlet
OC	oil in the crankshaft
OS	oil sump
OW	oil on the walls
P	cell point
Pi	piston
PP	piston pin
R600a	isobutane
Rey	hydrodynamic forces

s	suction
s	south
sat	saturation
stat	static
SG	shell gas
SG	solid part
t	turbulent
TDC	Top Dead Center
TNW	Thermal Network approach
UDF	User Defined Function
VOF	Volume of Fluid
w	wall
w	west

Operators and designations

d	complete derivative
D	substantial derivative
δ	incomplete derivative
∂	partial derivative
Δ	difference of two values
∇	nabla operator
$\sum$	sum
$(.)^*$	dimensionless
$(.)_\infty$	reference to characteristic value
$(.)^+$	wall coordinate
$\underline{(.)}$	mean term
$\tilde{(.)}$	mean term (Favre averaged)

1 Introduction

'Simulation' is one of the keywords in today's engineering language. Due to the dynamic development of simulation tools for the use in different engineering tasks, the confrontation with simulation is unavoidable for engineers in each field. Focusing on the field of mechanical engineering, aerospace and automotive industry were the leaders in the use of simulation tools in the development process achieving time reduction and enabling an earlier launch of their products on the global market. A great number of simulation tools are based on the application on automotive or aeronautic issues. The rapid increase of computational performance combined with a decrease of computer costs paved the way for other industrial sectors. As an example, the traditional experimental driven development of refrigeration appliances and their components can be mentioned. In the field of domestic refrigeration, the introduction of energy labels such as the Directive 2010/30 EU and as a consequence, the necessity of producing highly efficient appliances requires a deep understanding of the system and its physical effects. Experimental investigations are still essential in the development process but without the application of simulation, efficiency limits are reached sooner or later. Another aspect, which could be mentioned at this point, is the reduction of development duration. The development duration of a new refrigerator based on experimental investigations can take about two years which is comparable with the development duration of a passenger car. To be competitive on the world market and to create an advantage over the increasing number of Chinese manufacturers, a fast launch of new products is crucial especially for European manufacturers e.g. Liebherr or BSH.
In the field of refrigeration research and development simulation is used to investigate the entire system behavior like predicting energy consumption at different operation conditions or to analyze the system components as heat exchangers, capillary tube or compressor. Especially in the compressor research and development, simulation became indispensable in the last two decades. The range of simulation application includes simple semi-empirical or polynomial models for the integration of the compressor in holistic refrigeration cycle simulation or numerical models for the investigation of physical effects in the compressor or its sub systems. Common numerical simulations in the field of refrigeration compressors are Computational Fluid Dynamics (CFD) and Finite Element Analysis (FEA).
The further development of hermetic compressor numerical simulation is the main idea of the present work. Previous simulation activities were mainly focused on the investigation of sub systems like CFD of the refrigerant gas path including valve motion or structural analysis of crank drive parts, thus, a holistic evaluation concerning the

entire compressor behavior on the thermodynamic level is only possible to a limited extent. In the present work a method which enables the thermal evaluation of hermetic reciprocating compressors for refrigeration application is presented. The key to achieve a holistic treatment is to take also the oil flow into consideration. Due to the hermetic design of the compressor, sub systems as the electrical motor, the crank drive and the refrigerant path interact with each other. The lubrication oil acts as heat transport medium between the hot compressor parts and the shell and so to the ambient air, thus, the knowledge about the relevant physical effects concerning the compressor oil is crucial for the thermodynamic evaluation of the compressor.
However, before going into detail about the motivation forcing this work and the problem definition, some compressor basics and a fundamental compressor experiment is shown in the following sub chapters.

1.1 Reciprocating compressor basics

Compressor machines can be generally described by the fundamental functionality of increasing the pressure of a substance in gaseous phase by reducing its specific volume. The application field of compressors covers a wide range from refrigeration through chemical engineering to food engineering, just to mention a few examples. To meet the requirements of the respective application different types of compressors are available e.g. reciprocating compressors, screw compressors or scroll compressors. Reciprocating compressors are widely used and can be found in almost every household refrigerator. The following sub chapter gives an overview of the basics of a reciprocating compressor for refrigeration application in terms of its working principle and its role as a part in the refrigeration cycle. Furthermore, the design of such a compressor is explained by the compressor the present study is related on. Finally, a description of the common experimental investigation method for refrigeration compressors is given.

1.1.1 Working principle

Reciprocating compressors compress the gas by reducing the volume in a cylinder by means of a piston. The translational motion of the piston is induced via a crank drive which translates the rotational movement of the crankshaft. The required energy for the operation of the compressor is provided by a drive unit, for example an electric drive.
The efficiency of a compressor can be expressed by the ability of compressing the gas with as little work as possible. Generally, to value machines like compressors an ideal reference process is defined. Looking at a compressor, assuming that the system is adiabatic, the ideal process for the compression of the gas is an isentropic process. The relationship of the real and the isentropic process is given by the isentropic efficiency which is defined as the relation between the isentropic work divided by the inner work.

If the system is not adiabatic which is more applicable to reciprocating compressors the process with a minimum of inner work is the isothermal process.
A closer look on the ideal working process of a reciprocating compressor can be seen in Fig. 1.1. Starting at point 1 the piston is at the bottom dead center giving the maximum cylinder volume. The gas in the cylinder is compressed by the moving piston. Assuming adiabatic compression without friction point 2 is reached along an isentropic compression. At point 2 the discharge valve opens at discharge pressure and the compressed gas flows into the discharge line at constant pressure until the piston reaches the top dead center. The volume in the cylinder in point 3 is the minimum clearance volume. Trapped gas in the clearance volume expands by the increasing cylinder volume after the piston reverses at the top dead center along an isentropic expansion. Pressure decreases until the suction pressure is reached and the suction valve opens. Gas flows from the suction line into the cylinder until the piston reaches its bottom dead center and the cycle starts again.

The compression work per cycle can be expressed as the cycle integral of the pressure-volume work.

$$W_{\mathrm{i}} = \oint p \mathrm{d}V \tag{1.1}$$

Compared to the ideal working process, the working process of a real compressor looks quite different (Fig. 1.2). The ideal opening and closing of the suction and discharge valves are an assumption far away from real conditions. Real valves cause a pressure drop during the suction and discharge process and a pressure difference is required to open the valves. Furthermore, the compression and expansion processes are not isentropic due to occurring friction and heat transfer from or into the gas. Nevertheless, the calculation of the inner compressor work according Eq. 1.1 is still permitted.

1.1.2 Compressor as part of the refrigerator

The majority of the cooling circuits in cooling appliances like refrigerators or freezers are based on the compression refrigeration cycle. In contrast to absorption refrigeration cycles which are driven by heat, compression refrigeration cycles use a compressor which provides the required energy to run the system. In addition to the compressor a refrigeration cycle consists in its most simple case of two heat exchangers namely the condenser and the evaporator and an expansion device. An illustration of a compression refrigeration circuit layout is shown in Fig. 1.3. To explain the working principle of a refrigeration system working with isobutane, the compressor as the component which drives the cycle is chosen to start. After the refrigerant leaves the compressor at high pressure level it flows through the condenser. At the inlet of the condenser the refrigerant is superheated. Utilizing the latent heat the isobutane condenses and subcools until it enters the capillary tube. The capillary tube acts as expansion de-

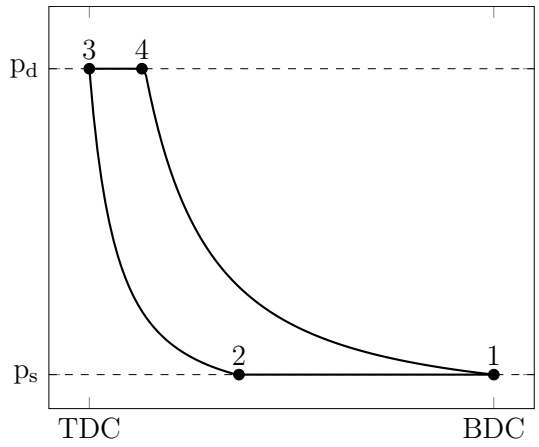

Fig. 1.1: Ideal working process of a reciprocating compressor

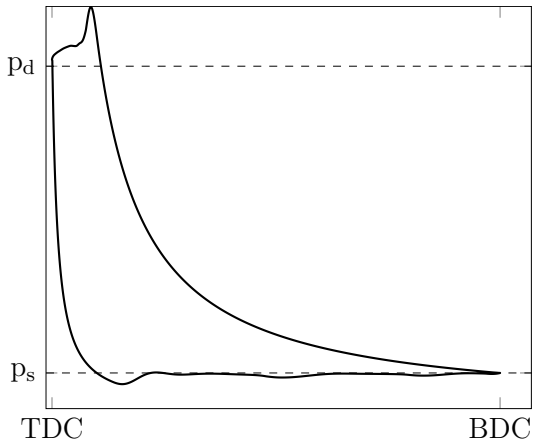

Fig. 1.2: Real working process of a reciprocating compressor

vice which can be either adiabatic or non-adiabatic depending on the regarded setup. Non-adiabatic capillary tubes are a special form of heat exchanger in a refrigerator. As shown in Fig. 1.3, the first part of the capillary tube can be joined with the end of the evaporator. This setup yields higher efficiency by increasing the cooling capacity and ensures superheated refrigerant at the inlet of the compressor. In the evaporator the saturated isobutane evaporates by utilization of latent heat and flows back into the compressor starting the cycle again.

Although the previous explanation of the refrigeration cycle working principle is quite more realistic as the ideal cycle assuming isentropic compression, neglecting superheating and subcooling, it is only applicable for a refrigeration system working at steady-state conditions. Real appliances can reach steady-state conditions only at unusual operation like pull-down mode. Independent of the used compressor logic, either if it is an On/Off controlled or a variable speed compressor, the working conditions of real appliances are of transient nature. [Hei15] presents transient data of the inlet and outlet conditions of the capillary tube and the compressor respectively, in an On/Off controlled refrigeration cycle gained by experiments. The data shown in Fig. 1.4 represents the transient operation conditions.

1.1.3 Design aspects

During the last five decades the principal design of hermetic reciprocating compressors for refrigeration application has not been changed fundamentally. A schematic illustration of a hermetic reciprocating compressor can be seen in Fig. 1.5. Depending on the type of compressor the crank drive is driven by a single-phase asynchronous motor for fix speed compressors or a direct current motor for variable speed compressors, respectively. Several plenum in the suction and the discharge line damp pressure waves

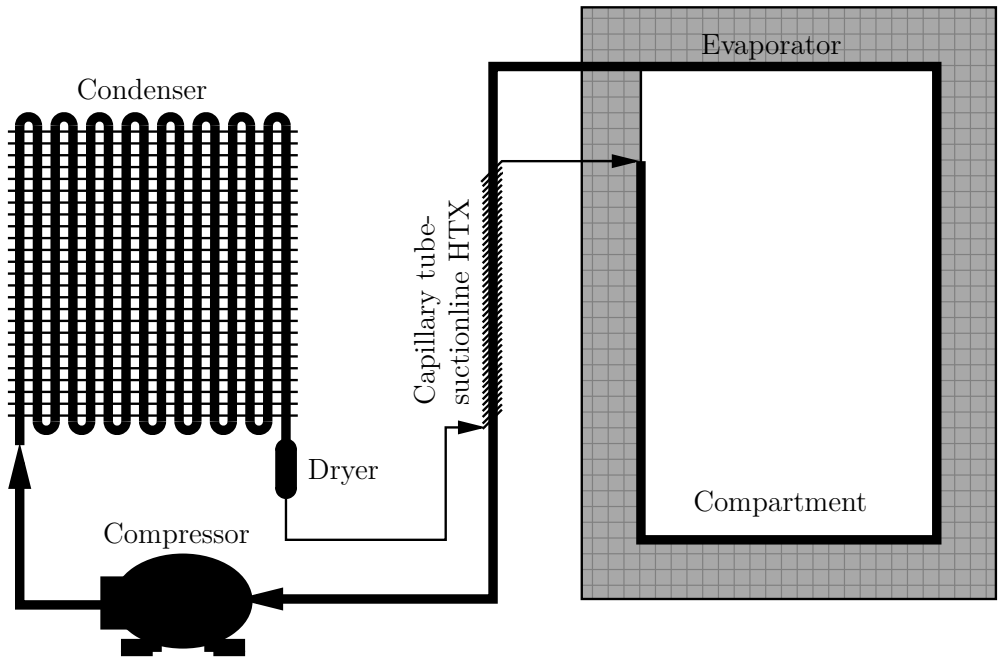

Fig. 1.3: Example of a refrigeration circuit

and thus, improve the acoustic behavior of the compressor. Flapper valves are used to control the suction and discharge process. The oil supply of the crank mechanism is provided by an oil pump in the crank shaft. The compressor parts are integrated into a hermetic steel shell and the connection to the refrigerator is done by soldering the copper suction and discharge tubes to the evaporator and condenser, respectively. A closer look on the design aspects of hermetic reciprocating compressors is given by means of the compressor the present study is related on. The characteristic data of the fix speed Delta series compressor HXD55 of the company Secop Austria GmbH is listed in Tab. 1.1. Fig. 1.6 shows the design of the regarded HXD55 compressor (the upper shell part is hidden for better illustration).

Tab. 1.1: Compressor Parameter HXD55

Parameter	Value	Unit
Speed	2950	rpm
Power consumption (at ASHRAE -23.3/55)	51.6	W
COP (at ASHRAE -23.3/55)	1.95	W/W
Displacement	55	cm^3

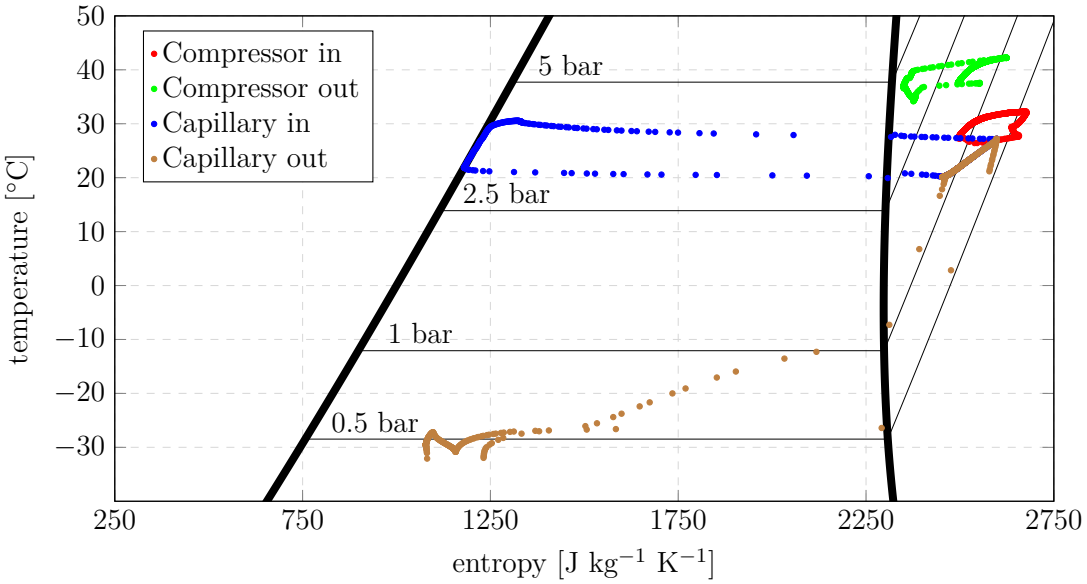

Fig. 1.4: Compressor and capillary boundary conditions during on On/Off cylce [Hei15]

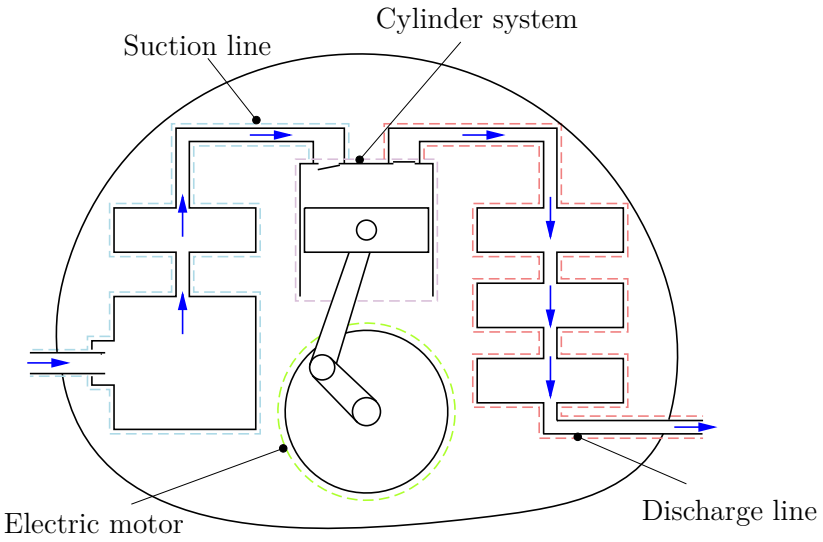

Fig. 1.5: Schematic illustration of a hermetic reciprocating compressor

Suction line

The design of the suction line (see Fig. 1.7) is crucial for the thermodynamic and acoustic behavior of a hermetic compressor. Due to the trade-off between minimum pressure loss and noise damping the suction line design requires the use of numerical tools like CFD. The suction line of the HXD55 consists of the suction tube and the suction plenum, the so called suction muffler. To minimize superheating of the suction

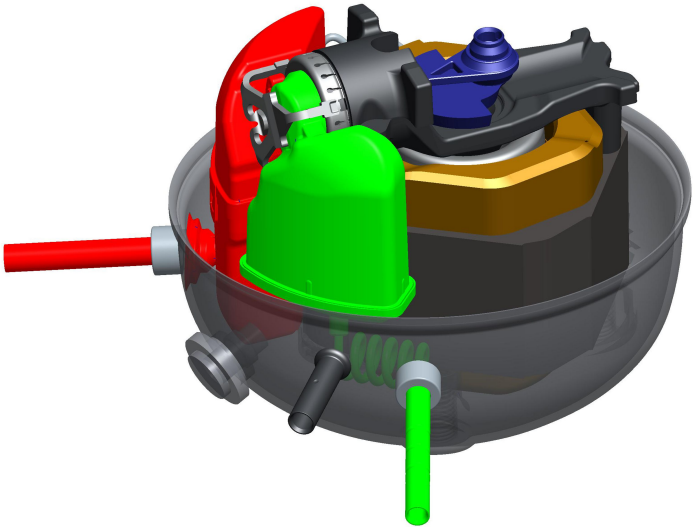

Fig. 1.6: HXD55 compressor

gas in the suction line the regarded compressor uses a direct suction concept and a plastic suction muffler. Direct suction means that the refrigerant is sucked directly from the evaporator and not from the gas inside the compressor shell. The suction muffler is designed as one volume with an oil drain hole and a second hole to equalize the pressure using the shell volume as an additional volume.

Discharge line

The discharge line (see Fig. 1.8) of the HXD55 compressor represents a novelty in the design of hermetic reciprocating compressors. In contrast to compressors with an integrated discharge line in the casted crank case, the discharge line of the regarded compressor is, similar to the suction muffler, a separate plastic part. Compared to integrated discharge lines in the crank case, a plastic discharge muffler minimizes the heat transfer between the hot refrigerant in the discharge line and the gas inside the compressor shell and thus decreases the temperature level of the entire compressor. To avoid the transport of valve induced pressure waves (the discharge process lasts approximately 30 °CA) to the condenser the discharge muffler consists of two volumes. A flexible plastic serpentine enables the connection of the swinging parts to the compressor shell.

Valves

Valves are the heart of a reciprocating compressor. They have a big influence on the thermodynamic behavior and several loss mechanism of a compressor. Reciprocating refrigeration compressors usually use flapper valve concepts. In contrast to active

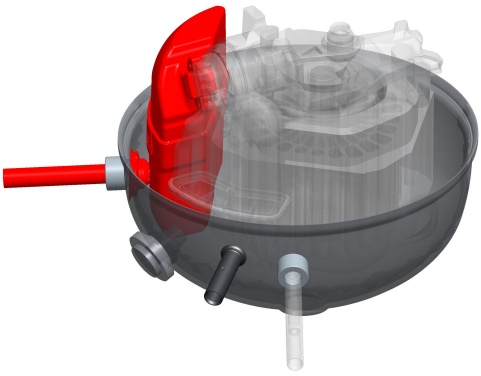

Fig. 1.7: Suction line of the HXD55 compressor

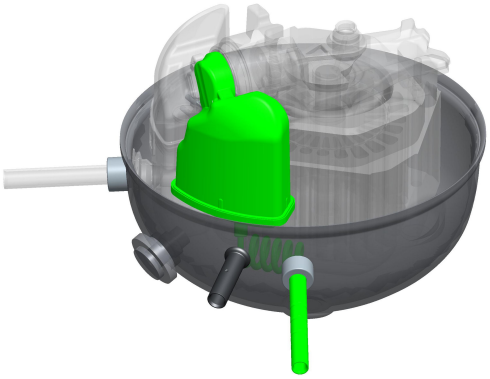

Fig. 1.8: Discharge line of the HXD55 compressor

controlled valves (e.g. used in internal combustion engines) which are actuated by an external force, flapper valves are actuated by the flow induced pressure difference. To realize specific opening and closing properties the valves can be preloaded. The suction valve of the HXD55 compressor for example has a preload which means that the valve in its neutral position is pressed on the valve plate. The preload yields in a faster valve closing decreasing the closing losses of the valve but increasing the opening losses due to the higher required opening force. The valve plate of the HXD55 compressor (suction valve - blue, discharge valve - red) can be seen in Fig. 1.9.

Crank drive

The crank drive of a reciprocating compressor consists of the usual parts of reciprocating machines namely a vertical oriented crankshaft, a connecting rod and a piston. The crank shaft is fixed with the rotor of the electric motor by press fit. In addition to the transformation of the rotational movement of the rotor into the translational movement of the piston, the crankshaft serves as oil pump of the compressor. The crankshaft is immersed in the oil sump and transports the oil via an arrangement of centrifugal and helical pumps to the bearings and distributes the oil inside the compressor shell. Two journal bearings and one roller bearing are used respectively for the radial and axial mounting of the crankshaft. To reduce friction and wear of the piston, axial offset of the piston pin is regarded. Fig. 1.10 shows the crank drive of the HXD55 compressor and its positioning.

1.1.4 Experimental investigation

The experimental investigation of refrigeration compressors is carried out in calorimeter test benches. In a calorimeter test bench, the compressor is tested at steady-state conditions in a predefined operation mode characterized by the pressure values at suc-

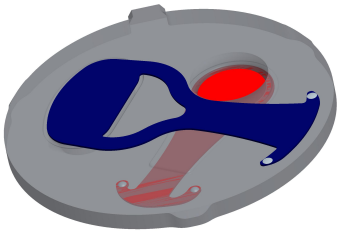

Fig. 1.9: Valve plate of the HXD55 compressor

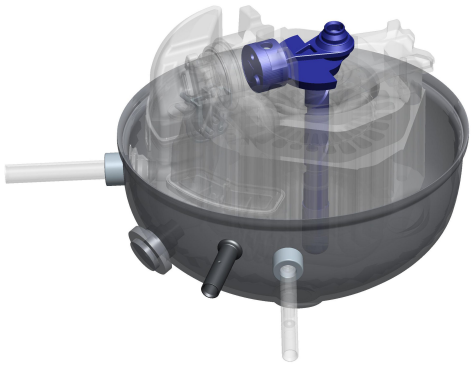

Fig. 1.10: Crank drive of the HXD55 compressor

tion and discharge. A schematic illustration of a calorimeter test bench can be seen in Fig. 1.11. The compressed refrigerant flows through the condenser giving off heat and after an accumulator, the liquid refrigerant is cooled down to a defined ambient temperature value. Via a valve in which the refrigerant is expanded and thus, pressure and temperature are decreased, the refrigerant enters the core element of a calorimeter test bench. The reservoir contains a second refrigerant (e.g. R404) at two-phase condition and ambient temperature. Due to the heat transport from the second refrigerant at ambient temperature to the refrigerant at low pressure condition, the temperature and thus the pressure of the second refrigerant would decrease. An electric heater keeps constant pressure and thus temperature in the reservoir (32 °C). The electrical input power of the compressor is measured by a wattmeter.

To quantify the efficiency of refrigeration compressors the Coefficient of Performance (COP) is introduced.

$$\mathrm{COP} = \frac{\dot{Q}_0}{P_{el}} \tag{1.2}$$

The determination of the compressor COP can be carried out at several standard operating conditions. As examples of common operating conditions, the ASHRAE conditions, well known in the compressor industry, can be mentioned. The term ASHRAE -23.3/45 for example means -23.3 °C evaporation, 45 °C condensing and 32.2 °C ambient temperature. Fig. 1.12 shows the Ts-diagram of the refrigeration cycle ASHRAE -23.3/45 for isobutane.

The cooling capacity which is needed to calculate the compressor COP is defined as

$$\dot{Q}_0 = \dot{m}_{\mathrm{R600a}} \left(h_6 - h_5\right) \tag{1.3}$$

In the previous described calorimeter test bench, the cooling capacity corresponds to the electrical power of the heater to get constant pressure in the reservoir. Assuming

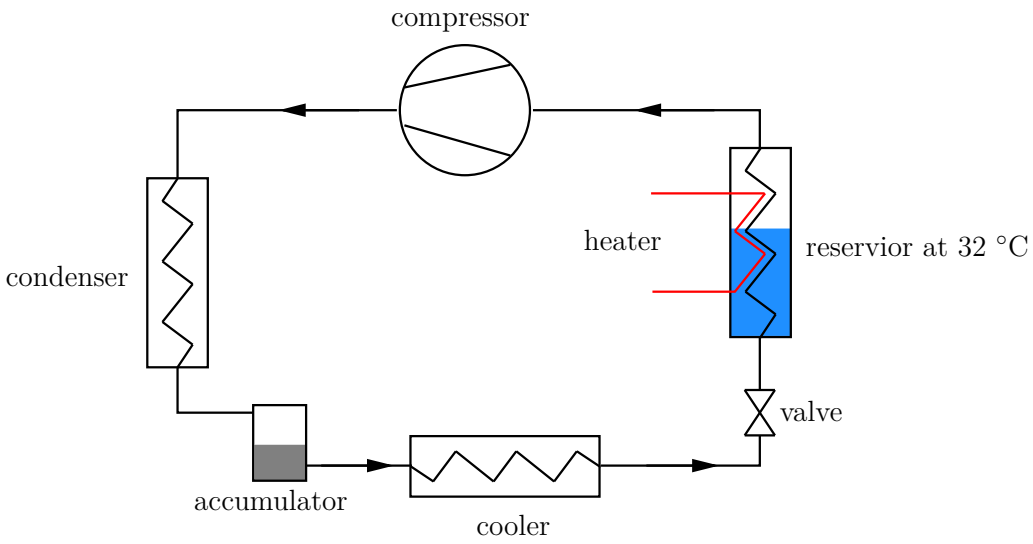

Fig. 1.11: Schematic illustration of a calorimeter

ASHRAE -23.3/45 standard conditions, the specific cooling capacity is 336.2 kJ kg^{-1} and thus the compressor mass flow rate can be determined. The measured electrical input power of the compressor and the electrical input power of the heater give the compressor COP.

1.1.5 Compressor oil

The proper selection of lubrication oil for the use in refrigeration systems depends on several factors. In addition to the compatibility of the refrigerant with the lubrication oil, the compressor type used in the refrigeration system plays an important role. Centrifugal, screw or reciprocating compressors differ in function and design and thus the demands on the lubrication oil vary. In reciprocating compressors the oil lubricates the moving parts and journal bearings, supports valve sealing and acts as heat transfer media. Due to the hermetic design of the regarded refrigeration compressor the oil and the refrigerant interacts with each other in different forms.
An important property of the refrigerant oil interaction is the solubility of refrigerant in the oil. Absorption of refrigerant in the lubrication oil depends on temperature and pressure and thus, from the compressor operation mode. Considering On/Off controlled compressors, the temperature decreases when the compressor is off. In case the off duration is long enough, ambient temperature is reached. At this temperature, the oil is able to absorb a considerable amount of refrigerant yielding in an equalizing pressure level below the refrigerant saturation pressure. Low equalizing pressure can lead to lower power consumption of the compressor at start-ups due to the low density of the refrigerant and one might conclude, that high solubility of the refrigerant in the

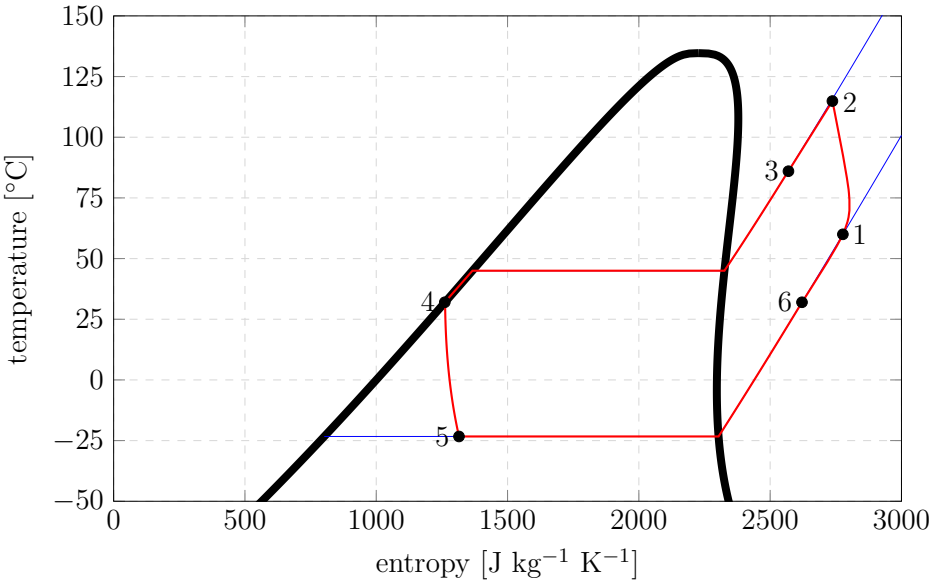

Fig. 1.12: ASHRAE standard conditions for isobutane (R600a)

oil might be desirable but here another effect plays an important role. At compressor start-ups the suction pressure decreases rapidly and thus the solubility decreases too. The dissolved refrigerant boils out influencing the oil pump efficiency and the lubrication capability of the oil.
Another property is the miscibility behavior of the oil with the refrigerant. The hermetic compressor design leads to oil transport into the refrigeration system. If miscibility of oil and refrigerant is not given, phase separation effects might occur yielding in efficiency decrease of the heat exchangers and furthermore, oil would be collected in the refrigeration circuit leading to compressor damage [Lav98].

Lubrication oil for hermetic reciprocating compressors used in household or light commercial refrigeration applications are usually mineral oil-based. Mineral oils perform well over a wide temperature range and show good chemical stability. To enable the use of these oils over the lifetime of hermetic refrigeration compressors, which is usually assumed to be 15 years, special anti-wear additives are used. As the basis for the investigations in the present thesis, the refrigeration oil Fuchs RENISO WF 5A which is the common lubrication oil in compressors of Secop Austria GmbH, is used. Fig. 1.13 shows the density and kinematic viscosity of the considered oil as a function of temperature. Furthermore, the influence of dissolved refrigerant R600a on the oil properties is illustrated [DS06].
The investigations of the present thesis are carried out by neglecting dissolved refrigerant in the oil.

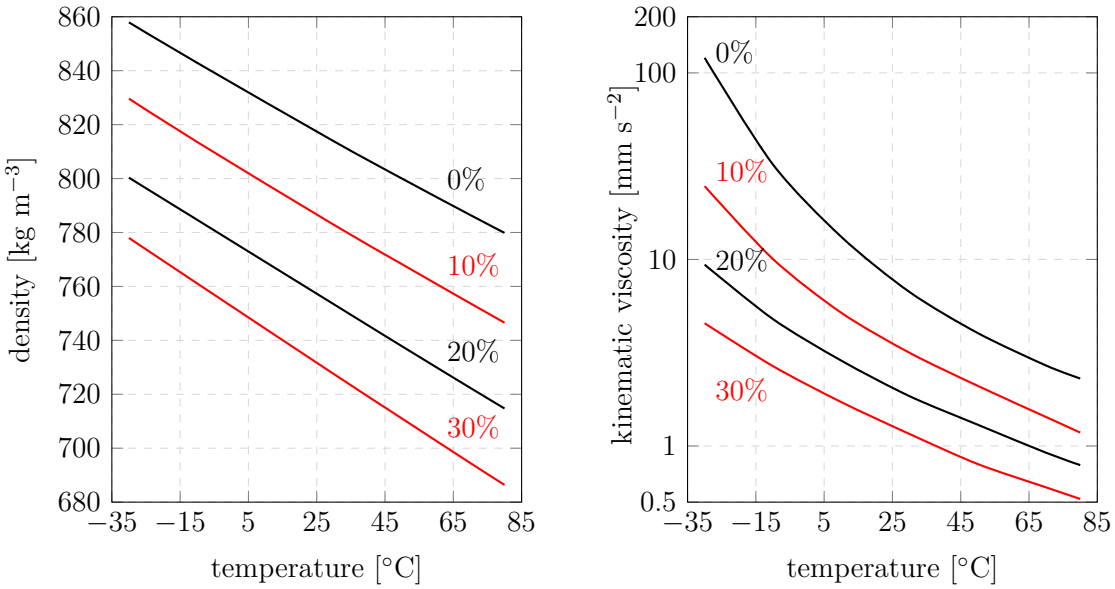

Fig. 1.13: Density and kinematic viscosity of RENISO WF 5A as a function of temperature and dissolved R600a [DS06]

1.2 Compressor cooling - a fundamental experiment

In order to increase the compressor COP, strategies must be developed which either increase the cooling capacity or decrease the electrical power input into the compressor. Looking at the cooling capacity, an increase can only be achieved by a higher refrigerant mass flow rate since the enthalpy difference for a specific test point is given. As the volume flow rate is given by the compressor geometry and the rotational speed, the density and thus the temperature of the refrigerant at the start of compression plays a significant role. Due to the hermetic design of the compressor and the installation of the suction line including the suction muffler inside the compressor shell, the refrigerant temperature at start of compression is considerably influenced by the temperature level of the entire compressor. In the compressor development, the heating of the refrigerant between compressor inlet and compression start and its resulting loss is known as superheating.
To investigate the influence of superheating on the compressor COP and thus the potential of increasing the compressor efficiency by measures in this area, an experimental investigation is carried out by the research group in which the compressor is cooled. Notwithstanding the practical implementation in an existing cooling appliance, the compressor is cooled by water flowing through a specially designed valve cover. A schematic illustration of the modified compressor for the cooling experiment can be seen in Fig. 1.14.

Although the compressor used in the experiment is from the Secop Kappa series,

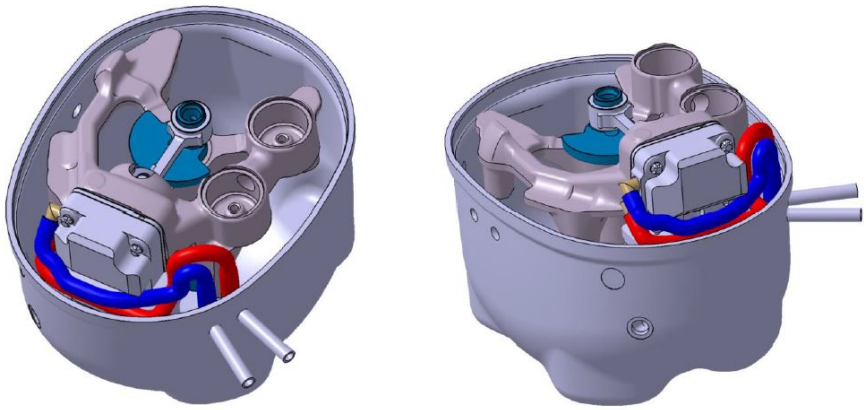

Fig. 1.14: Modified compressor for the cooling experiment

the fundamental findings can be assigned to the HXD55 compressor due to the similar design. The test procedure contains compressor efficiency measurements in the calorimeter test bench at different water cooling power $\dot{Q}_c$ applied on the water cooled valve cover. In addition to the measurement of the COP, the oil sump temperature as well as the cylinder temperature is determined. The results of the cooling experiment can be seen in Fig. 1.15.

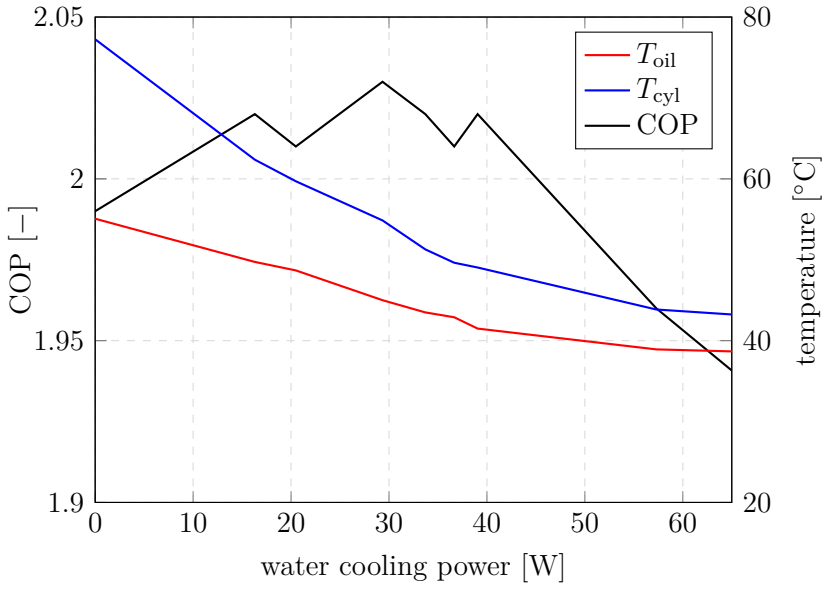

Fig. 1.15: Results of the cooling experiment

Looking at the results of the cooling experiment in Fig. 1.15 some interesting relationships can be observed. As expected, the temperatures of the cylinder and the oil in the sump decrease by increasing the water cooling power. Due to the lower temperature

level in the compressor and thus in the suction path, the temperature of the refrigerant at compression start is decreased compared to the compressor without water cooling leading to an increase of the refrigerant density. The resulting higher refrigerant mass flow yields in an increase of the compressor COP at moderate water cooling capacities. Contrary to the expectations, a further increase of the water cooling capacity does not lead to higher COP values of the compressor. As the results show, the compressor COP falls below the value of the original uncooled compressor. Analyzing the results of the cooling experiment the following question arises: "What is the limiting factor for the COP while decreasing the compressor temperature level?" As a consequence of the experimental results, it can be conclude that two effects might be responsible for the COP decrease. The first effect can be explained by thermal deformation of the compressor parts. The cooling of the compressor with water has a considerable influence on the temperature distribution inside the compressor. Due to the design of the water cooled valve cover, the crank case and the valve plate are mainly cooled on one side which may lead to temperature stresses and thus to deformations in the concerned compressor parts. Since the design, materials and machining of the compressor parts are adapted on the uncooled case, these deformations may lead to increasing friction losses and thus, to a lower COP. The second effect can be explained by looking at the oil temperature in the cooling experiment. Compared to the uncooled compressor, the oil temperature of the cooled compressor is decreased by approximately 17 °C. The oil of hermetic reciprocating compressors for refrigeration appliance is usually selected to fulfill the lubrication requirements at unfavorable conditions like in the pull-down mode. Unfavorable conditions mean high pressure ratios and thus high temperature levels in the compressor which is contrary to the present cooling experiment. The low oil temperature yields in an increase of the oil viscosity and thus in an increase of the friction losses. A distinction of the mentioned effects based on the experimental data is not possible.

1.3 Motivation

To meet the future requirements concerning efficiency and energy consumption, also the efficiency of the refrigerant sub systems as the compressor have to be increased. Despite water cooling of a compressor of this type is not realistic, decreasing the temperature level will be still an issue. As the cooling experiment shows, investigations solely executed by experiments are not enough to achieve accurate statements about the physical effects influencing the compressor COP. Numerical simulation instead of or in addition to experiments help to get a deeper understanding of the physical effects in the compressor. The aim of this work is to provide numerical simulation approaches for the oil relevant problems in hermetic reciprocating compressors and thus, enabling a holistic thermodynamic evaluation and loss analysis including the lubrication oil as heat transfer medium.

1.4 Problem definition and realization

The integration of the lubrication oil into the thermodynamic evaluation of hermetic compressors requires detailed understanding of the oil related effects. By tracking the oil on its path from the oil sump and back again, the relevant oil mechanisms can be shown. The oil is picked up by the oil pump from the sump feeding bearings and sliding surfaces. On its way through the oil pump the oil absorbs heat from the electric motor and the warm compressor parts. At the crank pin the oil is distributed inside the compressor shell, covering the shell walls and furthermore giving off heat. After the oil flows down the walls back into the oil sump, the process starts again. Considering the described oil path, the oil mechanisms which must be taken into account for the thermodynamic evaluation are the oil transport in the pump, the friction losses and the oil distribution inside the compressor including the resulting heat transfer.
The present work also goes along with the previous mentioned mechanisms. After an overview over the relevant theoretical background on which this work is based on, the calculation of the oil pump related parameters using numerical simulation is shown. In addition to the common modeling approach, an alternative method is proposed and validated against the common approach and measurement data. In chapter 4 the numerical simulation of the oil distribution inside the compressor shell is explained yielding in heat transfer coefficients between the lubrication oil and the oil covered walls. The determination of the compressor friction losses using both a self-coded program and a commercial software is shown in chapter 5. To enable the implementation of the gained results into the thermal evaluation of a compressor, a thermal compressor model is developed. The thermal model uses three-dimensional (3D) formulation as far as possible and its accuracy is validated by experimental data. Furthermore, a compressor loss analysis based on exergy formulation is shown. The loss analysis is able to reproduce exergy losses on different levels. Finally, the applicability of the presented simulation approaches is demonstrated on an artificially cooled compressor.

2 Theoretical basics

The following chapter provides an overview over the theoretical background for the applied numerical methods in this work. To keep the number of pages for this chapter within acceptable limits basic knowledge in fluid dynamics, thermodynamics and mechanics is assumed from the reader at this point.
Within this chapter the physical theory of flow process is explained in terms of the conservation equations of mass, momentum and energy. To get an idea about heat transfer, the difference between heat transfer mechanisms and their characteristics is explained. Furthermore, an overview over the lubrication theory and the necessary formulas is given. Finally, the second law of thermodynamics is examined in terms of entropy and exergy, respectively.

2.1 Conservation equations

Fluid flow problems are typical fields of activity for mechanical engineers. Especially since computational performance reaches acceptable values, the investigation of fluid dynamics applying numerical methods (CFD) is a common practice in research and industry. The base for the calculation of fluid flows is given by the so called Navier-Stokes equation, introduced in the first half of the 19^{th} century by Claude Louis Marie Henri Navier[1] and George Gabriel Stokes[2] (independently). In the proper sense of Navier-Stokes equation only the conservation equation of momentum is meant, but nowadays the term is used for the conservation equations of mass, momentum and energy. The mathematical equations of this sub chapter refer on [VM07] and [MMD15]. A more detailed derivation of the conservation equations can be found in these books. In the following expression of the conservation equations the Eulerian description is used. Compared to the Lagrangian description which follows fluid parcels as they move through space and time, the Eulerian approach concentrates on specific locations in the flow field resulting in flow variables as functions of time and position.

[1] Claude Louis Marie Henri Navier (1785-1836) Professor for mechanics and analytics at the École Polytechnique

[2] Sir George Gabriel Stokes (1819-1903) Lucasian Professor of Mathematics at the University of Cambridge

2.1.1 Conservation of mass

The conservation equation of mass (or continuity equation) indicates that without the presence of any mass source or sink the regarded system conserves its mass. The flux form of the continuity equation is given by

$$\frac{\partial \rho}{\partial t} + \nabla \cdot [\rho \mathbf{u}] = 0 \tag{2.1}$$

Assuming incompressible flow which means no significant absolute pressure or temperature changes, ρ does not change in the flow. The conservation equation for incompressible flow is obtained as

$$\nabla \cdot \mathbf{u} = 0 \tag{2.2}$$

Due to the absence of ρ in Eq. 2.2 the continuity equation cannot be used to calculate the density. The usage of the incompressible flow formulation is a good approximation for gases at low speeds (approx. 0.3 Ma). Incompressible flow does not mean that ρ is constant over the entire domain; it only means that each fluid element keeps its density as it moves. Density differences can occur for example due to temperature or pressure differences.

2.1.2 Conservation of momentum

Linear momentum is defined as the product of mass and velocity of a body resulting in a vectorial quantity. The direction of the momentum vector coincides with the movement direction of the body. According to Newton‘s second law of motion, a body will maintain its momentum until an external force acts on it. Applied on an arbitrary fluid, external forces can occur as surface or body forces. The conservative form of the momentum equation for incompressible fluids assuming constant viscosity can be expressed as

$$\frac{\partial}{\partial t}[\rho \mathbf{u}] + \nabla \cdot \rho \mathbf{u}\mathbf{u} = -\nabla p + \mu \nabla^2 \mathbf{u} + \mathbf{f}_\mathrm{b} \tag{2.3}$$

2.1.3 Conservation of energy

The conservation of energy is based on the first law of thermodynamics which states

Energy can be neither produced nor destroyed in a process, it can only be converted in another energy form [BK12]

Different forms of the energy equation can be used distinguished by the particular energy expression (e.g. specific total enthalpy). Under special conditions, the energy equation can be expressed in terms of temperature which gives the following form for ideal gases

$$\frac{\partial}{\partial t}(\rho c_p T) + \nabla \cdot [\rho c_p \mathbf{u} T] = \nabla \cdot [\lambda \nabla T] + \frac{\mathrm{D}p}{\mathrm{D}t} + \mu \Phi + \dot{q}_\mathrm{V} \tag{2.4}$$

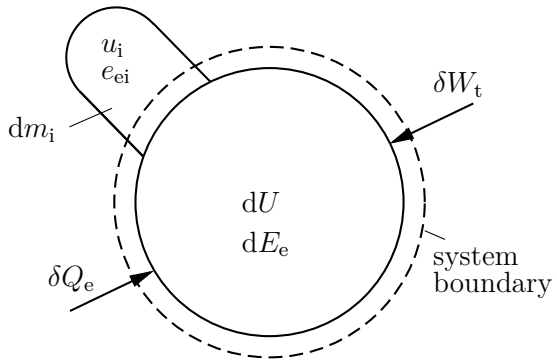

Fig. 2.1: Thermodynamic system [Eic10]

with

$$\Phi = 2\left[\left(\frac{\partial u}{\partial x}\right)^2 + \left(\frac{\partial v}{\partial y}\right)^2 + \left(\frac{\partial w}{\partial z}\right)^2\right] + \left(\frac{\partial u}{\partial y} + \frac{\partial v}{\partial x}\right)^2 + \left(\frac{\partial u}{\partial z} + \frac{\partial w}{\partial x}\right)^2 + \left(\frac{\partial v}{\partial z} + \frac{\partial w}{\partial y}\right)^2 \tag{2.5}$$

At this point, also the first law of thermodynamics applied on a thermodynamic system (Fig. 2.1) should be mentioned. It balances the energy inside of the thermodynamic system and the energy flows into the system across the system boundary. The energy inside the system is expressed as the internal and external energy. Energy flows across the system boundary are technical work, heat or energy transported with mass.

$$\delta W + \delta Q_\mathrm{e} + \sum_i \mathrm{d}m_\mathrm{i}(h_\mathrm{i} + e_\mathrm{ei}) = \mathrm{d}U + \mathrm{d}E_\mathrm{e} \tag{2.6}$$

2.1.4 General conservation equation

The structure of conservation equations is similar for every kind of conservative quantity. As Eq. 2.7 shows for an arbitrary property ϕ the equation contains a transient term, a convection term, a diffusion term and a source term.

$$\frac{\partial}{\partial t}(\rho\phi) + \nabla \cdot (\rho \mathbf{u}\phi) = \nabla \cdot (\Gamma^\phi \nabla\phi) + Q^\phi \tag{2.7}$$

Due to the similar structure, the numerical treatment of the equations does not require special methods for each regarded quantity. The discretization process and the structure of the numerical solution are independent of the conservative quantity.

2.1.5 Dimensionless numbers

A fundamental property of physical problems, and therefore also of velocity and temperature fields, is that the used reference system has no influence on the result. By intro-

ducing dimensionless quantities, the scaling of physical problems is simplified because the number of influencing variables is decreased to just a few characteristic numbers. The derivation of dimensionless quantities for the Navier-Stokes equations is carried out by using characteristic variables of length, velocity, density and temperature.

$$t^* = \frac{U_\infty t}{L}; \quad \mathbf{x}^* = \frac{\mathbf{x}}{L}; \quad \nabla^* = L\nabla \quad \mathbf{u}^* = \frac{\mathbf{u}}{U_\infty}; \quad \rho^* = \frac{\rho}{\rho_\infty}; \quad p^* = \frac{p}{\rho_\infty U_\infty^2}$$
$$\Theta = T - T_\infty; \quad \Theta_0 = T_\mathrm{W} - T_\infty; \quad \Theta^* = \frac{\Theta}{\Theta_0}$$

To derive the dimensionless forms of the momentum and energy equation, a temperature depending buoyancy term is introduced as a body force. The dimensionless forms of the equations for incompressible flow are given by

$$\frac{\partial}{\partial t^*}[\rho^*\mathbf{u}^*] + \nabla^* \cdot \rho^*\mathbf{u}^*\mathbf{u}^* = -\nabla^* p^* - \frac{\mathbf{g}\beta\Theta_0 L}{U_\infty^2}\rho^*\Theta^* + \frac{\mu}{\rho_\infty U_\infty L}(\nabla^*)^2\mathbf{u}^* \tag{2.8}$$

$$\begin{aligned}\frac{\partial}{\partial t^*}(\rho^*\Theta^*) + \nabla^* \cdot [\rho^*\mathbf{u}^*\Theta^*] = \frac{U_\infty^2}{c_p\Theta_0}\left(\frac{\partial p^*}{\partial t^*} + \mathbf{u}^* \cdot \nabla^* p^*\right) \\ + \frac{\lambda}{\rho_\infty U_\infty c_p L}\nabla^* \cdot [\nabla^*\Theta^*] + \frac{\mu U_\infty}{\rho_\infty \Theta_0 c_p L}\Phi^*\end{aligned} \tag{2.9}$$

with

$$\Phi^* = 2\left[\left(\frac{\partial u^*}{\partial x^*}\right)^2 + \left(\frac{\partial v^*}{\partial y^*}\right)^2 + \dots\right] + \dots$$

The obtained equations contain four independent dimensionless groups which characterize the physical problem and can be summarized in the following dimensionless numbers:

$$\mathrm{Re} := \frac{U_\infty L}{\nu} \tag{2.10}$$

$$\mathrm{Pr} := \frac{\nu}{a} \tag{2.11}$$

$$\mathrm{Gr} := \frac{g_\mathrm{i}\beta L^3\Theta_0}{\nu^2} \tag{2.12}$$

$$\mathrm{Ec} := \frac{U_\infty^2}{c_p\Theta_0} \tag{2.13}$$

The Reynolds[3] Re number gives the ratio of inertia to viscous forces. It plays a significant role in fluid dynamics due to its description of the boundary layer form. The Reynolds number is used to characterize fluid flows in terms of its dissipative properties and therefore to distinguish between laminar and turbulent flows. Next number only contains fluid properties ($a := \lambda/c_p\rho_\infty$) and is known as Prandtl[4] number Pr. The Prandtl number represents the ratio of hydrodynamic boundary layer to thermal boundary layer and thus, links temperature and velocity field. The Eckert[5] number Ec describes the ratio of kinetic energy to flow enthalpy. It only has to be considered in flows with velocities near speed of sound. The last dimensionless number gained from the dimensionless form of the momentum and energy equation is the Grashof[6] number Gr which gives the ratio of buoyancy to viscous forces. The Grashof number can be used to identify the type of convective heat transfer (forced or natural).

2.2 Heat transfer

The physical phenomenon of heat transfer plays an important role in the present thesis especially in the thermal investigation of the hermetic compressor. The following sub chapter gives a fundamental overview over the heat transfer mechanisms conduction, convection and radiation using the definitions and mathematical formulas of [BS04]. A closer look on the specific heat transfer mechanism will be given in the individual sub chapters.

2.2.1 Heat conduction

The transfer of heat due to conduction in a specific material requires a temperature gradient. Neighboring molecules or free electrons in metals enable the energy transport due to the temperature gradient. The basic law for heat conduction introduced by Jean Baptiste Fourier[7] in the early 19$^{\text{th}}$ century gives the relation between heat flow and temperature gradient by using the proportional factor λ. This factor is called thermal conductivity and is a material property depending on temperature and pressure.

$$\mathbf{q} = -\lambda \operatorname{grad} T \tag{2.14}$$

The heat flux density $\mathbf{q}$ is defined as a vector. To calculate the heat flux $\mathrm{d}\dot{Q}$ through an arbitrary orientated area element the unit vector of the area element has to be

[3] Osborne Reynolds (1842-1912) Professor of engineering at Owens College Manchester
[4] Ludwig Prandtl (1875-1953) Professor for applied mechanics at the University of Göttingen
[5] Ernst Rudolph Georg Eckert (1904-2004) Professor for mechanical engineering at the University of Minnesota
[6] Franz Grashof (1826-1893) Professor of applied mechanics at Karlsruhe University of Applied Sciences
[7] Jean Baptiste Joseph Fourier (1768-1830) Professor for mechanics and analytics at the École Polytechnique

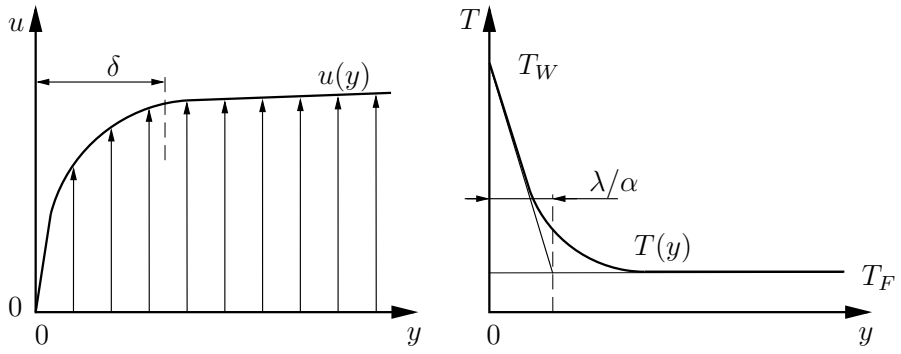

Fig. 2.2: Velocity and temperature of a fluid flow as a function of the distance to the wall [BS04]

considered.

$$\mathrm{d}\dot{Q} = \mathbf{q}\,\mathbf{n}\,\mathrm{d}A = -\lambda\,\mathrm{grad}\,T\,\mathbf{n}\,\mathrm{d}A \tag{2.15}$$

Thermal conductivity can vary significantly between different kinds of materials. Metals have very high thermal conductivities, fluids like gases and liquids have very little values of thermal conductivity. Depending on the specific technical field, the appropriate choice of material can have a significant influence on the function or efficiency of the application due to the thermal conductivity (e.g. isolation).

2.2.2 Convective heat transfer

In fluid flows, in addition to heat conduction due to a temperature gradient, energy is transported as enthalpy and kinetic energy of the fluid. This physical phenomenon is known as convective heat transfer. For technical applications, the heat transfer between a fluid flow and a solid wall is of particular significance. A characteristic property of convective heat transfer is the boundary layer, initially investigated by Ludwig Prandtl in 1904. The boundary layer is defined for the velocity and temperature field in the fluid flow, respectively. Fig. 2.2 illustrates the velocity and temperature of a fluid flow as a function of the distance to the wall. As the curves show, the heat transfer and, thus, the specific heat flux strongly depends on the velocity and temperature field. By introducing the local heat transfer coefficient α the specific heat flux is given by

$$\dot{q}_\mathrm{W} = \alpha(T_\mathrm{W} - T_\mathrm{F}) \tag{2.16}$$

A graphical illustration of the correlation between heat transfer coefficient and temperature profile is shown in Fig. 2.2. λ/α represents the sub tangent of the temperature profile at the wall which has the similar scale as the thermal boundary layer. The determination of the heat transfer coefficient can be reduced to the calculation of the

Nusselt number which was introduced by Wilhelm Nusselt[8] in 1915. The Nusselt number gives the ratio of real heat flux density to heat flux density at pure conduction in a stationary flow.

$$\mathrm{Nu} := \frac{\alpha L}{\lambda} \tag{2.17}$$

Generally, the Nusselt number only depends on the dimensionless number derived in chapter 2.1.5 and the dimensionless coordinate in surface direction (x^* and z^*). The Nusselt number and, thus, the convective heat transfer coefficient are related to the location on the body surface. If the Nusselt number is averaged over the body surface, the dependency to the dimensionless coordinate is dropped and it can be expressed as

$$\overline{\mathrm{Nu}} = f(\mathrm{Re}, \mathrm{Pr}, \mathrm{Gr}, \mathrm{Ec}) \tag{2.18}$$

Two different types of convective heat transfer can be distinguished. Forced convective heat transfer occurs in artificial driven fluid flows. It plays a significant role in technical applications like pipe flows or flows over bodies. Natural convection heat transfer occurs in buoyancy driven flows due to the density difference by temperature gradients in the gravitational field of the earth. To distinguish between forced and natural convection, the Reynolds number and the Grashof number are used and the following estimation can be drawn:

$Gr << Re^2$:	forced convection
	buoyancy forces << inertia forces
$Gr >> Re^2$:	natural convection
	buoyancy forces >> inertia forces
$Gr \approx Re^2$:	mixed convection
	buoyancy forces $\approx$ inertia forces

2.2.3 Radiation

Heat transfer due to radiation does not play a significant role in the present thesis and is therefore only mentioned for the sake of completeness. The following sub chapter should give a rough overview of the topic.
If the temperature of a body is higher than absolute zero (which can be stated for each practical appliance) heat is transferred from the body to its ambient due to radiation. Electromagnetic waves transport the inner energy of a body which is called emission. If the emitted electromagnetic waves hit another body, a part of the transported energy is absorbed, the rest is reflected or can be passed through, known as transmittance. Josef

[8] Wilhelm Nusselt (1882-1957) Professor of theoretical mechanics at Karlsruhe University of Applied Sciences

Stefan[9] stated that the maximum of the possible heat flux density due to radiation is given by

$$\dot{q} = \sigma T^4 \tag{2.19}$$

The universal constant σ was introduced by Ludwig Boltzmann[10] who derived it from the second law of thermodynamics. To calculate the specific radiation heat flux density of a real body the emissivity $\varepsilon(T)$ was introduced. The emissivity is defined as the ratio of radiant exitance of the real body to the radiant exitance of an ideal, called black body. Considering the emissivity the heat flux density due to radiation can be rewritten as

$$\dot{q} = \varepsilon(T)\sigma T^4 \tag{2.20}$$

2.3 Lubrication theory

Lubrication takes a significant role in the field of mechanical engineering regarding appliances with moving parts. The fluid film lubrication between two parts moving with differential speeds can be seen as fluid flow problem and thus, the Navier-Stokes equations form the base for its calculation. In 1886, Osborne Reynolds derived the basic differential equation of fluid film lubrication which links the pressure field and the fluid film height by adapting the Navier-stokes equations. The detailed derivation of the so called Reynolds equation is not given here but the interested reader can be referred to [Ham94] or [Bar10] which serves as the base literature sources for the following chapter. Reynolds assumed that inertia and body forces can be neglected in fluid film lubrication due to the dominating influence of pressure and viscous forces. Furthermore, he stated that the terms depending on the coordinate in fluid film height direction are negligible. By assuming small angles between the two surfaces the Reynolds equation can be written as

$$\frac{\partial}{\partial x}\left(\frac{\rho h^3}{12\mu}\frac{\partial p}{\partial x}\right) + \frac{\partial}{\partial y}\left(\frac{\rho h^3}{12\mu}\frac{\partial p}{\partial y}\right) = \frac{(U_\mathrm{I} + U_\mathrm{II})}{2}\frac{\partial(\rho h)}{\partial x} + \frac{(V_\mathrm{I} + V_\mathrm{II})}{2}\frac{\partial(\rho h)}{\partial y} + \frac{\partial(\rho h)}{\partial t} \tag{2.21}$$

The terms on the left-hand side of the Reynolds equation represent the Poiseuille flow, the terms on the right-hand side represent the Couette flow and the displacement flow, respectively. To solve the Reynolds equation pressure constraints have to be defined. At the boundaries of the regarded area the pressure is set to ambient condition. Oil supply areas are specified with oil supply pressure and in case of circular problems pressure value and pressure gradient have to be considered as periodic boundary condition. The solution of the Reynolds equation results in negative pressure values in areas with diverging fluid film height. Subambient pressure values lead to cavitation effects in the fluid film which can be distinguished between gaseous cavitation and vaporous

[9] Josef Stefan (1835-1893) Professor for physics at the University of Vienna
[10] Ludwig Boltzmann (1844-1906) Professor of Physics inter alia at the University of Graz

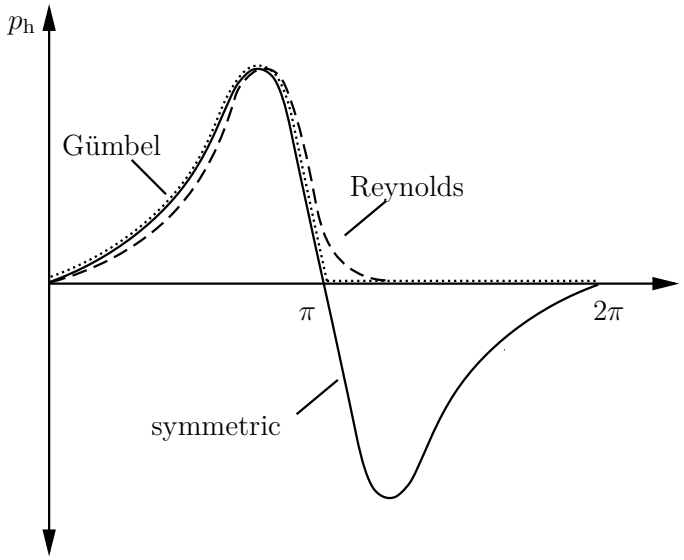

Fig. 2.3: Schematic pressure curve using non conservative cavitation models [LS78]

cavitation depending on the pressure level and the lubricant. Gaseous cavitation occurs if the pressure falls below the saturation pressure of dissolved gases in the lubricant which are then released. If the pressure level is decreased significantly and reaches its vapor pressure, the lubricant may boil at ambient pressure. Several approaches to model cavitation effects in lubrication systems are available and can be distinguished by their ability to conserve mass and fulfill continuity. Non conservative approaches were introduced by Gümbel[11] and Reynolds. Gümbel proposed to set negative pressure values to zero, whereas Reynolds set the pressure gradient to zero at the transition to cavitation region which has the disadvantage that the cavitation region is not known in advance so an iterative procedure is necessary (see Fig. 2.3). Compared to non-conservative approaches, conservative cavitation models for fluid film lubrication are quite more complex. A common used conservative cavitation algorithm was presented in [Elr81]. The author developed a numerical algorithm to calculate the lubricant flow in the cavitation region based on the models of [Flo57], [JF57] and [Ols65]. By introducing the gap filling level to calculate a mixture density of lubricant and gas, a modified form of the Reynolds equation is got, thus the cavitation algorithm requires the calculation of two variables: the gap filling level in the cavitation region and the hydrodynamic pressure in the remaining region.

For special cases, the Reynolds equation can be simplified and a closed solution can be obtained. As an example, the short cylindrical bearing can be mentioned. For the static loaded case the resulting shaft position diverges from the force direction as

[11] Ludwig Gümbel (1874-1923) naval architect

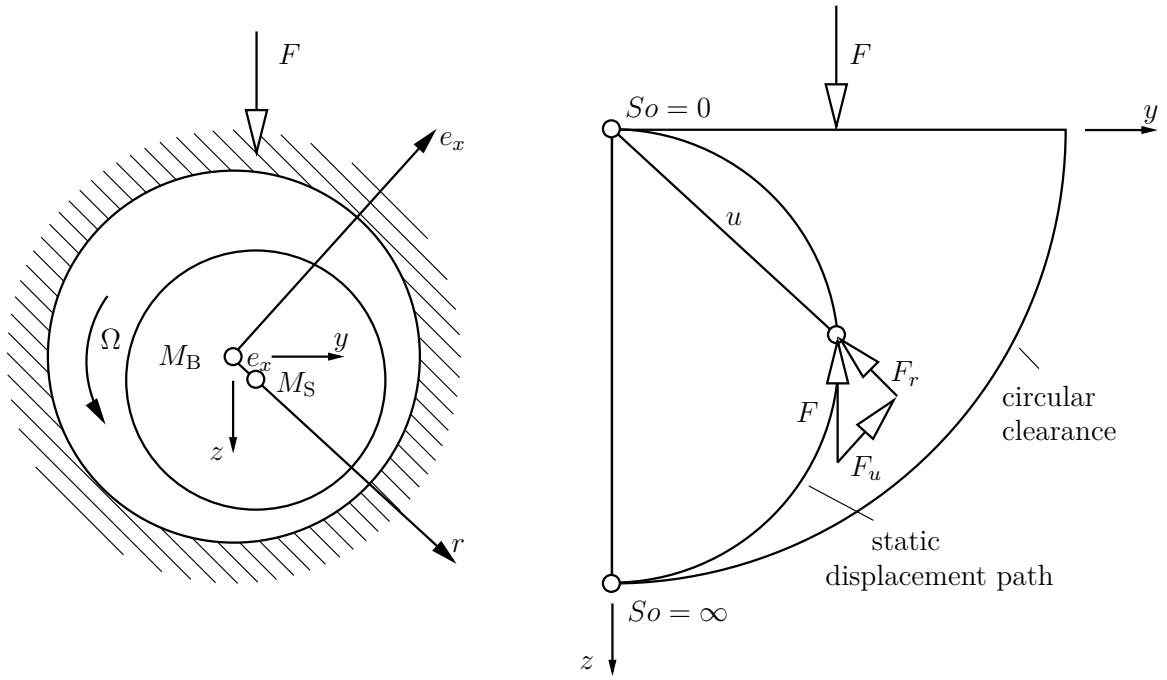

Fig. 2.4: Shaft position of a static loaded bearing depending on the Sommerfeld number [GNP05]

illustrated in Fig. 2.4. Sommerfeld[12] introduced a dimensionless number named after him which includes the influencing factors for this effect [GNP05].

$$\mathrm{So} := \frac{F\psi^2}{BD\mu\Omega} \tag{2.22}$$

The Sommerfeld number plays a significant role in the characterization of the static and dynamic behavior of cylindrical bearings. As shown in [GNP05], the Sommerfeld number is a function of the shaft eccentricity which is thereby depending on the bearing force, geometry, oil properties and rotational speed. Due to the predefinition of the bearing geometry the influence of the force, oil and rotational speed are of major interest. Reducing the rotational speed at constant remaining parameters has the same effect as increasing the bearing force. The shaft gets closer to the bearing shell as the Sommerfeld number is increased as shown in Fig. 2.4. Combining constant static and dynamic loads (e.g. rotor with constant unbalance under its specific weight) leads to trajectories of the shaft around the Sommerfeld number dependent static eccentricity proportional to the force amplitude.

Analytical calculation of the bearing behavior is only permitted in special cases like

[12] Arnold Sommerfeld (1868-1951) Professor for theoretical physics at University of Munich

the previous mentioned rotor with constant unbalance under its specific weight. For bearings under non constant loads like journal bearings in internal combustion engines or reciprocating compressors, analytical solutions of the Reynolds equation are not possible, thus, numerical methods have to be used.

The original Reynolds equation (Eq. 2.21) describes the link between the pressure field and the fluid film height which can be summarized to the so called macro effects. Detailed investigations of the journal bearing behavior require also the consideration of surface roughness influence on the pressure field which is known as micro effects. Taking into account the micro effects into the simulation of fluid film lubrication problems, a direct coupling or an indirect coupling approach can be used, respectively. The direct coupling approach includes the surface roughness into the definition of the fluid film height and thus, requires very fine geometric resolution of the desired bearing surface. Due to the fine resolution, direct coupling requires high computational resources and thus it can be used for very small simulation regions. The indirect coupling can be seen as the more practical method. In [PC78] and [PC79] an indirect method was first presented and it is still (or slightly adopted) state-of-the-art. The authors introduced so called flow factors to describe the difference between the fluid flow in rough and smooth bearing surfaces. By applying these flow factors to the original Reynolds equation, a modified version was developed which is given by

$$\begin{aligned}\frac{\partial}{\partial x}\left(\phi_{\mathrm{x}}\frac{\rho h^3}{12\mu}\frac{\partial \overline{p_h}}{\partial x}\right)+\frac{\partial}{\partial y}\left(\phi_{\mathrm{y}}\frac{\rho h^3}{12\mu}\frac{\partial \overline{p_h}}{\partial y}\right)=\frac{(U_{\mathrm{I}}+U_{\mathrm{II}})}{2}\frac{\partial(\rho\overline{h_{\mathrm{T}}})}{\partial x}+\frac{(V_{\mathrm{I}}+V_{\mathrm{II}})}{2}\frac{\partial(\rho\overline{h_{\mathrm{T}}})}{\partial y}\\ +\sigma_\delta\left(\frac{\partial\phi_{\mathrm{S}}}{\partial x}+\frac{\partial\phi_{\mathrm{S}}}{\partial y}\right)+\frac{\partial(\rho\overline{h_{\mathrm{T}}})}{\partial t}\end{aligned} \tag{2.23}$$

To determine the flow factors, the surface roughness parameters have to be known and the averaged fluid film height with respect to micro effects $\overline{h_{\mathrm{t}}}$ is introduced. At this point, a detailed description of the calculation of several flow factors is not given and the interested reader is referred to specific literature ([PC78] and [PC79]).

2.4 Second law of thermodynamics

In addition to the first law of thermodynamics which describes the conservation of energy in a thermodynamic system, the second law of thermodynamics plays a significant role in engineers' life to rate and understand the thermodynamic behavior of technical processes. The second law of thermodynamics enables conclusions about the direction of natural processes. It is an empirical finding and it cannot be reduced to another general law, it is only confirmed by experiences by studying natural processes [BK12]. The second law of thermodynamics can be expressed in different ways; the most general form is given by

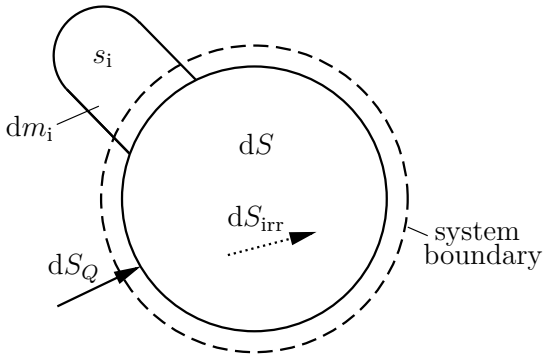

Fig. 2.5: Entropy balance [Kle12]

All natural processes are irreversible [BK12]

To formulate the second law of thermodynamics in mathematical form, the state variable entropy was introduced by Rudolf Clausius[13]. The entropy is defined as the measure of the irreversibility of processes resulting in a further form of the second law of thermodynamics

All natural processes produce irreversible entropy [BK12]

The entropy in a system can change due to heat transfer and mass transfer across the system boundary as well as irreversible entropy production inside the system. According to the system in Fig. 2.5 the entropy balance of a thermodynamic system can be written as follows

$$\mathrm{d}S_Q + \sum_i \mathrm{d}m_\mathrm{i} s_\mathrm{i} + \mathrm{d}S_\mathrm{irr} = \mathrm{d}S \tag{2.24}$$

The transport of work across the system boundary has no influence on the entropy of a system. Entropy is not a conserved quantity, it is only a quantity to rate the irreversibility and therefore the entropy balance is not denoted as conservation equation.

Additionally to the state variable entropy, the second law of thermodynamics can be described in terms of exergy and anergy. Exergy is the maximum useful energy of a thermodynamic system, anergy, in contrast, is the destroyed and not useful energy. Technical work and external energy are pure exergy, internal energy and heat are partly exergy. The first and second law of thermodynamics can be rewritten by the use of exergy and anergy as follows

The sum of exergy and anergy in natural processes stays constant [BK12]
In irreversible processes exergy is converted into anergy [BK12]

[13]Rudolf Julius Emanuel Clausius (1818-1888) Professor for theoretical physics inter alia at ETH Zurich

3 Oil pump

The oil pump in hermetic reciprocating compressors for refrigeration application is usually integrated into the compressor crankshaft. It pumps the lubrication oil from an oil sump at the bottom of the compressor shell via different pump parts to the crankshaft journal bearings and further to the conrod joints and the piston. In addition to the task of supplying the moving parts of the crank drive with oil, the oil pump distributes the oil inside the compressor shell and ensures proper heat transfer from the hot compressor parts to the shell and further on to the ambient air. The following descriptions are referred to the oil pump of the HXD55 compressor which is typical for many of the billions of hermetic reciprocating compressors. A cross section of the compressor can be seen in Fig. 3.1 which shows the assembly of the oil pump group. The crankshaft and thus the oil pump are connected with the rotor of the electrical motor via a press fit. In the considered case of the HXD55 compressor, the oil pump system consists of three individual pumps. The oil is sucked via a centrifugal pump, machined as an eccentric bore in the inside of the crankshaft. Due to the centrifugal force induced by the rotational movement of the crankshaft, an almost parabolic shape of the oil surface is developed. The eccentricity of the cyclic bore enables an asymmetric oil parabola shape and thus an oil flow at the outlet of the centrifugal pump. To increase the oil mass flow rate, a so-called catcher is mounted at the immersed end of the oil pump, which induces further rotational kinetic energy into the oil flow. After leaving the first centrifugal pump, the oil flows into a helical groove, machined on the outer surface of the crankshaft. To decrease the mechanical losses in that area, the gap between the crankshaft and the crankcase is increased. From the helical groove, the main journal bearings of the crankshaft are supplied with oil. The third pump is designed also as centrifugal pump. At the outlet of the helical groove, the oil is transported back into the inside of the crankshaft and further on, due to the centrifugal force, into the crank pin where the oil supplies the crank pin journal bearing and the piston. Finally, the oil leaves the pump and it is distributed inside the compressor shell, where it covers the walls and gives off the absorbed heat.

The design of oil pumps for hermetic reciprocating compressors is carried out according to different aspects. As the most important criterion, an adequate oil mass flow rate has to be ensured to supply the bearings and the piston with oil and, furthermore, to enable sufficient heat transfer. Especially for variable speed compressor, the design of the oil pump to guarantee sufficient oil mass flow at the whole speed range is an important task in the development process. For fixed speed compressors, an additional property of the oil pump has to be taken into account - the oil climbing time. The

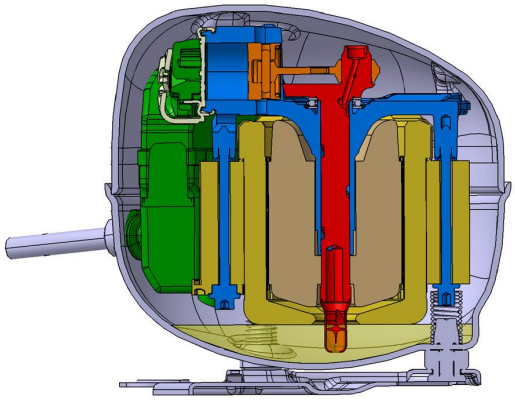

Fig. 3.1: Cross section of the HXD55 compressor

oil climbing time describes the time to transport the oil from the sump to the pump outlet and thus, to supply the bearings with oil. In addition to the maximum oil mass flow rate and the minimum climbing time, oil pumps have to be optimized in terms of power loss and acoustic behavior.
The development of compressor oil pumps is usually done by experimental work resulting in considerable time and cost expensive procedures. Since CFD plays a significant role in the development process of modern compressors, such methods are not only used for gas path simulations; also the calculation of the oil pump is performed applying these methods.

3.1 Literature review

The large number of published studies dealing with the oil pump modeling of hermetic compressors shows the significance of this topic in the development process of these kind of compressors. Various studies focus on only one specific part of the oil pump system as the works of [ABPR09] or [ABPR11] show which model can be applied for the helical oil pump with an analytical approach. The authors used the screw extrusion approach introduced by [LH94] which is derived from the Navier-Stokes equations and solve the resulting Poisson equation with mathematical methods like the Generalized Integral Transform Technique (GITT). Another example of analytical oil pump modeling is proposed in [KL03] and [KLKB02]. The aim of these studies was to transfer the oil pump system of a hermetic compressor into an equivalent electrical network which can be solved by numerical methods. Individual lubrication elements were modeled with electric elements applying coefficients gained by experimental or analytical methods. The increasing usage of CFD in the development process of modern hermetic compressors can also be seen in published papers related to this topic. Studies as presented in [LAB09], [ABP12], [KYO13] or [OSH+14] show the numerical simulation of

compressor oil pumps by the application of multiphase models embedded in commercial CFD software like ANSYS Fluent. The main objectives of these works are the determination of the oil mass flow and the oil climbing time. In addition to the consideration of the entire oil pump, studies as [THC+14] describe the uncoupled CFD simulation of individual oil pump parts as the helical groove. The uncoupled approach should enable an independent treatment of the helical groove without the need of simulating the entire oil pump resulting in a reduction of computational time but it also neglects any interactions of the considered part with the rest of the oil pump. In summary, the published studies reflect the typical trade-off of modeling accuracy and computational time. A modeling strategy as shown in the present thesis which tries to combine high geometrical resolution over the entire oil pump while keeping the computational time under reasonable limits cannot be found.

3.2 Oil pump simulation

The following chapter deals with the modeling of the compressor oil pump by the use of CFD. Starting with the conventional simulation approach, which can be found in several references, an alternative simulation method is presented. Finally, the simulation results are verified against experimental data of an oil pump test rig. Several simulations are carried out using the input data according to Tab. 3.1.

Tab. 3.1: Input data for the oil pump simulations

oil density	832 kg m^{-3}
oil viscosity	6.7e-3 Pa s
gas density	1.225 kg m^{-3}
gas viscosity	1.8e-5 Pa s
surface tension	2.8e-2 N m^{-1}
rotational speed	2950 min^{-1}

The following assumptions are made for each of the simulations:

- Isothermal flow.
- Physical properties of the fluids are constant.
- Dissolving of gaseous phase in liquid phase is neglected.
- Laminar flow.

3.3 Conventional oil pump simulation

The simulation of the compressor oil pump is usually performed by applying CFD methods on the entire pump geometry. Several studies, which can be found in open literature, deal with the application of CFD in compressor oil pump simulation. The following applied simulation approach is similar to the proposed method presented in [LAB09], [ABP12] or [KYO13].
If the entire pump geometry is considered, a closer look has to be taken on the filling situation in the pump domain. Due to the design of the HXD55 oil pump with its centrifugal pump which is immersed in the oil sump, the pump is only partly filled with oil, thus multiphase models are required. In contrast to single phase simulation, multiphase models can treat fluid flows with two or more fluids. Among the various numbers of different multiphase models, the Volume of Fluid (VOF) model, presented in [SZ99], is suitable for the oil pump flow. The VOF model is generally used to track the sharp interface between two or more immiscible fluids, thus two gases cannot be modeled due to their mixture at molecular level. Furthermore, the use of the VOF model requires interface length scales larger than the computational grid. The simulation of fluid flows using the VOF model is based on the introduction of the volume fraction χ of each fluid in the domain. Using Eq. 3.1 the movement of the phase interface can be described. Due to the discontinuity of the viscosity and density along the interface in the simulation domain, their values are calculated by Eq. 3.3 and Eq. 3.2.

$$\frac{\partial \chi}{\partial t} + \frac{\partial u_\mathrm{i} \chi}{\partial x_\mathrm{i}} = 0 \tag{3.1}$$

$$\rho = \rho_\mathrm{g} \chi + \rho_\mathrm{l} \left(1 - \chi\right) \tag{3.2}$$

$$\mu = \mu_\mathrm{g} \chi + \mu_\mathrm{l} \left(1 - \chi\right) \tag{3.3}$$

The VOF model is implemented in the commercial CFD software ANSYS Fluent which is used for the oil pump simulation applying the conventional approach. To consider the interaction between the oil sump and the immersed oil pump, the simulation domain contains a simplified oil sump in addition to the oil pump geometry. The entire mesh consists of approximately 800,000 mainly tetrahedral cells. To fulfill the overall mass balance, the oil mass flow at the pump outlet is filled back into the oil sump via a User Defined Function (UDF). At pump outlet, ventilation hole and oil sump surface pressure boundary conditions are adopted. To keep the number of cells under reasonable limits, the gap between shaft and crankcase at the helical groove area is neglected based on the modeling proposed in [LAB09] and [KYO13]. The relative velocity between crankshaft and crankcase is implemented as moving wall boundary condition. Fig. 3.2 shows the simulation domain and the applied boundary conditions for the conventional method. The simulation executed until steady-state conditions are reached by utilizing implicit time formulation using a constant time step of 1e-4 s.

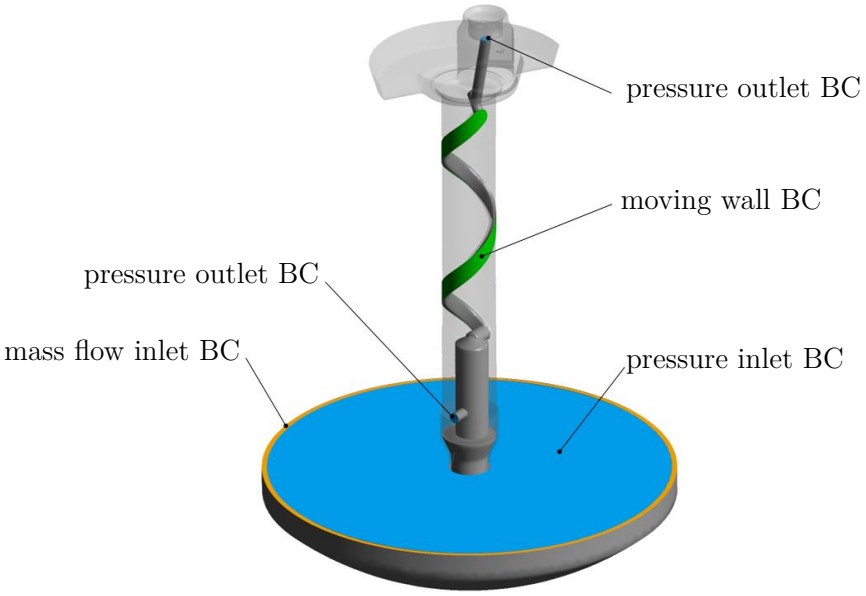

Fig. 3.2: Simulation domain and boundary conditions for the conventional method

The conventional simulation method is carried out for three different immersion depths which are 3 mm, 7 mm and 10 mm. Simulation results in terms of oil mass flow rate at the pump outlet and relative static pressure at the pump inlet can be seen in Fig. 3.3 and Fig. 3.4. As the oil mass flow rate results show, a decrease of the pump immersion depth leads to a decrease in the oil mass flow rate of the pump. Furthermore, smaller immersion depths have a significant impact on the oil climbing time. Decreasing the immersion depth from 7 mm to 3 mm does not only result in a climbing time increase of 0.22 s, but also the time to reach steady-state conditions rises significantly.

Regarding the static pressure at the oil pump inlet, a pressure drop can be seen in the first period after starting the compressor. Due to the increase of the pressure drop at higher immersion depth values, the pressure drop can be explained by the induced kinetic energy of the catcher giving higher dynamic pressure in that area. Although the static pressure values are too high to cause cavitation in the classical sense, outgasing effects of the dissolved refrigerant in the oil can occur and thus, can lead to a decrease of the oil mass flow rate. Fig. 3.5 shows the oil volume fraction in the regarded domain at different time steps. In addition to the induced vortex in the oil sump, the complete filling of the helical groove with oil can be seen.

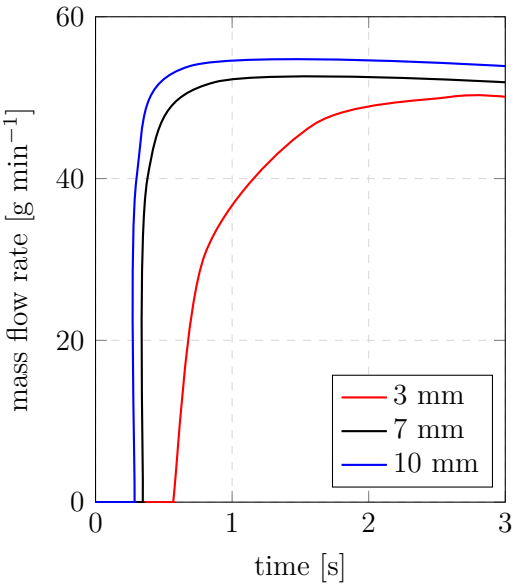

Fig. 3.3: Oil mass flow rate at the pump outlet

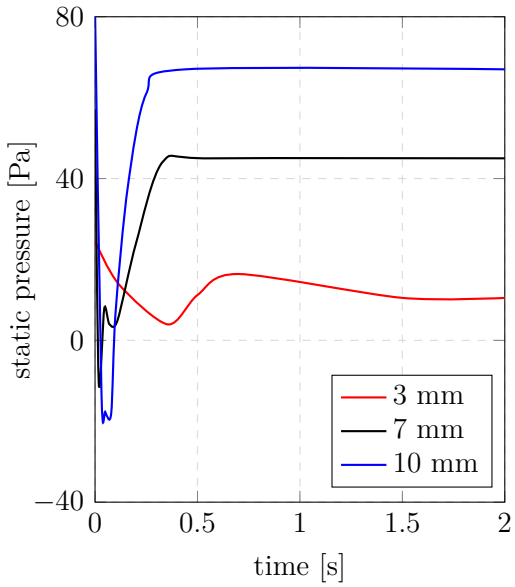

Fig. 3.4: Relative static pressure at the pump inlet

3.4 Split-up approach

Applying the previously mentioned conventional simulation method to determine the oil pump behavior, some drawbacks can be outlined. The time-consuming VOF method applied on each cell of the computational domain yields in considerable computation time due to the additional conservation equation of the volume fraction and the formulation of the fluid properties density and viscosity. Due to the time-expensive simulation, variant analyses of different geometries or operating parameters are only useful for a small number of variants. Therefore, the use of the conventional simulation method in the development process of hermetic reciprocating compressors is limited. Furthermore, to keep the computational time under reasonable limits, the resolution of geometric details has to be avoided. An example is the modeling of the gap between crankshaft and crankcase, which has a significant influence on the oil pump behavior.
In the following section, an innovative oil pump simulation approach is presented which avoids the disadvantages of the conventional method as far as possible and enables the use of CFD in the development of hermetic reciprocating compressor oil pumps. The method is based on the idea of splitting-up the oil pump into its individual pumping parts using appropriate simulation methods for each part. Regarding the HXD55 crankshaft, the oil pump consists of three individual pumps which are two centrifugal pumps at the inlet and outlet, and a helical groove, respectively (Fig. 3.6).

The simulation of each individual pump gives pump curves in terms of mass flow to pressure difference. To obtain the performance curve of the entire compressor oil pump

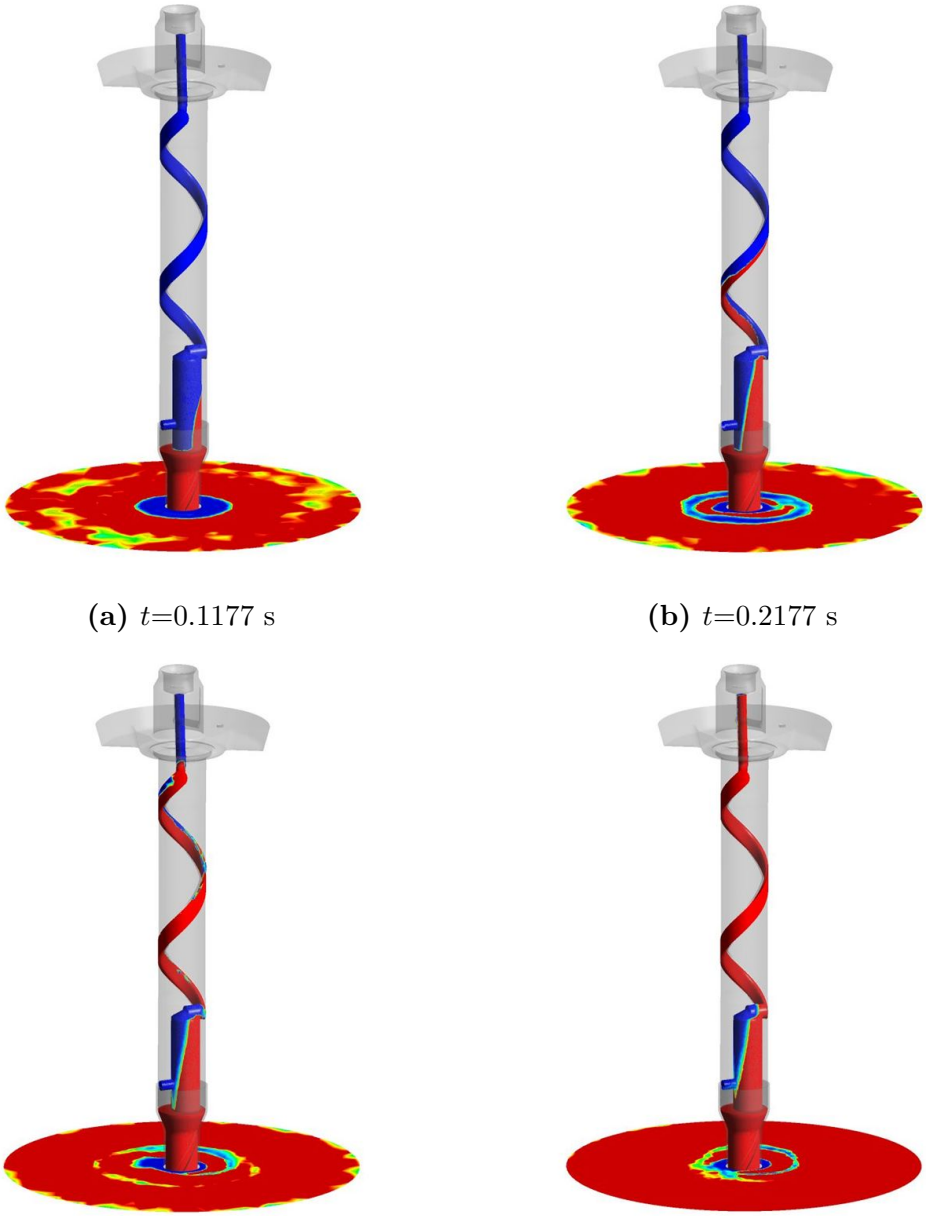

(a) t=0.1177 s **(b)** t=0.2177 s

(c) t=0.3177 s **(d)** t=1.0177 s

Fig. 3.5: Volumetric oil volume fraction gained by conventional simulation method (red = oil, blue = gas)

the individual pump curves can be summed up. The following sub sections give an insight into the modeling of each pumping part and the combination of the sub models

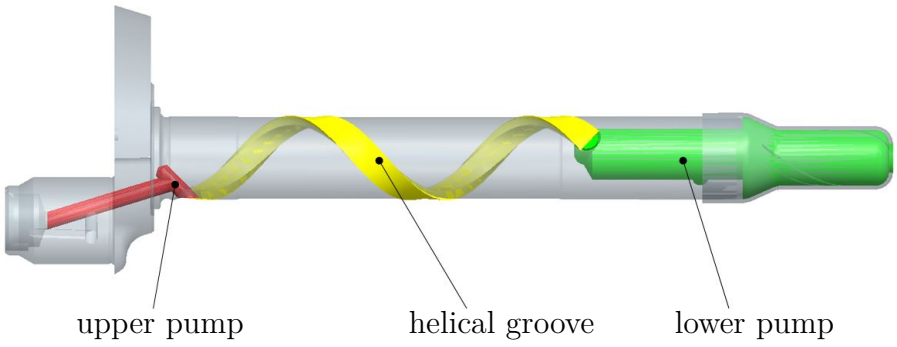

Fig. 3.6: Individual oil pump parts

to the entire oil pump model. To validate the approach, the simulation results are compared with measurement data of an oil pump test rig. Furthermore, the split-up method is compared with the conventional method in terms of computational effort. The split-up method has been published in [PHB+].

3.4.1 Lower centrifugal pump

The modeling of the lower centrifugal pump requires similar procedure as the simulation of the entire oil pump with the conventional approach. Due to the presence of liquid and gaseous phase, the use of the VOF method is necessary. Two different models are used to calculate the performance curve of the centrifugal pump and to determine the influence of the immersion depth on the oil pump behavior, respectively. The prediction of the performance curve is carried out utilizing the lower centrifugal pump domain without the compressor oil sump. A mesh with approximately 200,000 mainly tetrahedral cells is used. According to Fig. 3.7 pressure inlet and pressure outlet boundary conditions are applied on the interface to the oil sump and the helical groove. At the pressure inlet boundary condition, the oil volume fraction is set to one to simulate the immersion in the oil sump. The performance curve is generated by varying the pressure ratio between inlet and outlet. Results of the lower centrifugal pump simulation in terms of oil volume fraction at steady-state conditions can be seen in Fig. 3.8. The cross-section through the simulation domain shows the oil parabola which is cut off on one side due to the eccentricity of the cylindrical bore.

To determine the influence of the immersion depth on the oil pump behavior in the split-up approach, the simulation of the lower centrifugal pump in combination with the oil sump using the VOF model is carried out. Similar to the individual consideration of the lower centrifugal pump, pressure outlet boundary condition is implemented at the interface to the helical groove. The pressure value at the pressure outlet boundary condition is set to zero.

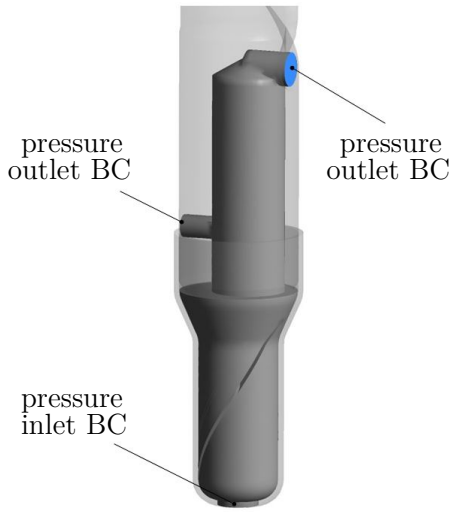

Fig. 3.7: Simulation domain and boundary conditions for the lower centrifugal pump

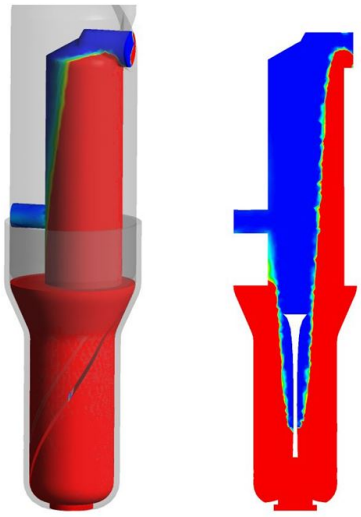

Fig. 3.8: Volumetric oil volume fraction gained in the lower centrifugal pump

3.4.2 Helical groove

The modeling of the helical groove is based on the assumption of a completely filled channel at steady-state conditions which can be confirmed by the simulation results of the conventional method. This assumption enables single phase simulation of the helical groove and thus, the time-consuming VOF method is not necessary. The flow in the helical groove channel is considered as fully developed and the cross-section flow can be regarded as independent from the transport velocity normal to the cross-section (in z-direction). As it is shown in [PHH+15], the transport velocity in z-direction can be treated as a passive scalar and only the two-dimensional flow field in the helical groove cross-section has to be calculated. Applying these assumptions and neglecting the body forces in y-direction gives the following formulations of the momentum equations:

$$\rho\left(u\frac{\partial u}{\partial x}+v\frac{\partial u}{\partial y}\right)=-\frac{\partial p}{\partial x}+\mu\left(\frac{\partial^2 u}{\partial x^2}+\frac{\partial^2 u}{\partial y^2}\right)+\rho g_x \tag{3.4}$$

$$\rho\left(u\frac{\partial v}{\partial x}+v\frac{\partial v}{\partial y}\right)=-\frac{\partial p}{\partial y}+\mu\left(\frac{\partial^2 v}{\partial x^2}+\frac{\partial^2 v}{\partial y^2}\right) \tag{3.5}$$

$$\rho\left(u\frac{\partial w}{\partial x}+v\frac{\partial w}{\partial y}\right)=-\frac{\partial p}{\partial z}+\mu\left(\frac{\partial^2 w}{\partial x^2}+\frac{\partial^2 w}{\partial y^2}\right)+\rho g_z \tag{3.6}$$

The body force terms in x- and z-direction include the gravitational force in the respective direction due to the helix angle. To predict the performance curve of the

helical groove, the pressure ratio between the interfaces to the lower and upper centrifugal pump is implemented via the pressure gradient term in the z-momentum equation, thus the total length of the helical groove has to be considered.
By the use of the commercial software ANSYS Fluent the two-dimensional cross-section flow is calculated. The determination of the transport velocity in channel direction is implemented via the passive scalar function in the software. Furthermore, the calculation of the performance curve of the helical groove is carried out utilizing an UDF. The determination of the simulation domain and the applied boundary conditions are shown in Fig. 3.9. As the illustration shows, the cross-section is given by the unwrapped channel which makes one full turn on the crankshaft. Therefore, periodic boundary conditions are applied at both sides of the channel gap. The simulation domain is meshed with approximately 50,000 almost quadrilateral cells to ensure an adequate resolution of the gap between crankshaft and crankcase.

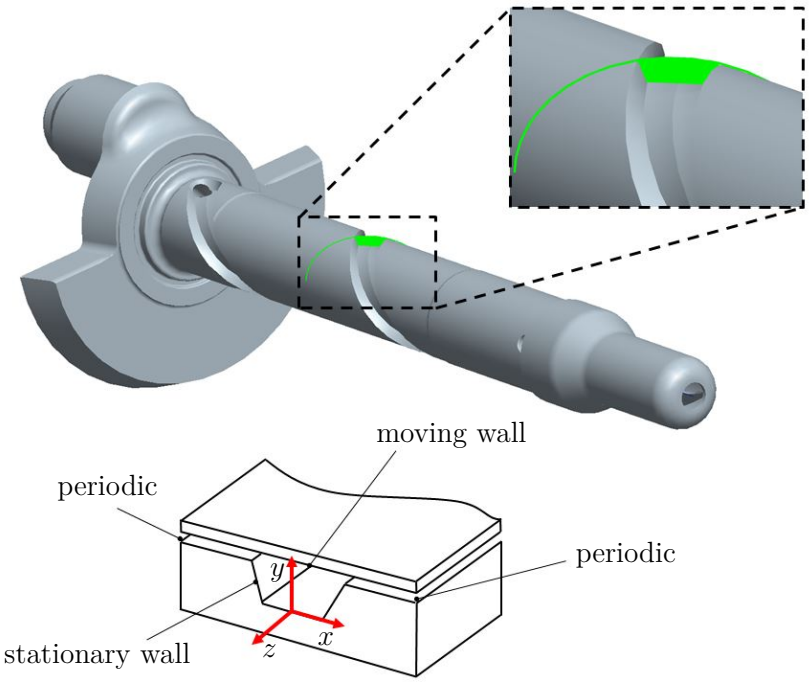

Fig. 3.9: Geometry of the helical groove and the applied boundary conditions

Results of the helical groove simulation can be seen in Fig. 3.10 and Fig. 3.11. The relative movement between the crankshaft and crankcase induces an asymmetric vortex in the channel cross section. Due to the treatment of the transport velocity in channel direction as a passive scalar, a flow field according to Fig. 3.11 occurs which shows asymmetric behavior too.

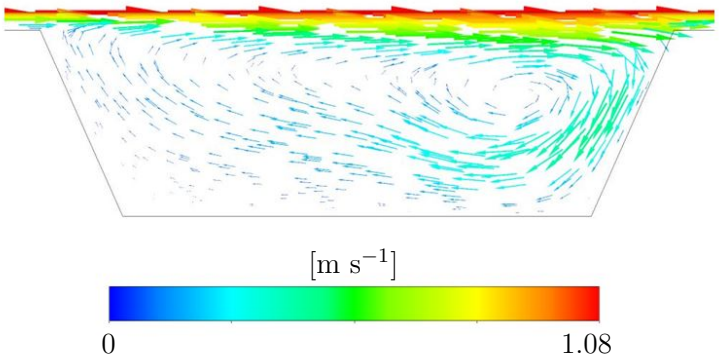

Fig. 3.10: Velocity in channel cross-section

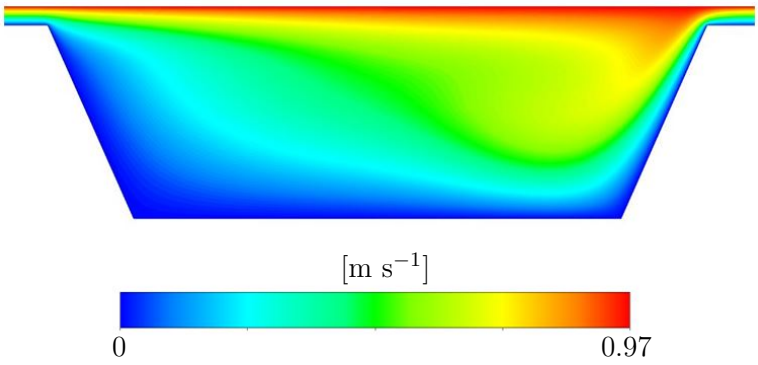

Fig. 3.11: Velocity in channel direction

3.4.3 Upper centrifugal pump

Similar to the treatment of the helical groove, the upper centrifugal pump is assumed to be filled with oil completely. Therefore, single phase simulation is permitted too. The simulation domain is meshed with approximately 200,000 tetrahedral cells. Utilizing inlet pressure and outlet pressure boundary conditions at the interface to the helical groove and the pump outlet, the pressure ratio to predict the pump performance curve can be implemented. The upper centrifugal pump simulation is performed in the commercial software ANSYS Fluent.

3.4.4 Combination of the sub models

The simulation of the individual pumping parts of the compressor oil pump according to the previously described methods yields to performance curves of each pump. In the next step, the combination of the individual performance curves to an entire performance curve has to be realized. Therefore, the individual pump curves are summed up (Fig. 3.12). To consider the influence of the immersion depth of the oil pump in the

oil sump, the simulation of the lower centrifugal pump combined with the oil sump has to be carried out giving the static pressure at the pump inlet. Assuming zero pressure at the outlet of the pump, the mass flow rate can be determined with the performance curve of the entire oil pump. Due to the partly filling of the lower centrifugal pump, the pressure difference in that pump has to be checked. The relative static pressure at the interface between the lower centrifugal pump and the helical groove has to be positive, otherwise gas would be sucked into the helical groove and the oil flow would break down, thus the lower centrifugal pump is the limiting factor in the investigated arrangement of individual pumps. The assumption of completely filled helical groove and upper centrifugal pump permits negative relative static pressure in the interface between these parts unless cavitation limits are not reached. Even if cavitation does not appear, outgasing effects of dissolved refrigerant may occur at negative static pressure values. A schematic illustration of the split-up approach can be seen in Fig. 3.13.

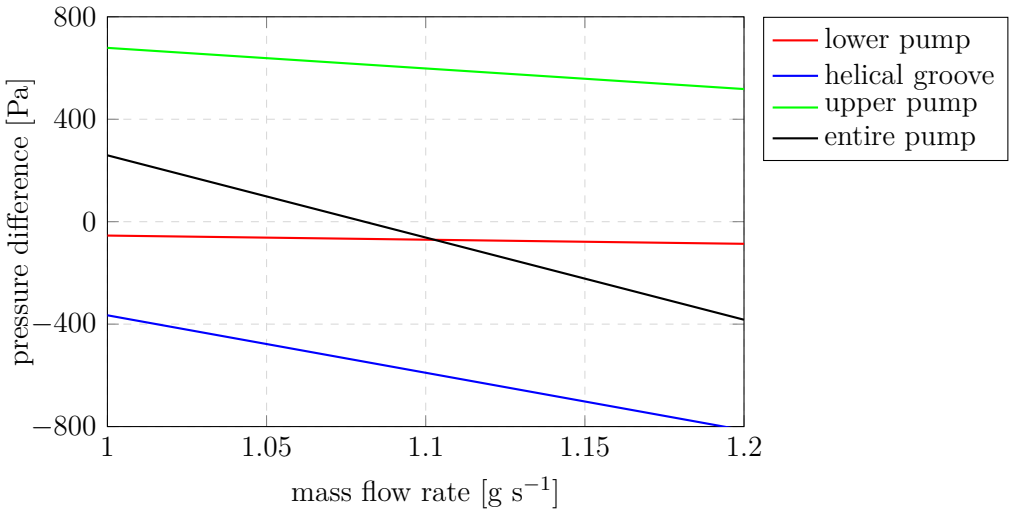

Fig. 3.12: Combination of the performance curves

3.5 Experimental work

To validate the results of the pump simulation, measurement data of an oil pump test rig are used. The validation is based on the comparison of the oil mass flow rate at steady-state conditions which serves as standard criterion for the evaluation of oil pump for On/Off controlled compressors. The measurement is based on the volumetric determination of the transported oil. A schematic illustration of the test rig is shown in Fig. 3.14. The lower part of the crankshaft is mounted on a motor module, which is vertically adjustable to enable oil flow measurements at different immersion depths. Rotation speed of the motor is kept constant at 3000 rpm. Due to the large surface of

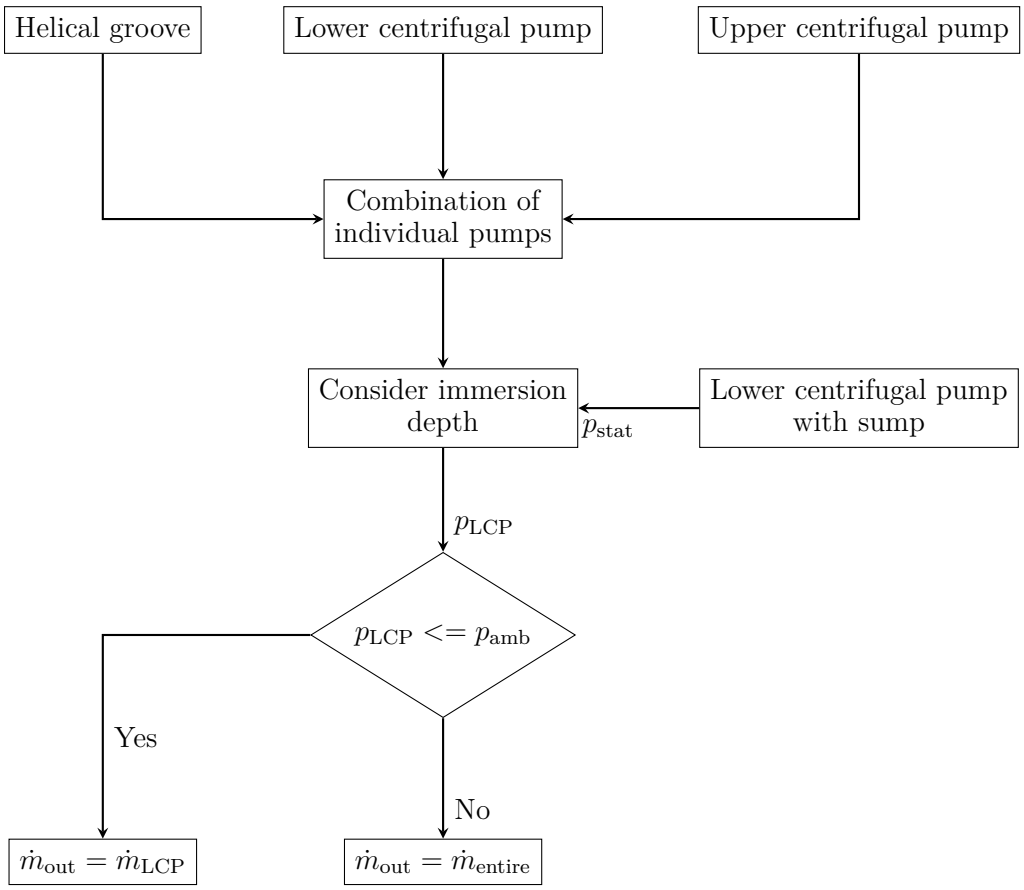

Fig. 3.13: Flow chart of the split-up solution algorithm

the oil pool, immersion depth fluctuations are widely compensated. A thermocouple is used to measure the oil temperature and an integrated heater is used to keep the oil temperature and thus, the viscosity at constant level. The expelled oil is collected in a collection tray and flows then into a graduated vessel via a plastic tube. For a given period the oil pump is operated and the oil volume is measured to get the flow rate. For each immersion depth ten measurements are carried out and the mean flow rate is determined by the arithmetic average. The standard deviation of the oil flow rate measurements is in the order of 2 %.

3.6 Application of the split-up approach

To show the ability of the developed split-up method to determine the steady-state oil mass flow rate of an hermetic compressor oil pump, two oil pump versions of the HXD55 compressor are used. In addition to the standard oil pump, a modified oil pump is investigated. The modified oil pump has an additional bore at the crank

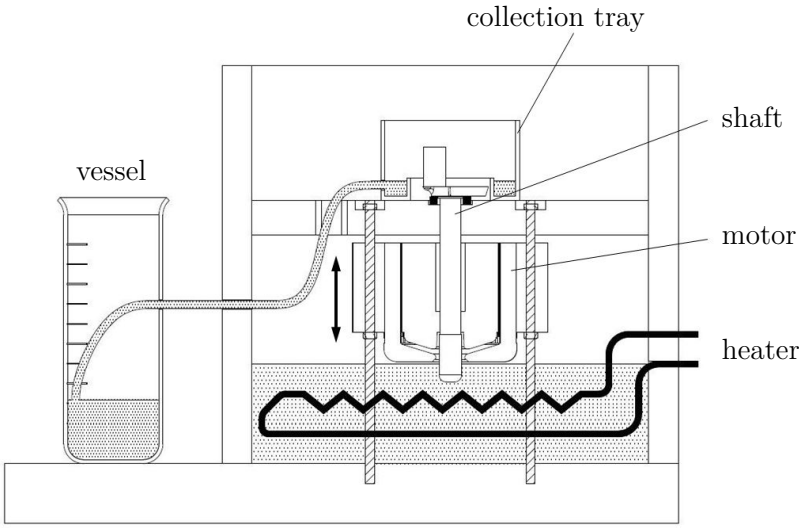

Fig. 3.14: Oil pump test rig

web which acts as a bypass of the upper centrifugal pump by equalizing the pressure at the interface between helical groove and upper centrifugal pump with ambient pressure. This leads to a disabling of the influence of the upper centrifugal pump on the behavior of the entire pump. The position of the bore can be seen in Fig. 3.15.

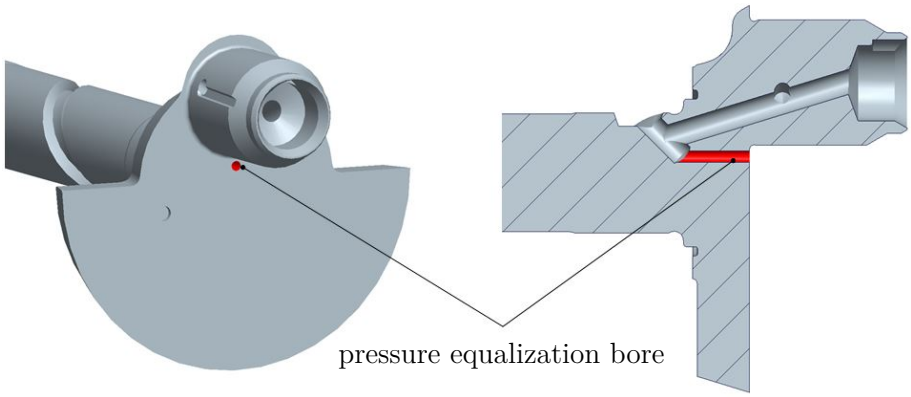

Fig. 3.15: Modified oil pump

Starting with the standard oil pump the workflow of the split-up method is explained. The oil mass flow rates are determined for three immersion depths which are 3 mm, 7 mm and 10 mm. Fig. 3.17 shows the operating point and the pressure along the crankshaft length of the regarded cases. Looking at the 3 mm case, the combination of the individual pump performance curves and the calculated static pressure at the pump inlet yields in an operating point above the intersection point of the entire and lower

centrifugal pump curves. The static pressure at the inlet of the lower centrifugal pump is not sufficient to ensure a complete filling of the helical groove and thus, the mass flow rate of the lower centrifugal pump is the maximum mass flow rate the oil pump is able to transport in this case. This circumstance can also be seen in the pressure along the crankshaft length. The static pressure at the interface between lower centrifugal pump and helical groove is negative, resulting in a breakdown of the oil flow.
Similar behavior can be observed at the 7 mm case. The position of the operating point and the static pressure value at the interface between lower centrifugal pump and helical groove yields in an oil mass flow rate limited by the lower centrifugal pump. Increasing the immersion depth to 10 mm gives a positive static pressure value at the interface between lower centrifugal pump and helical groove according to Fig. 3.17c. The operating point of the entire pump lies below the intersection point of the entire and lower centrifugal pump curves and thus, the complete filling of the helical groove and the upper centrifugal pump are ensured. In this case, the oil mass flow rate of the entire pump can be calculated by the combined performance curves of the individual pumps. Due to the complete filling above of the lower centrifugal pump, a negative static pressure occurs in the interface between helical groove and upper centrifugal pump leading to outgasing of dissolved refrigerant.

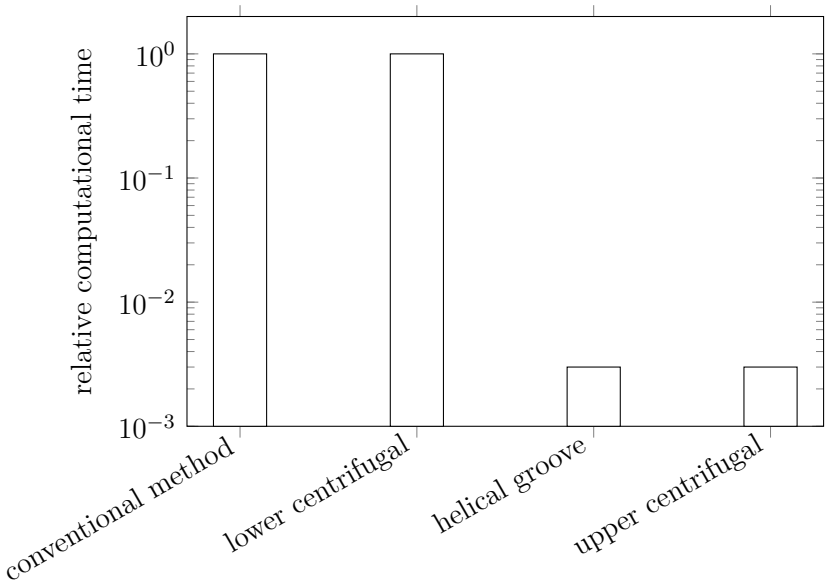

Fig. 3.16: Comparison of the computational time

The results of the split-up approach application on the modified oil pump can be seen in Fig. 3.18. Due to the pressure equalization hole, the pressure at the interface between helical groove and upper centrifugal pump is given by the ambient pressure, thus, the static pressure is zero. The investigation of the modified oil pump shows that in this configuration a limitation of the entire oil mass flow rate by the lower

centrifugal pump only occurs at 3 mm immersion depth. In case of 7mm and 10 mm immersion depth, the oil mass flow rate of the entire pump can be calculated by the split-up method and the combination of the individual pump performance curves.

Tab. 3.2 shows the results of the validation of the split-up approach and the conventional method with experimental data of the oil pump test rig. In addition to the validation of the proposed split-up method, the experimental data of the original and modified crankshaft can be used to interpret the made assumptions. As the experimental results show, the oil mass flow rates of the original geometry are higher than the measured rates of the modified crankshaft with the additional bore. One can conclude, that the theory of the three individual pumps influencing each other is confirmed. The upper centrifugal pump is able to build a significant pressure difference if it is filled with oil completely. Although the lower centrifugal pump may limit the oil mass flow rate of the entire pump at small immersion depths and thus, the upper centrifugal pump would have no impact on the pump behavior, higher oil mass flow rates of the oil pump without modifications occur. At this point, dynamic effects play a role. As high speed camera investigations of transparent oil pump parts, carried out at Secop Austria GmbH show, the upper centrifugal pump is filled with oil only for a short period of time until the oil flow breaks down and the helical groove and the upper centrifugal pump are filled up again. This short period of time is sufficient to increase the oil mass flow rate of the entire pump due to the significant influence of the upper centrifugal pump.
As the split-up method is used to determine the oil mass flow rate at steady-state conditions and the simulations of the individual pump parts are based on steady-state assumptions, dynamic effects as the breakdown and the following build up of the oil mass flow rate at small immersion depths are not modeled and thus, the conventional method of simulating the entire oil pump with CFD has its benefits. Comparing the simulated and experimental oil mass flow rates at immersion depths larger than 3 mm, the split-up method produces satisfying results with maximum deviation of 7 %.

Tab. 3.2: Results of the validation of the oil pump simulation ($\dot{m}$ in [g s^{-1}])

	split-up original			split-up modified			CFD		
h	exp	sim	dev	exp	sim	dev	exp	sim	dev
3 mm	0.827	0.746	10.9 %	0.670	0.746	10.2 %	0.827	0.880	6.00 %
7 mm	0.915	0.944	3.02 %	0.813	0.844	3.64 %	0.915	0.876	4.52 %
10 mm	1.031	1.109	7.07 %	0.837	0.863	2.96 %	1.031	0.899	14.6 %

To show the advantage of the split-up method, a comparison with the conventional method in terms of computational time is carried out. The several simulations are performed on the same workstation using one core per 100,000 cells. As mentioned

before, the advantage of the split-up method is the computational time reduction at the investigation of design changes. As the relative computational time in Fig. 3.16 shows, significant time reduction can be achieved if design changes are made at the helical groove or the upper centrifugal pump. The computational time can be decreased by the factor of 300 compared to the conventional method. Due to the time consuming VOF used in the calculation of the lower centrifugal pump, no significant time reduction can be observed.

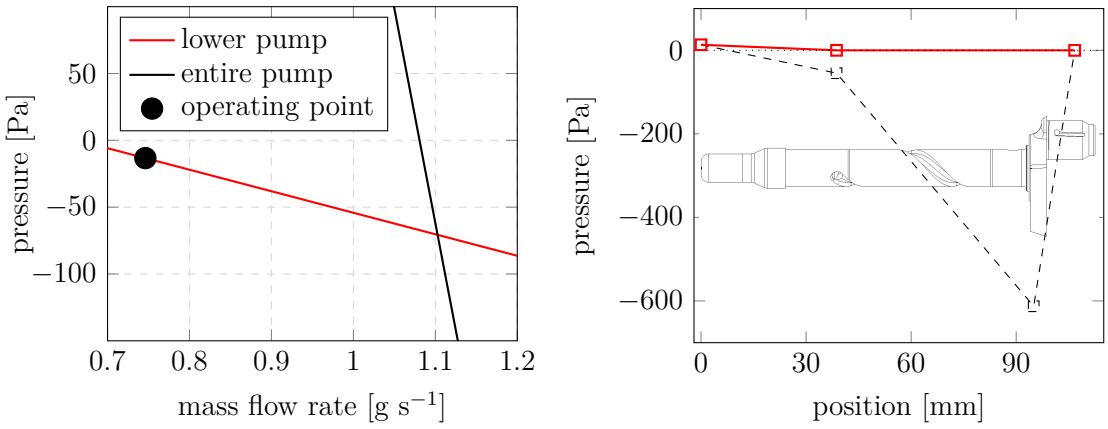

(a) 3 mm

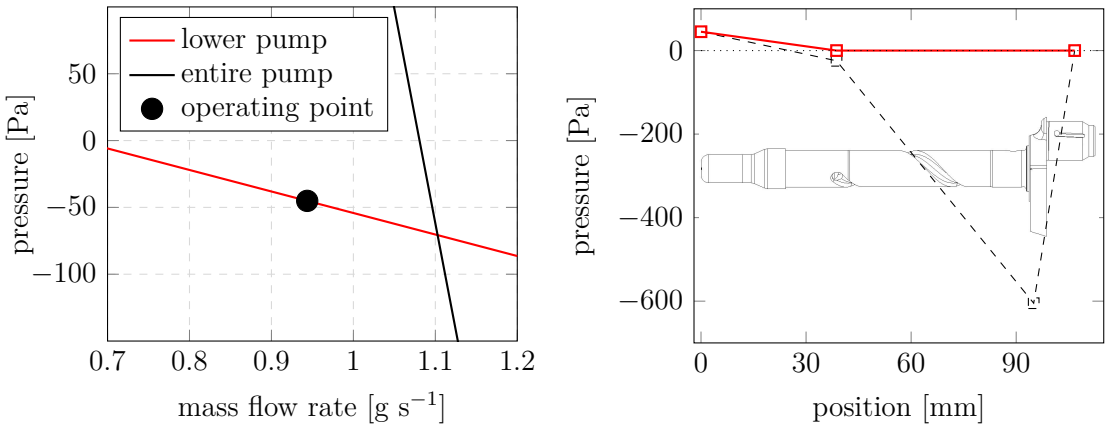

(b) 7 mm

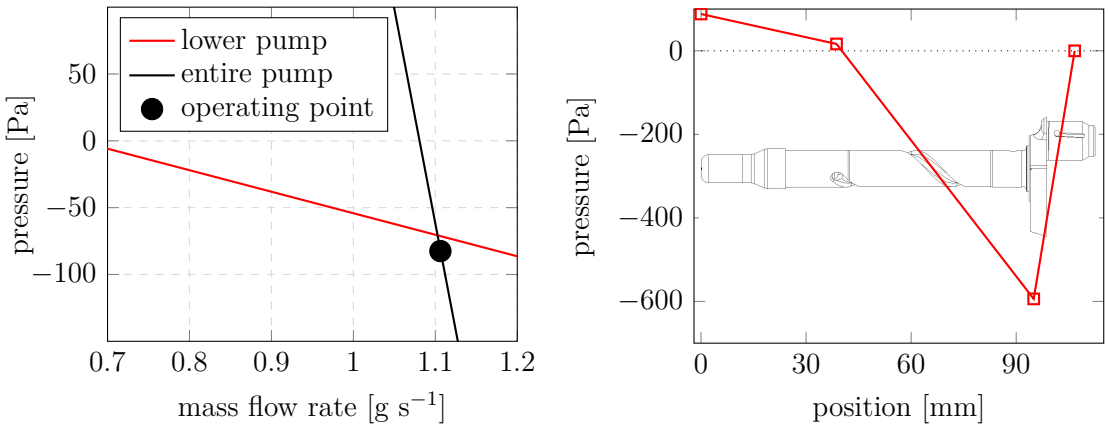

(c) 10 mm

Fig. 3.17: Application of the split-up method on the standard oil pump

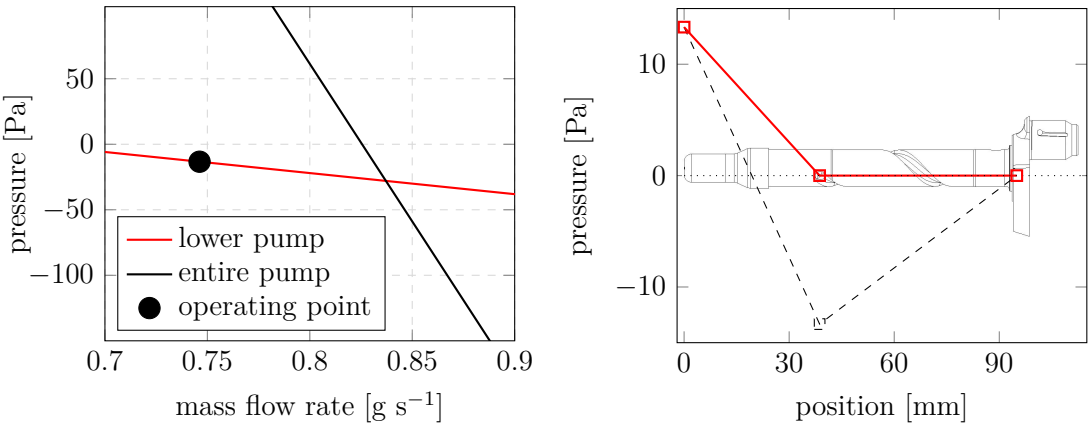

(a) 3 mm

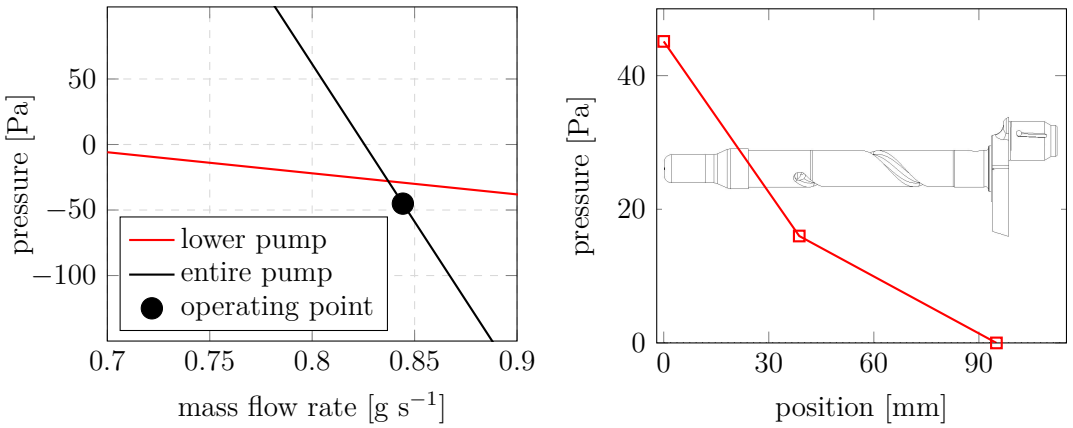

(b) 7 mm

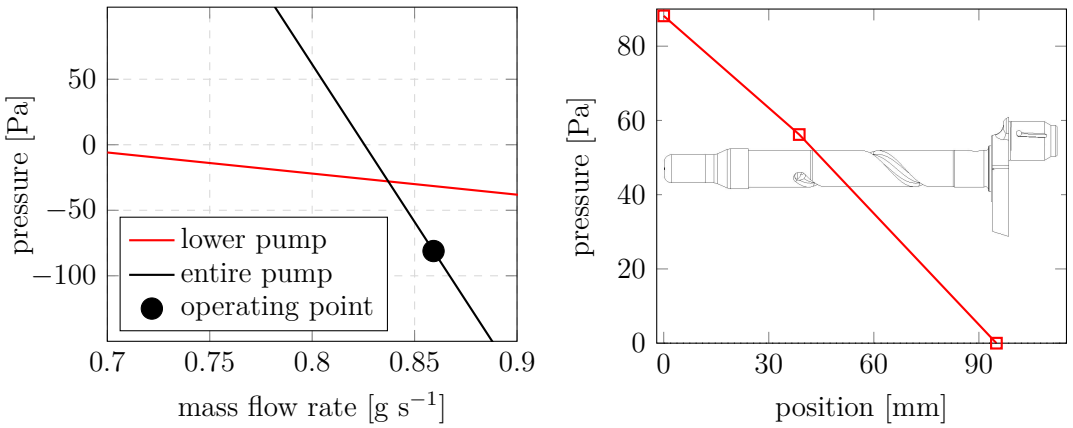

(c) 10 mm

Fig. 3.18: Application of the split-up method on the modified oil pump

4 Oil distribution

In order to investigate the oil influence on the behavior of a hermetic reciprocating compressor using numerical methods, the simulation of the oil distribution inside the compressor shell is indispensable. As already mentioned, in addition to the lubrication tasks of the moving compressor parts, the oil influences the thermal behavior of a compressor significantly by transporting heat from the hot compressor parts to the shell and further to the environment. To avoid uncertainties, caused by experimental works, the oil distribution and thus the heat transfer on the oil covered walls in the present thesis is determined by using numerical simulation. The modeling of the oil distribution and the heat transfer of the oil has been published in [PHB+17b]. In the following chapter, the procedure is shown in detail.

4.1 Literature review

Studies on the investigation of the oil distribution and its effects are quite rare and are restricted on experimental works. As an example, the work of [DD10] can be mentioned. The authors used heat flux sensors which were mounted on several positions inside the compressor. The disadvantages of these kinds of experiments are the complex feedthrough of the sensor wires through the hermetic compressor shell and especially the impact of the sensors on the measurements. Due to the different materials between compressor shell and heat flux sensor the heat flux is deflected and thus, the measured value can differ from the real value significantly. Numerical simulation of the oil distribution in hermetic compressors and its influence on the heat transfer has not been found in familiar literature sources.

4.2 Simulation model

Due to the lack of similar simulation tasks in open literature, a characterization of the expelled oil in terms of flow type has to be carried out to find an accurate simulation method. To characterize the flow type, a transparent compressor shell is used. By the use of a stroboscope the movement of the compressor crankshaft can be visualized as stationary image and thus, the oil flow type can be detected. Since the material of the transparent shell is acrylic glass, the compressor has to be operated at air with ambient pressure which is irrelevant for the desired outcome. The results of the strobe light

experiments can be seen in Fig. 4.1. In addition to find an accurate simulation method, the results of the strobe light experiments can be used to validate the simulation results qualitatively. As the images of the expelled oil show, the oil flow occurs as continuous jet. The appropriate method to model a continuous liquid jet in a gaseous environment is the VOF model which was already used for the two-phase flow simulation in the compressor oil pump (see chapter 3.3).

Fig. 4.1: Visualization of the oil flow

The oil distribution simulation domain covers the gas volume inside the compressor shell. To keep the number of cells in reasonable limits, regions which are covered by compressor parts (no oil is transported) are left out. The resulting mesh consists of approximately 700,000 mainly tetrahedral cells with hexahedral cells adjacent to the shell wall. Fig. 4.2 shows the computational mesh and its position inside the compressor shell.

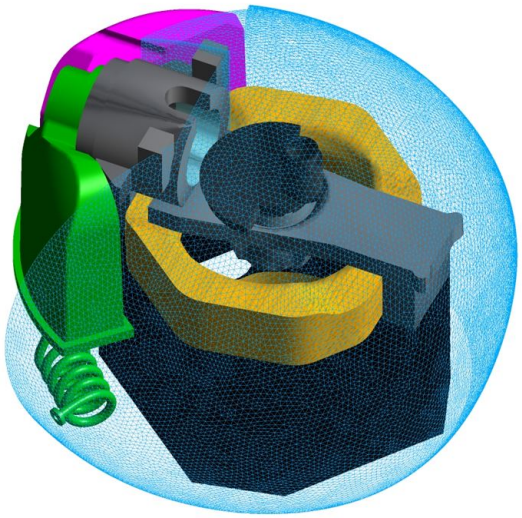

Fig. 4.2: Mesh of the oil distribution simulation

To increase the accuracy of the simulation, the movement of the gas inside the compressor shell is taken into account. The gas in the shell is driven by the rotational movement of the crankshaft and the rotor, and the translational movement of the piston. By using moving wall boundary conditions at the walls adjacent to the crankshaft applying rotational velocity according to the compressor speed, the rotational effect is considered. The translational movement of the piston is implemented via dynamic mesh technology (layering). Furthermore, the geometry of the crankshaft top end is modeled in detail and the oil flows into the domain via a velocity inlet boundary condition with constant oil density. The oil flow rate is used from the oil pump simulation results at an immersion depth of 7 mm according to chapter 3.4. A pressure outlet boundary condition enables the oil to flow out of the domain and simulates the interface between the shell gas and the oil sump. Fig. 4.3 illustrates the utilized boundary conditions for the oil distribution simulation.

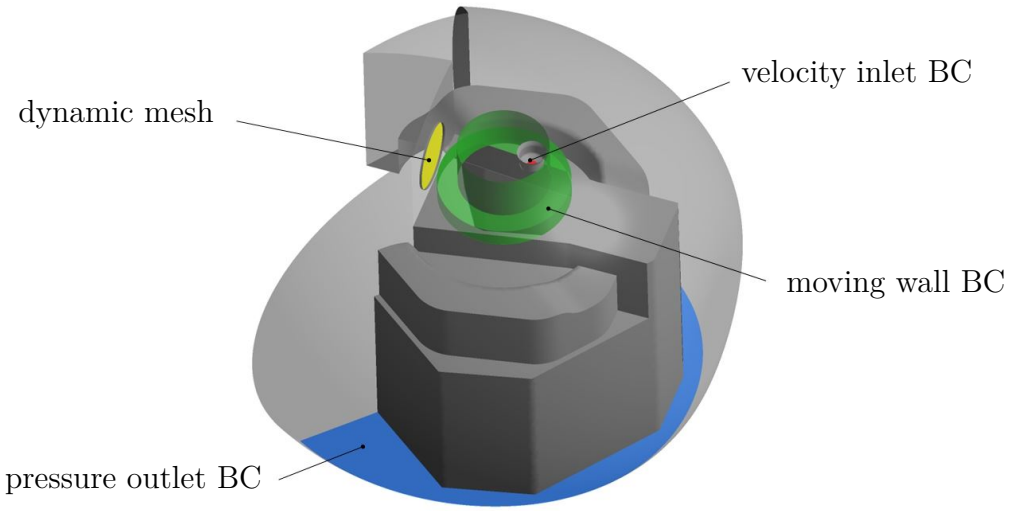

Fig. 4.3: Boundary conditions of the oil distribution simulation

Similar to the oil pump simulation, the simulation of the oil distribution is carried out in the commercial software ANSYS Fluent. Furthermore, similar assumptions and input data according to chapter 3 are used. The time step is set to 1e-4 s and is kept constant. By the use of implicit time formulation, the simulation is executed until steady-state conditions are reached which means that the oil flow rate at the pressure outlet boundary is constant.

4.3 Results

The results of the oil distribution simulation are analyzed in terms of oil jet, film thickness and resulting heat transfer coefficients on the compressor shell inner sur-

face. Regarding film thickness and heat transfer coefficient the results are evaluated at steady-state conditions which are achieved at 32 crankshaft revolutions.

4.3.1 Oil jet

The results of the oil distribution simulation in terms of oil jet behavior are visualized in Fig. 4.4. As the snapshots at different time steps show, the oil flows out of the upper centrifugal pump and hits the extended wall of the compressor crankshaft due to centrifugal force. Similar to the oil jet in the strobe light experiments the simulation shows the oil transport from the sharp edge of the crankshaft extended wall into the compressor interior. The dominant centrifugal forces result in an oil jet mainly in radial direction and thus, the upper area of the compressor shell is not moistened by the oil.

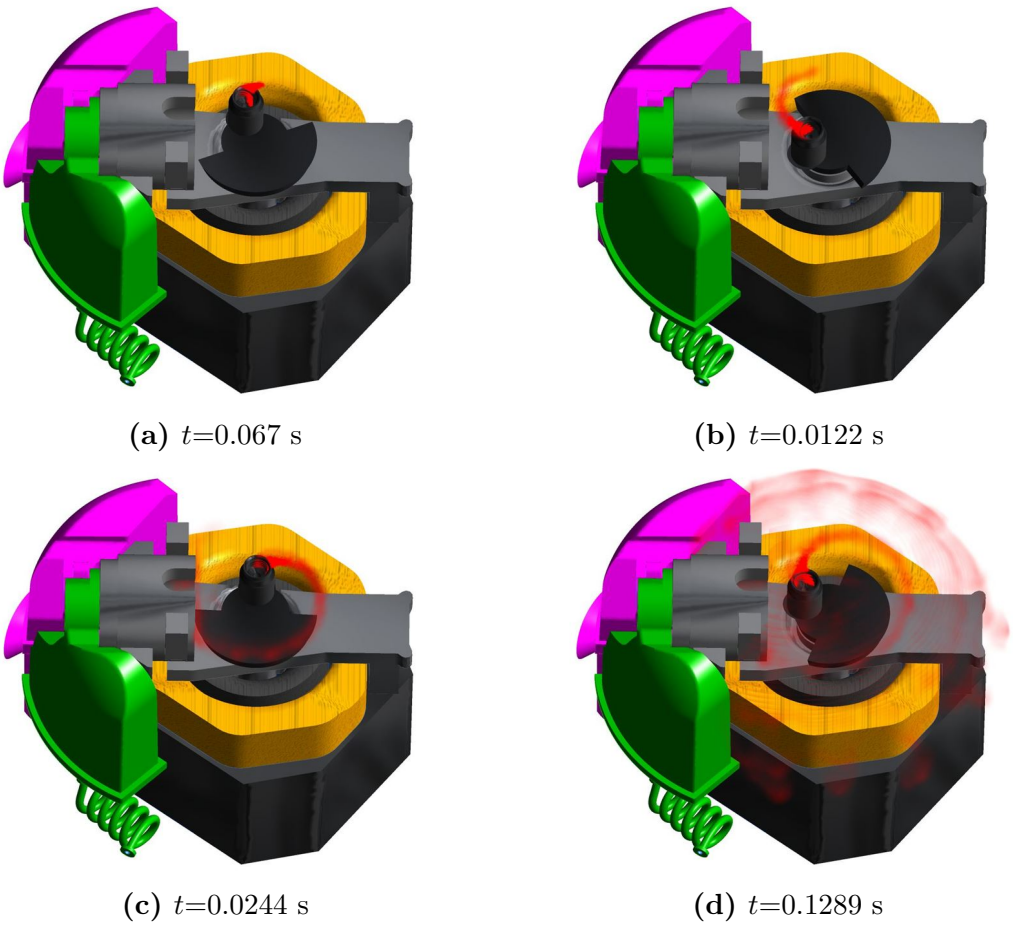

(a) t=0.067 s **(b)** t=0.0122 s

(c) t=0.0244 s **(d)** t=0.1289 s

Fig. 4.4: Oil distribution inside the compressor shell at several time steps

4.3.2 Oil film thickness

The oil distribution by the rotating crankshaft leads to a discontinuous oil film on the compressor shell which can also be observed in the strobe light experiments. In Fig. 4.5 the oil film thickness is visualized (to enable a proper overview only a characteristic area is shown) in terms of an iso-surface of the oil volume fraction (a) and the oil film thickness value (b). As the simulation results show, the oil film thickness is not constant along the fall film flow direction and also areas with significant oil film thicknesses can be detected. The mean oil film thickness of the oil covered shell walls is calculated using UDF and gives a value of 1.4 mm.

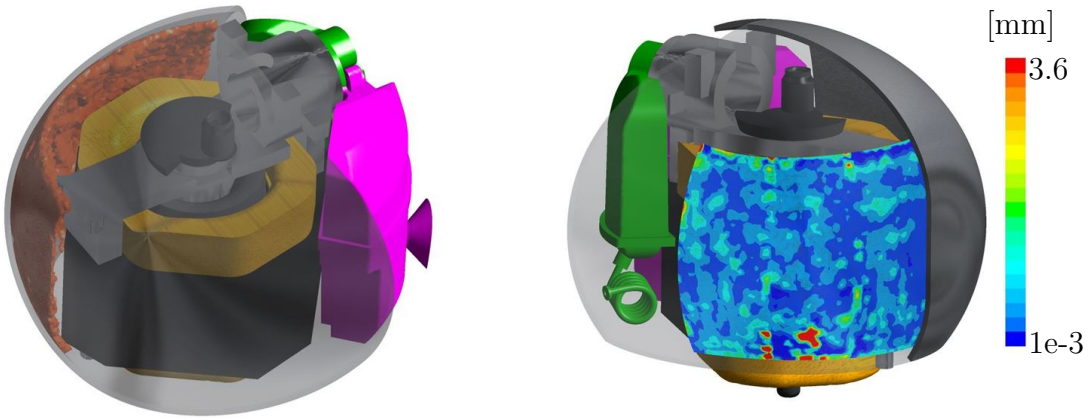

Fig. 4.5: Oil film (a) and oil film thickness (b)

4.3.3 Heat transfer

The major goal of the oil distribution simulation is the evaluation of the heat transfer coefficient due to the expelled oil to get reliable boundary values for the thermal compressor model. To keep the modeling effort of the oil distribution simulation in reasonable limits, the temperature of the compressor shell is kept constant. The calculation of the heat transfer coefficient is carried out via UDF by using the heat flux at the shell boundary cells and the temperature of the oil film. Results of the gained heat transfer coefficient values can be seen in Fig. 4.6(a). To enable the use of the oil distribution simulation results in the thermal model, the oil covered wall of the compressor shell is divided into 24 elements. The division of the area in circumferential direction is carried out with eight equidistant fields; in vertical direction the area is divided in three fields according to the area where the oil mainly hits the wall. In Fig. 4.6(b) the heat transfer coefficient values after the interpolation are shown.

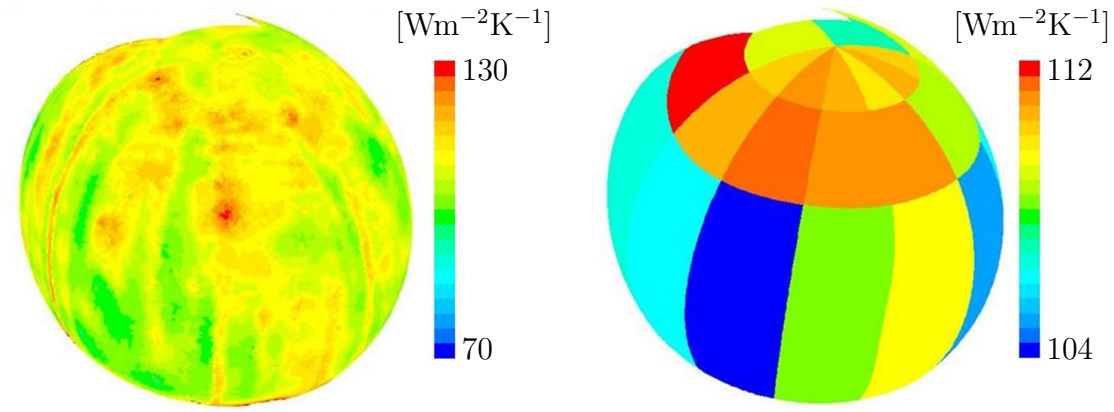

(a) **(b)**

Fig. 4.6: Heat transfer coefficient distribution on the inner surface of the compressor shell before (a) and after (b) the interpolation

5 Friction loss analysis

Investigating the oil influence on the thermodynamic behavior of a hermetic reciprocating compressor, the analysis of friction and friction caused losses is essential. Especially the hermetic design of the compressor yields in a significant influence of the friction induced heat and the temperature level of the entire compressor. Furthermore, friction losses, for example in the bearings or due to the relative movement between piston and cylinder, directly effect the compressor COP by reducing the available energy for the compression process. To analyze the friction losses in the previously mentioned joints, the equations presented in chapter 2.3 are applied. In the following chapter the investigation of compressor friction losses by the use of numerical methods is shown. To give an idea of the implementation of the required equations and the numerical algorithm for the solution process a self-written code is explained. The development of this code and the numerical issues are illustrated. It should give a deeper insight in the simulation of compressor crank mechanisms in terms of friction power losses and forms the base for the detailed analysis using the commercial software AVL EXCITE Power Unit. The use of the commercial software enables the holistic investigation of the friction behavior of the entire compressor and thus, the application of the software on the regarded compressor is shown.

5.1 Literature review

Due to the wide application field of friction loss analysis in mechanical engineering related tasks, the literature overview is concentrated on the field of hermetic reciprocating compressors. Published works mostly deal with the application of self-coded friction loss codes on the mechanical system of these compressors. A distinction of the studies can be made in terms of Reynolds equation modeling, investigated contact or model accuracy. Several studies address the use of simplified forms of the Reynolds equation like the short bearing approximation. In [KH04] the authors applied the short bearing approximation to the main journal bearings of a reciprocating compressor and compared the results with calculations using no simplification of the Reynolds equation. The authors stated that friction losses gained by short bearing approximation are less than the comparative case. Further examples of the short bearing approximation can be found in [KPC+12] or [CCP07]. To increase the accuracy of the Reynolds equation based bearing simulation, models have been developed which take into account oil refrigerant mixture (e.g. [GPP05]), shaft inclination (e.g. [MKI10]) or Elastohydrodynamic Lu-

brication (EHL) (e.g. [DD06]). In addition to the investigation of compressor journal bearings, the contact between piston and liner is of major interest. The calculation of the secondary piston movement by the use of the solution of the Reynolds equation is used to determine friction losses and gas leakage through the radial clearance. Studies dealing with this topic can be found in e.g. [PFF00] or [RPSO09].

5.2 Compressor friction loss code

Although commercial software for the analysis of the friction behavior of engine or compressor crank mechanism are available, the development of self-written simulation tools by mechanical engineers is sometimes necessary. Reasons are the high costs of commercial software and their insufficient applicability to the regarded problem. Furthermore, the level of detail which is provided by commercial codes is often not necessary. As an example, the compressor crank mechanism investigation can be mentioned. If the results are used for the rough comparison of several parameters or as an input for an overall thermal model, a self-written code is usually sufficient; but if the results should build the base for the compressor design, very detailed simulations are necessary and thus, a commercial software package is useful.
The following subchapter should give an overview over the development of a self-written code for friction loss analysis. Starting with the multi-body system and the formulation of its system of equations, the numerical treatment of the Reynolds equation using the Finite Volume Method (FVM) is described. Finally, results gained with the code are presented. An overview over the development and application of the code has been published in [PHH+16a].

5.2.1 Multi-body system

To determine the kinematics and thus the dynamic forces of a compressor crank mechanism, a multi-body system is set up. The system consists of the crank mechanism parts crankshaft, conrod and piston. Fig. 5.1 shows the coordinate system used for the kinematic description. The kinematic formulation of the crankshaft includes its misalignment due to the bearing eccentricity as well as the misalignment of the piston with respect to the initial coordinate system. Using the Newton-Euler formulation the equations of motion for each part can be expressed as follows:

Piston:

$$m_{\mathrm{Pi}} \cdot {}_{\mathrm{I}}\mathbf{a}_{\mathrm{Pi}} = {}_{\mathrm{I}}\mathbf{F}_p - {}_{\mathrm{I}}\mathbf{F}_4 + {}_{\mathrm{I}}\mathbf{F}_{\mathrm{Cyl}} \tag{5.1}$$

Connecting rod:

$$m_{\mathrm{Cr}} \cdot {}_{\mathrm{I}}\mathbf{a}_{\mathrm{Cr}} = {}_{\mathrm{I}}\mathbf{F}_4 - {}_{\mathrm{I}}\mathbf{F}_3 \tag{5.2}$$

$$ {}_{\mathrm{I}}\Theta_{\mathrm{Cr}} \cdot \dot{\omega}_{\mathrm{Cr}} + m_{\mathrm{Cr}} \cdot {}_{\mathrm{I}}\mathbf{r}_{3-\mathrm{Cr}} \times {}_{\mathrm{I}}\mathbf{a}_{\mathrm{Cr}} = {}_{\mathrm{I}}\mathbf{r}_{3-\mathrm{Cr}} \times {}_{\mathrm{I}}\mathbf{F}_4 \tag{5.3} $$

Crankshaft:

$$ m_{\mathrm{Cs}} \cdot {}_{\mathrm{I}}\mathbf{a}_{\mathrm{Cs}} = {}_{\mathrm{I}}\mathbf{F}_1 + {}_{\mathrm{I}}\mathbf{F}_2 + {}_{\mathrm{I}}\mathbf{F}_3 \tag{5.4} $$

$$ {}_{\mathrm{I}}\Theta_{\mathrm{Cs}} \cdot \dot{\omega}_{\mathrm{Cs}} + \omega_{Cs} \times ({}_{\mathrm{I}}\Theta_{\mathrm{Cs}} \cdot \omega_{Cs}) + m_{\mathrm{Cs}} \cdot {}_{\mathrm{I}}\mathbf{r}_{1-\mathrm{Cs}} \times {}_{\mathrm{I}}\mathbf{a}_{\mathrm{Cs}} = {}_{\mathrm{I}}\mathbf{r}_{1-\mathrm{Cs}} \times {}_{\mathrm{I}}\mathbf{F}_1 + {}_{\mathrm{I}}\mathbf{r}_{1-3} \times {}_{\mathrm{I}}\mathbf{F}_3 + \mathbf{T} \tag{5.5} $$

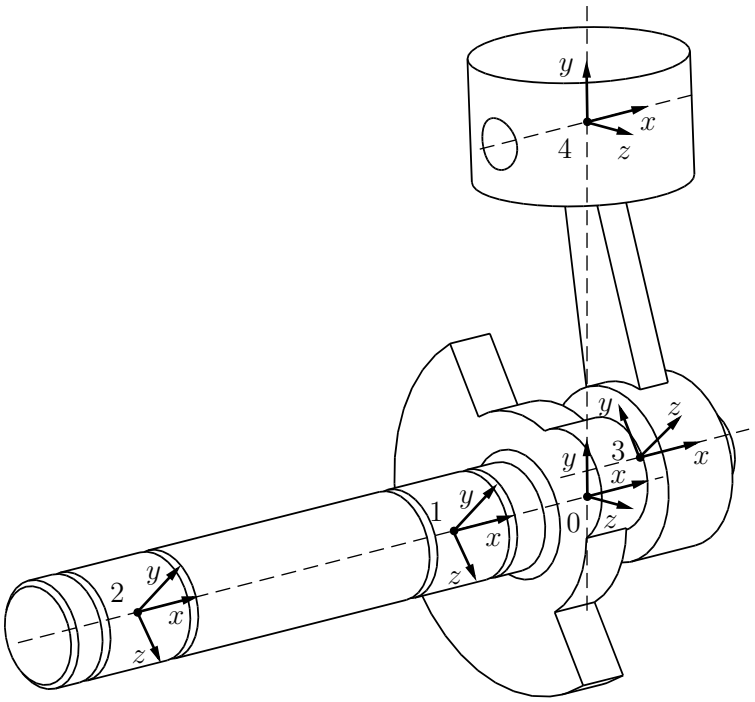

Fig. 5.1: Compressor crank drive with coordinate systems

In addition to the geometric and mass properties of the parts the time dependent pressure in the compressor cylinder has to be set as input data for the calculation of the joint forces. The cylinder pressure can be determined by experiments or CFD, respectively. For the present thesis the cylinder pressure is given by CFD simulation data. The simulations were carried out by the research group according the approach presented in [Hopss]. The data was gained by a holistic CFD simulation of the compressor gas path including the refrigerant flow in the mufflers and in the cylinder. Special focus was laid on the interaction between the gas flow and the flapper valve motion by using Fluid Structure Interaction (FSI). Fig. 5.2 illustrates the indicator diagram gained by

CFD simulation for -23.3/45 ASHRAE test conditions(R600a). The force vector due to the pressure in the cylinder regarding the initial coordinate system is then given by

$$ {}_{\mathrm{I}}\mathbf{F}_p = \begin{pmatrix} 0 \\ -p_{\mathrm{CFD}} \cdot A \\ 0 \end{pmatrix} $$

The kinematics of the compressor crank mechanism are calculated in symbolic formulation in the commercial software Wolfram Mathematica. Additionally to the several joint forces, the angular and radial displacement of the piston were set as unknown to solve the system of equations. To use the symbolic expressions in the numerical simulation of the joints, they have to be transferred into the commercial software Matlab which is used for the development of the friction loss code. The transferred symbolic expressions are embedded via a function in the code. Fig. 5.3 to Fig. 5.7 show results of the multi-body system. The forces are calculated using the Matlab input function setting the particular deflections of the crankshaft and piston to zero.

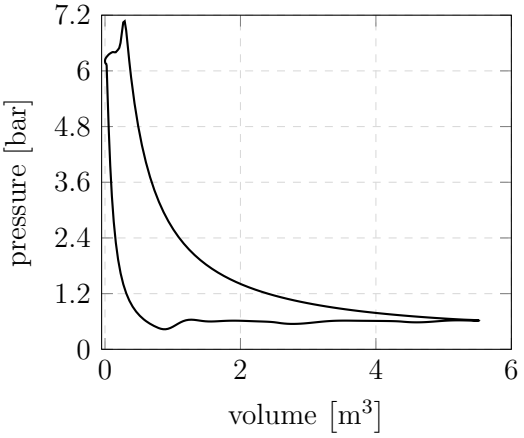

Fig. 5.2: Cylinder pressure from CFD results

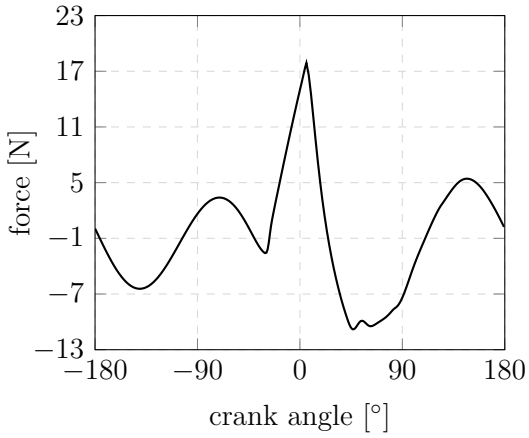

Fig. 5.3: Reaction forces at the cylinder liner

5.2.2 Numerical treatment of the Reynolds equation

In chapter 2.3 the fundamental equation of the lubrication theory, the Reynolds equation (Eq. 2.21) was presented. The Reynolds equation and its derivatives like the averaged Reynolds equation (Eq. 2.23) are partial differential equations. Therefore, analytical solutions are only available for restricted cases. To solve the Reynolds equation in general, numerical methods have to be used. The goal of the numerical treatment of this kind of equation is to transform the partial differential equation into an algebraic form by applying discretization techniques getting a system of linear equations

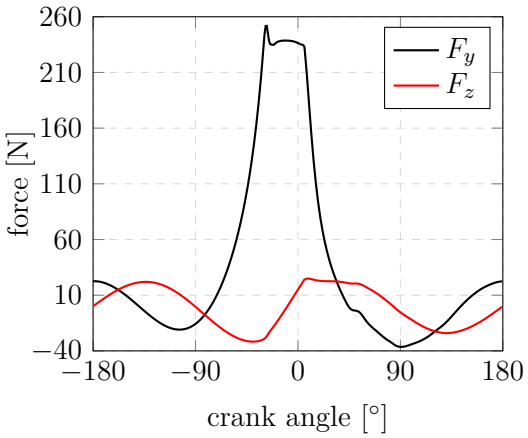

Fig. 5.4: Reaction forces at the conrod big end

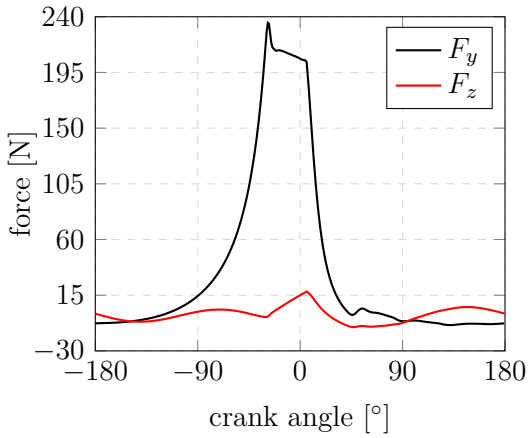

Fig. 5.5: Reaction forces at the conrod small end

which can be solved by numerical methods. Discretization techniques are the Finite Element Method (FEM), the Finite Volume Method (FVM) and the Finite Difference Method (FDM). The following numerical treatment of the Reynolds equation is based on the FVM. Therefore, the simulation domain is divided into a finite number of control volumes (Fig. 5.8). The FVM is based on the balancing of volume flows across the control volume. According to the well-known indexing of the regarded cell and its neighbors (P, N, S, E, W) by using FVM in CFD, the discretization of the Reynolds equation is carried out. To keep the discretization process clear, the single terms of the Reynolds equation are treated separately.

Poiseuille flow

To discretize the pressure flow also known as Poiseuille flow, the central differencing scheme is utilized. Integrating over the control volume boundaries the following formulations can be written

$$\iint_{\mathrm{Bo}} \frac{\partial}{\partial x}\left(\frac{h^3}{12\mu}\frac{\partial p}{\partial x}\right)\mathrm{d}x\mathrm{d}y = \left(\left(\frac{h^3}{12\mu}\frac{\partial p}{\partial x}\right)_{\mathrm{e}} - \left(\frac{h^3}{12\mu}\frac{\partial p}{\partial x}\right)_{\mathrm{w}}\right)\Delta y \tag{5.6}$$

$$\iint_{\mathrm{Bo}} \frac{\partial}{\partial y}\left(\frac{h^3}{12\mu}\frac{\partial p}{\partial y}\right)\mathrm{d}x\mathrm{d}y = \left(\left(\frac{h^3}{12\mu}\frac{\partial p}{\partial y}\right)_{\mathrm{n}} - \left(\frac{h^3}{12\mu}\frac{\partial p}{\partial y}\right)_{\mathrm{s}}\right)\Delta x \tag{5.7}$$

Interpolating the values of p at the boundaries of the control volume gives

$$\left(\left(\frac{h^3}{12\mu}\frac{\partial p}{\partial x}\right)_{\mathrm{e}} - \left(\frac{h^3}{12\mu}\frac{\partial p}{\partial x}\right)_{\mathrm{w}}\right)\Delta y = \left(\left(\frac{h_{\mathrm{e}}^3}{12\mu}\frac{p_{\mathrm{E}}-p_{\mathrm{P}}}{\Delta x}\right) - \left(\frac{h_{\mathrm{w}}^3}{12\mu}\frac{p_{\mathrm{P}}-p_{\mathrm{W}}}{\Delta x}\right)\right)\Delta y \tag{5.8}$$

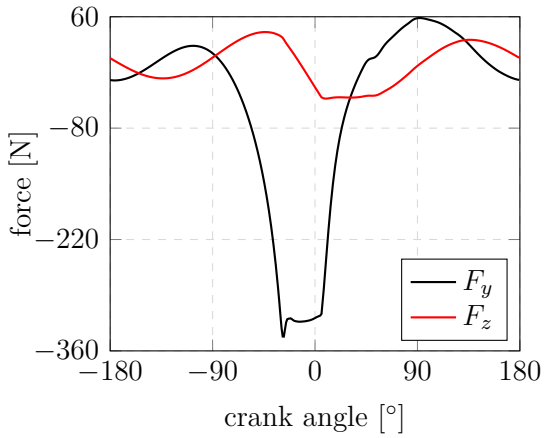

Fig. 5.6: Reaction forces at the crankshaft journal bearing 1

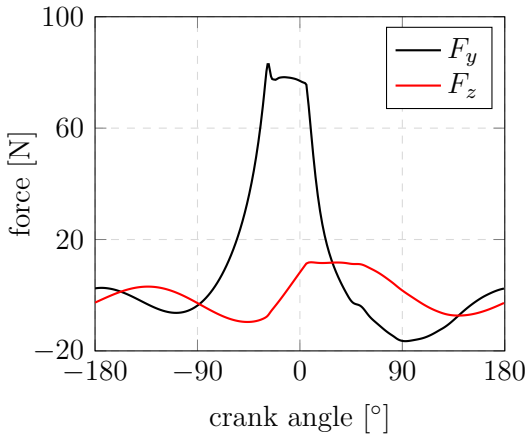

Fig. 5.7: Reaction forces at the crankshaft journal bearing 2

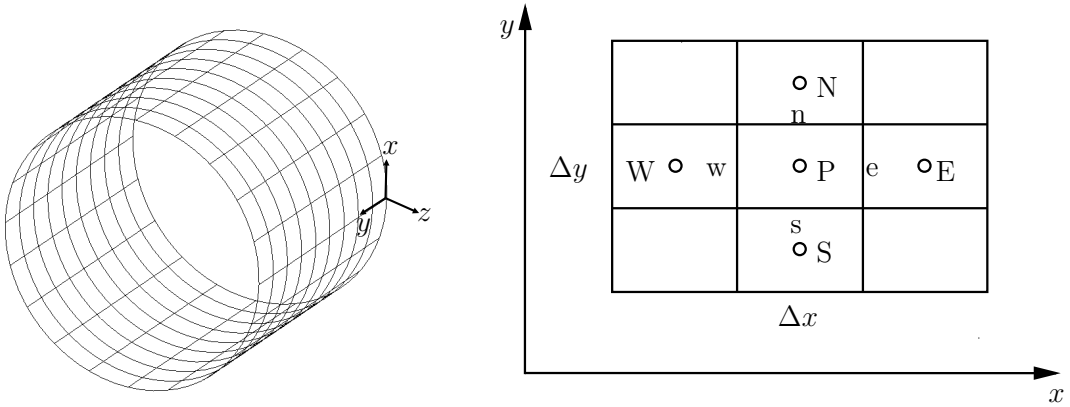

Fig. 5.8: Discretization of the simulation domain

$$\left(\left(\frac{h^3}{12\mu}\frac{\partial p}{\partial y}\right)_{\mathrm{n}} - \left(\frac{h^3}{12\mu}\frac{\partial p}{\partial y}\right)_{\mathrm{s}}\right)\Delta x = \left(\left(\frac{h_{\mathrm{n}}^3}{12\mu}\frac{p_{\mathrm{N}}-p_{\mathrm{P}}}{\Delta y}\right) - \left(\frac{h_{\mathrm{s}}^3}{12\mu}\frac{p_{\mathrm{P}}-p_{\mathrm{S}}}{\Delta y}\right)\right)\Delta x \tag{5.9}$$

The final form of the discretized Poiseuille flow can be written as

$$\begin{aligned}\iint_{\mathrm{Bo}} \frac{\partial}{\partial x}\left(\frac{h^3}{12\mu}\frac{\partial p}{\partial x}\right)\mathrm{d}x\mathrm{d}y + \iint_{\mathrm{Bo}} \frac{\partial}{\partial y}\left(\frac{h^3}{12\mu}\frac{\partial p}{\partial y}\right)\mathrm{d}x\mathrm{d}y = \\ A_{\mathrm{P}}p_{\mathrm{P}} + A_{\mathrm{W}}p_{\mathrm{W}} + A_{\mathrm{E}}p_{\mathrm{E}} + A_{\mathrm{N}}p_{\mathrm{N}} + A_{\mathrm{S}}p_{\mathrm{S}}\end{aligned} \tag{5.10}$$

The appropriate coefficients are

$$
\begin{aligned}
A_{\mathrm{W}} &= \frac{\left(\frac{1}{2}\left(h_{\mathrm{W}}+h_{\mathrm{P}}\right)\right)^{3}}{12\mu}\frac{\Delta y}{\Delta x} \quad A_{\mathrm{E}} = \frac{\left(\frac{1}{2}\left(h_{\mathrm{E}}+h_{\mathrm{P}}\right)\right)^{3}}{12\mu}\frac{\Delta y}{\Delta x} \\
A_{\mathrm{N}} &= \frac{\left(\frac{1}{2}\left(h_{\mathrm{N}}+h_{\mathrm{P}}\right)\right)^{3}}{12\mu}\frac{\Delta x}{\Delta y} \quad A_{\mathrm{S}} = \frac{\left(\frac{1}{2}\left(h_{\mathrm{S}}+h_{\mathrm{P}}\right)\right)^{3}}{12\mu}\frac{\Delta x}{\Delta y} \\
A_{\mathrm{P}} &= -\left(A_{\mathrm{W}}+A_{\mathrm{E}}+A_{\mathrm{N}}+A_{\mathrm{S}}\right)
\end{aligned}
\tag{5.11}
$$

Couette flow

The treatment of the Reynolds equation shear flow term differs from the Poiseuille flow treatment according the applied discretization method. To avoid oscillations in the solution in transition between converging and diverging gap, a first order upwind method is used. By introducing the mean circumferential speed u_{m} two cases can be distinguished: $u_{\mathrm{m}} > 0$ and $u_{\mathrm{m}} < 0$. Assuming the case $u_{\mathrm{m}} > 0$, the approximation of the values at the boundaries e and w can be carried out using the values in the control volumes P and W. The discretization of the Couette flow is then given by

$$
\begin{aligned}
\iint_{\mathrm{Bo}} u_{\mathrm{m}}\frac{\partial h}{\partial x}\mathrm{d}x\mathrm{d}y &= u_{\mathrm{m}}\left(h_{\mathrm{e}}-h_{\mathrm{w}}\right)\Delta y \\
&= u_{\mathrm{m}}\left(\frac{h_{\mathrm{E}}+h_{\mathrm{P}}}{2}-\frac{h_{\mathrm{P}}+h_{\mathrm{W}}}{2}\right)\Delta y \\
&= u_{\mathrm{m}}\left(\frac{h_{\mathrm{E}}-h_{\mathrm{W}}}{2}\right)\Delta y
\end{aligned}
\tag{5.12}
$$

Displacement flow

The time-dependent term of the Reynolds equation describes the damping influence of the lubricant due to the deviation of the fluid film thickness. To discretize the displacement flow term the forward Euler scheme is applied.

$$
\iint_{\mathrm{Bo}} \frac{\partial h}{\partial t}\mathrm{d}x\mathrm{d}y = \frac{h_{\mathrm{P}}^{n+1}-h_{\mathrm{P}}^{n}}{\Delta t}\Delta x\Delta y \tag{5.13}
$$

The presented discretization procedure can also be applied on the modified Reynolds equation (Eq. 2.23) by additional discretization of the several flow factors similar to the fluid film thickness h.

5.2.3 Gap kinematics

To link the general Reynolds equation to the regarded bearing geometry and the multibody system, the geometric properties of the fluid film have to be characterized. The presented compressor friction loss code is based on rigid body dynamics, so deformations of the crank drive bodies is not considered. To reduce the computational effort for the calculation of the friction losses between piston and liner, only the piston skirt surfaces according to Fig. 5.9 are taken into account.
Concerning the main journal bearings of the compressor crankshaft, the fluid film can be expressed as shown in Fig. 5.10 by assuming a parallel gap. The radial displacement of the crankshaft yields to an eccentric fluid film function along the circumferential direction [Wos13].

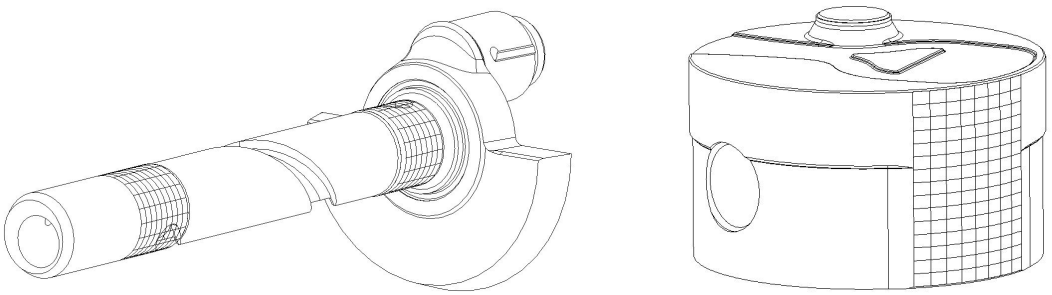

Fig. 5.9: Bearing and piston meshes

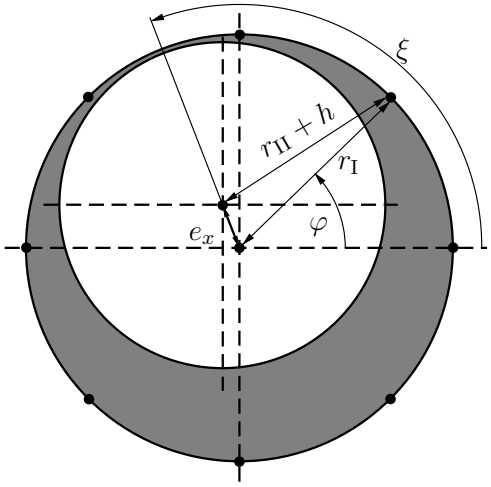

Fig. 5.10: Determination of the bearing fluid film thickness

Using the cosine theorem, the following expression according to Fig. 5.10 is given

$$(r_{II} + h)^2 = {r_I}^2 + e_x^2 - 2\, r_I\, e_x\, \cos(\varphi - \xi) \tag{5.14}$$

Transforming the equation gives the fluid film function depending on φ

$$h(\varphi) = -r_{\mathrm{II}} + \sqrt{[r_{\mathrm{I}} - e_x \cos(\varphi - \xi)]^2 + e_x^2 \sin^2(\varphi - \xi)} \tag{5.15}$$

Using the simplification $\frac{e_x}{r_{\mathrm{I}}} << 1$, the fluid film function can be expressed as

$$h(\varphi) = \Delta r - e_x \cos(\varphi - \xi) \tag{5.16}$$

Similar geometric considerations have to be made for the gap between piston and liner. The movement of the piston is assumed to occur only in radial direction normal to the piston pin axis and angular movement, respectively. Fig. 5.11 shows the geometric properties of the fluid film between piston and liner.

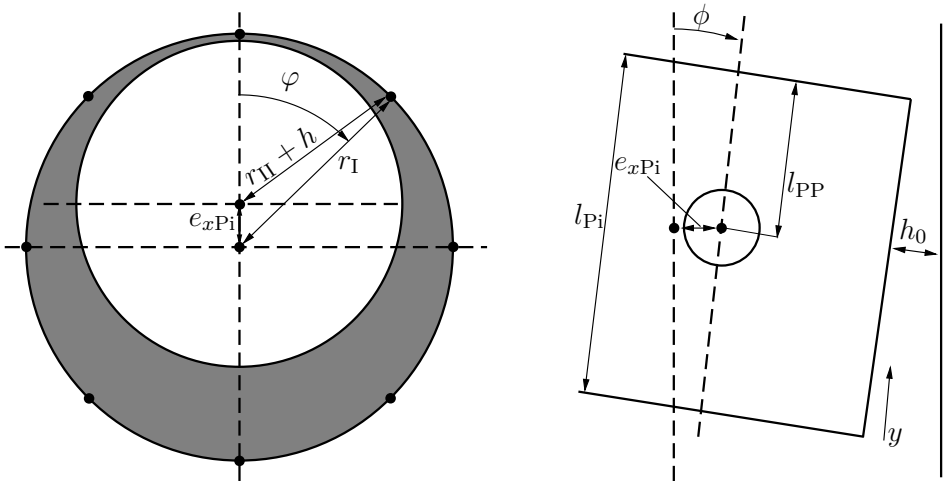

Fig. 5.11: Determination of the piston fluid film thickness

Applying the similar approach as for the bearing fluid film function, the fluid film function of the gap between the piston and the liner is given by

$$h_0 = \Delta r - \frac{e_x}{cos(\phi)} cos(\varphi) \tag{5.17}$$

$$h(y) = h_0 + (l_{\mathrm{Pi}} - l_{\mathrm{PP}} - y)\, tan(\phi) \tag{5.18}$$

The formulations have to be adapted to the mesh on the opposite site of the piston skirt.

5.2.4 Solution algorithm

The computational algorithm to solve the friction losses in the main journal bearings and in the contact between piston and liner starts with the input of the geometric data of the crank mechanism parts. Initial values of the unknown bearing parameters

eccentricity e_x and fluid film thickness angle ξ and the unknown piston parameters offset $e_{x\mathrm{Pi}}$ and tilting angle ϕ are set to zero. Using a constant time step or rather crank angle of two degree, the cylinder pressure gained by CFD simulation is read into the program. For the current time step the bearing and piston forces can be calculated by solving the multi-body dynamics system. The next step is the calculation of the hydrodynamic bearing forces starting with the determination of the fluid film functions according to Eq. 5.16 and Eq. 5.18 with the defined start values of the new time step. The start values are the unknown bearing and piston parameters of the previous time step or the initial values if it is the first time step. To get the unknown fluid film parameters of the regarded joints, a multi-dimensional Newton-algorithm according to Eq. 5.19 is used.

$$\begin{aligned} \mathbf{x} &= \left(e_{x1} \quad \xi_1 \quad e_{x2} \quad \xi_2 \quad e_{x\mathrm{Pi}} \quad \phi\right)^T \\ \mathbf{f}\left(\mathbf{x}\right) &= \mathbf{F}_{\mathrm{MBS}} - \mathbf{F}_{\mathrm{Rey}} \\ \mathbf{x}_{n+1} &= \mathbf{x}_n \left(\mathbf{J}_f\left(\mathbf{x}_n\right)\right)^{-1} \mathbf{f}\left(\mathbf{x}_n\right) \end{aligned} \tag{5.19}$$

The averaged Reynolds equation is solved numerically for each joint and the calculated bearing forces are compared with the results of the multi-body system regarding absolute value and force direction. If the resulting deviations are higher than the convergence criterion β_{F}, the iteration procedure is repeated; otherwise the algorithm proceeds to the next time step. Steady-state conditions are reached and the simulation is finished, if the deviation of the calculated values between the current and the previous cycle are under the convergence criterion β_{C}.

Tab. 5.1: Geometry data and oil viscosity for the code test

shaft diameter	10.5 mm
bearing width	6 mm
journal clearance	5 μm
oil viscosity	6.7e-3 Pa s

5.2.5 Code testing

The correct implementation of the previous shown formulations concerning multi-body system, discretization of the Reynolds equation, kinematics and the solution algorithm are tested by the example of a beam on two supports with a central acting force (Fig. 5.13).

Due to the symmetric distribution of the force on the two supports, only one joint has to be calculated. The test is carried out for a constant static force and the combination between a constant static force and a rotary unbalance. To validate the code, the shaft

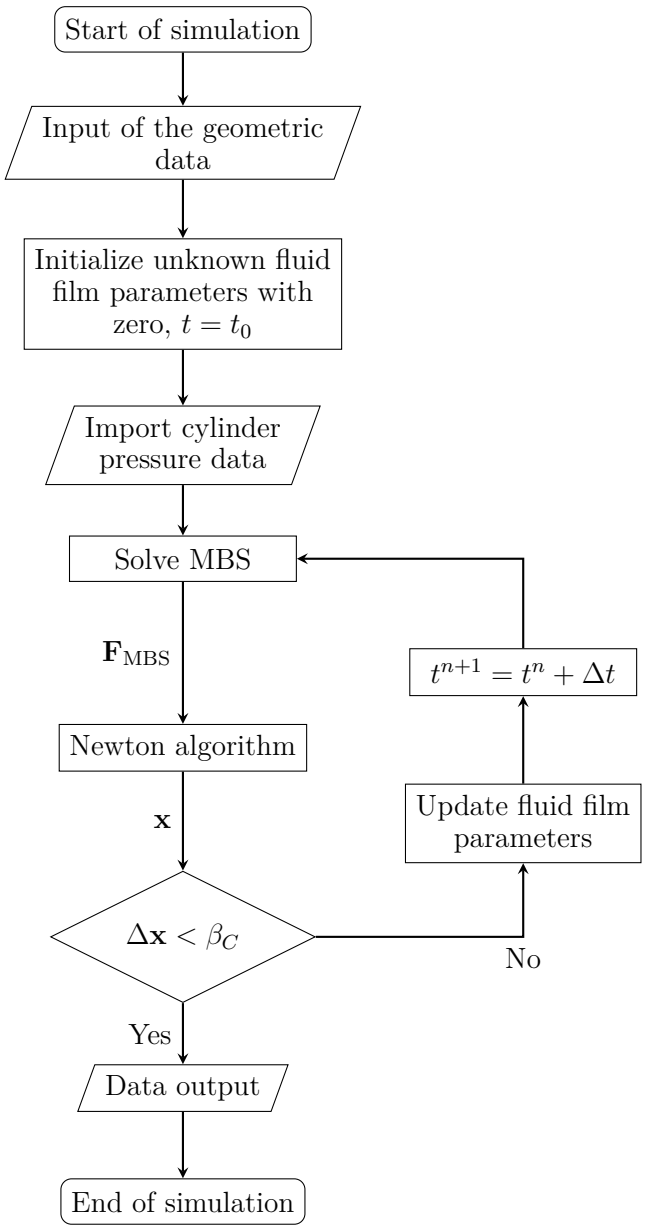

Fig. 5.12: Flow chart of the solution algorithm

trajectories for the static and dynamic loaded short bearing according [GNP05] should be reproduced. The input parameters for the code test are given in Tab. 5.1.

The simulation of the static loaded bearing is carried out by varying the force and the rotational speed, respectively. Fig. 5.14 and Fig. 5.15 show the eccentricity of the shaft under several force loads and rotational speeds. The shaft is initialized at zero eccentricity and the simulation is carried out until the movement of the shaft reaches steady-state conditions (four revolutions). Connecting the steady-state shaft positions

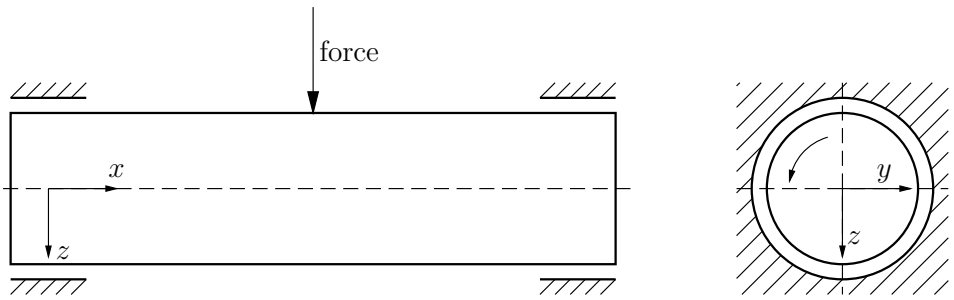

Fig. 5.13: Test case for the code validation

results in the static eccentricity curve of the regarded bearing. Increasing the force load has the same influence on the position of the shaft as decreasing the rotational speed yielding in higher eccentricity. The theoretical eccentricity curve of the regarded journal bearing describes a half circle from the bearing center to the maximum displacement in force direction depending on the force amplitude or rotational speed. Due to the small number of calculations, the eccentricity curves in Fig. 5.14 and Fig. 5.15 do not have a perfect circular shape but they are qualitative identical to the theoretical curve. The relationship between the Sommerfeld number and the relative eccentricity of the bearing can be seen in Fig. 5.16. In the considered test case the geometric parameters and the oil viscosity are fixed values and the Sommerfeld number depends only on the bearing force and the angular velocity (Eq. 2.22).

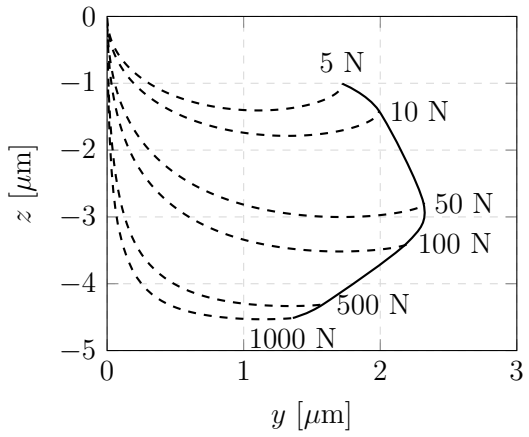

Fig. 5.14: Static eccentricity by force variation (n =1000 rpm)

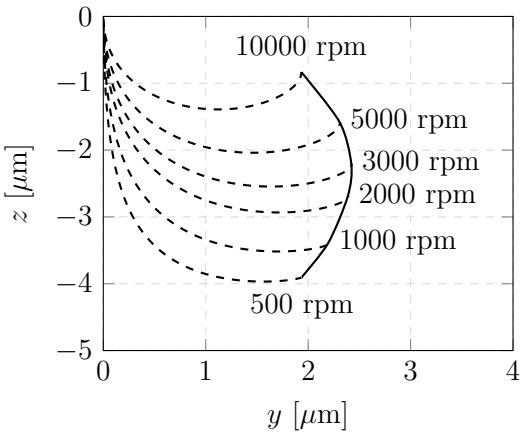

Fig. 5.15: Static eccentricity by speed variation (F =100 N)

To test the simulation of the journal bearing under dynamic load, a rotary unbalance is applied in addition to the static load. Fig. 5.17 shows the superposition of the static eccentricity and the trajectory due to the dynamic force. For $F = 0$ the shaft moves along a circular path around the center. Increasing the static load, the dynamic

trajectory moves along the eccentricity curve due to the static load. As the bearing is getting more and more rigid at higher eccentricities, the dynamic movement of the shaft decreases.
The test of the friction loss code gives similar results as shown in [GNP05]. Therefore, the ability to use the code for the investigation of the mechanical compressor losses is fundamentally proven.

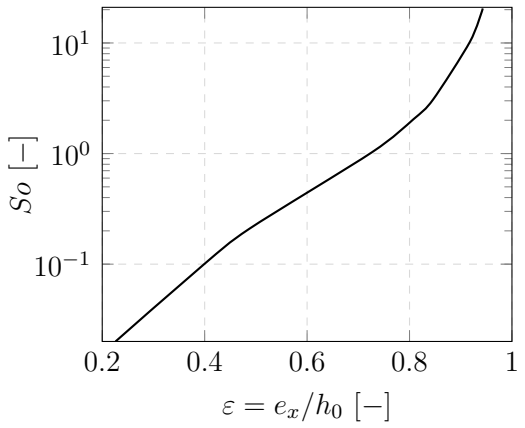

Fig. 5.16: *So*-relative eccentricity relationship

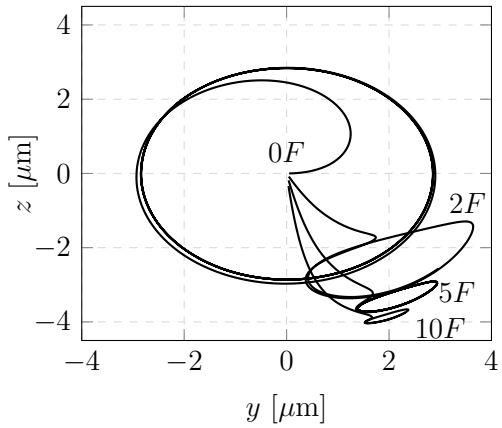

Fig. 5.17: Static eccentricity and dynamic trajectory

5.2.6 Results

The application of the friction loss code on the HXD55 compressor is carried out at a rotational speed of 3000 rpm assuming oil viscosity of 2.64e-3 Pa s at the journal bearings, 2.652e-3 Pa s at the conrod big end and 2.2e-3 Pa s at the piston-liner contact. Input data for geometric values, masses and moments of inertia are gained by Computer Aided Design (CAD) data. Steady-state conditions are reached after eight cycles for the journal bearing calculation and 35 cycles for the piston-liner contact calculation.
Fig. 5.18 and Fig. 5.19 show the piston secondary motion and the journal bearing orbital paths as examples for the results gained by the friction loss code.

The distribution of the mechanical losses can be seen in Fig. 5.20. As expected, the piston-liner contact is responsible for the major part of the losses. Furthermore, the losses in journal bearing 1 are higher than in bearing 2 due to the higher reaction forces.

5.3 AVL EXCITE Power Unit

In addition to the determination of the friction losses by the use of the self-coded friction loss code, the possibility of applying a commercial software should be mentioned

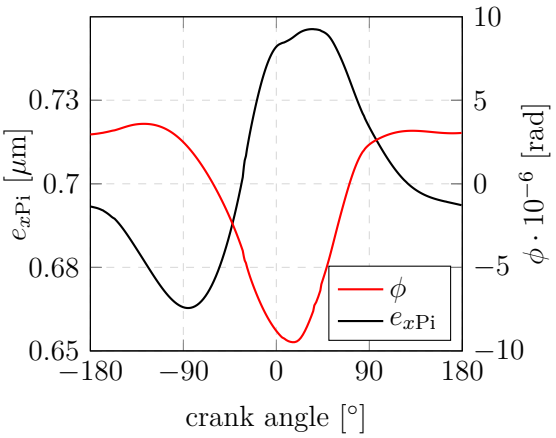

Fig. 5.18: Piston eccentricity and tilting angle

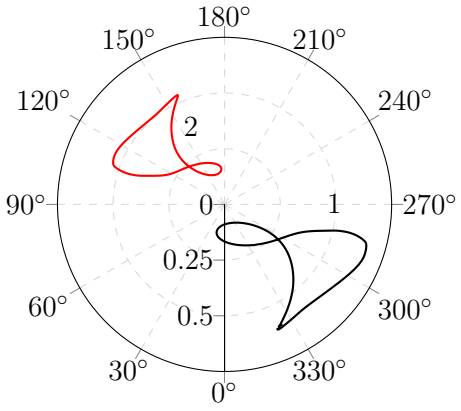

Fig. 5.19: Orbital paths of the crankshaft bearings

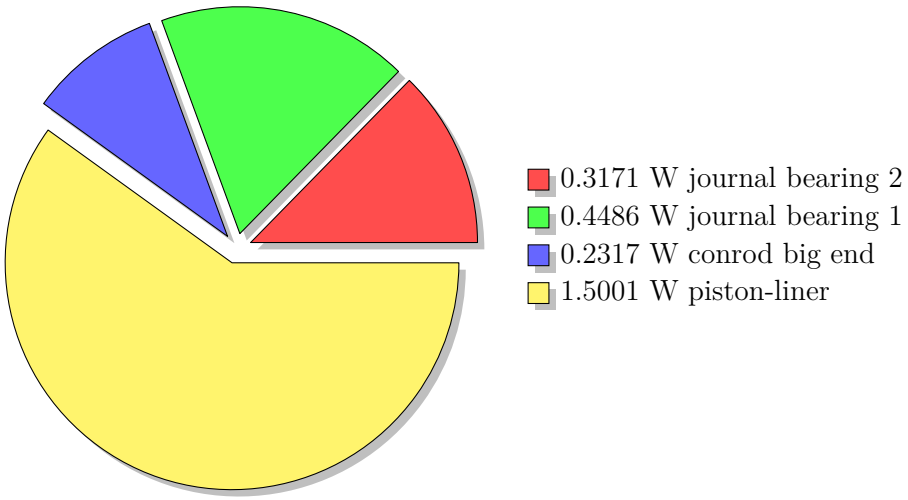

Fig. 5.20: Mechanical power losses gained by the friction loss code

at this point. An appropriate tool which could be used is the software package AVL EXCITE Power Unit. Nevertheless, this software is usually used for the application in combustion engines and drivetrain development, the similar structure of an internal combustion engine and a hermetic reciprocating compressor enables compressor friction loss calculation with this software. In the following sub chapter the development of a holistic friction loss analysis within AVL EXCITE Power Unit is shown. The present procedure has been published in [PHB+17a].

5.3.1 Model layout

AVL EXCITE Power Unit enables the simulation of EHL contacts taking into account the elastic deformation of the contact surfaces, thus, detailed information about the geometry of the crank mechanism parts is necessary. To get the necessary geometric input data to enable elastic deformation of the surfaces, the parts have to be condensed. The condensation process deletes unwanted degrees of freedom to reduce computational time significantly. As an example for the condensation process, the pre-processing of the compressor conrod is shown (Fig. 5.21). Starting from the 3D CAD model, a finite element model is prepared in the commercial software package SIMULIA Abaqus. Before defining the specific constraints in the finite element software, the type of contact model which is further applied in AVL EXCITE Power Unit must be selected. In the conrod example, the joint between the conrod big end and the crankshaft is regarded as EHL contact while the joint between the conrod small end and the piston pin is assumed as ordinary revolution contact. The EHL contact model requires seven nodes on the joint axis on which the surface nodes are condensed whereas the revolution contact only requires one node. For the EHL contact model six degrees of freedom and for the revolution contact one degree of freedom are implemented. The condensation process for the remaining crank drive parts (piston, crankshaft and crankcase) is similar to the condensation of the conrod.

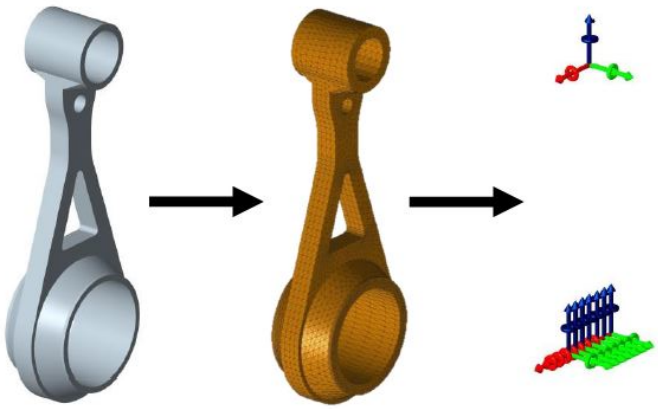

Fig. 5.21: Condensation process of the conrod

After the pre-processing step of preparing the geometry input data and loading into AVL EXCITE Power Unit, the specific contact models must be defined. Contacts which have a significant influence on the overall friction losses of the compressor are modeled as EHL contact. EHL contact model is applied on the crankshaft journal bearings, the conrod big end-crankshaft contact and the piston-liner contact. Here, the averaged Reynolds equation ([PC78], [PC79]) is used to take into account the roughness of the contact surfaces and, furthermore, the asperity contact model of Greenwood and Tripp ([GT70]) is applied. The remaining contacts between conrod and piston pin or piston

pin and piston are modeled as ordinary revolution joints. Similar to the self-written friction loss code, CFD data according to [Hopss] is used as input for the cylinder pressure and thus, for the multi-body system.
The simulation procedure is carried out using adaptive time step until periodic steady-state conditions are reached.

5.3.2 Results

The friction loss calculation with the commercial software AVL EXCITE Power Unit is carried out using similar boundary conditions as the friction loss code. Steady-state conditions are reached after five cycles. Results in terms of hydrodynamic pressure in the considered contacts at upper dead center piston position are shown in Fig. 5.23. Due to the high pressure acting on the piston and the resulting high reaction force in the conrod big end, the hydrodynamic pressure in the conrod big end joint reaches considerable values.

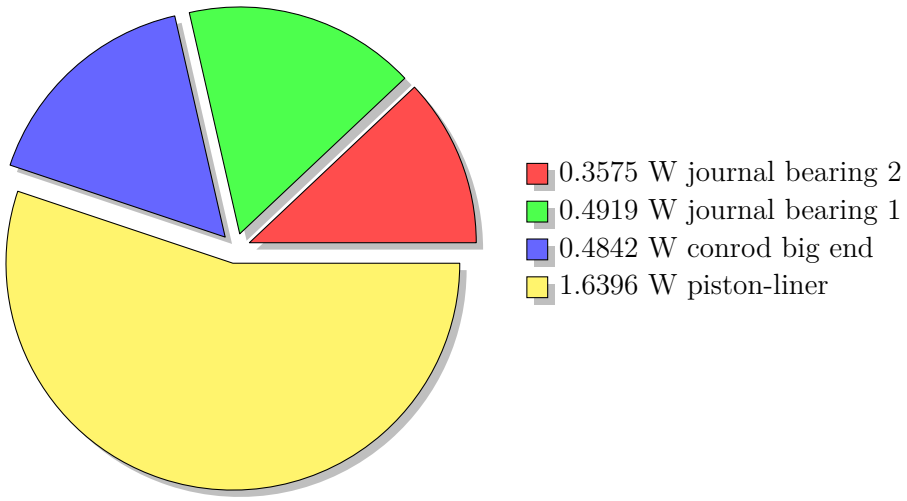

Fig. 5.22: Mechanical power losses gained by AVL EXCITE Power Unit

Similar to the self-written loss code, a loss distribution is carried out with the results gained by the commercial software. It can be pointed out that the friction losses in the journal bearings and the piston-liner contact do not show significant deviations between the two approaches. The results concerning conrod big end friction loss show that the simple model used in the self-written code underestimates the friction loss and thus the friction model based on the solution of the Reynolds equation should be used.

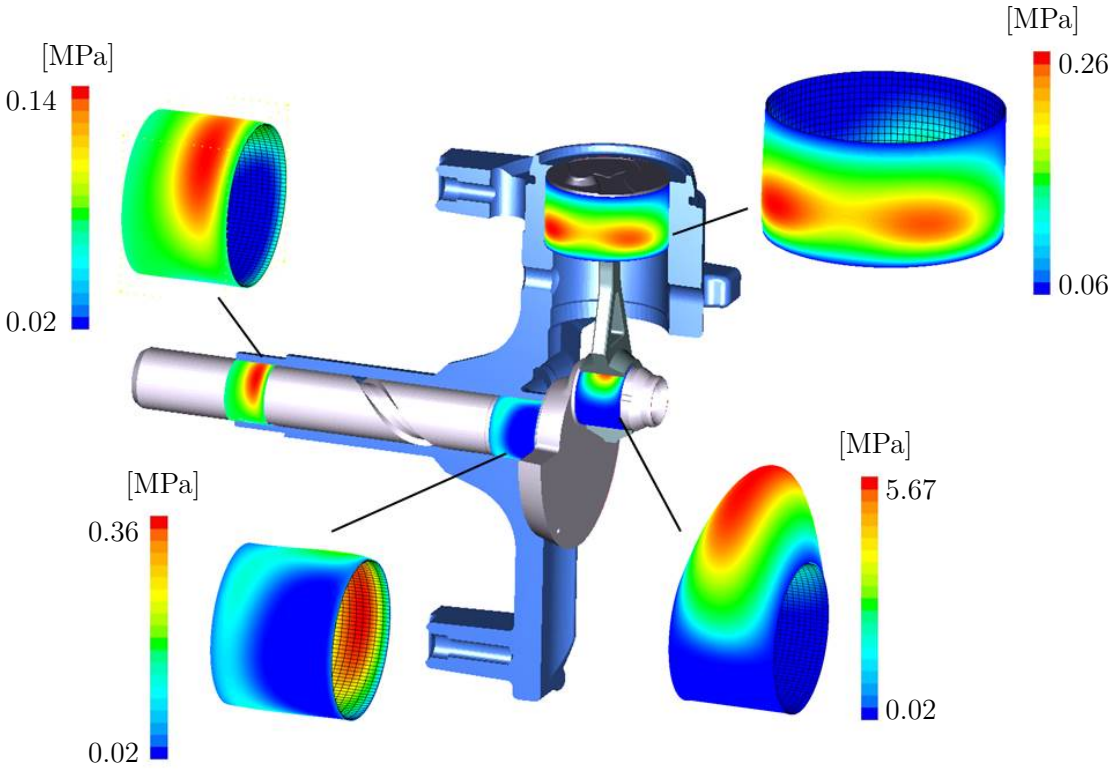

Fig. 5.23: Hydrodynamic pressure in the considered contacts

6 Thermal Compressor Model

After the simulation activities of the oil related sub systems, the influence of the lubrication oil on the overall thermal behavior of the hermetic compressor is investigated. For this purpose, a holistic thermal model of the compressor is created which links the results of the oil simulations with CFD simulations of the refrigerant gas path. Also for the thermal compressor model, the general rule for the development of numerical models is applicable to find a suitable ratio between accuracy and simulation effort. To solve this trade-off, different modeling strategies are available.
The simplest approaches use several lumped volumes which are connected via thermal conductance representing the individual compressor parts. Using the first law of thermodynamics, the temperature field inside the compressor can be calculated. Such models use mainly experimental data as input for heat transfer coefficients. In addition to the very low spatial resolution, the dependency on experimental data yields in an inflexible calculation of the temperature field in a hermetic compressor. An increase of flexibility can be achieved adopting the Thermal Network approach (TNW). Similar to the previously mentioned method, the TNW divides the compressor into several lumped mass points but it uses correlations from the literature to determine convective heat transfer coefficients and avoids the usage of experimental data as input parameter. The low spatial resolution can be also mentioned for the TNW which can cause uncertainties and can pose problems in the validation with experimental data because the measuring point may not represent the temperature of the lumped mass. An increase of accuracy and spatial resolution can be achieved by so-called hybrid models. Hybrid models use different combinations of complex 3D simulations and simple correlations. Since 3D simulations of the entire compressor and all physical phenomena are still not possible within reasonable time, hybrid models can be considered as suitable tool for the thermal modeling of hermetic compressors and are therefore used in the present work.
The present thermal compressor model is based on 3D formulation of the entire refrigerant gas path and 3D formulation of the solid compressor parts. It contains the results of the oil pump simulation and heat transfer coefficients determined by the oil distribution simulation. The oil and the refrigerant in the shell are modeled as lumped volumes. Due to this kind of hybrid model, the present approach has a high spatial resolution and is independent of experimental input data. The thermal model has been published in [PHH+16b] and [PHH+17].

6.1 Literature review

The origins of thermal modeling in the field of hermetic reciprocating compressors go back to the works of [MDT88] and [TFPF92] which are based on the simplest approach of dividing the compressor into several lumped volumes. Due to their limited computational power, the authors were restricted to a small number of lumped volumes and heat transfer coefficients gained by experiments or literature correlations. Examples for the application of TNW on hermetic compressors can be found in [SYM00] and [Ooi03]. In these studies the compressor is divided in up to 46 lumped volumes and furthermore, the heat transfer coefficients are modeled by literature correlations. Another example of TNW is given in [AABN06]. The compressor in this study is divided in 15 lumped volumes using heat transfer coefficients gained by numerical methods for heat flux calculation between solid parts and refrigerant gas flow. By the use of numerical determined Heat Transfer Factor (HTF) the heat transfer between the solid parts is modeled. Recent publications mostly deal with the application of hybrid models. Studies as published in [RJ07], [SD12] or [LDD15] deal with the combination of 3D solid part heat conduction formulation and gas path lumped formulation. Heat transfer is modeled by the use of experimental data or literature correlations. [ABAN06] applied the hybrid method with the focus on the cylinder solid domain which is modeled in 3D. The remaining compressor parts are regarded by lumped volumes and the heat transfer between the solid parts and the refrigerant gas path is determined by numerical methods. Even though hybrid models are state-of-the-art in the thermal modeling of hermetic reciprocating compressors, a holistic application using 3D formulation of the refrigerant gas path, 3D formulations of the compressor solid parts and detailed consideration of the oil influence cannot be found in the open literature.

6.2 Modeling

The present thermal compressor model based on hybrid formulation basically consists of three main parts which are the heat conduction in the solid parts, refrigerant gas flow in the compressor gas path and the lumped volume formulations of the lubrication oil and the refrigerant in the hermetic shell. In the following sub chapters, the modeling of the individual systems is explained; furthermore the interaction between the sub models and the solution algorithm is shown.

6.2.1 Solid parts

The heat conduction in the solid compressor parts is calculated solving the 3D energy equation in the commercial software ANSYS Fluent. Using the original CAD data, meshes of the individual compressor parts are created. The entire mesh consists of approximately 2.4 million cells with refinements at part interfaces. Thermal boundary

conditions are implemented via specifying heat flux values or heat transfer coefficients and medium temperature. In addition to the heat transfer determination with numerical methods, some heat transfer coefficients are calculated with correlations from the literature. The heat transfer coefficient between the external shell surface and the ambient air assuming spherical shape of the compressor, is calculated by the Nusselt number given by [Ing13]

$$\mathrm{Nu} = 0.56 \left[\left(\frac{\mathrm{Pr}}{0.846 + \mathrm{Pr}} \right) \mathrm{Ra} \right]^{1/4} + 2 \tag{6.1}$$

Inside the hermetic shell, the heat transfer coefficients between the solid parts and the refrigerant are unknown. Assuming constant velocity induced by the rotating crankshaft, the heat transfer coefficients are calculated with the correlations for flat plates as follows [Ing13]:

$$\mathrm{Nu} = \frac{0.037\,\mathrm{Re}^{0.8}\,\mathrm{Pr}}{1 + 2.443\,\mathrm{Re}^{-0.1}\left(\mathrm{Pr}^{2/3} - 1\right)} \tag{6.2}$$

The heat transfer between the lubrication oil and the crankshaft is specified using the heat flux value based on the simulation results of chapter 3 as well as the heat transfer between oil and oil covered walls is described by the heat transfer coefficients determined in chapter 4. Losses of the electrical motor are considered as heat input at the specific part. The values for the HXD55 compressor are related to the work of [Zac13].

6.2.2 Refrigerant gas path

The impact of the refrigerant gas flow on the compressor temperature field is considered using heat flux values determined by 3D CFD simulation carried out by the research group. Since the main task of the present work is not the simulation of the refrigerant gas path, the required data is referred to research activities within the research group. At this point, only the basics of the modeling should be presented. The gas flow simulation domain includes the entire refrigerant gas path which includes the suction line, suction muffler, valves, cylinder, ports, discharge muffler and discharge line. In order to keep the computational time in reasonable limits, the valves are assumed to be parallel moving flat plates. The valve motion is calculated solving the single-degree of freedom system considering oil stiction forces via UDF. Depending on the position of the piston, the mesh size varies between 3.1 and 5.5 million cells. Details of the gas path simulation can be found in [Hopss]. Fig. 6.1 shows the velocity in the cylinder at opened suction valve as an example of the gas path CFD results. The heat fluxes for the thermal model are given by the mean values of one crankshaft revolution at steady-state compressor conditions. At the valve plate, the heat flux values are specified in four areas which are the suction port, the discharge port, the discharge interface and

the area facing the cylinder. The heat flux values at the mufflers and inside the cylinder do not have high spatial differences which can be seen in Fig. 6.2.

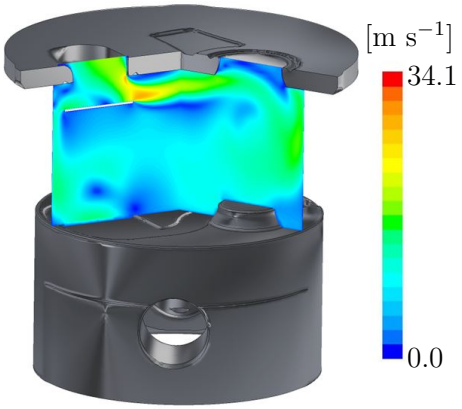

Fig. 6.1: Velocity field inside the cylinder

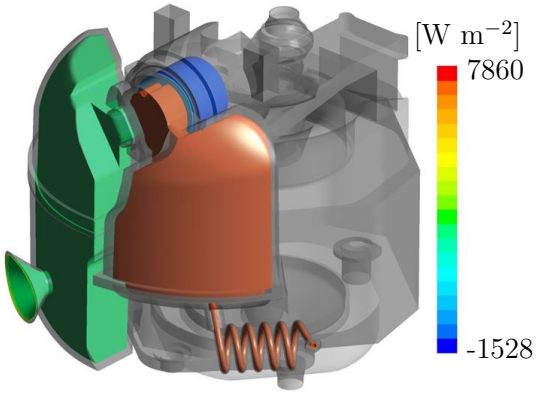

Fig. 6.2: Gas path wall heat flux values

6.2.3 Lumped volumes

As stated before, the present thermal compressor model should consider the lubrication oil and the refrigerant caught inside the compressor shell which is achieved by modeling the fluids as lumped volumes. In contrast to the refrigerant in the shell which is considered as one lumped volume, the lubrication oil is split-up into three individual lumped volumes which are the oil in the sump, the oil inside the oil pump and the oil on the oil covered walls. For each of the lumped volumes the energy equation can be stated:

$$T_{\mathrm{SG}}^{n+1} = T_{\mathrm{SG}}^{n} + \frac{\dot{Q}_{\mathrm{SG}} \cdot \Delta t}{m_{\mathrm{SG}} \cdot c_{v\mathrm{SG}}} \tag{6.3}$$

$$T_{\mathrm{OS}}^{n+1} = \frac{\dot{Q}_{\mathrm{OS}} + c_{\mathrm{oil}} \left(\dot{m}_{\mathrm{oil}} \cdot T_{\mathrm{OW}} + m_{\mathrm{OS}} \frac{T_{\mathrm{OS}}^{n}}{\Delta t} \right)}{c_{\mathrm{oil}} \left(\dot{m}_{\mathrm{oil}} + \frac{m_{\mathrm{OS}}}{\Delta t} \right)} \tag{6.4}$$

$$T_{\mathrm{OC}}^{n+1} = \frac{\dot{Q}_{\mathrm{OC}} + c_{\mathrm{oil}} \left(\dot{m}_{\mathrm{oil}} \cdot T_{\mathrm{OS}} + m_{\mathrm{OC}} \frac{T_{\mathrm{OC}}^{n}}{\Delta t} \right)}{c_{\mathrm{oil}} \left(\dot{m}_{\mathrm{oil}} + \frac{m_{\mathrm{OC}}}{\Delta t} \right)} \tag{6.5}$$

$$T_{\mathrm{OW}}^{n+1} = \frac{\dot{Q}_{\mathrm{OW}} + c_{\mathrm{oil}} \left(\dot{m}_{\mathrm{oil}} \cdot T_{\mathrm{OC}} + m_{\mathrm{OW}} \frac{T_{\mathrm{OW}}^{n}}{\Delta t} \right)}{c_{\mathrm{oil}} \left(\dot{m}_{\mathrm{oil}} + \frac{m_{\mathrm{OW}}}{\Delta t} \right)} \tag{6.6}$$

The heat flux values in the particular equation correspond to the values according to chapter 6.2.1 and the oil mass flow rate is given by the oil pump simulation results of chapter 3.

6.2.4 Solution algorithm

The simulation process starts with the initializing of the solid part temperature field, oil temperatures and refrigerant temperature using guessed values. In the following step, the CFD simulation of the refrigerant gas path using the initial solid part temperatures is utilized until cyclic steady-state conditions are reached. The gas path simulation results are averaged over one crankshaft revolution and are considered as heat flux values in the following calculation of the solid part temperature field. Since steady-state temperature fields should be calculated, the solid part simulation in ANSYS Fluent is set to steady. The solid part temperatures then act as boundary conditions for the solution of the quasi-transient energy balance of the refrigerant in the shell and the respective oil volumes using a constant time step. As the flow chart of the algorithm in Fig. 6.3 shows, two loops are integrated. The inner loop includes the calculation of the solid part temperature field and the solution of the lumped volumes energy equations which is carried out until heat flux deviation between two consecutive iteration steps is below a certain value. Gas flow CFD simulation and the solution of the inner loop forms the outer loop which is also continued until heat flux deviation between two consecutive iteration steps is below a certain convergence criterion.

6.3 Experimental work

The validation of the thermal compressor model is performed with experimental data of temperature measurements on the HXD55 compressor carried out from the research group. A total number of 22 thermocouples type T are distributed inside the compressor. For the validation of the thermal model eleven temperature positions according to Tab. 6.1 and Fig. 6.4 are used. The measurement inside hermetic systems like the compressor shell can cause difficulties due to the sealing of the Teflon®-insulated sensor wires. For the present experiment a special sealed feedthrough is used to enable the temperature measurement inside the hermetic shell. The compressor runs in a calorimeter test bench at -23.3 °C evaporating temperature, 45 °C condensing temperature and 32 °C ambient temperature at steady-state conditions.

6.4 Results

The thermal compressor model is applied on the HXD55 compressor working at steady-state conditions according to the operation point the calorimeter experiments are carried out. In addition to the use of the heat transfer coefficients gained in the oil distribution simulation of chapter 4, heat transfer coefficients calculated with Eq. 6.2 are implemented. The results of the two approaches can be validated with the temperature measurements on the calorimeter test bench and, furthermore, an assessment of the accuracy increase by the use of numerical calculated heat transfer coefficients can

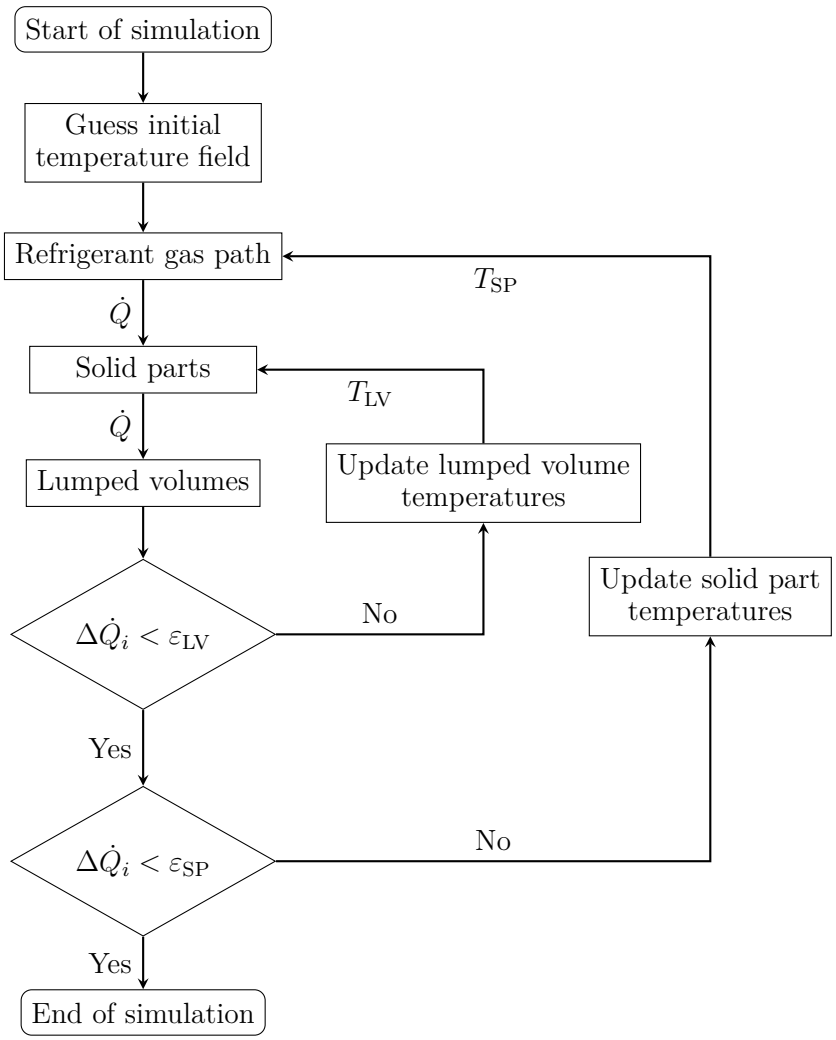

Fig. 6.3: Flow chart of the thermal model solution algorithm

be given.
In Fig. 6.5 the temperatures at the different sensor positions of the measurements, the thermal model using numerical calculated heat transfer coefficients and the thermal model using heat transfer coefficients gained by literature correlation are shown. As the results show, the solid part temperatures can be predicted accurately. Due to the generally lower heat transfer coefficients calculated by the literature correlation compared to the numerical simulation values, the temperature level of the solid parts inside the compressor is higher using the literature correlation. The maximum deviation between the experiment and the thermal model using numerical heat transfer coefficients is 4.2 °C which occurs at the discharge muffler surface. An important aspect which can be concluded on the basis of the simulation results is the significant influence of the heat transfer coefficient between shell and ambiance. Since the thermal resistance

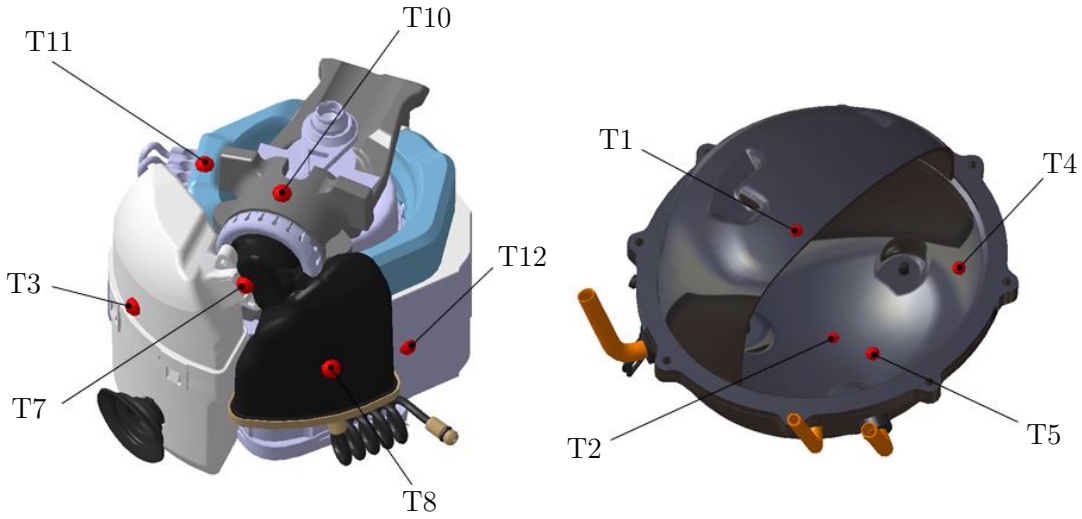

Fig. 6.4: Schematic overview of the sensor positions

Tab. 6.1: Thermocouple measuring points

No.	Measuring point description
T1	surface shell outside top
T2	surface shell outside bottom
T3	surface suction muffler
T4	surface shell inside opposite mufflers
T5	oil sump
T6	surface shell inside at mufflers
T7	valve plate
T8	surface discharge muffler
T9	shell gas
T10	cylinder
T11	surface stator windings
T12	surface stator lamination

of the heat transfer between compressor inside and outside is determined by the heat transfer from the shell to ambiance, the shell temperature is slightly influenced by the heat transfer coefficient between oil and shell. As the temperature values at the top of the compressor shell show, the constant heat transfer coefficient applied on the shell outer surface leads to a larger overestimation of the temperature value (4.6 °C) compared to the shell bottom (2.6 °C).

Fig. 6.6 shows the 3D temperature field in the inner compressor parts and on the compressor shell. The results are based on the simulation using the numerical calculated heat transfer coefficients between lubrication oil and oil covered shell walls. As the 3D

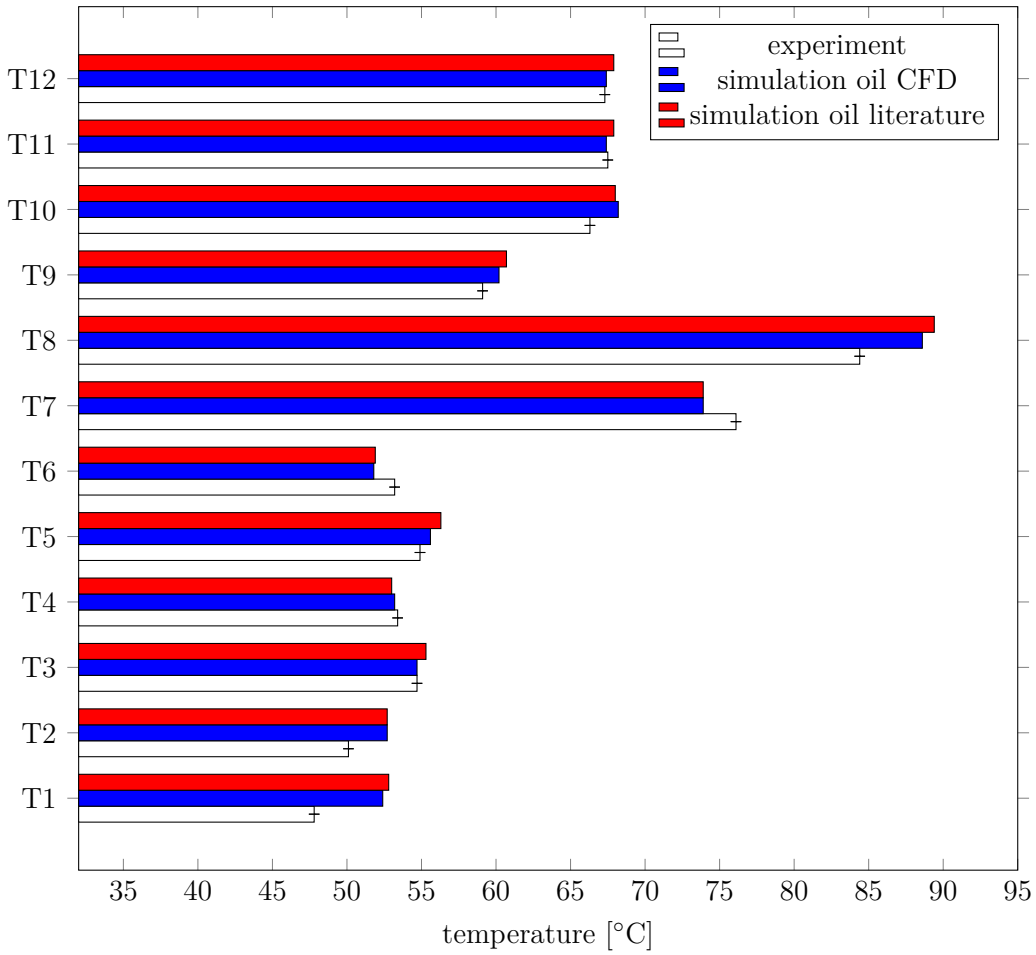

Fig. 6.5: Comparison between measured and simulated temperatures

temperature field of the inner compressor parts show, the highest temperature values occur at the discharge muffler and not, as often expected, at the valve plate. This can be explained by the relatively long duration of the hot refrigerant gas in the discharge muffler and the cooling of the valve plate by the suction gas. The accuracy of the temperature determination could be increased by introducing a higher number of zones with different heat flux values at parts with significant temperature gradients which is the case for the suction and discharge muffler. As the shell temperature field shows, the temperature values at the oil covered walls are higher than in the vicinity of the mufflers where the walls are not covered with oil. Using temperature dependent heat transfer coefficients in combination with several zones at the shell outer surface, the accuracy of the thermal model could by increased.

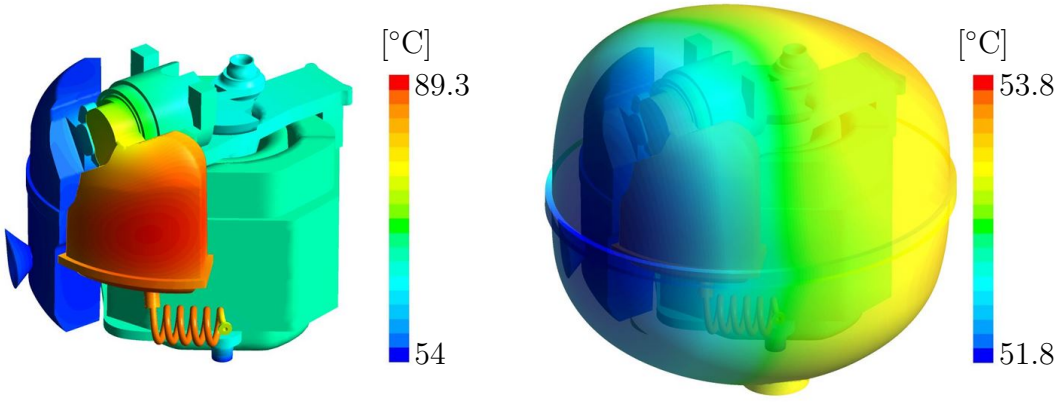

(a) **(b)**

Fig. 6.6: Temperature field of the solid parts inside the compressor (a) and on the compressor shell (b)

7 Exergy loss analysis

In addition to the thermodynamic modeling of the hermetic compressor in consideration of the oil influence, an evaluation of the losses which occur in the investigated compressor is given. For this purpose, the characteristic values of the second law of thermodynamics which are the entropy generation and the exergy loss are used. The loss analysis starts with a characterization of the several loss mechanisms in a compressor which are basically electrical, mechanical and thermodynamic losses. In the next step, different levels of the individual losses and their ensuing determination are shown. Finally, a holistic analysis of the compressor losses with respect to different levels is shown.

7.1 Literature review

Various studies published in the open literature deal with the investigation of hermetic compressor efficiency analysis based on the application of the energy equation disregarding the second law of thermodynamics. Furthermore, the focus of the majority of the studies lies on only one loss mechanism like thermodynamic losses. An example of compressor loss analysis based on the second law of thermodynamics can be found in [MGH92] and [MGH95]. The authors identified the losses due to friction, irreversible heat transfer, fluid throttling and irreversible fluid mixing. Describing these losses in terms of exergy destruction rates, their locations are shown. Another study using the thermodynamic property exergy to characterize compressor losses can be found in [PSRSO05]. In addition to the well-known isentropic and volumetric efficiencies, the authors introduced a combined mechanical-electrical efficiency and related it to the transferred and destroyed exergy. The mentioned works are based on analytical investigations and do hardly use any data gained by CFD simulations resulting in low spatial resolution.

7.2 Loss mechanism

The present analysis of the compressor losses is based on the three main loss mechanisms which are the electrical, the mechanical and thermodynamic losses. Due to the hermetic shell, the individual loss mechanism cannot be treated separately. The interaction between the loss mechanisms must be kept in mind when exergy losses are evaluated

for the entire system. In the following sub chapter, the determination of the several loss mechanisms is shown and, furthermore, an approach to evaluate the losses is proposed.

7.2.1 Electrical losses

Since the investigation of the electrical motor is not part of the present thesis, the electrical losses are calculated with data given in [Zac13]. The electrical losses of the motor are divided into copper losses, iron losses and aluminum losses. By the use of the efficiency values, the power dissipation of each electrical loss can be calculated. The power dissipation is assumed to occur as pure heat. Due to the hermetic compressor shell this heat is not directly given off to the environment. It is kept inside the compressor and thus, the heat does not consist of pure anergy but also of a small percentage of exergy. The exergy of the heat is determined by the Carnot factor according to

$$\dot{E} = \dot{Q}\left(1 - \frac{T_{\mathrm{amb}}}{T}\right) \tag{7.1}$$

The temperatures of the particular parts are given by the results of the thermodynamic model. Fig. 7.1 shows the proportional distribution of the electrical exergy losses.

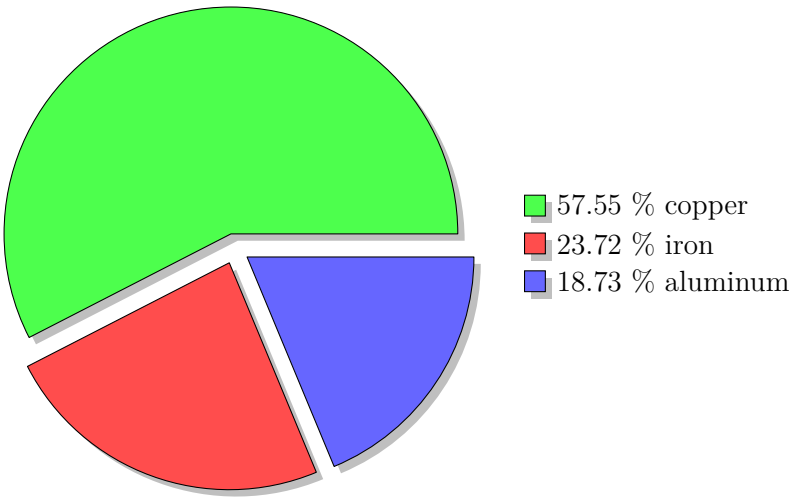

Fig. 7.1: Electrical exergy losses

7.2.2 Mechanical losses

The evaluation of the mechanical losses in terms of exergy is carried out using the similar approach as for the electrical losses. Using the results of the friction loss analysis performed in the commercial software AVL Excite Power Unit (see chapter 5.3) the

exergy amount of the occurred heat is calculated. The considered mechanical losses are confined to the piston liner contact, the big end conrod bearing and the main journal bearings at the crankshaft. In Fig. 7.2 the mechanical exergy losses can be seen.

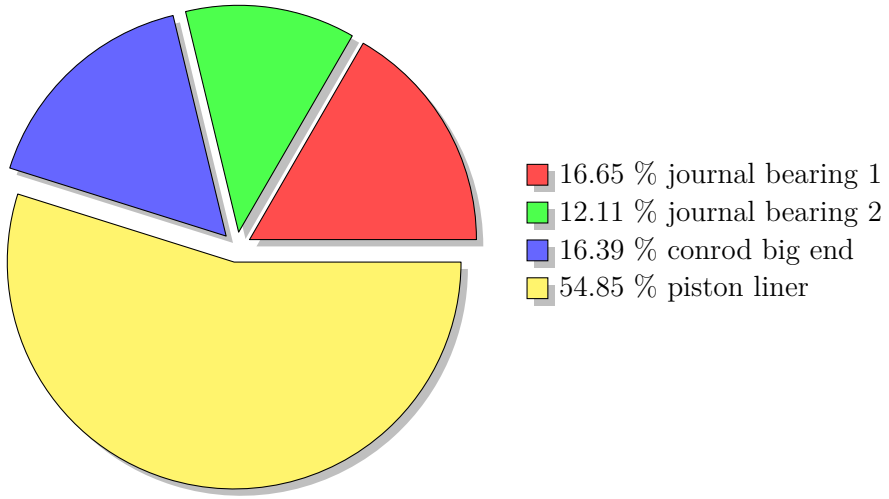

Fig. 7.2: Mechanical exergy losses

7.2.3 Thermodynamic losses

The determination of the thermodynamic exergy losses are based on the distinction between exergy losses in the refrigerant gas path, exergy losses due to heat conduction in the solid parts and exergy losses due to heat fluxes between the solid parts and the lubrication oil or refrigerant in the compressor shell.
The definition of the gas path losses depends on the calculation of the entropy generation which is linked to the exergy loss via the ambient temperature:

$$\mathrm{d}\dot{E}_{\mathrm{loss}} = T_{\mathrm{amb}} \cdot \mathrm{d}\dot{S}_{\mathrm{g}} \tag{7.2}$$

Although electrical and mechanical losses can be characterized directly as exergy losses, these losses are considered as heat sources due to their influence on the overall system in the hermetic compressor shell. The entropy generation rate due to this heat transfer can be calculated with the general formula of the irreversibility of heat transfer mechanism from temperature A to B:

$$\mathrm{d}\dot{S}_{\mathrm{g}} = \frac{T_{\mathrm{B}} - T_{\mathrm{A}}}{T_{\mathrm{B}} T_{\mathrm{A}}} \mathrm{d}\dot{Q} \tag{7.3}$$

A similar formula is used to determine the entropy generation rate of the transferred heat from the solid parts to the oil and gas inside the compressor shell and the

transferred heat from the compressor shell to the ambience. Temperature values are calculated in the thermodynamic compressor model.
To model the irreversibility in the gas path of the compressor a modeling approach based on the entropy equation is used [HW12]:

$$\rho\frac{\mathrm{D}s}{\mathrm{D}t} = -\nabla\cdot\left(\frac{\mathbf{q}}{T}\right) - \frac{1}{T^2}\mathbf{q}\cdot\nabla T + \frac{1}{T}\tau : \nabla\mathbf{u} \tag{7.4}$$

where the entropy generation rate per unit volume can be expressed as

$$s_\mathrm{g} = -\frac{1}{T^2}\mathbf{q}\cdot\nabla T + \frac{1}{T}\tau : \nabla\mathbf{u} \tag{7.5}$$

The entropy generation rate can be split into two parts due to a specific transport phenomenon which are the heat transfer term and viscous dissipation term:

$$s_\mathrm{g} = s_\mathrm{g}\,|_h + s_\mathrm{g}\,|_\mu \tag{7.6}$$

$$s_\mathrm{g}\,|_h = -\frac{1}{T^2}\mathbf{q}\cdot\nabla T \tag{7.7}$$

$$s_\mathrm{g}\,|_\mu = \frac{1}{T}\tau : \nabla\mathbf{u} \tag{7.8}$$

Similar to the treatment of the momentum equation, the conservation equation of entropy needs be time averaged in turbulent flows and the unclosed terms must be modeled. The method presented by [HK06] divides the entropy generation rate into a contribution of the mean gradients and a contribution of the fluctuating components:

$$\tilde{s_\mathrm{g}} = \langle s_\mathrm{g}\rangle_\mathrm{m} + \langle s_\mathrm{g}\rangle_\mathrm{fluc} \tag{7.9}$$

The entropy generation rates due to mean gradients can be written as:

$$\langle s_\mathrm{g}\,|_h\rangle_\mathrm{m} = \frac{\lambda}{T^2}\left[\left(\frac{\partial\tilde{T}}{\partial x}\right)^2 + \left(\frac{\partial\tilde{T}}{\partial y}\right)^2 + \left(\frac{\partial\tilde{T}}{\partial z}\right)^2\right] \tag{7.10}$$

$$\begin{aligned}\langle s_\mathrm{g}\,|_\mu\rangle_\mathrm{m} =& \frac{\mu}{T}\left[2\left\{\left(\frac{\partial\tilde{u}}{\partial x}\right)^2 + \left(\frac{\partial\tilde{v}}{\partial y}\right)^2 + \left(\frac{\partial\tilde{w}}{\partial z}\right)^2\right\} + \left(\frac{\partial\tilde{u}}{\partial y} + \frac{\partial\tilde{v}}{\partial x}\right)^2\right.\\ &\left. + \left(\frac{\partial\tilde{u}}{\partial z} + \frac{\partial\tilde{w}}{\partial x}\right)^2 + \left(\frac{\partial\tilde{v}}{\partial z} + \frac{\partial\tilde{w}}{\partial y}\right)^2\right]\end{aligned} \tag{7.11}$$

and the entropy generation rates due to fluctuating components are given by:

$$\langle s_\mathrm{g}\,|_h\rangle_\mathrm{fluc} = \frac{a_\mathrm{T}}{\alpha}\langle s_\mathrm{g}\,|_h\rangle_\mathrm{m} \tag{7.12}$$

$$\langle s_{\mathrm{g}} \mid_{\mu} \rangle_{\mathrm{fluc}} = \frac{\bar{\rho}\bar{\varepsilon}}{\tilde{T}} \tag{7.13}$$

In cells adjacent to walls, special care is needed to calculate the entropy generation rate. [WM08] proposed a method based on the applied wall function. The entropy generation rate per unit area is given by:

$$s'_{\mathrm{g}} = \left(\frac{\rho u_{\tau}^{3}}{T}\right) \int_{0}^{y^{+}} \left(\frac{\partial u^{+}}{\partial y^{+}}\right) \mathrm{d}y^{+} \tag{7.14}$$

The presented methodology, known as the direct method, can be applied on the results of the gas path CFD simulation in the post-processing phase. Details about the CFD simulations which were performed by the research group can be found in [Hopss]. Due to the lack of entropy generation calculation in ANSYS Fluent, the direct method is applied via an UDF. As an example of the irreversibility calculation in the compressor gas path, Fig. 7.3 shows the entropy generation in the suction valve area.

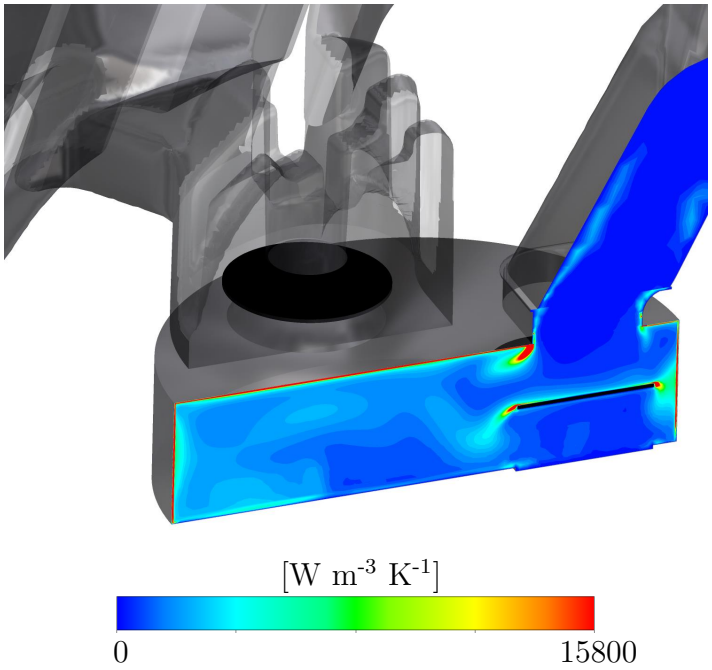

Fig. 7.3: Entropy generation in the area of the suction valve

The evaluation of the entropy generation in the refrigerant gas path yields in exergy losses according to Fig. 7.4. Looking at the results, the significant proportion of the losses in the cylinder must be seen critically. Since the distribution of the losses in the gas path depends on the mesh topology of the CFD model, the major part of the suction valve losses can be seen in the compressor cylinder.

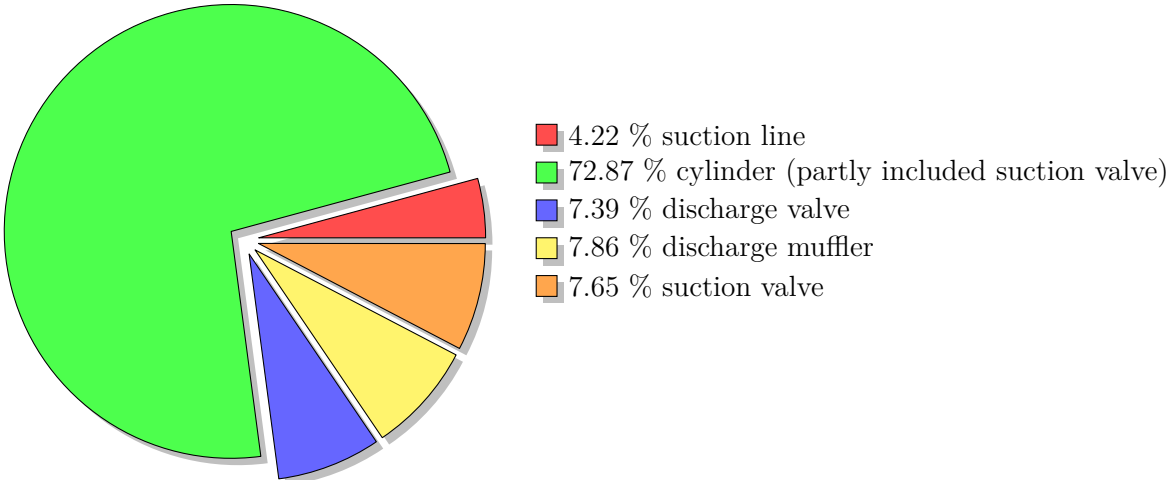

Fig. 7.4: Exergy losses in the gas path

The heat flux from the compressor shell to the environment is treated similar to the heat fluxes given off by the electrical and mechanical system but since the heat is not stored inside the hermetic shell, the exergy of the heat to the environment cannot be used and yields directly in an exergy loss. Thermal exergy losses due to the heat conduction in the solid parts of the compressor are calculated applying Eq. 7.10 on the temperature distribution gained by the thermodynamic compressor model. The entropy generation due to heat transfer between the solid parts and fluids is determined by

$$\mathrm{d}\dot{S}_\mathrm{g} = \frac{T_\mathrm{B} - T_\mathrm{A}}{T_\mathrm{B} T_\mathrm{A}} \mathrm{d}\dot{Q} \tag{7.15}$$

The summing up of the entire exergy losses due to thermodynamic effects yields in a loss distribution according Fig. 7.5. As expected, the exergy losses in the gas path account for the majority of the thermal losses. The exergy losses due to heat transfer, especially due to heat conduction in the solid compressor parts, play only a minor role.

7.2.4 Outlet temperature

In contrast to loss analysis simply based on the energy balance, the approach using exergy and thus the second law of thermodynamics values the energy of the refrigerant at the compressor outlet in terms of thermodynamic usability. Since the discharge pressure is given by the ASHRAE test case, the exergy difference between the refrigerant at the compressor outlet and the saturated state at discharge pressure is regarded as exergy loss (see Fig. 7.6). Although the real compressor process is similar to an isentropic process, the exergetic ideal process is assumed to end at saturated state. The exergy difference and thus the exergy loss is given by

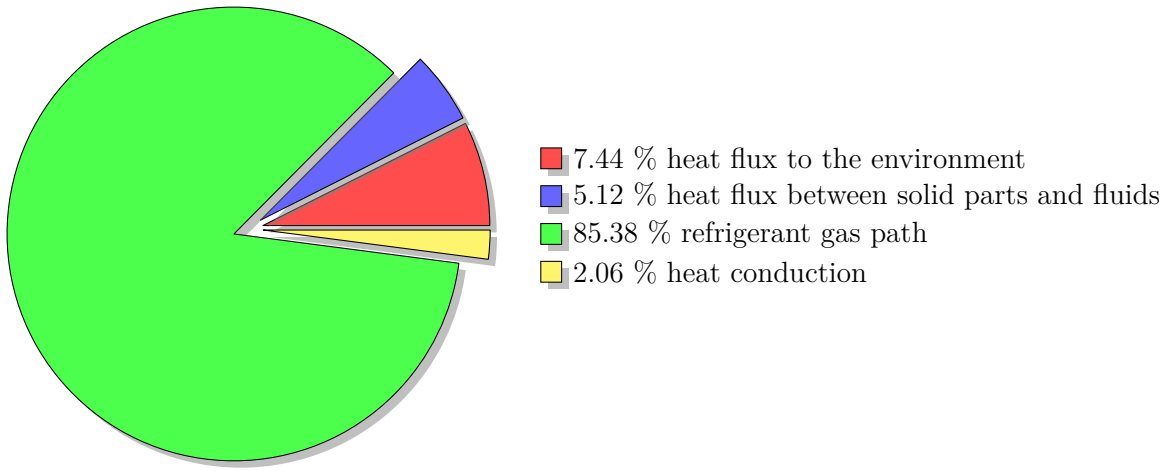

Fig. 7.5: Thermal exergy losses

$$\dot{E}_{\text{loss}} = \dot{m}\left[h_{\text{out}} - h''_{\text{sat}} - T_{\text{amb}}\left(s_{\text{out}} - s''_{\text{sat}}\right)\right] \tag{7.16}$$

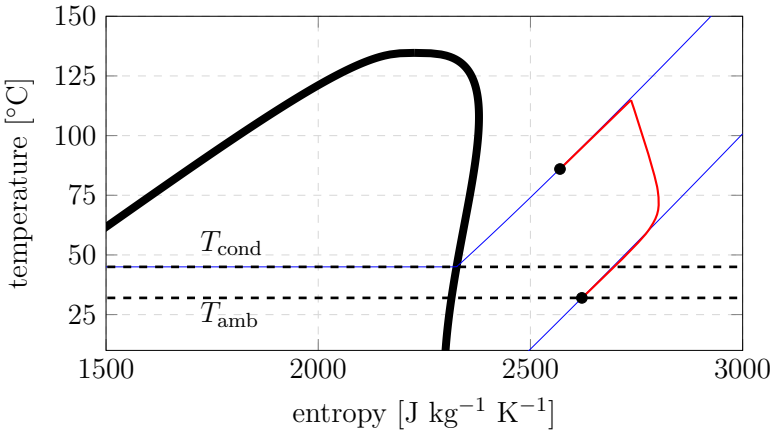

Fig. 7.6: Schematic compressor process at ASHRAE -23.3/45 test conditions

7.3 Entire compressor losses

The combination of the previously described individual losses results in the exergy loss distribution of the entire compressor. As Fig. 7.7 illustrates, the major part of the losses in the investigated compressor occur in the electric motor and in the thermodynamic system including the refrigerant gas path and losses due to heat transport. The thermodynamic system, leaving the electric motor aside, shows large potential for

improvements from the exergy point of view, especially in the refrigerant gas path. By evaluating the CFD results, a major part of the refrigerant gas path losses occur in the vicinity of the suction valve. Further developments on the opening and closing behavior of the suction valve would lead to a decrease of the losses. The definition of the outlet exergy loss shows exergetic influence of the refrigerant sensible heat at compressor outlet. It can be interpreted as an overshoot of the compression process beyond the necessary temperature. Due to the hermetic design of the compressor an independent decrease of this loss would not be useful. The outlet temperature could be decreased by holding the refrigerant in an uninsulated discharge muffler which would also lead to better acoustic behavior of the compressor but this would consequently increase the temperature level of the entire compressor and thus the refrigerant mass flow would decrease by the low density of the gas at compression start. Especially the investigated compressor with its plastic discharge muffler is designed to avoid the increase of the temperature level due to the hot refrigerant and thus produces high outlet exergy loss. Although the mechanical losses are responsible for only 11.6 % of the overall compressor losses, their influence on the compressor efficiency should not be disregarded. The mechanical losses produce heat which is directly transported to the lubrication oil. Higher temperature levels of the oil lead to higher compressor temperature level yielding in the previously mentioned decrease of refrigerant mass flow.

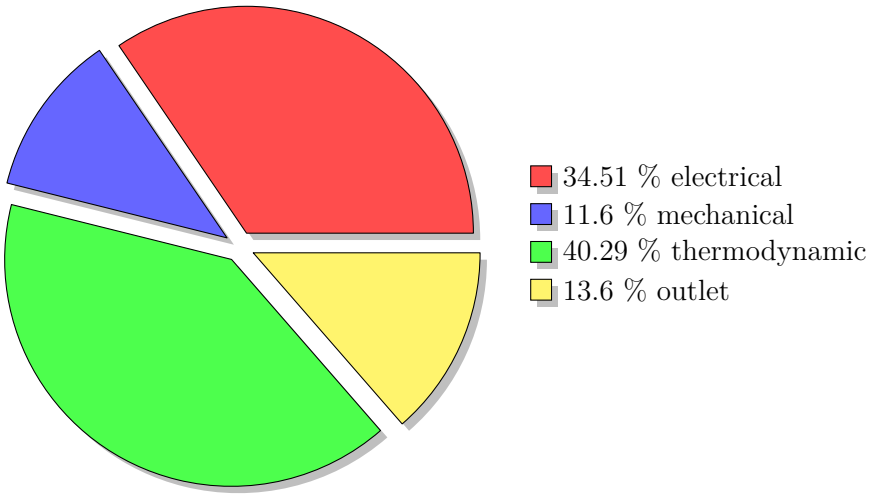

Fig. 7.7: Exergy losses of the entire compressor

The holistic simulation of the compressor enables the calculation of the compressor COP. By summing up the indicated power gained by the gas path CFD simulation, the friction loss power and the electrical loss power, the input power of the compressor can be determined. The cooling capacity is given by the reference points of the ASHRAE -23.3/45 test conditions and the refrigerant mass flow gained by the gas path CFD simulation. The obtained compressor COP is 2.12 which differs by 4.3 % from the catalog data (COP 2.04) which can be seen as satisfying result for the present approach.

8 Application example

In the following chapter, the ability to use the present methodology in the compressor research should be shown. Based on the compressor cooling experiment in chapter 1.2 the effects of a decrease in the temperature level of the entire compressor are investigated. In the following considerations, the compressor cooling is induced artificially, which means that restrictions due to the technical realization are ignored.
The investigation starts with the specification of compressor part temperatures. In addition to the discharge muffler, the valve plate is the compressor part where high temperature levels occur. Since the cold refrigerant has to pass the hot valve plate before entering the compression chamber, a decrease in the valve plate temperature leads to lower superheating effects. Therefore, the major part of the cooling in this investigation is assumed to effect the valve plate temperature. Furthermore, the temperatures of the mufflers and remaining parts are estimated. Fig. 8.1 shows the estimated temperatures of the important solid parts.

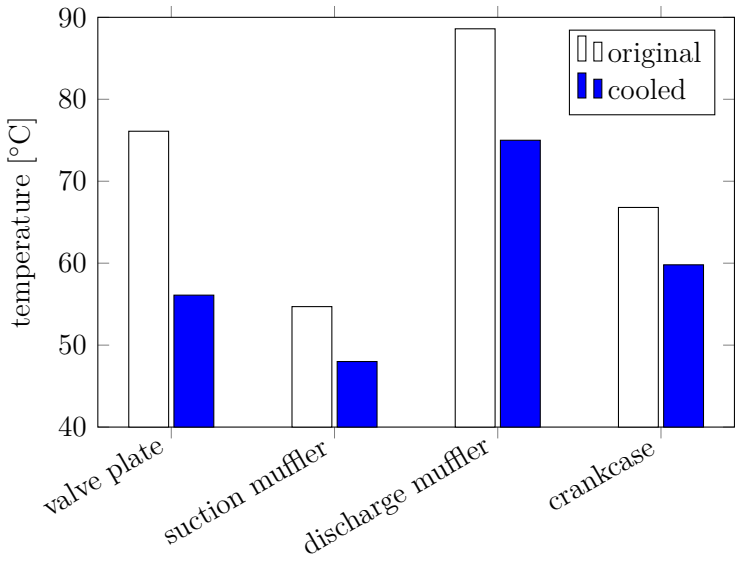

Fig. 8.1: Estimated temperatures for the artificial cooling example

In the next step, the estimated solid part temperatures are used as input data for the thermal model. By keeping the solid part temperatures constant, the lumped volume temperatures can be calculated. The results for the lumped volume temperatures can

be seen in Fig. 8.2.
To determine the influence of the artificially cooling on the thermodynamic system, the CFD simulation of the refrigerant gas path is carried out using the estimated solid part temperature values. The CFD simulation gives the inner work of the compression process and the refrigerant mass flow rate to calculate the compressor COP. Furthermore, the estimated solid part temperatures lead to higher heat flux values between the refrigerant and the solid parts. The difference between the heat flux values of the original compressor and the artificially cooled compressor results in the required cooling power which is 11.2 W for the investigated case.

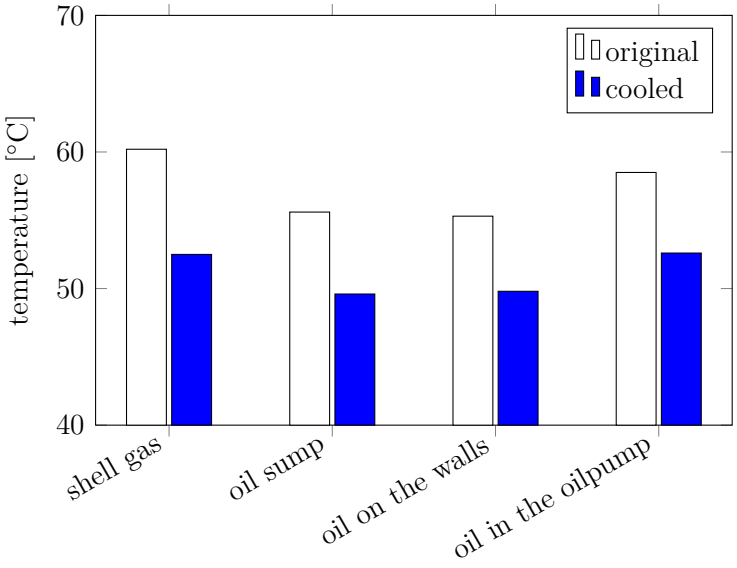

Fig. 8.2: Lumped volume temperatures of the artificial cooling example

Finally, the results of the thermal model are used to update the calculation of the mechanical losses. Since the oil properties depend on the oil temperatures, the viscosity and density values are updated according to the thermal model results. The losses due to the electric motor are kept constant compared to the original uncooled compressor. An overview of the investigation results can be seen in Fig. 8.3. As expected, the refrigerant mass flow is increased in the cooled version due to the higher density of the refrigerant at compression start. The mass flow increase of 2.63 % is equivalent to the increase of the cooling capacity due to the standardized points of the ASHRAE test. Furthermore, the higher density of the refrigerant due to the lower temperature level leads to a slight increase of the inner work which can be almost neglected. The influence of the temperature decrease in the compressor and thus the lower oil temperature leads to an increase of the oil viscosity. Applying the updated oil viscosity values, the mechanical losses are increased by 15.7 % compared to the original version. The final calculation of the compressor COP results in an increase of 1.57 % for the cooled

version.

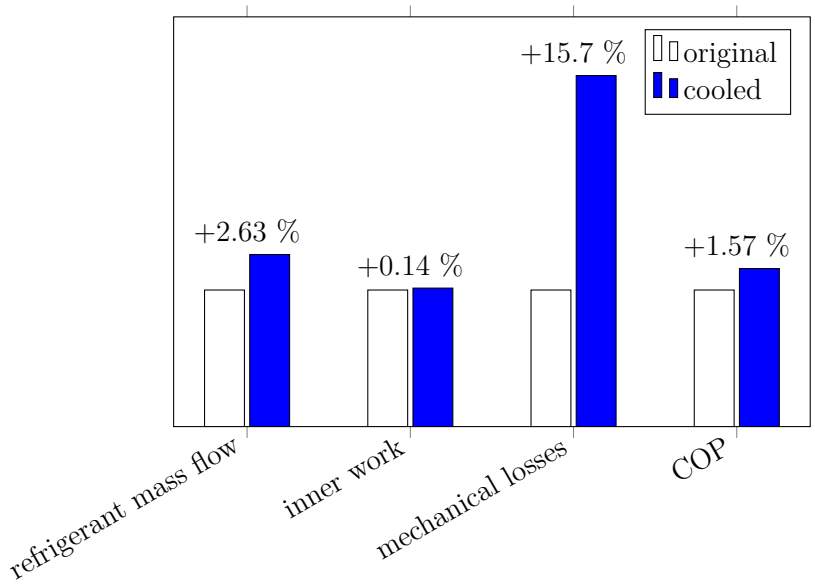

Fig. 8.3: Results of the artificial cooling example

As the results of the artificially cooled compressor investigation show, the compressor COP can be increased but a considerable proportion of the efficiency improvement is destroyed by the higher mechanical losses. It can be concluded that measures to decrease the compressor temperature level must go along with an adjustment of the lubrication oil. The optimum solution would be a constant temperature level of the lubrication oil in each operating mode.

9 Summary and conclusions

A brief overview of the tasks which were carried out in the course of the present work and the main conclusions are given in the following chapter.

- An innovative simulation approach to model the oil pump of a hermetic reciprocating compressor has been developed. The new approach splits-up the oil pump in its individual pumping parts and combines the individual performance curves to an entire performance curve. A validation of the developed method against experimental data shows satisfying agreement. Comparing the split-up method with the conventional approach, a reduction by a factor of 300 in terms of computational effort in case of design changes in the helical groove or the upper centrifugal pump can be achieved.

- The oil distribution inside the compressor shell has been analyzed by the use of numerical simulation. Results of the oil distribution simulation have been used to determine the heat transfer coefficients between the lubrication oil and the oil covered walls. To enable the use of the heat transfer coefficient values in a thermal model, the compressor shell has been divided into several zones on which the heat transfer coefficients have been averaged. The simulation of the oil distribution is highly computational time expensive and thus not practical in the development process of hermetic compressors.

- The influence of the lubrication oil on the mechanical losses of the compressor has been investigated by a self-written friction loss code and a commercial software, respectively. Although the commercial software uses complex EHL models to describe the lubrication behavior in bearings or in the piston-liner contact, the deviation between the results of the self-written code and the commercial software are in acceptable limits. It can be concluded that for an accurate investigation of the compressor friction losses, the use of commercial software is recommended but if commercial software is not available, a self-coded simulation tool fulfills the requirements.

- A holistic thermal model of the compressor has been developed. The model includes 3D simulation of the refrigerant gas path and the solid part heat conduction as well as lumped formulation of the refrigerant gas and lubrication oil inside the compressor shell. To couple the individual models, an algorithm has been introduced. The thermal model contains oil dependent results of the oil

pump, oil distribution and friction loss simulation. Validation results show satisfying agreement between the simulation and temperature measurements on a calorimeter test bench.

- The determination of the compressor losses is based on the second law of thermodynamics, thus the individual loss mechanisms are described in terms of entropy or exergy. Applying the proposed method on hermetic reciprocating compressors, it is possible to describe the exergy losses at different levels. In this case, different levels mean that the losses can be distinguished in terms of location and loss mechanism.

- To show the influence of the lubrication oil on the compressor COP, an artificially cooled compressor has been investigated. The results show that a significant proportion of the efficiency increase gained by the cooling is destroyed by higher friction losses.

10 Future work

The final chapter of this work is used to give an outlook into future research activities which are based on the findings of the present thesis.

- As the simulation of the oil pump has shown, the use of multiphase models like VOF increases the computational time significantly. Even the proposed split-up method does not achieve noteworthy time reduction if design changes occur at the lower centrifugal pump. Ideas to avoid the use of multiphase models in the oil pump simulation have been considered in the course of the present work and will be further investigated in future projects.

- Another aspect concerning the compressor oil pump which is interesting for future investigations is the outgasing of dissolved refrigerant. Especially after long periods in which the compressor is shut off, the amount of refrigerant dissolved in the lubrication oil can reach considerable values and thus, outgasing effects in the oil pump after the compressor is switched on can play an important role. Furthermore, outgasing may also occur at standard operation conditions in low pressure areas inside the compressor oil pump. The modeling of outgasing effects requires accurate material properties of the oil refrigerant mixture and the development of special outgasing models.

- The thermal decoupling between lubrication oil temperature and operation point will be investigated in future works. Due to the partial redirecting of the oil flow, the controlling of the oil temperature can be realized and thus, the oil must not be selected for unfavorable operation conditions like the pull-down mode.

Bibliography

[AABN06] Z. Abidin, R. Almbauer, A. Burgstaller, and D. Nagy. One-dimensional and thermal network application for a complete thermodynamic analysis of a piston compression machine. In *International Conference on Fluid and Thermal Energy Conversion, Jakarta, Indonesia*, 2006.

[ABAN06] R. Almbauer, A. Burgstaller, Z. Abidin, and D. Nagy. 3-dimensional simulation for obtaining the heat transfer correlations of a thermal network calculation for a hermetic reciprocating compressor. In *International Compressor Engineering Conference at Purdue, West Lafayette, USA*, 2006.

[ABP12] M.C.A. Alves, Jr.J.R. Barbosa, and A.T. Prata. Analytical and cfd modeling of the fluid flow in an eccentric-tube centrifugal oil pump for hermetic compressors. In *International Compressor Engineering Conference at Purdue, West Lafayette, USA*, 2012.

[ABPR09] M.C.A. Alves, Jr.J.R. Barbosa, A.T. Prata, and Jr.F.A Ribas. Analytical solution of single screw extrusion applicable to intermediate values of screw channel aspect ratio. *Journal of Food Engineering*, 92:152–156, 2009.

[ABPR11] M.C.A. Alves, Jr.J.R. Barbosa, A.T. Prata, and Jr.F.A Ribas. Fluid flow in a screw pump oil supply system for reciprocating compressors. *International Journal of Refrigeration*, 34:74–83, 2011.

[Bar10] D. Bartel. *Simulation von Tribosystemen*. Vieweg + Teubner, 2010.

[BK12] H.D. Baehr and S. Kabelac. *Thermodynamik*. Springer, 2012.

[BS04] H.D. Baehr and K. Stephan. *Wärme und Stoffübertragung*. Springer, 2004.

[CCP07] H. Chieh, P.R.C. Couto, and A.T. Prata. An integral analysis and simulation of the complete bearing system in reciprocating hermetic compressors. In *International Conference on Compressors and their Systems, London, GB*, 2007.

[DD06] M. Duyar and Z. Dursunkaya. Design improvement based on wear of a journal bearing using an elastohydrodynamic lubrication model. In *International Compressor Engineering Conference at Purdue, West Lafayette, USA*, 2006.

[DD10] T. Dutra and C.J. Deschamps. Experimental investigation of heat transfer in components of a hermetic reciprocating compressor. In *International Compressor Engineering Conference at Purdue, West Lafayette, USA*, 2010.

[DS06] M. Dischner and J. Schenk. Bestimmung physikalischer Eigenschaften eines Öls gemischt mit R600a. In *Institut für Luft- und Kältetechnik gemeinnützige Gesellschaft mbH, Bertolt-Brecht-Allee 20, Dresden, Germany*, 2006.

[Eic10] H. Eichlseder. Thermodynamik. University Lecture, 2010.

[Elr81] H.G. Elrod. A cavitation algorithm. *Journal of Lubrication Technology*, 103:350–354, 1981.

[Flo57] L. Floberg. The infinite journal bearing considering vaporization. *Transactions of Chalmers University of Technology*, 189, 1957.

[GNP05] R. Gasch, R. Nordmann, and H. Pfützner. *Rotordynamik*. Springer, 2005.

[GPP05] F.P. Grando, M. Priest, and A.T. Prata. Lubrication in refrigeration systems: Performance of journal bearing lubricated with oil and refrigerant mixtures. *Life Cylce Tribology*, pages 481–491, 2005.

[GT70] J.A. Greenwood and J.H. Tripp. The contact of two nominally flat rough surfaces. *Proceedings of the Institution of Mechanical Engineers*, 185:625–633, 1970.

[Ham94] B.J. Hamrock. *Fundamentals of Fluid Film Lubrication*. McGraw-Hill, 1994.

[Hei15] M. Heimel. *Simulation and experimental validation of adiabatic and non-adiabatic capillary tubes*. PhD thesis, Graz University of Technology, 2015.

[HK06] H. Herwig and F. Kock. Direct and indirect methods of calculating entropy generation rates in turbulent convective heat transfer problems. *Heat Mass Transfer*, 43:207–215, 2006.

[Hopss] J. Hopfgartner. *Untersuchung von Verbesserungspotentialen hermetischer Kolbenkompressoren mit Hilfe numerischer Methoden*. PhD thesis, Graz University of Technology, in press.

[HW12] H. Herwig and T Wenterodt. *Entropie für Ingenieure*. Vieweg+Teubner, 2012.

[Ing13] Verein Deutscher Ingenieure. *VDI-Wärmeatlas*. Springer, 2013.

[JF57] B. Jakobsson and L. Floberg. The finite journal bearing considering vaporization. *Transactions of Chalmers University of Technology*, 190, 1957.

[KH04] T.-J. Kim and J.-S Han. Comparison of the dynamic behavior and lubrication characteristics of a reciprocating compressor crankshaft in both finite and short bearing models. *Tribology Transactions*, 47:61–69, 2004.

[KL03] H.J. Kim and T.W. Lancey. Numerical study on the lubrication oil distribution in a refrigeration rotary compressor. *International Journal of Refrigeration*, 26:800–808, 2003.

[Kle12] M. Klell. University Lecture, 2012.

[KLKB02] H. J. Kim, T. J. Lee, K. H. Kim, and Y. J. Bae. Numerical simulation of oil supply system of reciprocating compressor for household refrigerators. In *International Compressor Engineering Conference at Purdue, West Lafayette, USA*, 2002.

[KPC+12] J. Kim, S. Park, I. Cho, I. Baek, J. Jo, and J. Jung. Journal bearing lubrication characteristics in a reciprocating compressor. In *International Compressor Engineering Conference at Purdue, West Lafayette, USA*, 2012.

[KYO13] H. Kerpicci, A. Yagci, and S.U. Onbasioglu. Investigation of oil flow in a hermetic reciprocating compressor. *International Journal of Refrigeration*, 36:215–221, 2013.

[LAB09] A.J. Lueckmann, M.V.C. Alves, and J.R.Jr. Barbosa. Analysis of oil pumping in a reciprocating compressor. *Applied Thermal Engineering*, 29:3118–3123, 2009.

[Lav98] J.P. Lavelle. Oil miscibility and oil return characteristics of alternative refrigerants and blends. In *International Compressor Engineering Conference at Purdue, West Lafayette, USA*, 1998.

[LDD15] S.K. Lohn, M.C. Diniz, and C.J. Deschamps. A thermal model for analysis of hermetic reciprocating compressors under the on-off cycling operating condition. In *International Conference on Compressors and their Systems, London, GB*, 2015.

[LH94] Y. Li and F. Hsieh. Modeling of flow in a single screw extruder. *Journal of Food Engineering*, 27:353–375, 1994.

[LS78] O.R. Lang and W. Steinhilper. *Gleitlager: Berechnung und Konstruktion von Gleitlagern mit konstanter und zeitlich veränderlicher Belastung.* Springer, 1978.

[MDT88] W.A. Meyer and H. Doyle Thompson. An analytical model of heat transfer to the suction gas in a low-side hermetic refrigeration compressor. In *International Compressor Engineering Conference at Purdue, West Lafayette, USA*, 1988.

[MGH92] J.A. Mc Govern and S. Hart. Computer simulation of exergy destruction within a reciprocating compressor. In *International Compressor Engineering Conference at Purdue, West Lafayette, USA*, 1992.

[MGH95] J.A. Mc Govern and S. Hart. An exergy method for compressor performance analysis. *International Journal of Refrigeration*, 18:421–433, 1995.

[MKI10] M. Matsui, Y. Kitsunai, and K. Inagaki. High efficiency development of a reciprocating compressor by clarification of loss generation in bearings. In *International Compressor Engineering Conference at Purdue, West Lafayette, USA*, 2010.

[MMD15] F. Moukalled, L. Mangani, and M. Darwish. *The Finite Volume Method in Computational Fluid Dynamics*. Springer, 2015.

[Ols65] K.O. Olsson. Cavitation in dynamically loaded bearings. *Transactions of Chalmers University of Technology*, 308, 1965.

[Ooi03] K.T. Ooi. Heat transfer study of a hermetic refrigeration compressor. *Applied Thermal Engineering*, 23:1931–1945, 2003.

[OSH+14] M. Ozsipahi, C. Sertac, G. Hasan, K. Sarioglu, and H. Kerpicci. A numerical study on the lubrication system for a hermetic reciprocating compressor used in household refrigerators. *International Journal of Refrigeration*, 48:210–220, 2014.

[PC78] N. Patir and H.S. Cheng. An average flow model for determining effects of three dimensional roughness on partial hydrodynamic lubrication. *Journal of Lubrication Technology*, 100:12–17, 1978.

[PC79] N. Patir and H.S. Cheng. Application of average flow model to lubrication between rough sliding surfaces. *Journal of Lubrication Technology*, 101:220–230, 1979.

[PFF00] A. T. Prata, J.R.S. Fernandes, and F. Fagotti. Dynamic analysis of piston secondary motion for small reciprocating compressors. *Journal of Tribology*, 122:752–760, 2000.

[PHB+] S. Posch, J. Hopfgartner, E. Berger, B. Zuber, P. Schoellauf, and R. Almbauer. Numerical analysis of a hermetic reciprocating compressor oil pump system. *International Journal of Refrigeration*, In Press.

[PHB+17a] S. Posch, J. Hopfgartner, E. Berger, B. Zuber, R. Almbauer, and P. Schoellauf. Comprehensive 3d-elastohydrodynamic simulation of hermetic compressor crank drive. In *International Conference on Compressors and their Systems, London, GB*, 2017.

[PHB+17b] S. Posch, J. Hopfgartner, E. Berger, B. Zuber, R. Almbauer, and P. Schoellauf. Determination of the oil distribution in a hermetic compressor using numerical simulation. In *International Conference on Compressors and their Systems, London, GB*, 2017.

[PHH+15] S. Posch, J. Hopfgartner, M. Heimel, E. Berger, R. Almbauer, and P. Schoellauf. Fluid flow in the oil pumping system of a hermetic compressor. In *International Conference on Compressors and their Systems, London, GB*, 2015.

[PHH+16a] S. Posch, J. Hopfgartner, M. Heimel, E. Berger, R. Almbauer, and P. Schöllauf. A numerical friction loss analysis of the journal bearings in a hermetic reciprocating compressor. In *International Compressor Engineering Conference at Purdue, West Lafayette, USA, paper 1214*, 2016.

[PHH+16b] S. Posch, J. Hopfgartner, M. Heimel, E. Berger, R. Almbauer, and S. Stangl. Thermal analysis of a hermetic reciprocating compressor using numerical methods. In *International Compressor Engineering Conference at Purdue, West Lafayette, USA*, 2016.

[PHH+17] S. Posch, J. Hopfgartner, M. Heimel, E. Berger, R. Almbauer, and S. Stangl. Numerical analysis of the thermal behavior of a hermetic reciprocating compressor. *Journal of Earth Science and Engineering*, 7:1–9, 2017.

[PSRSO05] C.D. Perez-Segarra, J. Rigola, M. Soria, and A. Oliva. Detailed thermodynamic characterization of hermetic reciprocating compressors. *International Journal of Refrigeration*, 28:579–593, 2005.

[RJ07] F.A. Ribas Jr. Thermal analysis of reciprocating compressors. In *International Conference on Compressors and their Systems, London, GB*, 2007.

[RPSO09] J. Rigola, C.D. Perez-Segarra, and A. Oliva. Numerical simulation of piston leakage over hermetic reciprocating compressors behavior. In *International Conference on Compressors and their Systems, London, GB*, 2009.

[SD12] J. Sanvezzo and C. Deschamps. A heat transfer model combining differential and integral formulations for thermal analysis of reciprocating compressors. In *International Compressor Engineering Conference at Purdue, West Lafayette, USA*, 2012.

[SYM00] Y.H. Sim, Y. Youn, and M.K. Min. A study on heat transfer and performance analysis of hermetic reciprocating compressors for refrigerators. In *International Compressor Engineering Conference at Purdue, West Lafayette, USA*, 2000.

[SZ99] R. Scardovelli and S. Zaleski. Direct numerical simulation of free-surface and interfacial flow. *Annual Review Fluid Dynamics*, 31:567–603, 1999.

[TFPF92] M.L. Todescat, F. Fagotti, A. T. Prata, and R.T.S. Ferreira. Thermal energy analysis in reciprocating hermetic compressors. In *International Compressor Engineering Conference at Purdue, West Lafayette, USA*, 1992.

[THC+14] M.P. Tada, T. Hoffmann, P.R.C. Couto, A.L. Manke, and M.G.D. de Bortoli. Numerical and experimental examination for oil pump system using a simplified uncoupled simulation model. In *International Compressor Engineering Conference at Purdue, West Lafayette, USA*, 2014.

[VM07] H.K. Versteeg and W. Malalasekera. *An Introduction to Computational Fluid Dynamics, The Finite Volume Method*. Harlow: Pearson Prentice-Hall, 2007.

[WM08] E.J. Walsh and D. McEgliot. Relation of entropy generation to wall laws for turbulent flows. *International Journal of Computational Fluid Dynamics*, 22:649–657, 2008.

[Wos13] E. Woschke. *Simulation gleitgelagerter Systeme in Mehrkörperprogrammen unter Berücksichtigung mechanischer und thermischer Deformationen*. PhD thesis, Otto von Guericke University Magdeburg, 2013.

[Zac13] D. Zach. *Verlustteilung hermetischer Kältemittelkompressoren*. Master's thesis, Graz University of Technology, 2013.

Appendix

A Paper 1

S. Posch, J. Hopfgartner, M. Heimel, E. Berger, R. Almbauer, P. Schöllauf

A NUMERICAL FRICTION LOSS ANALYSIS OF THE JOURNAL BEARINGS IN A HERMETIC RECIPROCATING COMPRESSOR

23rd International Compressor Engineering Conference at Purdue, USA, 2016

A Numerical Friction Loss Analysis of the Journal Bearings in a Hermetic Reciprocating Compressor

Stefan POSCH[1]*, Johann HOPFGARTNER[1], Martin HEIMEL[1], Erwin BERGER[1], Raimund ALMBAUER[1], Peter SCHÖLLAUF[2]

[1] Institute of Internal Combustion Engines and Thermodynamics, Graz University of Technology, Inffeldgasse 19, 8010 Graz, Austria

posch@ivt.tugraz.at, +43 316 873 30233
hopfgartner@ivt.tugraz.at, +43 316 873 30240
heimel@ivt.tugraz.at, +43 316 873 30235
berger@ivt.tugraz.at, +43 316 873 30234
almbauer@ivt.tugraz.at, +43 316 873 30230

[2] Secop Austria GmbH, Jahnstraße 30, 8280 Fürstenfeld, Austria

p.schoellauf@secop.com, +43 3382 5010 984

* Corresponding Author

ABSTRACT

In addition to the electrical and the thermodynamic losses in hermetic compressors, mechanical losses have a significant influence on the performance of the compressor. In the present paper the friction losses in the journal bearings of a hermetic reciprocating compressor are investigated using numerical methods. A dynamic model is set up to solve the Reynolds equation using a finite volume approach to calculate the pressure field in each journal bearing. The calculation of the fluid film thickness is accomplished with the formulas of the parallel gap. The resulting hydrodynamic forces are equated with forces obtained by a dynamic multibody model of the compressor crank drive to calculate the transient orbit movement of the bearing. Based on the movement of the crankshaft at steady-state conditions, the shear stresses in the gap between crankshaft and housing can be calculated. Thus the cycle averaged friction power loss can be determined. To consider effects such as surface roughness of the bearings or possible contacts between the solids, correlations found in literature are implemented. The present method is used to assess the friction power loss of the journal bearings during the operation with different oil viscosities. The simulated data is verified by simple analytical friction loss calculations based on shear stresses in the Couette flow between bearing and housing.

1. INTRODUCTION

Hermetic compressors either running in ON-OFF or variable speed mode are widely used in domestic refrigeration appliances. The hermetic design of the compressors requests a durability of all the compressor parts of at least 15 years, which is specified by the producer of the cooling appliance. Another difficulty caused by the hermetic design is the complex interaction between electrical, mechanical and thermodynamic losses. The identification of the individual losses is one of the main tasks in the development process of modern hermetic reciprocating compressors. In addition to challenging experimental investigations, simulation models are increasingly used. An example of simulation application in compressor development is the quantification of friction losses in moving parts, especially in journal bearings. Due to the low absolute level of friction power losses (relative level with regard to compressor power is about 15 %) and the hermetic design, classical strip-down methods which are used in engine development are not suitable for the investigation of friction losses in reciprocating compressors for domestic refrigeration appliance. Several studies dealing with the modelling of the journal bearing dynamic behaviour are available. The studies resemble each other concerning the procedure to solve the friction loss problem of journal bearings. The procedure can be summarized as follows: (i) a multi body simulation of the compressor crank drive is carried out to get the dynamic loads on the journal bearings, (ii) the Reynolds equation is solved using numerical schemes to calculate the hydrodynamic forces in the bearings, (iii) a Newton-Raphson algorithm is used to get the movement of the shaft orbit and (iv) based on the shaft movement the friction losses can be determined. A distinction between these studies can be made concerning the modelling of the Reynolds equation or the model accuracy. The use of the short bearing approximation can be

found in e.g. Estupinan and Santos (2009) or Kim *et al.* (2012). A comparison between results of the short bearing approximation and the finite bearing model was carried out by Chieh *et al.* (2007). Duyar and Dursunkaya (2002 and 2006) analysed the dynamic behaviour of compressor journal bearings considering the elastic deformation of the shaft using finite element discretization. An investigation of compressor journal bearings considering mixed lubrication was presented in the work of Matsui *et al.* (2010).
The present paper deals with the investigation of the friction losses in compressor journal bearings for being used as input data for a holistic thermal model of a hermetic compressor. The method is similar to the previous explained procedure using finite bearing model for the solution of the Reynolds equation. Furthermore, mixed lubrication models found in the literature are considered. The gap in the bearing is approximated as parallel. The simulation is used to calculate the influence of the oil viscosity and gap width on the friction losses. The simulated data is compared to simple analytical friction loss calculations based on shear stresses in the Couette flow to give an assessment of the required accuracy of the model to fulfil the requirements of a thermal compressor model.

2. KINEMATICS AND DYNAMICS

The friction analysis of the compressor journal bearings requires the determination of the bearing forces. For this purpose a multibody dynamics model of the piston-conrod-crankshaft system is developed. A detailed description of the friction behaviour of the junctions between piston and conrod respectively conrod and crankshaft is not carried out in the present study. Moreover, the misalignment of the piston is not considered. Figure 1 shows the coordinate systems used for the kinematic description of the crank mechanism parts. The inertial coordinate system is located in the static position of bearing A. The misalignment of the crankshaft due to the bearing eccentricity is considered in the distance and rotating vector of the crankshaft regarding to the initial coordinate system.

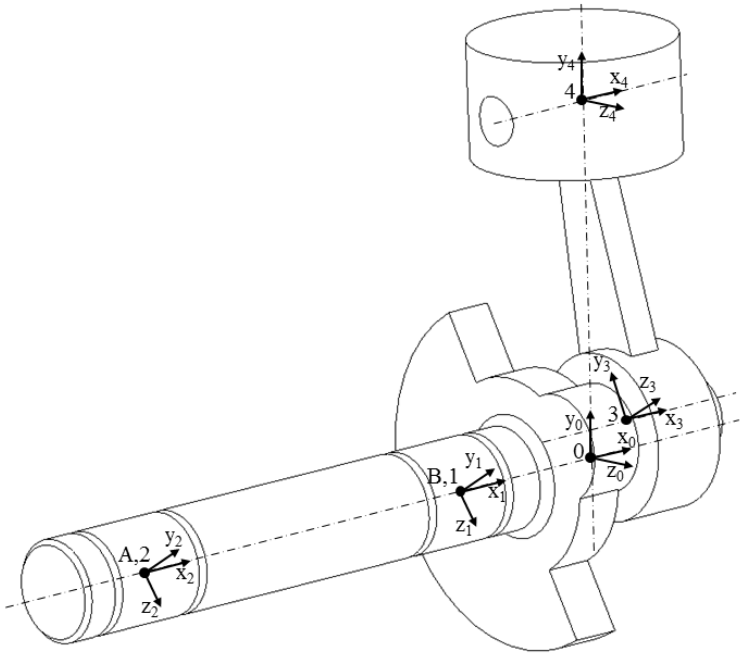

Figure 1: Coordinate systems

Using the Newton-Euler method the equations of motion can be expressed for each part.

Piston:

$$m_{Pi} \cdot {}_I\boldsymbol{a}_{Pi} = {}_I\boldsymbol{F}_p - {}_I\boldsymbol{F}_4 + {}_I\boldsymbol{F}_{Cyl} \tag{1}$$

Conrod:

$$m_{Cr} \cdot {}_I\boldsymbol{a}_{Cr} = {}_I\boldsymbol{F}_4 - {}_I\boldsymbol{F}_3 \tag{2}$$

$${}_I\Theta_{Cr} \cdot \dot{\omega}_{Cr} + m_{Cr} \cdot {}_I\boldsymbol{r}_{3-Cr} \times {}_I\boldsymbol{a}_{Cr} = {}_I\boldsymbol{r}_{3-4} \times {}_I\boldsymbol{F}_4 \tag{3}$$

Crankshaft:

$$m_{Cs} \cdot {}_I\boldsymbol{a}_{Cs} = {}_I\boldsymbol{F}_A + {}_I\boldsymbol{F}_B + {}_I\boldsymbol{F}_3 \tag{4}$$

$${}_I\Theta_{Cs} \cdot \dot{\omega}_{Cs} + \omega_{Cs} \times \left({}_I\Theta_{Cs} \cdot \omega_{Cs} \right) + m_{Cs} \cdot {}_I\boldsymbol{r}_{1-Cs} \times {}_I\boldsymbol{a}_{Cs} = {}_I\boldsymbol{r}_{1-2} \times {}_I\boldsymbol{F}_A + {}_I\boldsymbol{r}_{1-3} \times {}_I\boldsymbol{F}_3 + \boldsymbol{T} \tag{5}$$

The set of equations gives the time dependent functions of the reaction forces in the main journal bearings according to the cylinder pressure. The cylinder pressure can be determined by experiments or computational fluid dynamics (CFD), respectively. In the present study the cylinder pressure is given by CFD simulation of the compressor gas line.

$${}_I\boldsymbol{F}_p = \begin{pmatrix} 0 \\ p_{CFD} \cdot A \\ 0 \end{pmatrix} \tag{6}$$

3. HYDRODYNAMIC FORCES

The modelling of the hydrodynamic forces in the journal bearings is carried out by solving the Reynolds equation which links the hydrodynamic pressure and the fluid film thickness.

$$\frac{\partial}{\partial x}\left(\frac{\rho\, h^3}{12\eta}\frac{\partial p_h}{\partial x}\right) + \frac{\partial}{\partial y}\left(\frac{\rho\, h^3}{12\eta}\frac{\partial p_h}{\partial y}\right) = \frac{(u_I + u_{II})}{2}\frac{\partial(\rho h)}{\partial x} + \frac{\partial(\rho h)}{\partial t} \tag{7}$$

The terms on the left-hand side of the Reynolds equation represent the Poiseuille flow, the terms on the right-hand side represent the Couette flow and the displacement flow, respectively. To solve this kind of partial, inhomogeneous elliptic differential equation, numerical methods have to be applied. In the present study the Reynolds equation is solved using the finite volume approach. The fluid film area in each bearing is divided in a certain number of cells and the terms of the Reynolds equation can be discretised. To avoid negative fluid film pressures, the Gümbel boundary condition is used which sets negative pressure values to zero. Figure 2 shows the hydrodynamic pressure distribution in bearing A without (a) and with (b) Gümbel boundary condition.

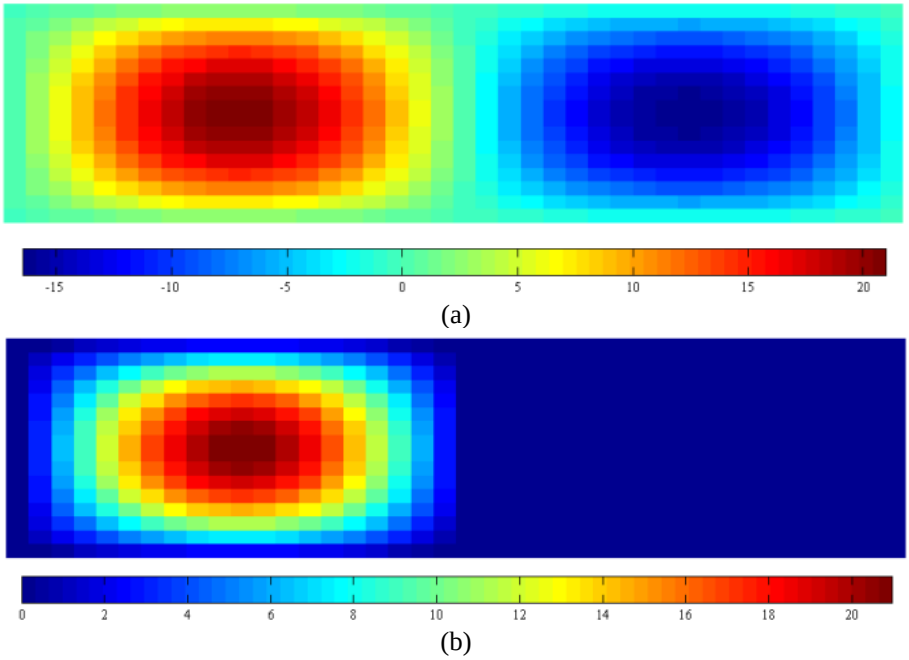

Figure 2: Hydrodynamic pressure in bearing A without (a) and with (b) Gümbel boundary condition [MPa]

To create a link between the eccentricity of the bearing and the fluid film thickness, the gap in the bearing is assumed to be parallel. According to the geometric relations shown in Figure 3 the fluid film thickness can be expressed as follows (Woschke, 2013):

$$h(\varphi) = (r_I - r_{II}) - ex \cdot \cos(\varphi - \xi) \tag{8}$$

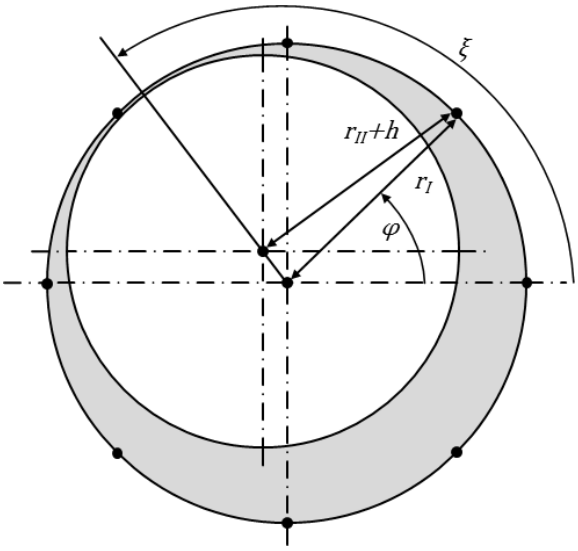

Figure 3: Determination of the fluid film thickness

The basic form of the Reynolds equation (7) considers only the macro geometry of the bearing parts. Patir and Cheng (1978 and 1979) introduced an extended form of the Reynolds equation to consider also micro effects due to surface roughness. The authors used flow factors which depend on the roughness of the bearing surface and called the new form Average Reynolds Equation.

$$\frac{\partial}{\partial x}\left(\phi_x \frac{\rho\, h^3}{12\eta}\frac{\partial \overline{p_h}}{\partial x}\right)+\frac{\partial}{\partial y}\left(\phi_y \frac{\rho\, h^3}{12\eta}\frac{\partial \overline{p_h}}{\partial y}\right)=\frac{(u_I+u_{II})}{2}\left(\frac{\partial\left(\rho\overline{h_T}\right)}{\partial x}+\sigma_\delta\frac{\partial \phi_S}{\partial x}\right)+\frac{\partial\left(\rho\overline{h_T}\right)}{\partial t} \tag{9}$$

For a more detailed description of the flow factor determination the interested reader is referred to the primary works by Patir and Cheng (1978 and 1979). To calculate the possible solid contact between the surfaces the model of Greenwood and Tripp (1970) is used in the present study.

4. NUMERICAL ALGORITHM

The solving procedure starts with the input of the geometric data of the compressor crank mechanism parts. Initial values of eccentricity *ex* and minimum fluid film thickness angle ξ are set to zero as well as their time derivatives. Time resolution is fixed for the whole procedure and corresponds to a crank angle of two degrees. Starting at a certain position of the crankshaft (here crankshaft angle is zero) the cylinder pressure of the CFD calculation is read into the bearing simulation program. Solving the multibody dynamic system, the bearing forces can be calculated for the current crank angle. The calculation of the hydrodynamic bearing forces starts with the determination of the fluid film thickness according to (8) with the defined start values of the new time step. The start values of the new time step are the calculated eccentricity *ex* and minimum fluid film thickness angle ξ of the previous time step or the initial values if it is the first time step, respectively. To get the orbit of the crankshaft for the current time step, a two-dimensional Newton algorithm depending on *ex* and ξ is used (10). In each iteration step the Averaged Reynold Equation (9) is solved numerically for both bearings and the hydrodynamic bearing forces are compared with the calculated bearing forces of the multibody system regarding absolute value and force direction. If the deviation between hydrodynamic and multibody forces in both bearings is higher than the convergence criteria β_F the iteration procedure is repeated, otherwise the algorithm proceeds to the next time step. The numerical algorithm is carried out until the deviation of the time-dependent shaft orbit between the current and the previous cycle is lower than the convergence criteria β_C and steady-state conditions are reached.

$$\begin{aligned} \boldsymbol{x} &= \begin{pmatrix} ex \\ \xi \end{pmatrix} \\ \boldsymbol{f}(\boldsymbol{x}) &= \boldsymbol{F}_{MBS} - \boldsymbol{F}_{Rey} \\ \boldsymbol{x}_{n+1} &= \boldsymbol{x}_n - \left(\boldsymbol{J}_f(\boldsymbol{x}_n)\right)^{-1}\boldsymbol{f}(\boldsymbol{x}_n) \end{aligned} \tag{10}$$

5. RESULTS

The present numerical bearing model is used to simulate hydrodynamic bearings of a hermetic reciprocating compressor running at 3000 rpm. The pressure in the cylinder is determined by CFD simulation of the compressor gas line considering fluid-structure interaction of the compressor valves. Operating conditions are set to -23 °C for evaporating temperature and 45 °C for condensing temperature (R600a), respectively. The baseline value for oil viscosity is 8 cSt and bearing clearance is 5 µm. Bearing width of bearing A is one quarter less than bearing B, whereas the shaft diameter is equal for both bearings.

Figure 4 shows the shaft orbits of both bearings as a function of the oil viscosity. The illustrated curves represent one crankshaft revolution after steady-state conditions are reached which is the case after 7-8 cycles depending on the considered configuration. According to the higher forces due to the compression process at bearing B the eccentricity ratio of bearing B is higher than bearing A. An increase of the oil viscosity results in a decrease of the shaft deflection. Furthermore, higher oil viscosities damp the relative motion between the bearing parts and thus the crankshaft orbit is focused on a smaller region. The influence of the shaft orbit on the bearing clearance is shown in Figure 5. The curves show an increase of the eccentricity ratio of both bearings with an increased bearing clearance. This behaviour is a result of the nonlinear relation between the bearing pressure and the local oil film thickness. Small bearing clearance already yields in higher oil pressure at small shaft movement, so the deflection of the crankshaft is kept at low values. This effect can be seen in the shape of the crank orbit which is smoother at smaller bearing clearance values.

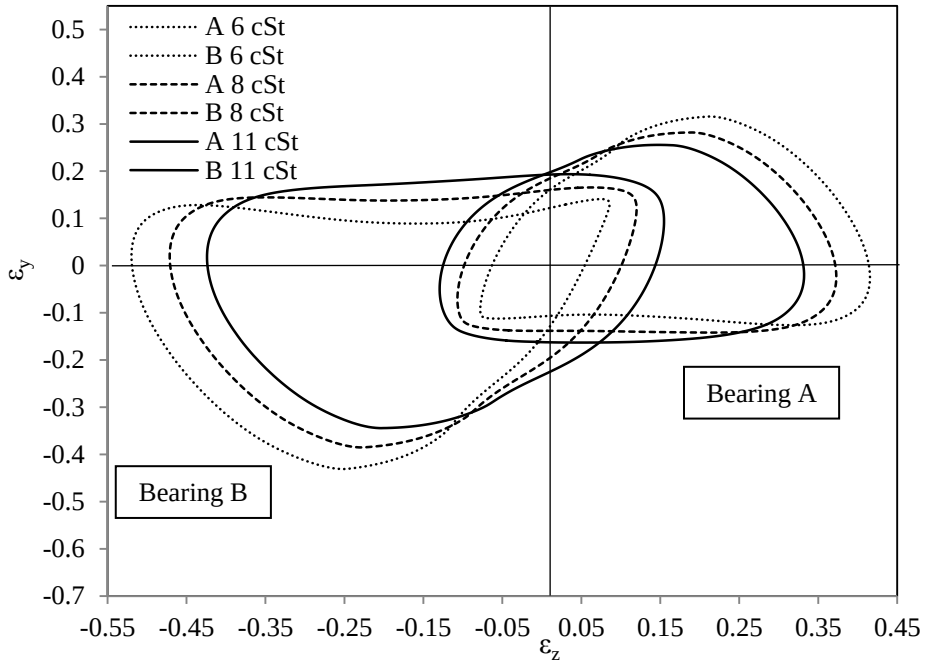

Figure 4: Shaft orbits with different oil viscosity

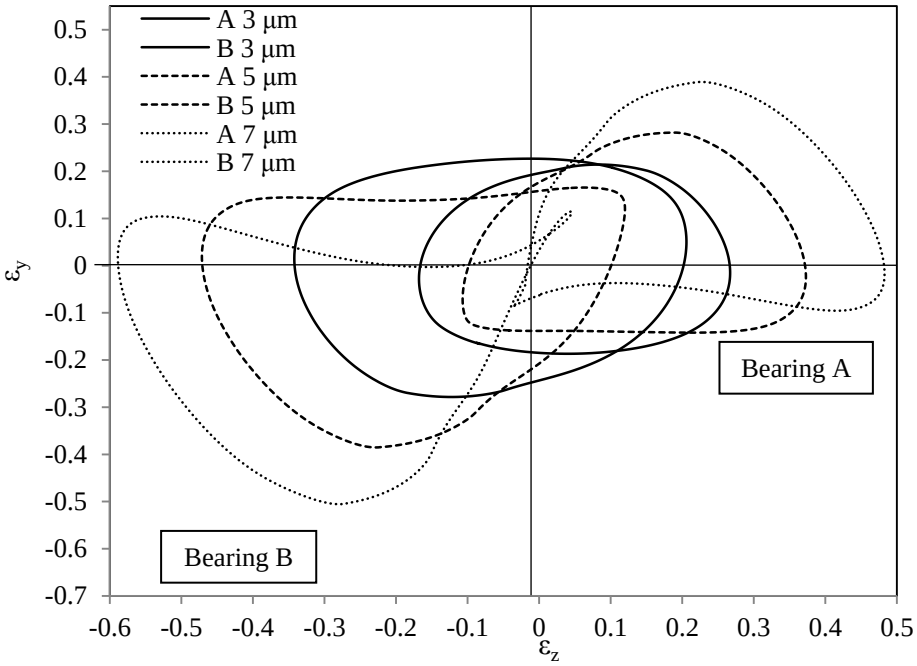

Figure 5: Shaft orbits with different bearing clearances

An addition illustration of the simulated shaft movement in terms of the absolute eccentricity ratio ε over the crank angle φ can be seen in Figure 6 and 7. According to the shaft orbit curves the eccentricity ratio of bearing B is higher than of bearing A. The figures show the peak in the eccentricity curve in the area of the top-dead centre of the compressor piston and the resulting high reaction forces in the piston-conrod-crankshaft system. The nonlinear dependence between bearing pressure and local oil film thickness (and its time derivatives) can also be seen in the eccentricity ratio curves. Curves of different viscosity or gap width can intersect especially in regions of low reaction forces and small eccentricity ratios.

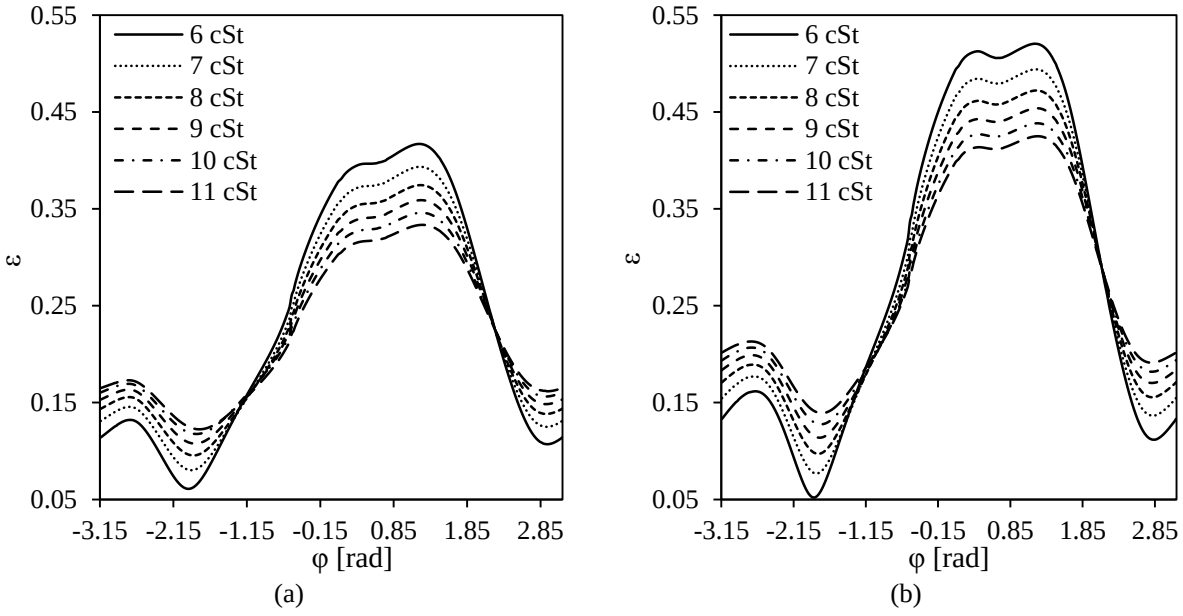

Figure 6: Eccentricity ratio over one crank shaft revolution of bearing A (a) and bearing B (b)

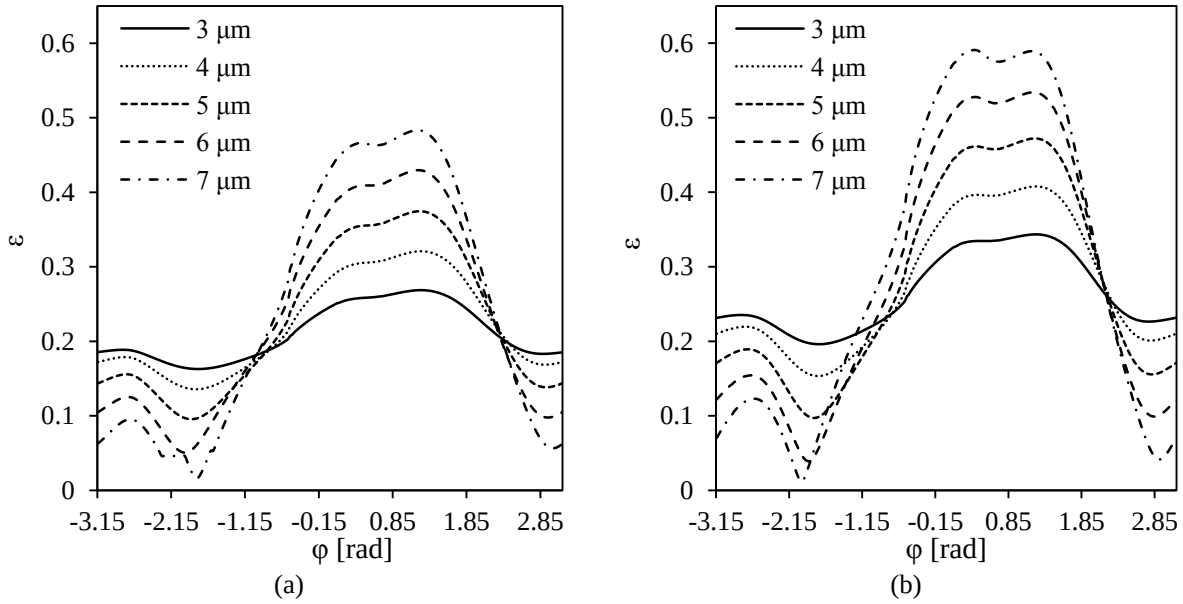

Figure 7: Eccentricity ratio over one crank shaft revolution of bearing A (a) and bearing B (b)

Results of the determination of the friction power loss in the bearings are shown in Figure 8. Friction power loss values of bearing B are higher than of bearing A. This is because of the higher reaction forces in addition with the larger bearing width of bearing B which results in higher friction surface. Viscosity variations show a linear dependency of the friction power loss increasing with higher viscosities. The numerical simulation of the friction power loss with different gap widths shows a stronger power loss increase at smaller gap widths. A comparison between numerical results and simple analytical Couette flow calculation show constant curve offset for a viscosity variation. For gap width investigation, the offset between numerical and analytical results increases for higher gap widths. Generally, the deviation between numerical and analytical results is significantly higher for higher loaded bearings like bearing B in the present study.

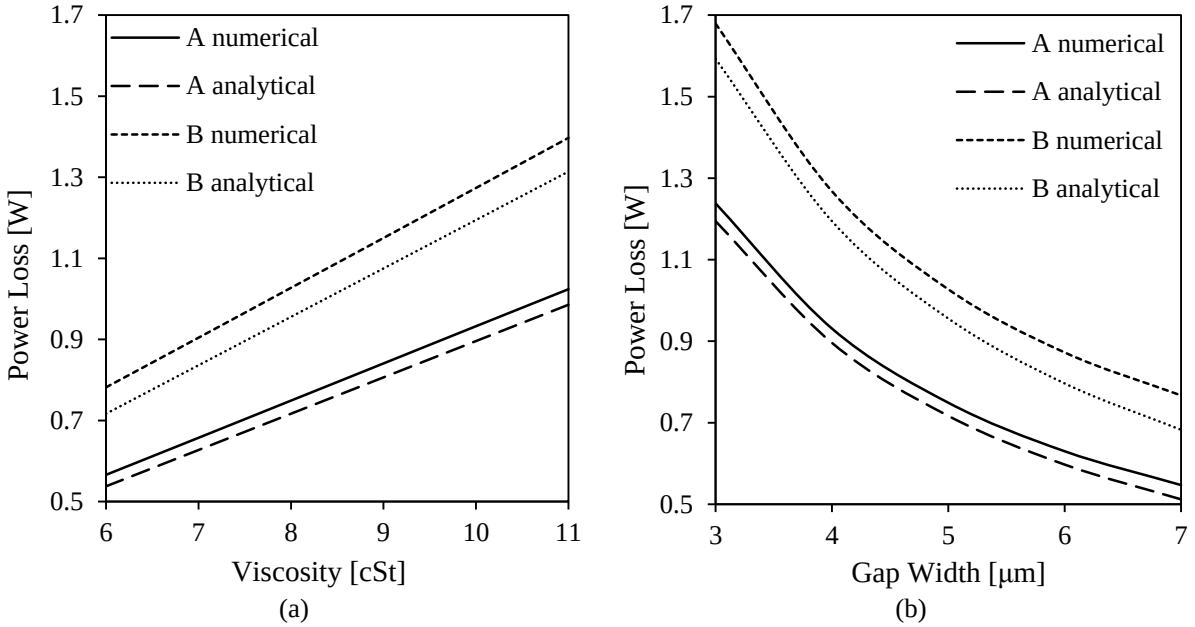

Figure 8: Power loss as function of viscosity (a) and gap width (b)

A comparison between the simulations with and without the usage of Patir and Cheng's (1978 and 1979) Average Reynolds Equation yields in friction power loss deviations below 1 %. It should be mentioned, that the maximum determined eccentricity ratios of both bearings in the present study are significant smaller than 1 so the influence of the surface roughness on the friction power loss is also small. In simulations of compressor

operating points with higher cylinder pressure which results in higher reaction forces in the bearings the eccentricity ratio will increase and thus the surface roughness influence on the friction power loss will also increase. Similar considerations can be made regarding the influence of the shaft movement in the multibody dynamics. Stronger shaft movement influences the dynamics of the piston-conrod-crankshaft system and consequently the hydrodynamics of the bearings. In the present study the influence of the shaft movement consideration on the friction power loss is below 1 %.

6. CONCLUSION

A numerical investigation of the hydrodynamic bearing system of a hermetic reciprocating compressor is shown in this study. The model is based on the solution of the Average Reynolds Equation of Patir and Cheng (1978 and 1979) to compare hydrodynamic bearing forces with reaction forces gained by multibody dynamics calculation which results in a two-dimensional Newton algorithm problem for the fluid film properties *ex* and ξ. The presented algorithm is used to calculate the dynamic behaviour of the journal bearings of the compressor operating at -23 °C evaporating temperature and 45 °C condensing temperature (R600a). A parameter study for several oil viscosities and gap widths are carried out to show the abilities of the method for the compressor development. Additionally, the present algorithm is used to calculate the friction power losses of the journal bearings. In terms of the friction power loss modelling, the following conclusions can be emphasized:

- The comparison between numerical and analytical (simple Couette flow) simulations show a similar dependence of the parameters, but analytical simulation underestimates friction power losses especially at higher loaded bearings.
- The use of the complex Averaged Reynolds Equation of Patir and Cheng (1978 and 1979) can be avoided at lower loaded bearings with small shaft movements. In this case, the classical Reynolds equation can be used.
- A similar conclusion can be made for the consideration of the shaft movement in the multibody dynamics. Small shaft movements can be neglected here.

NOMENCLATURE

$\boldsymbol{a}$	acceleration vector	(m/s²)	Cyl	cylinder	
A	area	(m²)	I	inertial system	
ex	eccentricity	(m)	I, II	shaft, bearing	
$\boldsymbol{F}$	force vector	(N)	MBS	multi body system	
h	fluid film thickness	(m)	Pi	piston	
m	mass	(kg)	Rey	Reynolds forces	
p	pressure	(N/m²)	**Greek symbols**		
$\boldsymbol{r}, \boldsymbol{x}$	distance vector	(m)	β	convergence criteria	(-)
t	time	(s)	ε	relative eccentricity	(-)
$\boldsymbol{T}$	torque moment vector	(N m)	η	dynamic viscosity	(N s/m²)
u	velocity	(m/s)	Θ	inertia tensor	(kg m²)
x, y, z	distance components	(m)	ξ	minimum fluid film thickness angle	(°)
Subscripts			ϕ_x, ϕ_y, ϕ_s	flow factors	(-)
0, 1, 2, 3, 4	coordinate system index		φ	attitude angle	(°)
A, B	bearing index		ω	rotational speed	(s^{-1})
Cr	conrod		ρ	density	(kg/m³)
Cs	crankshaft		σ_δ	standard deviation of the combined roughness	(m)

REFERENCES

Chieh, H., Couto, P.R.C., Prata, A.T. (2007). An Integral Analysis and Simulation of the Complete Bearing System in Reciprocating Hermetic Compressors. *Proceedings of the International Conference on Compressors and their Systems*, City University, London, GB, paper 658054.

Duyar, M., Dursunkaya, Z. (2002). Design Improvement of a Compressor Bearing Using an Elastohydrodynamic Lubrication Model. *Proceedings of the International Compressor Engineering Conference at Purdue*, Purdue University, IN, USA, paper 1537.

Duyar, M., Dursunkaya, Z. (2006). Design Improvement Based on Wear of a Journal Bearing Using an Elastohydrodynamic Lubrication Model. *Proceedings of the International Compressor Engineering Conference at Purdue*, Purdue University, IN, USA, paper 1821.

Estupinan, E.A., Santos, I.F. (2009). Modelling Hermetic Compressors Using Different Constraint Equations to Accommodate Multibody Dynamics and Hydrodynamic Lubrication. *Journal of the Brazilian Society of Mechanical Science and Engineering*, Volume 31, pages 35-46.

Greenwood, J.A., Tripp, J.H. (1970). The contact of two nominally flat rough surfaces. *Proceedings of the Institution of Mechanical Engineers*, Volume 185, pages 635-633.

Kim, J., Park, S., Cho, I., Baek, I., Jo, J., Jung, J. (2012). Journal Bearing Lubrication Characteristics in a Reciprocating Compressor. *Proceedings of the International Compressor Engineering Conference at Purdue*, Purdue University, IN, USA, paper 1263.

Matsui, M., Kitsunai, Y., Inagaki, K. (2010). High Efficiency Development of a Reciprocating Compressor by Clarification of Loss Generation in Bearings. *Proceedings of the International Compressor Engineering Conference at Purdue*, Purdue University, IN, USA, paper 2025.

Patir, N., Cheng, H.S. (1978). An average model for determining effects of three-dimensional roughness on partial hydrodynamic lubrication. *Journal of Lubrication Technology*, Volume 100, pages 12-17.

Patir, N., Cheng, H.S. (1979). Application of average flow model to lubrication between rough sliding surfaces. *Journal of Lubrication Technology*, Volume 101, pages 220-230.

Woschke, E. (2013). Simulation gleitgelagerter Systeme in Mehrkörperprogrammen unter Berücksichtigung mechanischer und thermischer Deformation. *PhD Thesis*, Otto von Guericke University Magdeburg, GER.

ACKNOWLEDGEMENT

This work has been carried out within the framework of ECO-COOL, a research project initiated and funded by the FFG (Austrian Research Promotion Agency). Furthermore the authors particularly acknowledge the technical support by Secop Austria GmbH, formerly ACC Austria GmbH and Liebherr-Hausgeräte Lienz GmbH.

B Paper 2

S. Posch, J. Hopfgartner, M. Heimel, E. Berger, R. Almbauer, P. Schöllauf

A NUMERICAL INVESTIGATION OF THE OIL PUMP SUCTION BEHAVIOR IN A HERMETIC RECIPROCATING COMPRESSOR

23rd International Compressor Engineering Conference at Purdue, USA, 2016

A Numerical Investigation of the Oil Pump Suction Behaviour in a Hermetic Reciprocating Compressor

Stefan POSCH[1]*, Johann HOPFGARTNER[1], Martin HEIMEL[1], Erwin BERGER[1], Raimund ALMBAUER[1], Peter SCHÖLLAUF[2]

[1] Institute of Internal Combustion Engines and Thermodynamics, Graz University of Technology, Inffeldgasse 19, 8010 Graz, Austria

posch@ivt.tugraz.at, +43 316 873 30233
hopfgartner@ivt.tugraz.at, +43 316 873 30240
heimel@ivt.tugraz.at, +43 316 873 30235
berger@ivt.tugraz.at, +43 316 873 30234
almbauer@ivt.tugraz.at, +43 316 873 30230

[2] Secop Austria GmbH, Jahnstraße 30, 8280 Fürstenfeld, Austria
p.schoellauf@secop.com, +43 3382 5010 984

* Corresponding Author

ABSTRACT

In addition to the adequate lubrication of the moving parts, the oil flow in a hermetic reciprocating compressor has a significant influence on the thermal characteristics of a compressor. The present work is concerned with the investigation of the oil pump system of a reciprocating hermetic compressor used in household refrigeration appliances. The considered oil pump system consists of a centrifugal pump immersed in the oil sump of the hermetic compressor and a helical groove machined on the crankshaft. The focus of this work lies on the immersed part of the centrifugal oil pump and its interaction with the oil in the oil sump. To analyse the flow in the immersed area of the oil pump, the commercial computational fluid dynamics (CFD) software ANSYS Fluent is used. The free surface of the oil flow is modelled with the Volume of Fluid (VOF) method. A numerical investigation is used to study the influence of the immersion depth and the oil pump design on oil mass flow rate and flow field at the oil pump intake. To evaluate the oil pump regarding the applicability in variable speed compressors, the influence of the rotational speed on the oil mass flow is also explored.

1. INTRODUCTION

The most common compressor type used in domestic refrigeration appliance is the hermetic reciprocating compressor. This kind of compressor uses a reciprocating piston driven by a slider-crank mechanism for suction, compression and discharge of the refrigerant. Small-scale hermetic reciprocating compressors have a crankshaft which is directly driven by the electric motor. In addition to the energy transfer from the motor to the piston, the crankshaft acts also as oil pump device. Depending on the compressor type and the required amount of oil, different oil pump designs are used which differ in the arrangement of centrifugal and helical pumps. Several studies are available which deal with the investigation of single pumping parts or the entire oil pump, respectively. A numerical study of a compressor oil pump using commercial CFD software can be found in Lückmann *et al.* (2009) and Kerpicci *et al.* (2013). The authors used the Volume of Fluid (VOF) technique to model the two-phase flow in three dimensions. Besides the calculation of the oil mass flow rate, specific focus was laid on the determination of the oil climbing time. To keep the number of cells and therefore the computational time under a tolerable limit, several simplifications like the neglect of the gap between shaft and crankcase in the helical grove have to be made. Kim *et al.* (2002) used the analogy between the oil supply system of a reciprocating compressor and an electric circuit. The authors described the pumping parts by equivalent electric elements to get a mathematical model of the system. A validation of the simulation results by experimental data showed good agreement in terms of the oil flow rate. The fluid flow in helical pumps using analytical models is analysed in the works of Alves *et al.* (2009 and 2010). Thereby, the Navier-Stokes equations were adapted to a finite channel with specific boundary conditions. The gap between shaft and crankcase was neglected in these studies. Different techniques like generalized integral transform technique have been presented to solve the resulting equation. A more detailed investigation of helical groove oil pumps was

presented by Posch *et al.* (2015). In this study, the oil flow in channel direction is assumed to be fully developed and the 2d flow in the channel cross section has been calculated considering the gap between shaft and crankcase. The pressure gradient in channel direction can be considered to get the ability to couple the helical groove with other pumping parts. In Tada *et al.* (2014) an uncoupled simulation of the helical pump of a reciprocating compressor using commercial CFD software is shown. The method has been utilized to analyse the applicability of an oil pump for the use in variable speed compressors. The authors calculated the volumetric oil flow depending on the rotational speed and immersion depth of the shaft in the compressor oil sump. Another example of the use of commercial CFD software to analyse the performance of a compressor lubrication system can be found in Ozsipah *et al.* (2014). In addition to the investigation of the influence of geometric parameters on the pumped oil mass flow, the suction behaviour of the oil pump was analysed. Therefore, the oil sump of the compressor was also modelled, assuming that the oil expelled from the oil pump does not flow back into the oil sump. A calculation of the oil mass flow rate, transient oil distribution and pressure fluctuations at the pump inlet, depending on geometrical parameters, was carried out.
The present paper focuses on the investigation of the suction behaviour of a hermetic reciprocating compressor oil pump. Therefore, an uncoupled simulation of the immersed centrifugal pump interacting with the oil sump using commercial CFD software ANSYS Fluent is carried out. To increase the accuracy of the simulation, the expelled oil is assumed to be transported back into the oil sump. The approach is utilized to get an insight in the suction behaviour of the oil pump in dependence on the immersion depth, pump design and rotational speed. Additionally, an assessment according to the oil mass flow rate of the different cases is presented.

2. MODELLING

2.1 Theoretical background

Computational fluid dynamics (CFD) simulation is based on the solution of the flow governing equations using numerical methods. The governing equations for mass and momentum are as follows (Moukalled *et al.*, 2015):

$$\frac{\partial \rho}{\partial t} + \nabla \cdot [\rho \boldsymbol{v}] = 0 \tag{1}$$

$$\frac{\partial}{\partial t}[\rho \boldsymbol{v}] + \nabla \cdot \{\rho \boldsymbol{v}\boldsymbol{v}\} = -\nabla p + \mu \nabla^2 \boldsymbol{v} + \boldsymbol{f}_b \tag{2}$$

The simulation domain is divided into a finite number of cells, the so called control volumes. The governing equations are spatial discretized on the control volumes using the finite volume method to get a linear system of equations which is solved by mathematical methods. Commercial CFD software like ANSYS Fluent, which is used in the present study, executes these steps automatically.
Two phase flows with sharp interface are calculated with the volume of fluid approach (VOF) by Scardovelli and Zaleski (1999) which is implemented in ANSYS Fluent. The VOF approach models two or more immiscible fluids by tracking the volume fraction of each fluid in the domain, solving the volume fraction equation (3). Fluid properties like density or viscosity can be determined by summing up the volume fraction weighted values (4 and 5).

$$\frac{\partial \chi}{\partial t} + \frac{\partial (u_i \chi)}{\partial x_i} = 0 \tag{3}$$

$$\rho = \rho_g \chi + \rho_l (1 - \chi) \tag{4}$$

$$\mu = \mu_g \chi + \mu_l (1 - \chi) \tag{5}$$

Further information about the VOF method can be found in the work of Scardovelli and Zaleski (1999) and the Fluent User Guide (2011).

2.2 Simulation domain

The investigated compressor oil pump consists of three single pump parts: a helical pump and two centrifugal pumps at the inlet and outlet of the crankshaft, respectively. To increase the oil mass flow rate, the considered oil pump is designed with a spiral sheet (catcher) at the pump inlet. The aim of the present study is to investigate the suction behaviour of the oil pump and the flow conditions at the pump inlet. Therefore, an uncoupled simulation of the centrifugal pump at the crankshaft inlet in combination with a simplified oil sump is carried out. The computational mesh is created with about 250.000 cells for the pump and about 400.000 cells for the sump,

respectively. The mesh is refined at interfaces, inlet and outlet to increase simulation accuracy. Figure 1 shows the position of the centrifugal pump in the crankshaft (a) and the computational mesh (b).

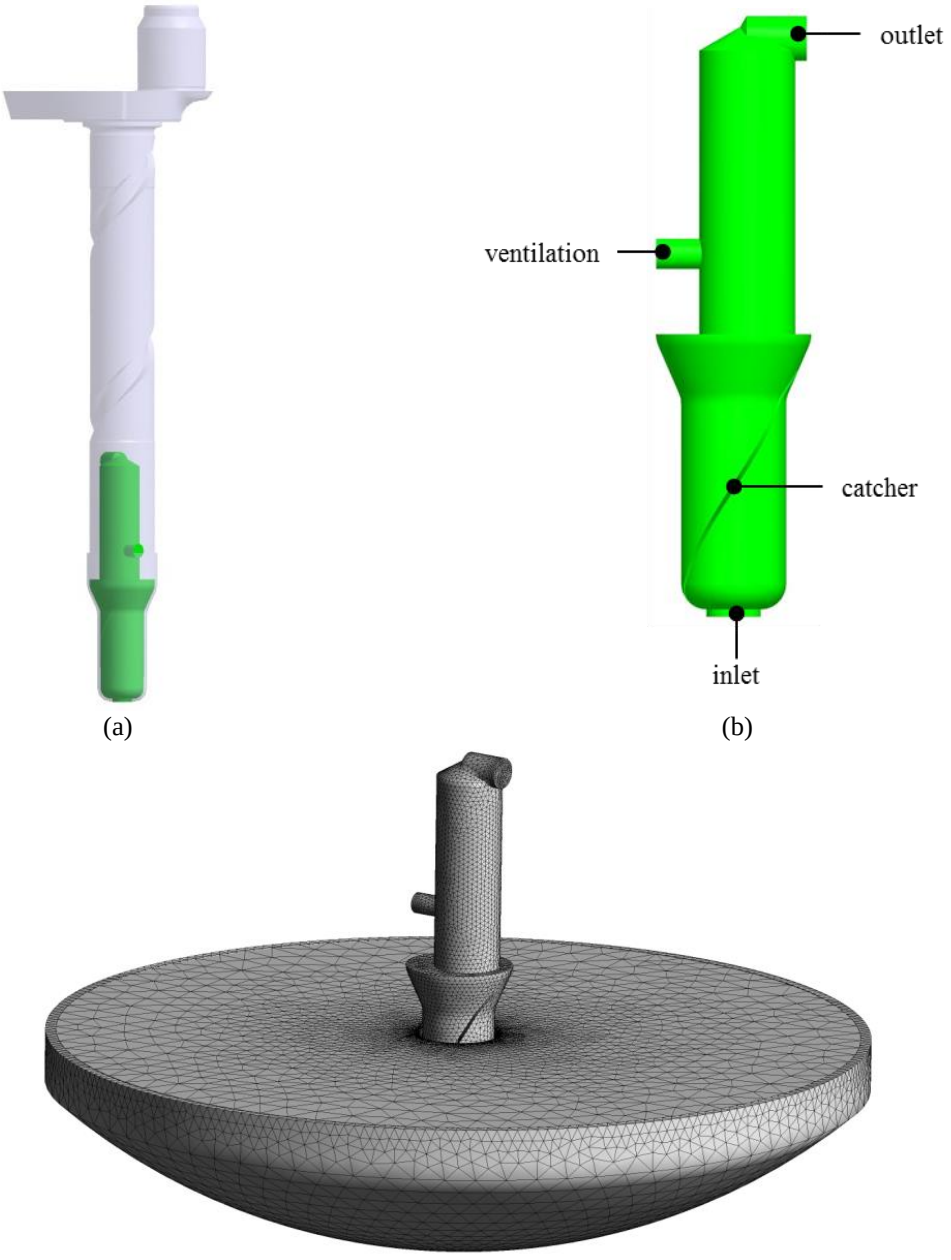

Figure 1: Position of the centrifugal pump (a), geometrical domain (b) and computational mesh (c)

To fulfil the overall mass balance, the oil at the outlet of the pump is filled back into the oil sump at the outer area of the oil sump surface to reproduce the wall oil flow. A mass flow boundary condition which is linked to the pump outlet via user defined function (UDF) is applied on the outer area of the oil sump surface. On the rest of the oil sump surface, a pressure inlet boundary condition with zero relative pressure is applied. At pump outlet and ventilation hole, a pressure outlet boundary condition is used with also zero relative pressure. To decrease computational time, the pump is filled with oil according to the current immersion depth at the initialization process. The simulation is carried out until pressure at the pump/sump interface and oil mass flow at the pump outlet show a steady-state behaviour.

2.3 Assumptions and Settings

The following assumptions are made for the simulation of the centrifugal pump and the compressor oil sump:

- Isothermal flow.
- Acceleration at the compressor start-up is infinite.
- Air is used for the gaseous phase.
- Dissolving of gaseous phase in liquid phase is neglected.
- Physical properties of the fluids are constant.
- Laminar flow.

The oil density is set to 832 kg m^{-3} and the oil viscosity is set to 6.7 x 10^{-3} Pa s. Surface tension is considered and is set to 0.028 N m^{-1}.

The simulation is carried out using implicit VOF method in combination with bounded second order implicit time formulation. The spatial discretization of the momentum equation is utilized with a second order upwind scheme (Moukalled *et al.*, 2015) and, for the volume fraction equation, the compressive scheme is used. The pressure-velocity coupling is executed with the PISO (pressure-implicit with splitting of operators) algorithm (Isaa, 1986). Time step is set to 10^{-4} s and double precision mode is utilized.

3. RESULTS

The important properties to value the functionality of oil pumps for the usage in hermetic compressors are the oil mass flow rate, the oil climbing time and the oil distribution. To quantify the influence of the immersion depth, the rotational speed and the pump design on the mentioned parameters, a basic configuration with 7 mm immersion depth and 3000 rpm rotational speed in combination with the original geometry is used.
Figure 2 shows the oil volume fraction depending on the immersion depth at different time steps during the compressor start-up until and after reaching stead-state conditions. The figures show the development of the oil parabola due to the centrifugal forces. Although the variant with the highest immersion depth gives the highest static pressure at the pump inlet due to the hydrostatic pressure, the oil parabola sinks nearly to the pump inlet at the beginning of compressor start-up. This can be explained by the increasing friction forces on the outer surface which induce centrifugal forces. The centrifugal forces reduce the static pressure at the pump inlet. If the oil parabola would reach the pump inlet, the oil flow would break down immediately.

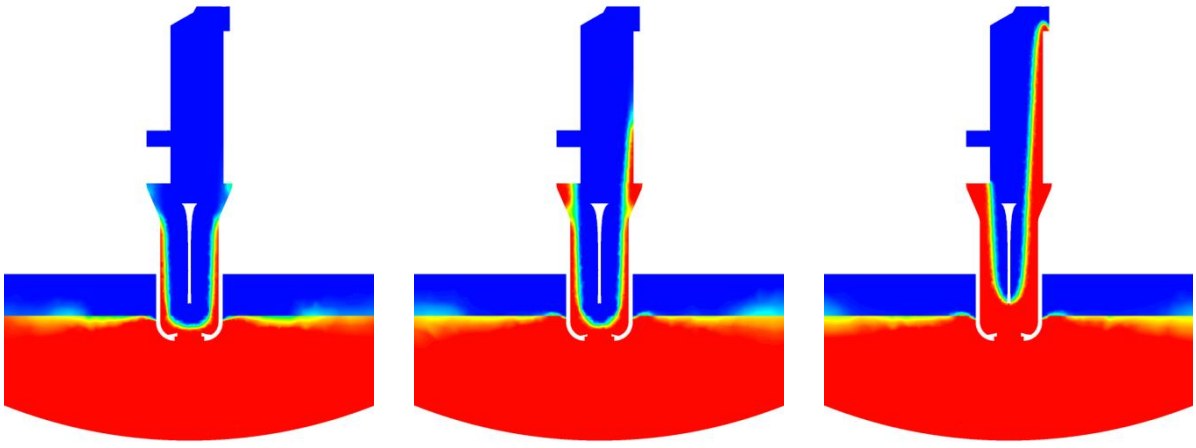

0.12s (a) 0.24s (b) 1s (c)

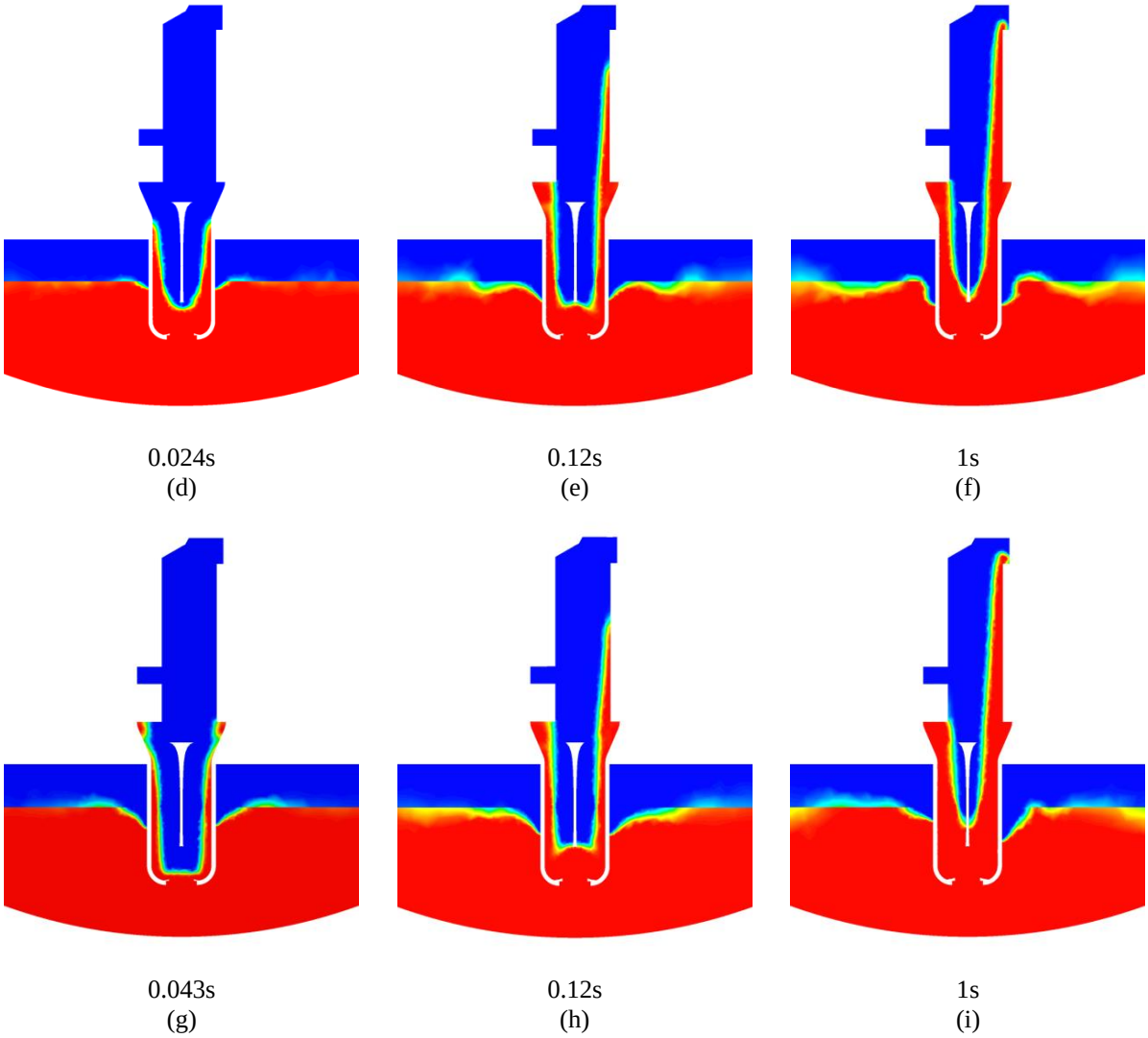

Figure 2: Oil volume fraction of 3 mm (a) - (c), 7 mm (d) - (e) and 9 mm (g) - (i) immersion depth at different flow time

The oil volume fraction at steady-state conditions for rotational speed variations and two different design variants can be seen in Figure 3. The results of the simulation show the increasing steepness of the oil parabola at higher rotational speed which leads to a lower oil level inside the pump. As already mentioned, if the oil parabola reaches the pump inlet, the oil mass flow would break down. Figure 3 (c) and Figure 3 (d) show two different design variants. Design 1 has a larger pump inlet diameter compared to the original geometry. Design 2 has the same diameter at the pump inlet, but compared to the original geometry, the conical shape is replaced by a cylindrical shape, thus the volume in the lower region of the pump is larger. The oil volume fraction of pump design 1 shows an uneven shape of the oil parabola due to the influence of the spiral sheet which interacts with the oil in the sump. A comparison between design 2 and the original geometry shows similar shape of the oil parabola and an increased amount of oil in the catcher due to the higher volume of design 2.

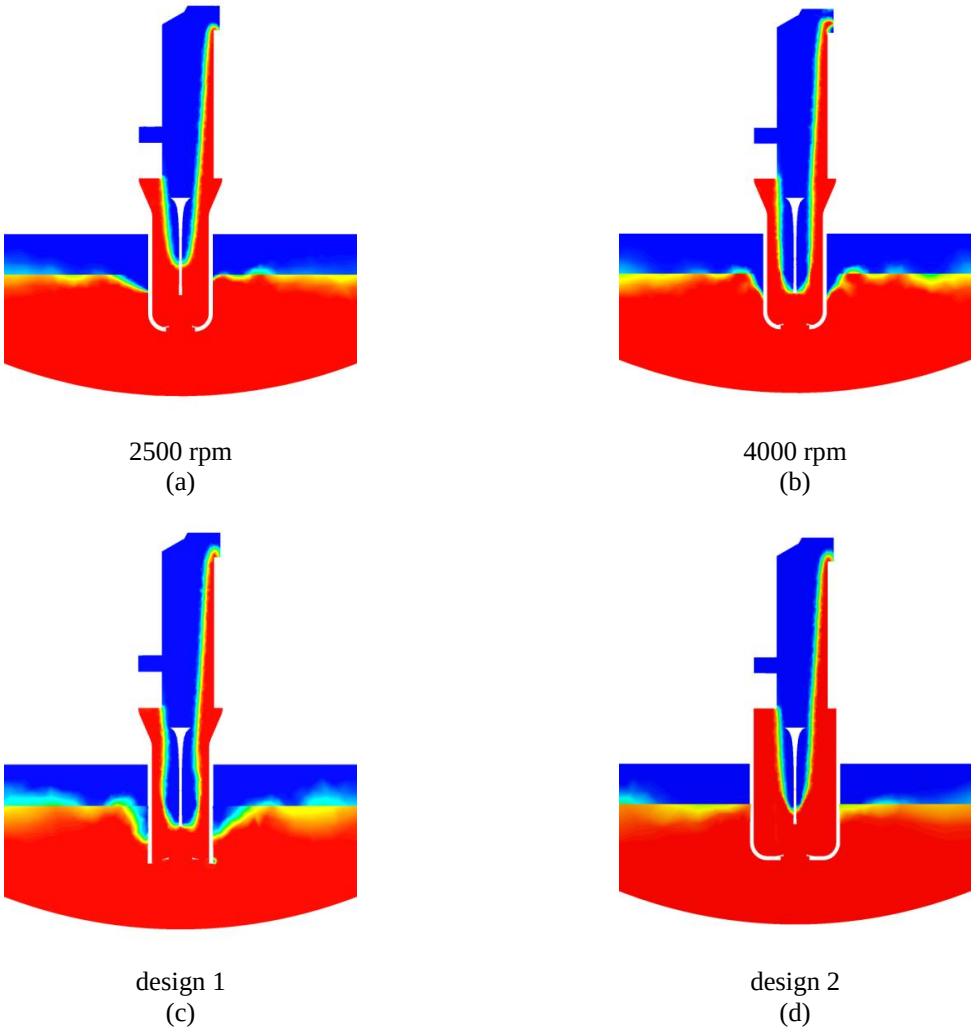

2500 rpm
(a)

4000 rpm
(b)

design 1
(c)

design 2
(d)

Figure 3: Steady-state oil volume fraction

Figure 4 shows the pressure distribution and the flow field of the basic configuration in the vicinity of the pump inlet. It can be seen that the main flow of the oil is situated around the centreline of the pump until the flow develops the oil parabola. Apart from the centreline, hardly oil is transported, thus the oil in that region undergoes only a rotational movement. The tangential velocity at the outer surface of the pump is a function of the distance from the centreline and increases with growing radius. Due to the higher velocities, the pressure decreases in the vicinity of the surface and oil is transported to low pressure regions causing vortexes. The vortexes spread out in the oil sump and can cause acoustic problems. High velocities at the inlet of the pump result in a decrease of the static pressure. Table 1 gives an overview of the static pressure reduction for the observed variants compared to the analytically determined geodetic pressure. It can be pointed out, that the major part of the static pressure reduction occurs due to the flow in axial direction. The influence of tangential and radial flow on the reduction of the static pressure can be considered as efficiency loss. Especially higher rotational speed induces higher tangential and radial velocities at the pump inlet due to higher frictional forces.

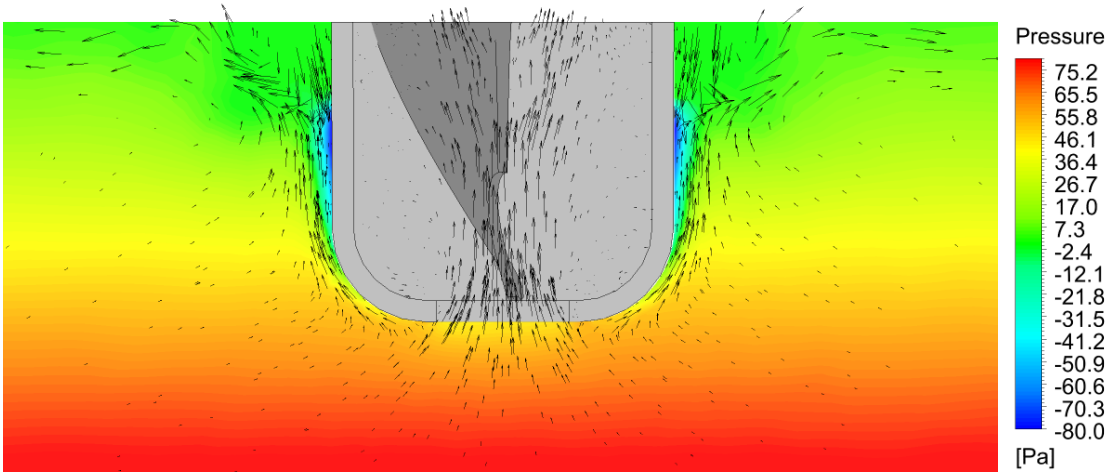

Figure 4: Pressure distribution and flow field in the vicinity of the suction hole

The Figures 5, 6 and 7 illustrate the mass flow rate at pump outlet as a function of time of the investigated variants. Simulated mass flow rates are normalized to the basic configuration. Variations of the immersed depth of the oil pump show the dependence of the oil mass flow rate on the immersion depth and therefore on the static pressure. Reduction of the immersion depth of ~50 % yields a decrease of the mass flow rate of 20 % and an increase of the oil climbing time of 0.4 s. The results also show that higher immersion depths do not affect the oil climbing time significantly but yield higher oil mass flow rates as expected. The comparison between the original geometry, design 1 and design 2 shows deviations of the oil mass flow rate of about 10 %. A shorter oil climbing time could be achieved with design 1 compared to the original geometry. Design 2 requires significant longer time for the oil reaching the pump outlet. This can be explained due to the higher volume in design 2 which has to be filled with oil until it is furtherly transported.

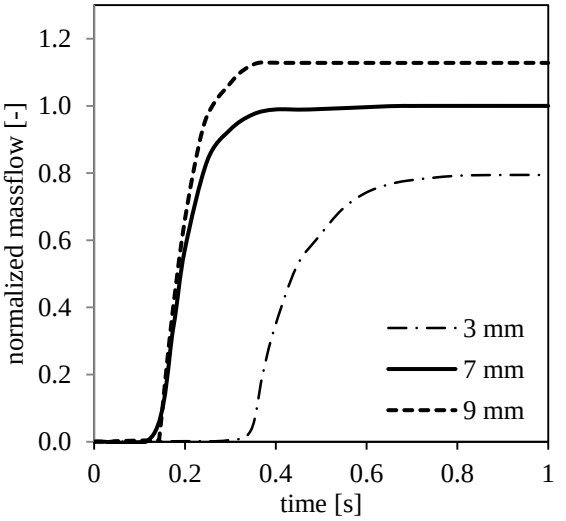

Figure 5: Normalized oil mass flow as a function of immersion depth

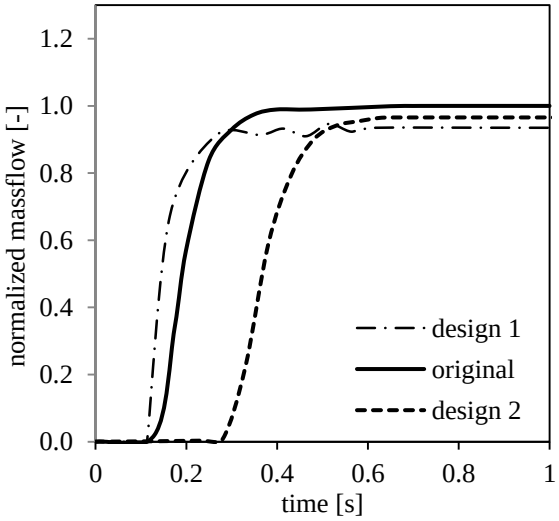

Figure 6: Normalized oil mass flow as a function of pump design

Rotational speed variations influence the oil mass flow rate and the oil climbing time in the same intent. Increasing the rotational speed by a third yields an increase of the oil mass flow rate by a factor of 2.2. The results also show the behaviour of the oil pump at low rotational speeds. A reduction of 500 rpm compared to the basic configuration results in an oil mass flow decrease of 60%. Simulations with reduced rotational speed show that no oil is transported under 2000 rpm, thus the use of the investigated pump design in variable speed compressors is unsuitable.

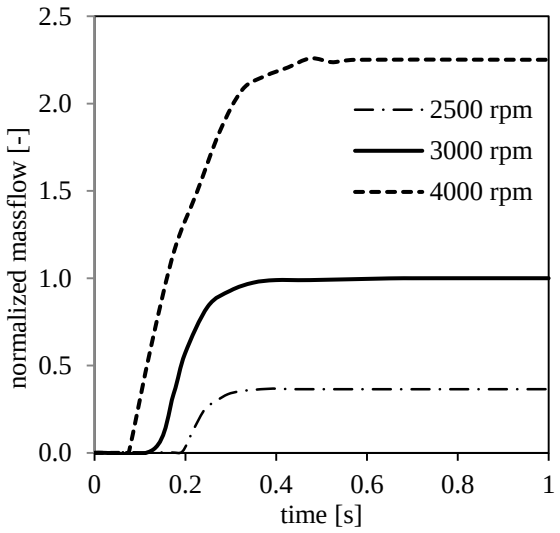

Figure 7: Normalized oil mass flow as a function of rotational speed

Table 1: Reduction of the static pressure between analytic (geodetic pressure) and numerical (CFD) calculation

Variant	Value [%]
basic model	21.0
3 mm immersion depth	45.5
9 mm immersion depth	24.1
2500 rpm	9.2
4000 rpm	71.2
design 1	55.3
design 2	52.5

4. CONCLUSION

A numerical investigation of the suction behaviour of the oil pump of a hermetic compressor is shown. The simulations are carried out using the commercial software ANSYS Fluent and they concentrate on the immersed centrifugal pump and its interaction with the oil sump. Special focus lies on the oil volume fraction in the pump, the oil mass flow rate, the oil climbing time and the static pressure at pump inlet. After analysing the simulation results the following conclusions can be drawn:

- Especially in the start-up phase of the compressor, the oil parabola can sink significantly which has to be taken into account in the pump design.
- Frictional forces reduce the static pressure at the pump inlet due to high radial and tangential velocities which occurs at high rotational speed.
- Vortexes are developed on the immersed pump surface which are spread out in the oil sump and can lead to acoustic problems.
- Volumes in the lower area of the pump should be kept small to decrease the oil climbing time considering the development of the oil parabola.
- The investigated oil pump is not suitable for the use in variable speed compressors because the oil transport fails below 2000 rpm.

NOMENCLATURE

$\boldsymbol{f}_b$	body force vector	(N/m³)
p	pressure	(N/m²)
t	time	(s)
u_i	velocity component	(m/s)
$\boldsymbol{v}_i$	velocity vector	(m/s)
x_i	coordinate component	(m)

Subscripts

g	gaseous phase	
l	liquid phase	

Greek symbols

μ	dynamic viscosity	(N s/m²)
ρ	density	(kg/m³)
χ	gas volume fraction	(-)

REFERENCES

Alves, M.V.C., Barbosa Jr, J.R., Prata, A.T. (2009). Analytical solution of single screw extrusion applicable to intermediate values of screw channel aspect ratio. *Journal of Food Engineering*, Volume 92, pages 152-156.

Alves, M.V.C., Barbosa Jr, J.R., Prata, A.T., Ribas Jr, A.T. (2010). Fluid Flow in a Screw Pump Oil Supply System for Reciprocating Compressors. *Proceedings of the International Compressor Engineering Conference at Purdue*, Purdue University, IN, USA, paper 1326.

Fluent 14 (2011). *User Guide*. Fluent Inc., USA, 2498.

Isaa, R.I. (1986). Solution of the Implicitly Discretised Fluid Flow Equations by Operator-Splitting. *Journal of Computational Physics*, Volume 62, pages 40-65.

Kerpicci, H., Alper, Y., Onbasioglu, S.U. (2013). Investigation of Oil Flow in a Hermetic Reciprocating Compressor. *International Journal of Refrigeration*, Volume 36, pages 215-221.

Kim, H.J., Lee, T.J., Kim, K.H., Bae, Y.J. (2002). Numerical Simulation of Oil Supply System of Reciprocating Compressor for Household Refrigerators. *Proceedings of the International Compressor Engineering Conference at Purdue*, Purdue University, IN, USA, paper 1533.

Lückamnn, A.J., Alves, M.V.C., Barbosa Jr, J.R. (2009). Analysis of Oil Pumping in a Reciprocating Compressor. *Applied Thermal Engineering*, Volume 29, pages 3188-3123.

Moukalled, F., Mangani, L., Darwish, M., (2015). *The Finite Volume Method in Computational Fluid Dynamics*. Springer, Switzerland, 791.

Ozsipah, M., Cadirci, S., Gunes, H., Sarioglu, K., Kerpicci, H. (2014). A Numerical Study on the Lubrication System for a Hermetic Reciprocating Compressor used in Household Refrigerators. *International Journal of Refrigeration*, Volume 48, pages 210-220.

Posch, S., Berger, E., Heimel, M., Hopfgartner, J., Almbauer, R., Schöllauf, P. (2015). Fluid Flow in the Oil Pumping System of a Hermetic Compressor. *Proceedings of the International Conference on Compressors and their Systems*, City University, London, GB, paper 012028.

Scardovelli, R., Zaleski, S. (1999). Direct numerical simulation of free-surface and interfacial flow. *Annual Review Fluid Dynamics*, Volume 31, pages 567-603.

Tada, M.P., Hoffmann, T., Couto, P.R., Manke, A.L., de Bortoli, G.D. (2014). Numerical and Experimental Examination for Oil Pump System Using a Simplified Uncoupled Simulation. *Proceedings of the International Compressor Engineering Conference at Purdue*, Purdue University, IN, USA, paper 1248.

ACKNOWLEDGEMENT

This work has been carried out within the framework of ECO-COOL, a research project initiated and funded by the FFG (Austrian Research Promotion Agency). Furthermore the authors particularly acknowledge the technical support by Secop Austria GmbH, formerly ACC Austria GmbH and Liebherr-Hausgeräte Lienz GmbH.

C Paper 3

S. Posch, J. Hopfgartner, E. Berger, B. Zuber, L. Dür, S. Stangl, R. Almbauer

NUMERICAL ANALYSIS OF THE THERMAL BEHAVIOR OF A HERMETIC RECIPROCATING COMPRESSOR

Journal of Earth Science and Engineering **7**, 1-9, 2017

Journal of Earth Science and Engineering 7 (2017) 1-9
doi: 10.17265/2159-581X/2017.01.001

Numerical Analysis of the Thermal Behavior of a Hermetic Reciprocating Compressor

Stefan Posch[1], Johann Hopfgartner[1], Erwin Berger[1], Bernhard Zuber[1], Lukas Dür[1], Stefan Stangl[2] and Raimund Almbauer[1]

1. Institute of Internal Combustion Engines and Thermodynamics, Graz University of Technology, Inffeldgasse 19, 8010 Graz, Austria

2. Secop Austria GmbH, Jahnstraße 30, 8280 Fürstenfeld, Austria

Abstract: A numerical model to predict the temperature field in a hermetic reciprocating compressor for household refrigeration appliances is presented in this work. The model combines a high resolution three-dimensional heat conduction formulation of the compressor's solid parts, a three-dimensional CFD (computational fluid dynamics) approach for the gas line domain and lumped formulations of the shell gas and the lubrication oil. Heat transfer coefficients are determined by applying CFD to the gas line side and correlations from the literature on the shell gas and oil side, respectively. The valve in the gas line simulation is modelled as a parallel moving flat plate. By means of an iterative loop the temperature field of the solid parts acts as boundary condition for the CFD calculation of the gas line which returns a cycle averaged quantity of heat to the solid parts. Using an iteration method which is based on the temperature deviation between two iteration steps, the total number of iterations and consequently the computational time can be reduced. The loop is continued until a steady-state temperature field is obtained. Calculated temperatures of the solid parts are verified by temperature measurements of a calorimeter test bench.

Key words: Compressor, simulation, CFD.

Nomenclature

c	specific heat capacity	(J/kg K)
$\dot{m}$	mass flow rate	(kg/s)
m	mass	(kg)
n	iteration step	
$\dot{Q}$	heat flux	(W)
T	temperature	(K)
t	time	(s)

Subscripts

CV	control volumes
OC	oil in the crankshaft
OS	oil in the sump
OW	oil on the walls
oil	compressor oil
SG	shell gas
SP	solid parts
v	isochoric

Greek symbols

Δ	difference	(-)
ε	convergence criteria	(-)

1. Introduction

Thermal management is one of the main topics in the development process of modern hermetic reciprocating compressors for household refrigeration application. Due to the hermetic design of the compressor, electrical and mechanical losses influence the thermodynamic efficiency of the compressor. Heat transfer mechanisms like convection and conduction determine the temperature field inside the compressor and consequently, the compressor performance. The knowledge of the temperature field inside the compressor is essential to quantify loss mechanisms like superheating.

One possibility to obtain the heat transfer and the temperature field inside the compressor is the

Corresponding author: Stefan Posch, M.Sc., B.Sc., research fields: hermetic compressors and refrigeration systems.

experimental investigation using heat flux sensors [2] or thermocouples [3]. The spatial resolution of these methods is low, they are not suitable for compressors in the design phase and the usage of sensors may affect the compressor behaviour. Another possibility to investigate the thermal performance of a hermetic reciprocating compressor is the use of simulation tools. Several strategies to model the temperature field and heat transfer mechanism inside the compressor have been developed and can be found in the open literature.

Simple approaches split the compressor into several lumped volumes using the first law of thermodynamics to calculate the temperature field (e.g. [5] and [11]). Such models use either experimental data or correlations for the convective heat transfer formulation. The lumped volumes are connected via thermal conductance adjusted to experimental data. The low spatial resolution of these models and the dependence on experimental data yield a very rough and inflexible estimation of the temperature field in a hermetic reciprocating compressor.

A more flexible modelling strategy is the TNW (thermal network approach). The usage of TNW for thermal modelling of a hermetic reciprocating compressor for refrigeration application can be found in e.g. [9] and [6]. TNW uses mass points to model the considered compressor parts and the heat transfer between the mass points is represented with the Lumped Conductance Method. Convective heat transfer is modelled with correlations based on forced or natural convection Nusselt number. Due to the reduction of geometrical information, the heat transfer modelling is characterized by a high level of uncertainty especially for regions with transient 3d flows like in the suction or discharge line. Also the validation of TNW with experimental data can cause problems because it is not clear if the chosen measuring points represent the temperature of the lumped mass.

The use of CFD (computational fluid dynamics) in the development process of hermetic reciprocating compressors leads to another approach for thermal modelling, the so called hybrid simulation models. Although the performance of CPUs increased significantly over the last years, an overall 3d simulation of a compressor is still not possible within a reasonable time. Hybrid models use different combinations of complex 3d formulations and simple correlations for convective and conductive heat transfer, respectively. In Ref. [1], the authors applied 1d flow simulation of the gas line, 3d formulation of the cylinder solid domain and lumped formulation of the remaining compressor parts. In Refs. [4], [8] and [10] 3d heat conduction formulation for the solid parts of the compressor and lumped formulation of the gas path were combined. The authors used either experimental data or correlations from the literature to model the heat transfer.

The model in the present study is based on the hybrid approach. Compared to the hybrid models found in the literature, this work contains 3d formulation of the full gas line and 3d formulation of solid components of the entire compressor in combination with lumped volume formulation of the gas inside the compressor shell and the lubrication oil. The simulation of the fluid flow in the gas line considers 3d phenomena in the suction and discharge mufflers, the flow in the cylinder as well as interactions with the compressor valves. Special focus is laid on the high geometric resolution of the solid compressor parts. A simulation algorithm is presented to combine the transient flow calculation and the steady-state heat conduction calculation to model the thermal behaviour of a hermetic reciprocating compressor running at calorimeter test conditions. The simulation results are verified by experimental data of a calorimeter test bench.

2. Simulation Model

The R600a (isobutane) hermetic reciprocating compressor used in the present study has a displacement of 5.5 cm^3 and the COP (ASHRAE test

conditions -23.3 °C/55 °C) is approximately 1.8. A schematic view of the compressor is shown in Fig. 1. The simulation model can basically be split up into three main parts: (i) simulation of the gas flow using commercial CFD software, (ii) heat conduction in the solid parts also using commercial CFD software and (iii) the energy balance for oil and refrigerant by assuming lumped control volumes. The three simulation parts exchange data in terms of heat flux and temperatures.

2.1 Gas Flow

The simulation of the gas flow is done with the commercial CFD software package ANSYS Fluent. The simulation domain includes suction line, suction muffler, valves, cylinder, ports, discharge muffler and discharge line. To reduce the computational time the valves are assumed to be parallel moving flat plates. The valve motion is calculated via User Defined Functions solving the single-degree of freedom system considering oil stiction forces. The number of cells in the computational mesh varies between 3.1 and 5.5 million cells depending on the position of the piston. The k-ε turbulence model is used and 1st order spatial discretization of density, momentum, energy and turbulence is applied. Pressure-velocity coupling is used with coupled solver setting.

2.2 Conduction in the Solid Parts

Heat conduction in the solid parts of the hermetic compressor is also solved with the commercial software package ANSYS Fluent. The whole domain is meshed with about 2.4 million cells with refinements at the interfaces between the single parts. Heat flux boundary conditions are applied on the surfaces of the solid parts depending on the flow conditions. Surfaces that are in contact with the gas flow use area-weighted average heat flux values determined by the CFD calculation of the gas flow. Heat flux values for the convective heat transfer between the solid parts, the compressor oil and the gas inside the shell are calculated with correlations from the literature (e.g. flow over flat plates, flow inside pipes). The heat flux between the compressor shell and the ambient air is modelled by means of a natural convection correlation. Electrical power losses are considered as volumetric source terms in the energy equation of the corresponding part. Mechanical power losses are considered as heat input to the compressor oil [12].

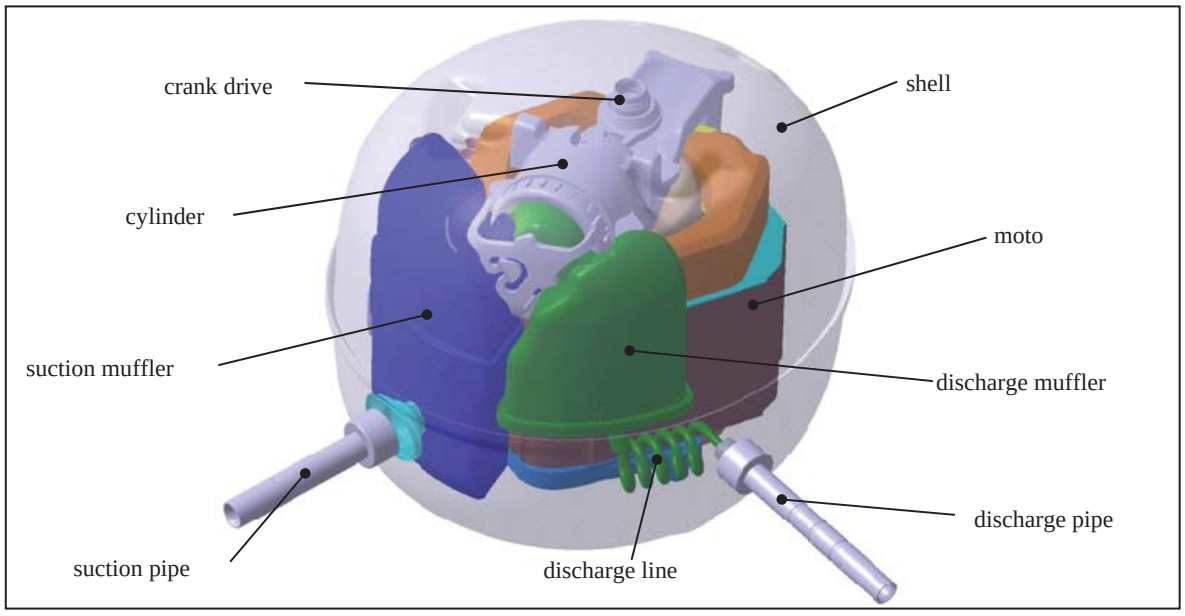

Fig. 1 Schematic view of the investigated compressor.

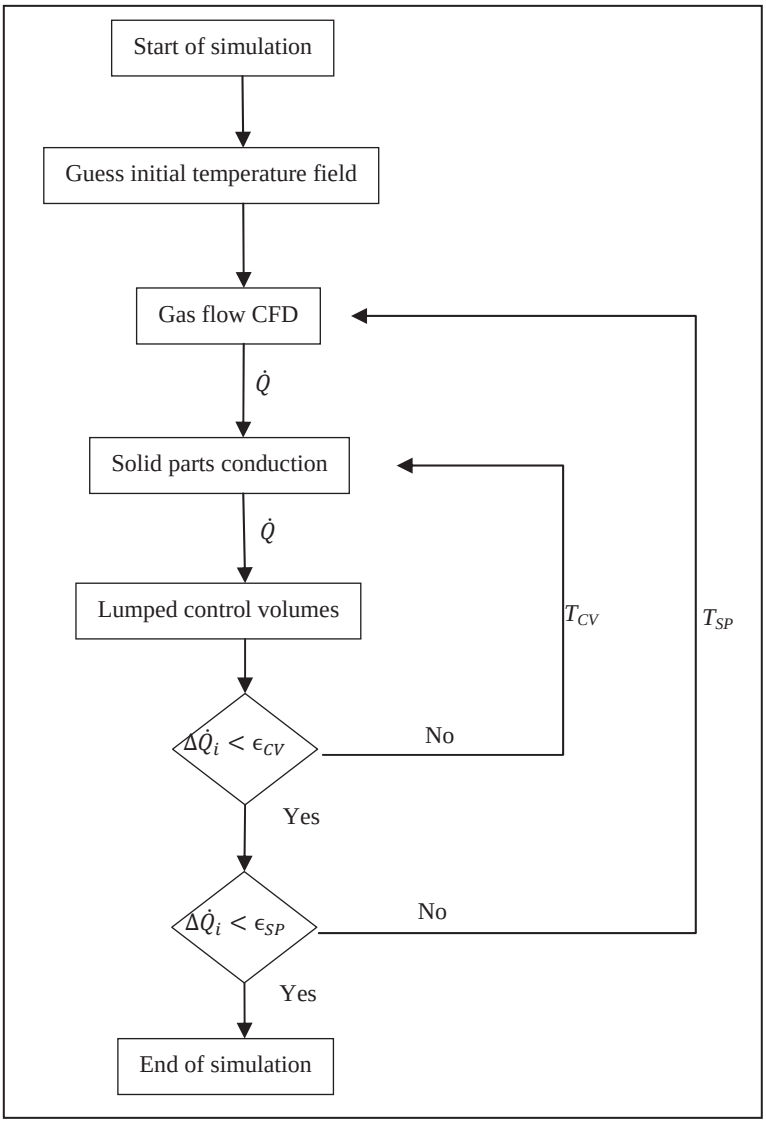

Fig. 2 Flow chart of the solution algorithm.

2.3 Lumped Control Volumes

To complete the thermal modelling of the entire hermetic compressor, the refrigerant and the oil inside the compressor shell have to be taken into account. The gas caught inside the shell is regarded as one control volume. Leakage mass flow rates are neglected and the gas is assumed to be in thermal equilibrium. The sum of the heat fluxes between the shell gas and the adjacent parts Q_{SG} are calculated with the results of the solid part conduction simulation. The temperature of the gas can be calculated by applying the energy balance to the control volume:

$$T_{SG}^{n+1} = T_{SG}^{n} + \frac{\dot{Q}_{SG} \cdot \Delta t}{m_{SG} \cdot c_{v\,SG}} \tag{1}$$

The oil inside the compressor shell is divided into three control volumes, namely the oil in the sump, the oil transported by the oil pump and the expelled oil on the oil covered walls. The oil mass flow rate at steady-state operating conditions is determined by experiments [7]. Applying a first order upwind scheme for the calculation of the outlet enthalpy flow, the energy balance of the considered control volume yields the following equations for the oil temperatures:

$$T_{OS}^{n+1} = \frac{\dot{Q}_{OS} + c_{oil}\left(\dot{m}_{oil} \cdot T_{OW} + m_{OS}\frac{T_{OS}^{n}}{\Delta t}\right)}{c_{oil}\left(\dot{m}_{oil} + \frac{m_{OS}}{\Delta t}\right)} \quad (2)$$

$$T_{OC}^{n+1} = \frac{\dot{Q}_{OC} + c_{oil}\left(\dot{m}_{oil} \cdot T_{OS} + m_{OC}\frac{T_{OC}^{n}}{\Delta t}\right)}{c_{oil}\left(\dot{m}_{oil} + \frac{m_{OC}}{\Delta t}\right)} \quad (3)$$

$$T_{OW}^{n+1} = \frac{\dot{Q}_{OW} + c_{oil}\left(\dot{m}_{oil} \cdot T_{OC} + m_{OW}\frac{T_{OW}^{n}}{\Delta t}\right)}{c_{oil}\left(\dot{m}_{oil} + \frac{m_{OW}}{\Delta t}\right)} \quad (4)$$

2.4 Solution Algorithm

At the beginning of the simulation process an initial temperature field in all solid parts, refrigerant and oil in the compressor is guessed. The solid part temperatures are used as boundary conditions for the following CFD simulation of the gas flow. The results of the CFD simulation are averaged over one rotation of the compressor and are considered as heat flux boundary conditions for the simulation of the solid part heat conduction. Since a steady-state temperature field of the compressor should be calculated, the solid part heat conduction model in ANSYS Fluent is set to steady. After calculating the temperature distribution in the solid parts, the energy balance for the refrigerant in the shell and the respective oil volumes are carried out using the CFD heat fluxes. The lumped control volumes are modelled as quasi-transient using a time step of 1s. The boundary conditions for the solid part conduction simulation are updated with the gas and oil temperatures. Lumped volume energy balance and solid part conduction forms an iteration loop which is continued until heat flux deviation between two consecutive iteration steps is below a certain limit. Using the new solid part temperature field the CFD simulation is carried out again. The iteration loop between CFD simulation of the gas line and the solid part heat conduction calculation is executed until heat flux deviations between two consecutive iteration steps are also below a certain convergence criteria.

3. Experimental Work

To validate the thermal modelling of the hermetic compressor, temperature measurements on several positions in the compressor are carried out. Twenty-two thermocouples type T are distributed inside the compressor, on the shell and in the gas line. Furthermore, two pressure sensors are placed in the suction and discharge muffler. A special sealed feedthrough is used to pass the Teflon®-insulated sensor wires through the hermetic shell. Table 1 gives an overview of the thermocouples which are used for the validation of the present thermal model. A schematic overview of the sensor positions is illustrated in Fig. 3.

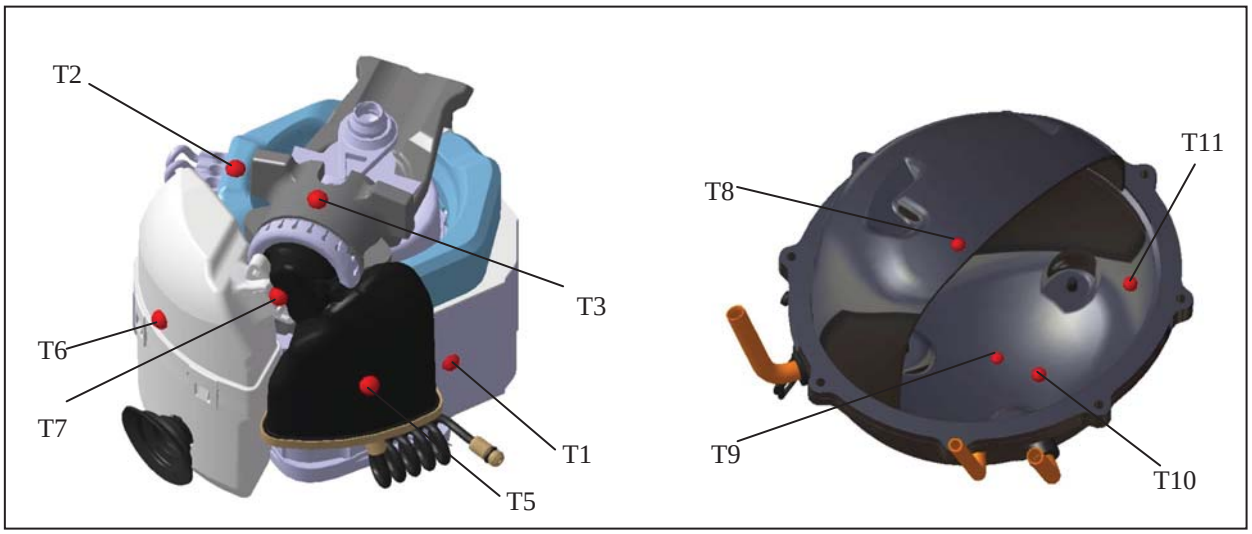

Fig. 3 Schematic overview of the sensor positions.

Table 1 Thermocouple measuring points.

No.	Measuring point description
T1	Stator lamination (surface)
T2	Stator windings (surface)
T3	Cylinder (surface)
T4	Shell (gas)
T5	Discharge muffler (surface)
T6	Suction muffler (surface)
T7	Valve plate (surface)
T8	Shell top outside (surface)
T9	Shell bottom outside (surface)
T10	Oil sump
T11	Shell inside (surface)

4. Results

The presented thermal model is used to simulate the temperature distribution in solid parts, gas and oil of a hermetic reciprocating compressor. The operating conditions of the compressor are set to -23 °C evaporating temperature, 45 °C condensing temperature and 32 °C ambient temperature, respectively. The compressor works at constant speed of 2,950 rpm.

Fig. 4 shows exemplarily the velocity field in the cylinder of the gas flow obtained by CFD simulation. Regions with high local gradients of the heat transfer coefficient like suction and discharge port are treated as separated areas in the iteration loop between gas flow simulation and solid part conduction. Specific heat flux values for the individual regions can be seen in Table 2. The sign of the values is related to the heat flux direction from solid part to gas flow. The specific heat flux acts as boundary condition for the heat conduction simulation of the solid parts.

As described in chapter two the present model consists of two iteration loops. The outer iteration loop links the gas flow simulation with the simulation of the solid parts, shell gas and oil. The inner iteration loop links the solid part conduction with the energy balance of the lumped volumes of gas and oil in the compressor shell. The calculation time of the whole procedure is significantly depending on the outer iteration loop due to the time-consuming CFD simulation of the gas flow. To contain the number of

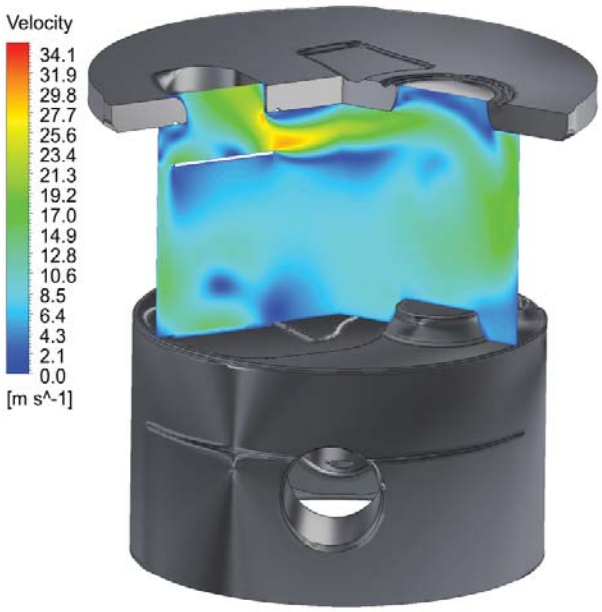

Fig. 4 CFD simulation of the gas flow.

Table 2 Specific heat flux from solid to gas [W/m²].

Solid	Value
Piston	-7,199
Discharge Muffler	-1,289
Suction muffler	351
Valve plate cylinder	239
Cylinder	2,082
Valve plate suction	414
Valve plate discharge	-24,421
Discharge port	-10,216
Suction port	7,485
Serpentine	-3,799

iterations for the outer loop, the initial temperature field of the compressor has to be guessed well. In the present study, five iterations for the outer loop had to be carried out to fulfil the convergence criteria. Due to the fast calculation of the conduction in the solids and of the energy balance, the inner iteration loop has no significant impact on the overall computation time. The number of iterations for the inner loop in the present study is between 50 and 60. Fig. 5 shows the temperature development over the number of iterations of the lumped volumes during the inner iteration loop.

The comparison between the simulated and measured temperatures at the specific measuring

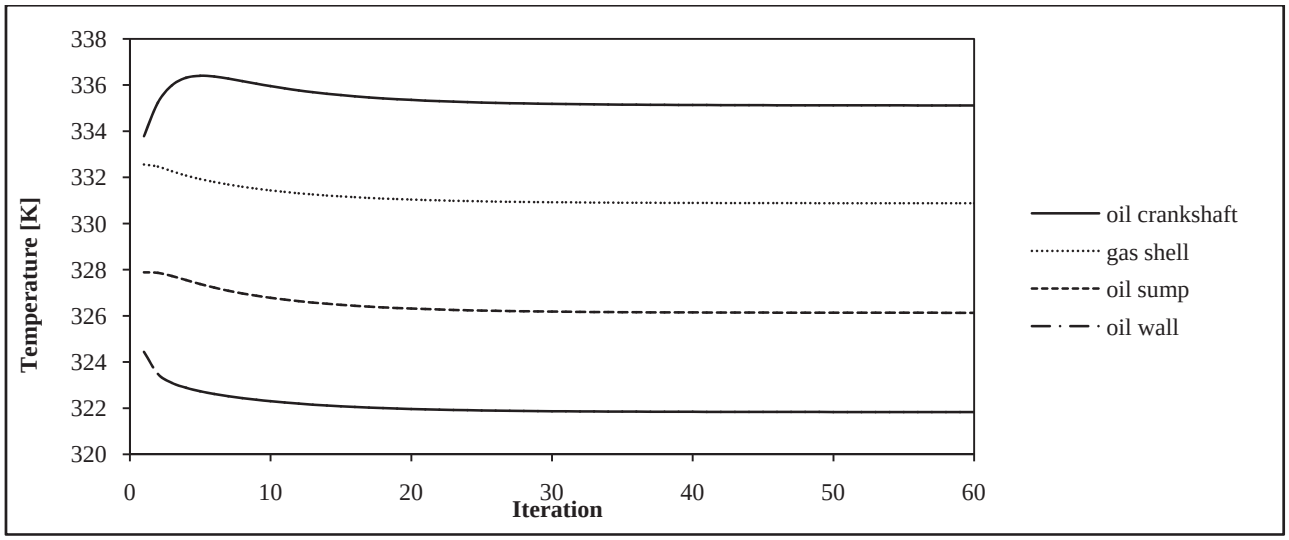

Fig. 5 Temperature development during the inner iteration loop [K].

Table 3 Comparison between measured and simulated temperatures [K].

No.	Measuring point description	Measurement	Simulation	ΔT
T1	Stator lamination (surface)	332.9	333.4	0.5
T2	Stator windings (surface)	333.7	333.4	0.3
T3	Cylinder (surface)	337.7	338.3	0.6
T4	Shell (gas)	331.6	330.9	0.7
T5	Discharge muffler (surface)	350.9	350.9	0.0
T6	Suction muffler (surface)	328.2	326.8	1.4
T7	Valve plate (surface)	345.0	342.6	2.4
T8	Shell top outside (surface)	318.9	321.2	2.3
T9	Shell bottom outside (surface)	321.8	322.0	0.2
T10	Oil sump	327.8	326.1	1.7
T11	Shell inside (surface)	324.7	320.5	4.2

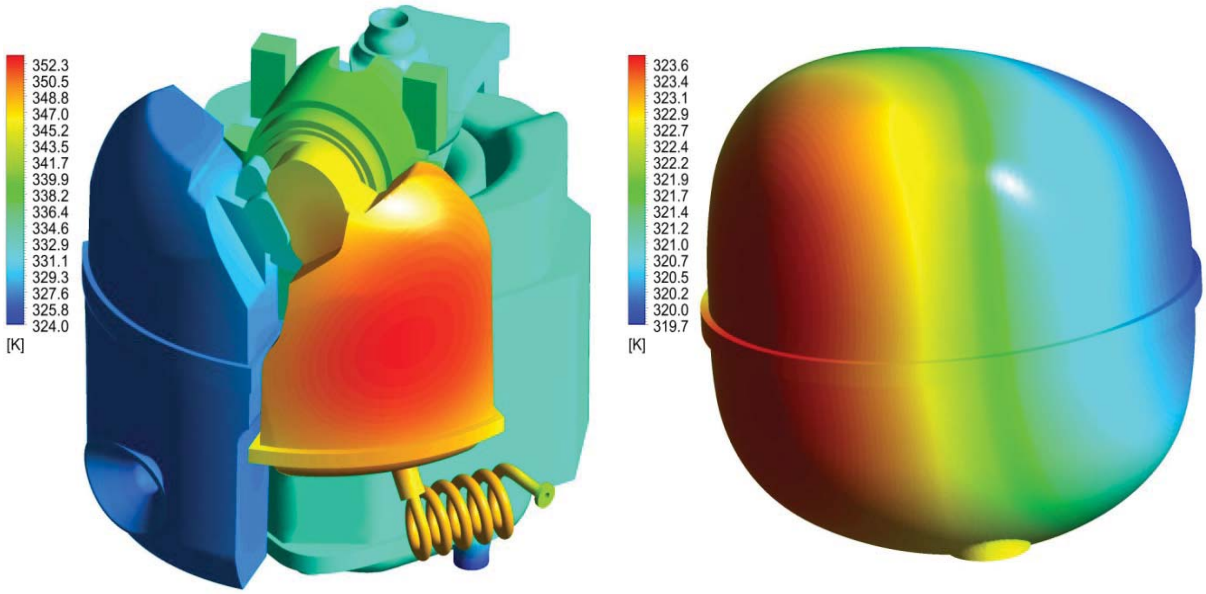

Fig. 6 Temperature field of the solid parts.

points is illustrated in Table 3. The results of the thermal model are in agreement with calorimeter test data. Maximum absolute temperature difference between simulation and measurement is less than 4.2 K. Especially the temperatures of the solid parts inside the compressor and the lumped volumes are met very well. Although the thermal modelling of the hermetic compressor in the present study matches the experiment well, the uncertainties in the determination of the heat transfer coefficients should be discussed briefly. In general heat transfer can be modelled in two different ways: On the one hand by detailed CFD simulation of the complex gas flow inside the shell or by means of empirical correlations. With the CFD approach not only the model accuracy should increase but also the computation effort. If choosing empirical correlations a bad agreement between simulation and experimental data could turn out, that requires a slight calibration of the empirical correlations by experimental data. The temperature distribution in the solid parts of the compressor can be seen in Fig. 6.

5. Conclusion

In this study a thermal model for the investigation of a hermetic reciprocating compressor is shown using mainly numerical methods. The method combines CFD simulation of the gas flow, numerical calculation of the heat conduction in the solid parts and simple lumped formulations of the refrigerant and oil in the compressor shell. Although some heat transfer coefficients are determined by simple correlations from literature, the results of the thermal modelling are in good agreement with experimental data gained by calorimeter tests. The present method is an advisable tool in the compressor development process along with detailed CFD simulation of the gas flow to validate thermodynamic compressor behavior. Unavoidable uncertainties in the determination of the heat transfer coefficients between the solid parts and the fluids (refrigerant and oil) have to be considered in the evaluation of the results. To get a thermal model for the usage in thermodynamic parameter studies it is useful to calibrate the heat transfer coefficients with experimental data.

Acknowledgement

This work has been carried out within the framework of ECO-COOL, a research project initiated and funded by the FFG (Austrian Research Promotion Agency). Furthermore the authors particularly acknowledge the technical support by Secop Austria GmbH, formerly ACC Austria GmbH and Liebherr-Hausgeräte Lienz GmbH.

References

[1] Almbauer, R., Burgstaller, A., Abidin, Z., and Nagy, D. 2006. 3-Dimensional Simulation for Obtaining the Heat Transfer Correlations of a Thermal Network Calculation for a Hermetic Reciprocating Compressor. *Proceedings of the International Compressor Engineering Conference at Purdue*, Purdue University, IN, USA, paper 1794.

[2] Dutra, T., and Deschamps, C. 2010. Experimental Investigation of Heat Transfer in Components of a Hermetic Reciprocating Compressor. *Proceedings of the International Compressor Engineering Conference at Purdue*, Purdue University, IN, USA, paper 1346.

[3] Kara, S., and Oguz, D. H. 2010. Thermal Analysis of a Small Hermetic Reciprocating Compressor, *Proceedings of the International Compressor Engineering Conference at Purdue*. Purdue University, IN, USA, paper 1307.

[4] Lohn, S. K., Diniz, M. C., and Deschamps, C. J. 2015. A Thermal Model for Analysis of Hermetic Reciprocating Compressors under the On-Off Cycling Operating Condition. *Proceedings of the International Conference on Compressors and their Systems*, City University, London, GB, paper 012068.

[5] Meyer, W. A., and Thompson, E. 2010. An Analytical Model of Heat Transfer to the Suction Gas in a Low-Side Hermetic Refrigeration Compressor. *Proceedings of the International Compressor Engineering Conference at Purdue*, Purdue University, IN, USA, paper 662.

[6] Ooi, K. T. 2003. “Heat Transfer Study of a Hermetic Refrigeration Compressor.” *Applied Thermal Engineering*, Volume 23, pages 1931-1945.

[7] Posch, S., Berger, E., Heimel, M., Hopfgartner, J., Almbauer, R., and Schöllauf, P. 2015. “Fluid Flow in the Oil Pumping System of a Hermetic Compressor.” *Proceedings of the International Conference on*

Compressors and Their Systems, City University, London, GB, paper 012028.

[8] Ribas Jr., F. A. 2007. "Thermal Analysis of Reciprocating Compressors." *Proceedings of the International Conference on Compressors and Their Systems*, City University, London, GB, 277-87.

[9] Sim, Y. H., Youn, Y., and Min, M. K. 2000. "A Study on Heat Transfer and Performance Analysis of Hermetic Reciprocating Compressors for Refrigerators." *Proceedings of the International Compressor Engineering Conference at Purdue*, Purdue University, IN, USA, paper 1390.

[10] Sanvezzo Jr, J., and Deschamps, C. J. 2012. "A Heat Transfer Model Combining Differential and Integral Formulations for Thermal Analysis of Reciprocating Compressors." *Proceedings of the International Compressor Engineering Conference at Purdue*, Purdue University, IN, USA, paper 2104.

[11] Todescat, M. L., Fagotti, F., Prata, A. T., and Ferreira, R. T. S. 1992. "Thermal Energy Analysis in Reciprocating Hermetic Compressors." *Proceedings of the International Compressor Engineering Conference at Purdue*, Purdue University, IN, USA, paper 936.

[12] Zach, D. 2013. "Verlustteilung hermetischer Kältemittelkompressoren." M.Sc. thesis, Graz University of Technology, AUT.

D Paper 4

S. Posch, J. Hopfgartner, E. Berger, B. Zuber, R. Almbauer, P. Schöllauf

DETERMINATION OF THE OIL DISTRIBUTION IN A HERMETIC COMPRESSOR USING NUMERICAL SIMULATION

10th International Conference on Compressors and their Systems, London, GB, 2017

CITY UNIVERSITY LONDON

Determination of the Oil Distribution in a Hermetic Compressor Using Numerical Simulation

S Posch[1], J Hopfgartner[1], E Berger[1], B Zuber[1], R Almbauer[1] and P Schöllauf[2]

[1] Graz University of Technology, 8010 Graz, Austria
[2] Secop Austria GmbH, 8280 Fürstenfeld, Austria

posch@ivt.tugraz.at

Abstract. *In addition to the reduction of friction the oil in a hermetic compressor is very important for the transfer of heat from hot parts to the compressor shell. The simulation of the oil distribution in a hermetic reciprocating compressor for refrigeration application is shown in the present work. Using the commercial Computational Fluid Dynamics (CFD) software ANSYS Fluent, the oil flow inside the compressor shell from the oil pump outlet to the oil sump is calculated. A comprehensive overview of the used models and the boundary conditions is given. After reaching steady-state conditions the oil covered surfaces are analysed concerning heat transfer coefficients. The gained heat transfer coefficients are used as input parameters for a thermal model of a hermetic compressor. An increase in accuracy of the thermal model with the simulated heat transfer coefficients compared to values from literature is shown by model validation with experimental data.*

Nomenclature

Roman symbols

c_p	specific heat capacity
$\boldsymbol{f}_b$	body force vector
p	pressure
$\dot{q}_V$	rate of heat source/sink per volume
t	time
T	temperature
$\boldsymbol{v}$	velocity vector

Greek symbols

λ	thermal conductivity
μ	dynamic viscosity
ρ	density
Φ	viscous dissipation term

1. Introduction

The use of simulation in different fields of engineering has been increased in the last two decades due to the new possibilities of applying numerical methods in combination with raising computational performance. Additionally to the early pioneers of using simulation in the development process like the automotive or aeronautic industry the decreasing costs allow the use of simulation tools in other fields of mechanical engineering. As an example, the traditionally experimentally driven development of hermetic reciprocating compressors for refrigeration appliances can be mentioned. To meet future regulations concerning the energy consumption of refrigeration devices comprehensive research on the level of the overall cooling cycle and on the component level is needed. Especially for the hermetic compressor which serves as the core element of a refrigeration cycle, considerable efforts have to be

made to find energy saving potentials. The development of innovative compressors requires the knowledge of its thermal behaviour and occurring loss mechanisms. Due to the hermetic shell an individual consideration of the electrical, mechanical and thermodynamic losses is not expedient. Electrical and mechanical losses produce heat which influences the thermodynamic behaviour of the entire compressor. Several studies have been published and can be found in the open literature which deal with the thermal modelling of hermetic reciprocating compressors. The following survey of thermal compressor models should give an overview without any claim of completeness.

Generally, thermal compressor models can be characterized due to their complexity and geometrical resolution. Studies presented in [1] or [2] split up the compressor in several lumped volumes representing the appropriate compressor part. Using the first law of thermodynamics the temperature field is calculated. Heat transfer coefficients are determined either by simple correlations or experimental data. These studies represent the early stage of thermal compressor modelling and show the limitations due to low computational performance in the late 80s and early 90s. The models are only able to give a rough estimation of the temperature field.

The Thermal Network approach (TNW) can be considered as more flexible compared to the previous described models. Examples of TNW for thermal compressor modelling can be found in [3] and [4]. Using the Lumped Conductance Method the heat transfer between mass points representing the several compressor parts is modelled. The authors calculate the convective heat transfer with correlations for forced or natural convection based on the Nusselt number which can cause uncertainties especially in regions with transient flow like in the suction or discharge muffler. Low geometric resolution is also critical for the validation of the models using experimental data due to significant temperature differences in parts with a low thermal conductivity.

Modern thermal models integrate Computational Fluid Dynamics (CFD) resulting in so called hybrid models. Hybrid models combine 3d numerical simulation (e.g. solid part conduction) and simple correlation (e.g. convective heat transfer) in one model to gain high geometrical resolution by keeping the calculation time at acceptable limits. Examples for hybrid models using 3d heat conduction of the solid parts in combination with lumped volume formulation for the compressor gas path can be found in [5], [6] and [7]. The modelling of the heat transfer in these models was carried out either by using experimental data or correlations from the literature. In [8] special care was laid on the cylinder of the compressor. The authors combined 1d flow simulation of the compressor gas line, 3d formulation of the compressor cylinder and lumped formulation of the remaining compressor parts.

A more detailed hybrid model using 3d formulation of the full gas line and 3d formulation of the solid components can be found in [9]. The authors introduced a simulation algorithm to combine transient flow calculation with steady-state heat conduction calculation. Heat transfer coefficients calculation between the oil and the oil covered walls is carried out with correlations from literature. The authors remark that the results of thermal compressor models should not be trusted without considering the modelling of the heat transfer coefficients especially between oil and oil covered walls. Generally, considerable influence on the thermodynamic compressor behaviour is caused by the lubrication oil. Additionally to the lubrication of the moving parts and reduction of wear losses, the oil acts as heat transfer media between the hot compressor parts, the shell and hence the ambience. Based on the thermal compressor model presented in [9] the present study increases the accuracy of the model by calculating the heat transfer coefficients between oil and compressor shell applying 3d CFD. Therefore, a simulation of the oil distribution inside the compressor shell is performed in the commercial software ANSYS Fluent. The two phase flow (oil/refrigerant) is modelled with the Volume of Fluid (VOF) approach. A comparison between the results of the thermal model with heat transfer gained with correlations from the literature and by CFD, respectively, is carried out and the results are validated with experimental data of a calorimeter test bench.

The compressor used in the present study works with R600a (isobutane) and has a displacement of 5.5 ccm at a rotational speed of 2950 rpm. Its COP at ASHRAE test conditions (-23.3 °C/55 °C) is approximately 1.8.

2. Modelling

An overview of the used CFD methods and solution strategy is given in the following chapter. The fluid flow of the distributed oil is assumed to be a continuous jet which can also be seen in experimental tests using a transparent compressor shell and a stroboscope light, therefore the volume of fluid approach (VOF) is used for fluid flow simulation.

2.1. Theoretical background

The basic idea of CFD is the transformation of governing equations from the partial differential equation form into an algebraic form using finite volume discretization. For the present study the governing equations for mass, momentum and energy are essential [10]:

$$\frac{\partial \rho}{\partial t} + \nabla \cdot [\rho \boldsymbol{v}] = 0 \tag{1}$$

$$\frac{\partial}{\partial t}[\rho \boldsymbol{v}] + \nabla \cdot \{\rho \boldsymbol{v}\boldsymbol{v}\} = -\nabla p + \mu \nabla^2 \boldsymbol{v} + \boldsymbol{f}_b \tag{2}$$

$$\frac{\partial}{\partial t}\left[\rho c_p T\right] + \nabla \cdot \left\{\rho c_p \boldsymbol{v} T\right\} = \nabla \cdot \{\lambda \nabla T\} + \frac{\mathrm{D}p}{\mathrm{D}t} + \mu \Phi + \dot{q}_V \tag{3}$$

Commercial software packages like ANSYS Fluent discretize the governing equations automatically on the regarded flow domain and solves the system of equations by means of appropriate numerical methods. The modelling of the oil flow in the gaseous environment inside the compressor shell, the previous mentioned VOF approach presented in [11] is used thus an additional value, the volume fraction χ is introduced. It describes the volumetric amount of oil in a finite volume of the solution domain. The use of χ requires the solution of an additional governing equation and the volume fraction is used to determine density and viscosity of a partial filled finite volume by applying the following equations:

$$\frac{\partial \chi}{\partial t} + \nabla \cdot [\chi \boldsymbol{v}] = \boldsymbol{0} \tag{4}$$

$$\rho = \rho_g \chi + \rho_l (1 - \chi) \tag{5}$$

$$\mu = \mu_g \chi + \mu_l (1 - \chi) \tag{6}$$

For more details about the VOF approach the interested reader is referred to [11] and [12].

2.2. Solution domain and computational settings

The gas volume inside the compressor shell is meshed for the present simulation with approximately 700.000 mainly tetrahedral cells with hexahedral cells adjacent to the shell wall. To keep the number of cells in reasonable boarders regions which are covered by compressor parts and thus no oil is transported are left out. Moving mesh techniques like layering are taken to model the piston and crankpin movement to consider the induced secondary movement of the gas in the shell which influences the oil jet.

Oil mass flow rate at the oil pump outlet is determined by simulating the lower pump geometry according to [13] assuming constant oil mass flow rate in the rest of the pump and thus at the pump outlet. The properties of the oil are assumed to be constant over the entire simulation. Values for density and viscosity are set to 832 kg m^{-3} and 6.7 x 10^{-3} Pa s, respectively. Surface tension is also set constant at 0.028 N m^{-1}. Additionally, the following assumptions are made for the simulation of the oil distribution:

- Wall temperatures are constant.
- Flow is isothermal.
- Laminar flow.

- Dissolving of gaseous phase in liquid phase is neglected.

The oil distribution simulation is carried out with the following solver settings:

- free surface model: implicit VOF
- time discretization: bounded second order implicit, time step 10^{-4} s
- spatial discretization: second order upwind for momentum [10], compressive scheme for volume fraction [12]
- pressure-velocity coupling: PISO [14]
- double precision mode

3. Results

The presentation of the results is divided into the individual work steps until the oil distribution results can be used in the thermal compressor model.

3.1. Oil flow distribution

The simulation of the oil flow distribution is carried out until steady-state conditions are reached. In the present work steady-state means that the difference in the absolute oil mass flow rate into the compressor oil sump between two time steps becomes approximately constant which is obtained after 32 crankshaft revolutions. Illustrations of the simulation results with the starting oil flow can be seen in Figure 1.

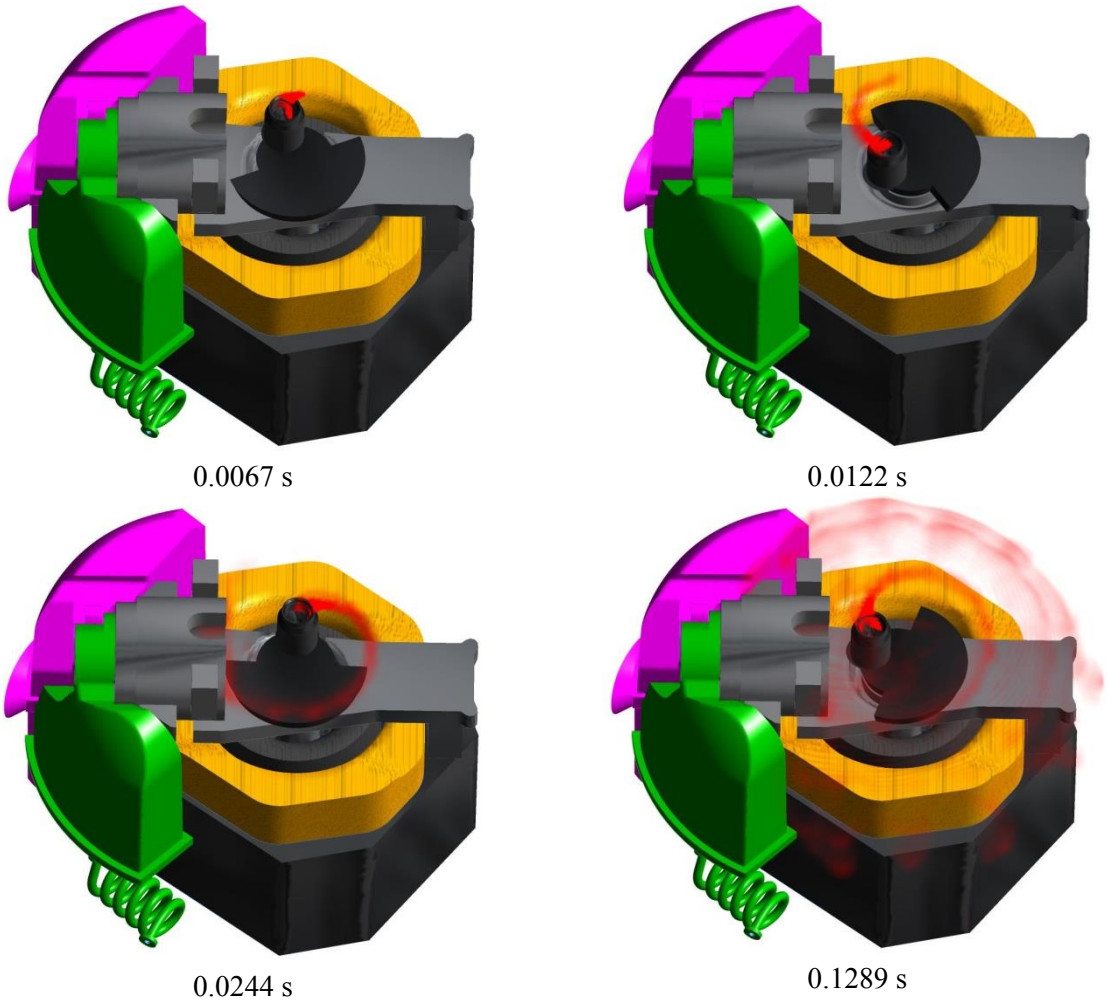

Figure 1. Oil distribution inside the compressor shell at several time steps.

The oil film thickness as a result of the oil distribution simulation can be seen in Figure 2 (only a characteristic area is shown to enable a proper overview). Figure 2a shows the iso-surface of the oil volume fraction and Figure 2b the oil film thickness value. The oil film thickness is not constant along the fall film flow direction which can be explained by the periodic impingement of the oil. By the use of a user defined function (UDF) the mean oil film thickness of 1.4 mm was calculated.

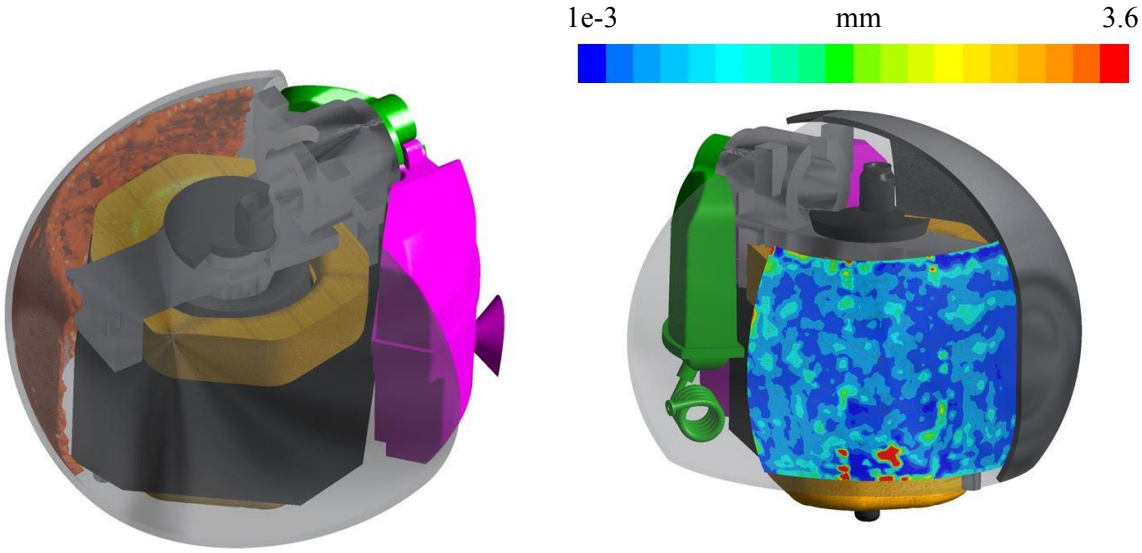

(a) (b)

Figure 2. Oil film (a) and oil film thickness (b).

3.2. Heat transfer coefficient

The simulation of the oil distribution inside the compressor and furthermore on the compressor shell enables the determination of heat transfer coefficients on the oil covered shell walls. Additionally to the main task of lubricating the moving compressor parts the oil acts as the main heat transfer media between the hot compressor parts and the compressor shell and thus to the ambience. High heat transfer coefficients result in increased heat transfer and improved compressor performance by decreasing the overall compressor temperature.

Results of the determination of the heat transfer coefficient on the oil covered shell walls can be seen in Figure 3a. Areas on which the oil jet hits the walls show higher heat transfer coefficients compared to areas where the heat transfer is affected by the falling oil film.

To enable the use of the oil distribution simulation results in the thermal model, the oil covered wall of the compressor shell is divided into 24 elements. The division of the area in circumferential direction is carried out with eight equidistant fields; in vertical direction the area is divided in three fields whereby the middle field represents the shell area where the oil jet mainly hits the shell wall. Figure 3b shows the distribution of the heat transfer coefficient on the shell after the interpolation process.

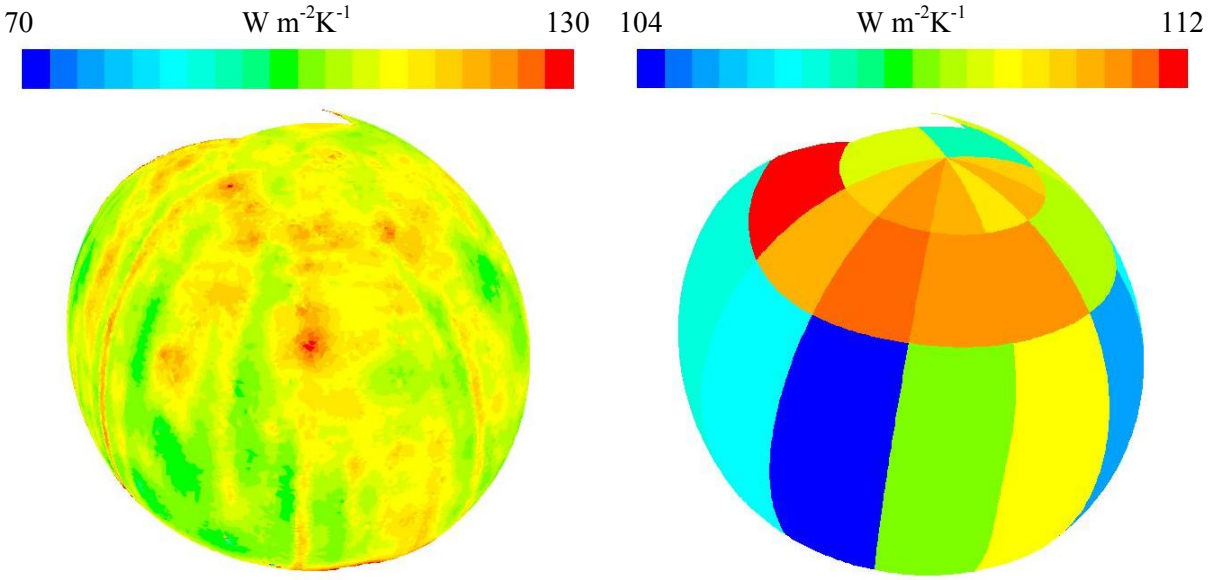

Figure 3. Heat transfer coefficient distribution on the inner surface of the compressor shell before (a) and after (b) the interpolation.

3.3. Thermal model

The determination of the temperature field in the hermetic reciprocating compressor using the thermal modelling approach published in [9] is carried out with the heat transfer values gained either by oil distribution CFD results and correlations from the literature. To value the prediction accuracy of the two methods the simulation results are compared with temperature measurements on twelve significant measuring points. The positon of the measuring points in the compressor can be seen in [9]. For the validation of the simulation the experimental data are gained in a calorimeter test bench with -23.3 °C evaporating temperature, 45 °C condensing temperature and 32 °C ambient temperature, respectively.

The results of the comparison between the simulation results and the experiment can be seen in the diagram in Figure 4 (the temperatures are referred to the temperature of the shell gas in the experiment). As the diagram shows, the temperatures of solid parts inside the compressor, shell gas and oil sump can be predicted accurately. Due to the generally lower heat transfer coefficients gained by literature correlations compared to those determined by CFD, the heat transfer between the hot compressor parts to the ambience is smaller. So the literature correlation case results in higher temperatures of the inner solid parts compared to the case with CFD heat transfer values. The highest deviation between experiment and simulation with CFD oil distribution regarding the inner compressor parts occurs at the discharge muffler surface with a value of 4.2 K. Using similar heat transfer coefficients between compressor shell and ambient air, the temperature deviation of the shell between the two simulation cases is very small which shows the significant influence of the heat transfer coefficient on the shell outer surface. Generally, the deviation between shell temperatures determined by simulation and experiment is higher compared to the deviation of the inner compressor parts. The maximum temperature deviation occurs at the top of the shell with 4.6 K. As the diagram in Figure 3 illustrates, the prediction accuracy is improved using heat transfer coefficients of the compressor oil gained by CFD compared to correlations of the literature.

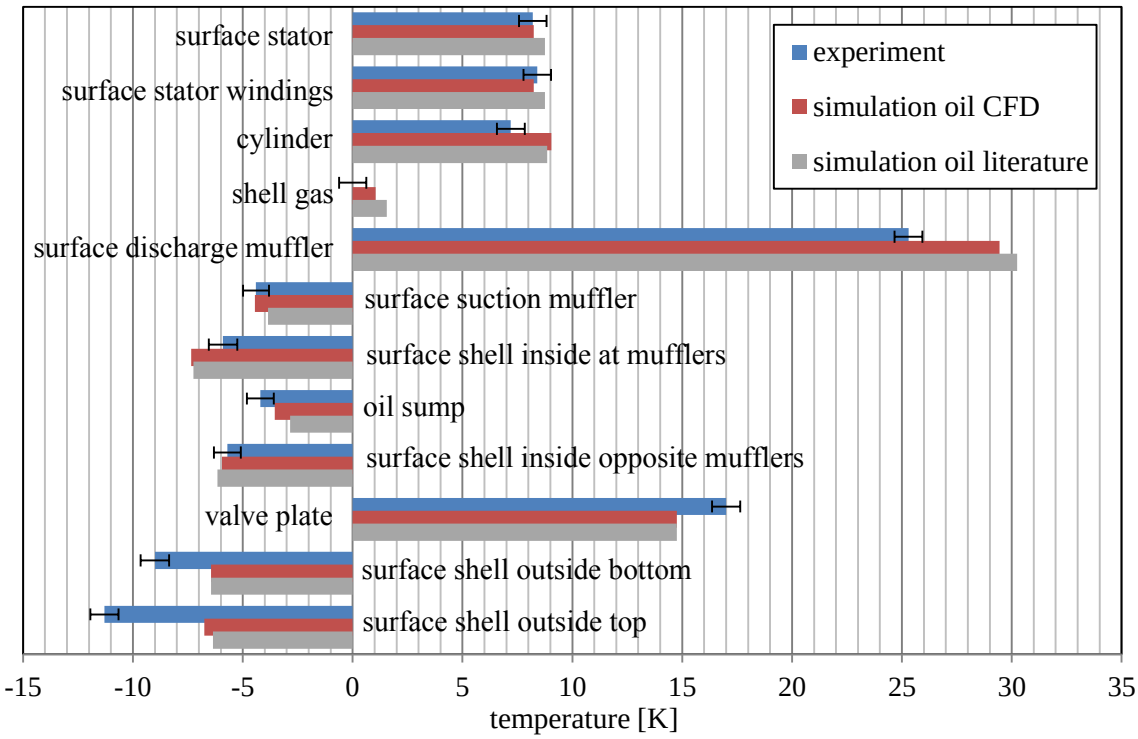

Figure 4. Comparison between simulation results and experiment (related to shell gas experiment temperature).

Figure 5 shows the results of the simulation with CFD heat transfer correlations for the compressor oil in terms of solid parts temperature field. The highest temperature values occur at the discharge muffler and not as often expected at the valve plate which can be explained by the relatively long duration of the hot refrigerant gas in the discharge muffler and the cooling of the valve plate by the suction gas. As the shell temperature field shows, the temperature values at the oil covered walls are higher than in the vicinity of the mufflers where the walls are not covered with oil.

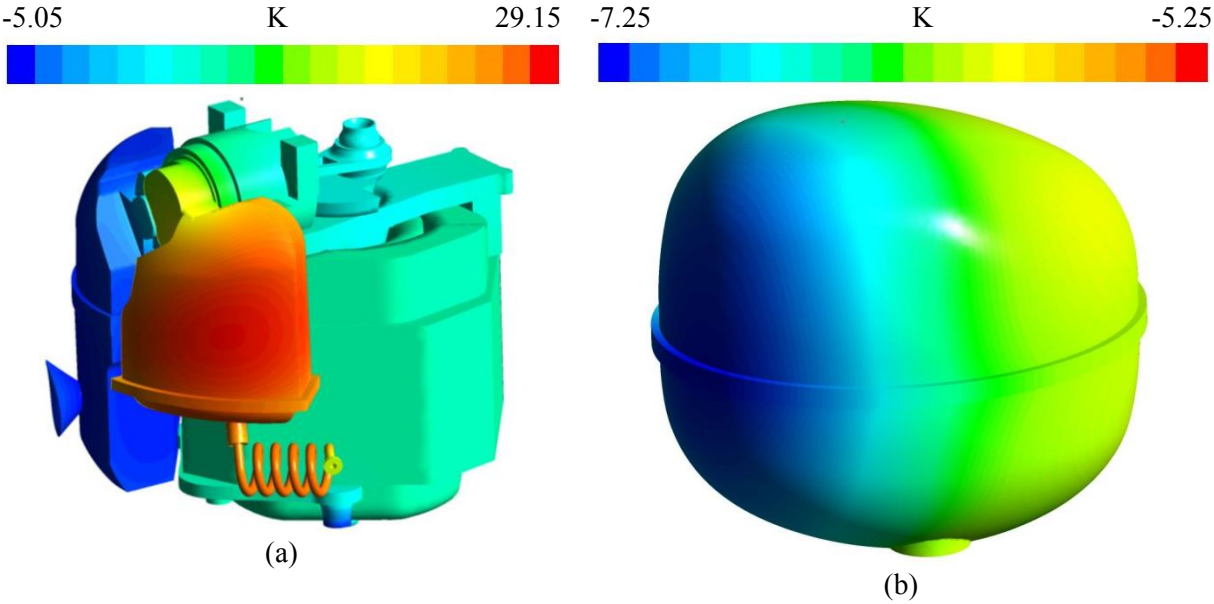

Figure 5. Solid part temperature field (related to shell gas experiment temperature) inside the compressor (a) and on the compressor shell (b).

The accuracy of the temperature determination of the inner compressor parts could be increased by introducing a higher number of zones with different heat flux values at parts with significant temperature gradients which is the case for the suction and discharge muffler. Furthermore, the use of temperature dependent heat transfer coefficients in combination with several zones at the shell outer surface could increase the accuracy of the thermal model.

An important aspect which should be mentioned at this point, is the application of the present model to different operating conditions. If the compressor load is increased and thus the temperature field inside the compressor rises also the oil and shell temperature increase. Assuming similar temperature difference between oil and shell, the determined heat transfer coefficients could be used for other operating points. More accurate results at other operating points can be gained by carrying out the simulation procedure again.

Due to the investigation of a constant speed compressor the oil distribution at several speeds is not part of the present study. Since the oil transport is highly influenced by the rotational speed of the compressor, the oil distribution would be different and thus the heat transfer.

4. Conclusion

In the presented study the simulation of the oil distribution in a hermetic reciprocating compressor for refrigeration application using commercial CFD software ANSYS Fluent is shown. The simulation was carried out by applying the VOF method to calculate the oil jet flow in the refrigerant environment inside the compressor shell. Furthermore, the CFD results were analysed in terms of heat transfer coefficient between the compressor oil and the oil covered shell walls. The calculated heat transfer coefficients were then used in a thermal model of the entire compressor according to [9]. A comparison of the determined temperature fields with the results of a simulation with heat transfer values gained by literature correlations was carried out and furthermore, the prediction accuracy of the simulations was analysed by a validation with experimental results of a calorimeter test bench. The maximum temperature deviation between simulation results with CFD heat transfer coefficients and experiment was 4.6 K which shows generally good agreement. Due to the lower heat transfer coefficients of

literature correlations, the temperature level inside the compressor is predicted too high compared to the CFD method. Although the temperature prediction of the case using CFD heat transfer coefficients for oil covered shell walls is better compared to the case using literature correlations, the application of this approach has to be reviewed closely in terms of benefit and time. Due to the high computational effort for the CFD simulation this method can only be applied in research and not in the development phase of a compressor. Additionally, the fact that the heat transfer coefficients between solid parts and shell gas were still determined with literature correlations gives scope for further improvements.

Acknowledgements
This work has been carried out within the framework of ECO-COOL, a research project initiated and funded by the FFG (Austrian Research Promotion Agency). Furthermore the authors particularly acknowledge the technical support by Secop Austria GmbH, formerly ACC Austria GmbH and Liebherr-Hausgeräte Lienz GmbH.

References

[1] Todescat M L, Fagotti F, Prata A T and Ferreira R T S 1992 Thermal Energy Analysis in Reciprocating Hermetic Compressors *Proc. Int. Compr. Eng. Conf. at Purdue* **936**
[2] Meyer W A and Thompson E 1998 An Analytical Model of Heat Transfer to the Suction Gas in a Low-Side Hermetic Refrigeration Compressor *Proc. Int. Compr. Eng. Conf. at Purdue* **662**
[3] Ooi K T 2003 Heat Transfer Study of a Hermetic Refrigeration Compressor *Appl. Thermal Eng.* **23** 1931-1945
[4] Sim Y H, Youn Y and Min M K 2000 A Study on Heat Transfer and Performance Analysis of Hermetic Reciprocating Compressor for Refrigeration *Proc. Int. Compr. Eng. Conf. at Purdue* **1390**
[5] Sanvezzo J Jr and Deschamps C J 2012 A Heat Transfer Model Combining Differential and Integral Formulations for Thermal Analysis of Reciprocating Compressors *Proc. Int. Compr. Eng. Conf. at Purdue* **2104**
[6] Lohn S K, Diniz M C and Deschamps C J 2015 A Thermal Model for Analysis of Hermetic Reciprocating Compressors und the On-Off Cycling Operation Condition *Proc. Int. Conf. Compr. and their Sys.(London)* **012068**
[7] Ribas Jr F A 2007 Thermal Analysis of Reciprocating Compressors *Proc. Int. Conf. Compr. and their Sys.(London)* **C65804207**
[8] Almbauer R, Burgstaller A, Abisid Z and Nagy D 2006 3-Dimensional Simulation for Obtaining the Heat Transfer Correlations pf a Thermal Network Calculation for a Hermetic Reciprocating Compressor *Proc. Int. Compr. Eng. Conf. at Purdue* **1794**
[9] Posch S, Hopfgartner J, Heimel M, Berger E, Almbauer R and Stangl S 2016 Thermal Analysis of a Hermetic Reciprocating Compressor using Numerical Methods *Proc. Int. Compr. Eng. Conf. at Purdue* **1215**
[10] Moukalled F, Mangani L and Darwish M 2015 The Finite Volume Method in Computational Fluid Dynamics (Springer**)**
[11] Scardovelli R and Zaleski S 1999 Direct numerical simulation of free-surface and interfacial flow *Annual Review Fluid Dynamics* **31** 567-603
[12] Fluent 14 2011 User Guide (Fluent Inc.**)**
[13] Posch S, Hopfgartner J, Heimel M, Berger E, Almbauer R and Schöllauf S 2016 A Numerical Investigation of the Oil Pump Suction Behaviour in a Hermetic Reciprocating Compressor *Proc. Int. Compr. Eng. Conf. at Purdue* **1215**
[14] Isaa R I 1986 Solution of the Implicitly Discretised Fluid Flow Equations by Operator-Splitting *J. of Comp. Physics* **62** 40-65

E Paper 5

S. Posch, J. Hopfgartner, E. Berger, B. Zuber, R. Almbauer, P. Schöllauf

COMPREHENSIVE 3D-ELASTOHYDRODYNAMIC SIMULATION OF HERMETIC COMPRESSOR CRANK DRIVE

10th International Conference on Compressors and their Systems, London, GB, 2017

CITY UNIVERSITY LONDON

Comprehensive 3d-Elastohydrodynamic Simulation of Hermetic Compressor Crank Drive

S Posch[1], J Hopfgartner[1], E Berger[1], B Zuber[1], R Almbauer[1] and P Schöllauf[2]

[1] Graz University of Technology, 8010 Graz, Austria
[2] Secop Austria GmbH, 8280 Fürstenfeld, Austria

posch@ivt.tugraz.at

Abstract. *Mechanical, electrical and thermodynamic losses form the major loss mechanisms of hermetic compressors for refrigeration application. The present work deals with the investigation of the mechanical losses of a hermetic compressor crank drive. Focus is on 3d-elastohydrodynamic (EHD) modelling of the journal bearings, piston-liner contact and piston secondary motion in combination with multi-body and structural dynamics of the crank drive elements. A detailed description of the model development within the commercial software AVL EXCITE Power Unit is given in the work. The model is used to create a comprehensive analysis of the mechanical losses of a hermetic compressor. Further on, a parametric study concerning oil viscosity and compressor speed is carried out which shows the possibilities of the usage of the model in the development process of hermetic compressors for refrigeration application. Additionally, the usage of the results in an overall thermal network for the determination of the thermal compressor behaviour is discussed.*

Nomenclature

Roman symbols		Greek symbols	
h	fluid film thickness	μ	dynamic viscosity
p	pressure	ϕ_x, ϕ_y, ϕ_s	flow factors
t	time	ρ	density
u	velocity	σ_δ	standard deviation of the combined roughness
x, y	coordinate		

1. Introduction

The compressor is the core element of the cooling circuit of a refrigeration appliance. In addition to the improvement of the entire refrigeration cycle in terms of energy efficiency to meet the energy standards, the further development of the single components like the compressor is driven forward. The determination of the loss mechanisms namely electrical, mechanical and thermodynamic is indispensable in the development of innovative efficient hermetic reciprocating compressors. Due to the hermetic design of the compressors, the different loss mechanisms interact with each other and thus a holistic consideration of the overall thermal compressor behaviour is necessary. Several studies presented thermal compressor models trying to use as much physical information as possible. In [1] and [2], the authors combined 3d heat conduction formulation for solid parts and lumped formulation of the gas path with experimental data or correlations from the literature to model the heat transfer coef-

ficients. A more detailed method is used in [3]. Additionally to the 3d heat conduction formulation of the solid parts the refrigerant gas path was simulated 3d using commercial CFD software. Mechanical and electrical losses were considered via heat sources in the particular part or in the lubrication oil. The determination of the mechanical losses in the compressor, mainly the journal bearing losses and the piston losses, has been published in several studies. A majority of the studies uses the similar general simulation strategy embedded in self coded simulation codes. The simulation strategy can be summarized in the following steps: (i) determination of the dynamic loads by applying multi body simulation, (ii) calculation of the hydrodynamic forces solving the Reynolds equation with numerical methods, (iii) calculation of displacements using a Newton-Raphson algorithm and (iv) calculation of the friction losses based on the displacements. A short overview of some studies and their statements concerning the modelling of the Reynolds equation and the model accuracy should be given at this point: [4] applied three different approaches to simulate the motion of the crank shaft and furthermore the journal bearing forces, whereby one approach takes into account lateral and tilting oscillations of the crank shaft. The modelling of the journal bearing forces was carried out applying the so-called short bearing approximation. The authors stated that no significant difference in the estimation of the journal bearing forces and the fluid film pressure between the different cases was found. A comparison between short and finite bearing approach can be found in [5]. As the authors concluded, the short bearing approach can be used as a first approximation to predict the bearing performance. In order to predict good results for piston cylinder contact, the finite bearing approach should be used. A more detailed calculation of the journal bearings of a hermetic compressor by using the averaged Reynolds equation introduced in [6] and [7] was presented in [8]. By applying the finite bearing approximation, the authors determined the friction power losses for the two journal bearings and investigated the influence of the oil viscosity and the gap width in the bearing. The method was verified by simple analytical friction loss calculations based on Couette shear stress.

The present study deals with the detailed calculation of the friction losses in a hermetic reciprocating compressor using the commercial software package AVL EXCITE Power Unit. An example of an application of the software can be found in [9]. The study analyses the piston secondary movement and its impact on the structure-borne noise behaviour of a direct injection Diesel engine. Although the software is usually used in engine development, the present study should show the ability of the software for the usage in reciprocating compressor investigations. The software is able to simulate the friction forces taking into account the elastic deformation of the crank drive parts. A general workflow for the use of AVL EXCITE Power Unit in the simulation of the mechanical losses of a hermetic reciprocating compressor is given and the model is utilised to investigate the influence of compressor speed and oil viscosity.

The compressor used in the present study works with R600a (isobutane) and contains a displacement of 5.5 cm³. Its COP at ASHRAE test conditions (-23.3 °C/55 °C) is approximately 1.8.

2. Simulation

The software AVL EXCITE Power Unit is an advanced tool for the simulation of rigid and flexible multi-body dynamics for the application in combustion engine and drivetrain development. Due to the similar structure of reciprocating compressors and combustion engines, the usage of the software for the calculation of mechanical losses in refrigeration compressors is useful. An overview of the workflow for setting up the simulation of the compressor crank drive with AVL EXCITE is given in this chapter. Furthermore, the pre-processing steps concerning condensation of the compressor parts and the theoretical background of the hydrodynamic force modelling are given.

2.1 Layout

An illustration of the simulation layout within the used software can be seen in Figure 1. The model is built up with subsystems representing several compressor parts connected with relevant types of joints. In the present study, a mechanical loss calculation of the overall compressor crank drive is carried out. Therefore, all crank drive parts and the crankcase are considered. Additionally, detailed modelling of

the friction behaviour in the journal bearings of the crank shaft, connecting rod big end and the piston-liner with elastohydrodynamic (EHD) contacts is carried out. Joints with little influence on the overall mechanical losses like the piston-piston pin and the connecting rod-piston pin connection are modelled with simple revolution joints by setting linear or non-linear spring/damper functions [10].

Geometric input data of the crank drive enable the calculation of the compressor dynamics via multi body simulation.

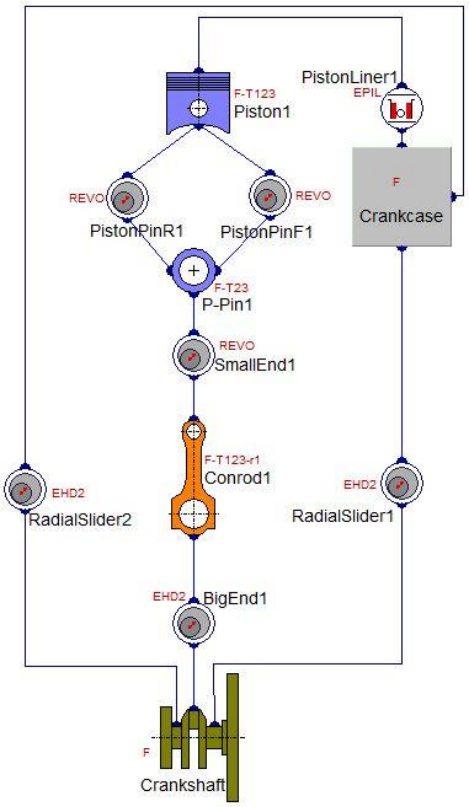

Figure 1. Layout of the simulation model.

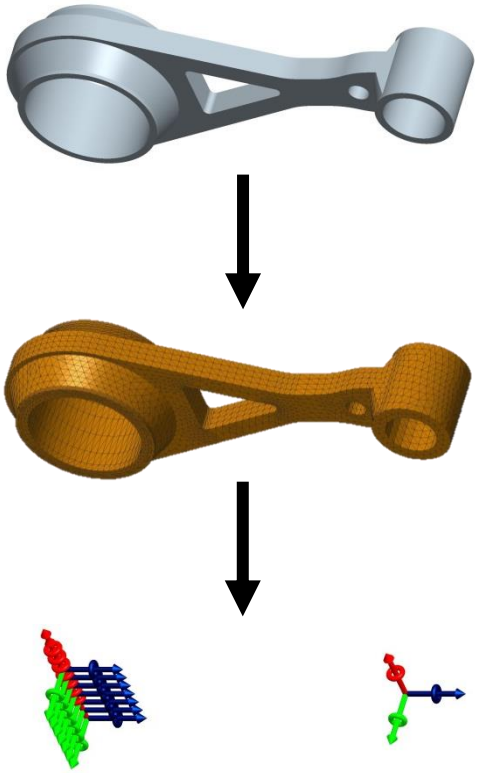

Figure 2. Condensation process.

2.2 Pre-processing

EHD simulation requires detailed information about the elastic behaviour of the considered parts. In the pre-processing phase of the simulation, the body input data for the use in AVL EXCITE Power Unit is generated. Starting from the 3d-CAD model, a finite element model with defined degrees of freedom is generated in the commercial software SIMULIA Abaqus. A predefined interface between the two software packages ensures the implementation of the input data in correct syntax. Figure 2 shows exemplarily the condensation process of the connecting rod. At the big end of the connecting rod seven node points with defined degrees of freedom are created which have to be aligned with the appropriate nodes on the crank shaft. Due to the simple modelling of the connecting rod small end, the part is condensed to only one node with defined degrees of freedom.

2.3 Simulation handling

After the several compressor parts are loaded into the software and are linked by appropriate contacts, the compressor load must be defined. In the present study, a pressure profile gained by CFD simulation is used. The CFD simulation was carried out in the commercial software ANSYS Fluent at the previous mentioned ASHRAE test conditions modelling the valve motions by the use of ideal moving

flat plates. Assuming equal pressure profile for every crankshaft revolution, the pressure is set to be periodic. Depending on the surface contact model, the roughness values of the several bearing partners must be specified and the material properties are necessary. Since the software AVL EXCITE Power Unit is mainly used for the simulation of combustion engines, the oil database does not contain the used compressor oil, therefore, the oil properties must be specified by the user. Gravitational forces are neglected to avoid the implementation of axial bearings.

2.4 Lubrication theory

The calculation of the hydrodynamic forces is carried out by solving the average Reynolds equation introduced in [6] and [7] which links the hydrodynamic pressure to the fluid film thickness.

$$\frac{\partial}{\partial x}\left(\phi_x \frac{\rho\, h^3}{12\mu}\frac{\partial \overline{p_h}}{\partial x}\right)+\frac{\partial}{\partial y}\left(\phi_y \frac{\rho\, h^3}{12\mu}\frac{\partial \overline{p_h}}{\partial y}\right)=\frac{(u_I+u_{II})}{2}\left(\frac{\partial\left(\rho\overline{h_T}\right)}{\partial x}+\sigma_\delta\frac{\partial \phi_S}{\partial x}\right)+\frac{\partial\left(\rho\overline{h_T}\right)}{\partial t} \tag{1}$$

The terms in the average Reynolds equation can be interpreted as follows: the term on the left-hand side represents the Poiseuille flow, the terms on the right-hand side represent the Couette flow and the time dependent displacement flow, respectively. Compared to the original Reynolds equation, several flow factors which depend on the roughness properties of the surfaces are introduced. Additionally to the hydrodynamic contact, an elastic-plastic asperity contact can occur which is considered with the model presented in [11]. The oil supply of the regarded contacts is not modelled specially, therefore, the contacts are assumed to be filled with oil. To fulfil the continuity balance, a cavitation approach similar to the model in [12] is used in the software.

3. Results

Before presenting the results of the comparison in terms of friction power loss, results of the predefined standard case are shown. The standard case is defined as the previous described compressor working in steady-state mode for R600a at a suction pressure of 0.629 bar and a discharge pressure of 6.04 bar corresponding to -23.3 °C evaporating temperature and 45 °C condensing temperature, respectively. Compressor speed is set to 3000 rpm and the oil viscosity is assumed to be constant at 8 cSt. The usage of the commercial software AVL EXCITE Power Unit enables easy post-processing. A visualisation of the hydraulic pressure in the regarded EHD contacts is shown in Figure 3. It can be seen that the region in the piston-liner contact shows two peaks in the hydrodynamic pressure field, indicating increased wear in this region.

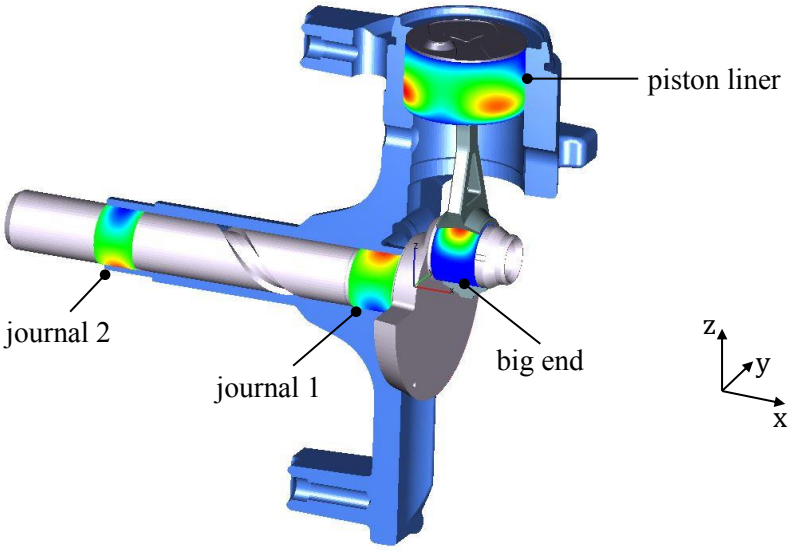

Figure 3. Visualisation of the hydraulic pressure in the EHD contacts.

The simulation of the standard case is carried out until steady-state conditions between two consecutive time steps are reached. For the standard case five crankshaft revolutions are needed to reach steady-state conditions yielding in a computational time of 20 hours on a quad core 3.50 GHz processor.

Figure 4 and Figure 5 illustrate results in terms of the reaction forces in the particular EHD contacts for one crankshaft revolution at steady-state conditions. The force curves reflect the crank mechanism behaviour and show the high forces at the connecting rod big end joint. Furthermore, the reaction forces at the piston liner contact and at the connecting rod big end joint have approximately sinusoidal character. In contrast, the amplitude reaction forces at the journal bearings of the crankshaft are smaller compared to the connecting rod big end and the curves do not show sinusoidal character.

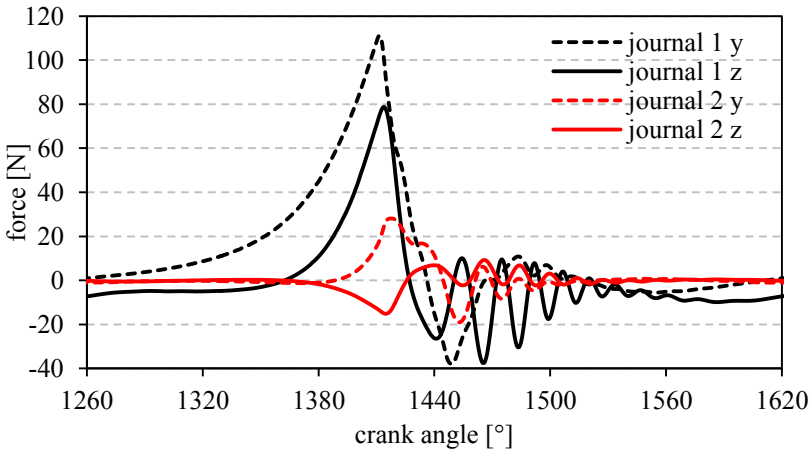

Figure 4. Reaction forces in the crankshaft journal bearings.

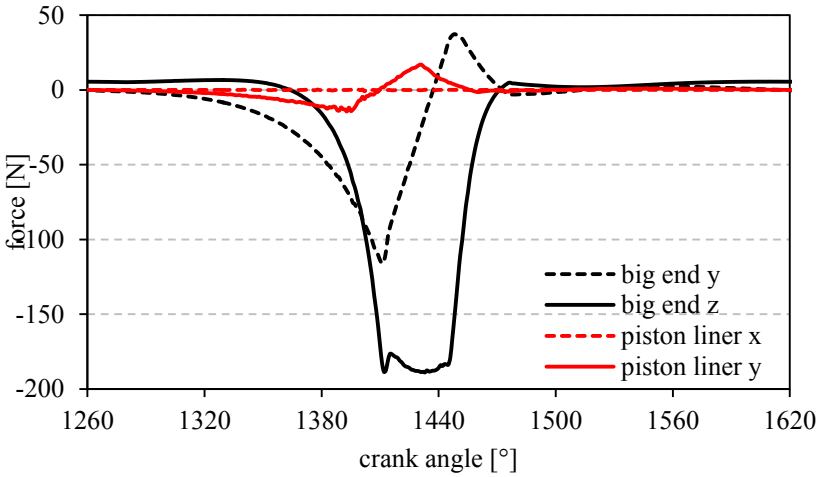

Figure 5. Reaction forces in the connecting rod big end and the piston liner contact.

Simulation results of the body kinematics can be seen in Figure 6 and Figure 7. The combination of piston pin offset and partly one-sided piston side load yields in tilting angle curve according Figure 6. As the orbital paths of the crankshaft journal bearings show, the displacement of the crankshaft at journal bearing 2 is smaller compared to bearing 1 due to the lower force amplitude acting on it. Furthermore, the higher loads according to Figure 4 at bearing 1 lead to a not perfectly cyclical orbital path. The lower force amplitude also yields in an almost circular displacement curve of journal bearing 2 and furthermore, to a faster achievement of the final shape of the orbital path compared to bearing 1.

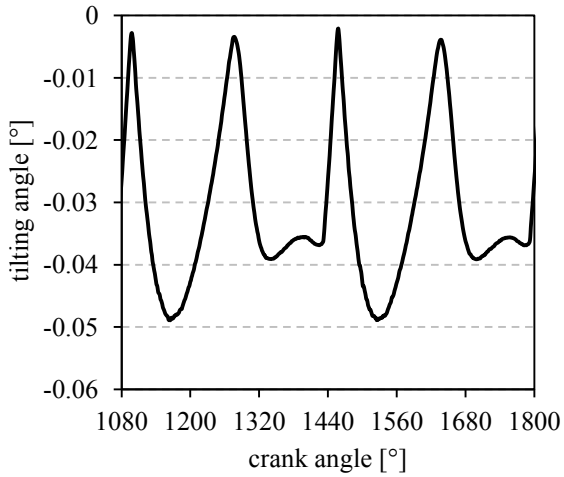

Figure 6. Piston tilting angle.

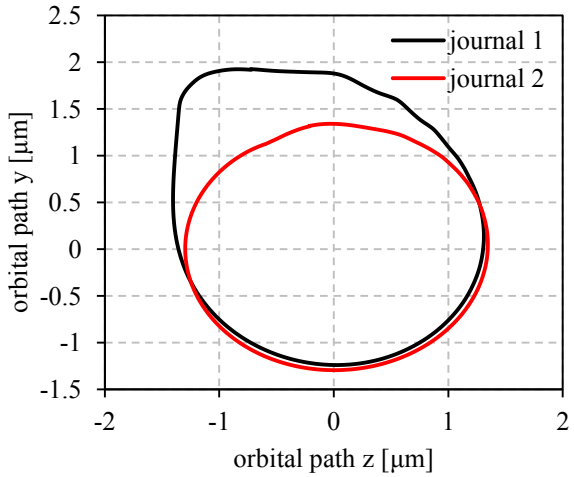

Figure 7. Orbital path of the crankshaft journal bearings.

The investigation of the friction loss behaviour of the considered joints is carried out by varying the oil viscosity and the rotational speed of the crankshaft. Figure 8 and Figure 9 illustrate the calculated friction power loss according to their occurrence. It is assumed, that the cylinder pressure gained by CFD results can be obtained for every variant. The viscosity variation (at constant speed of 3000 rpm) shows almost linear dependency of the friction power loss in the several joints and thus the overall friction loss.

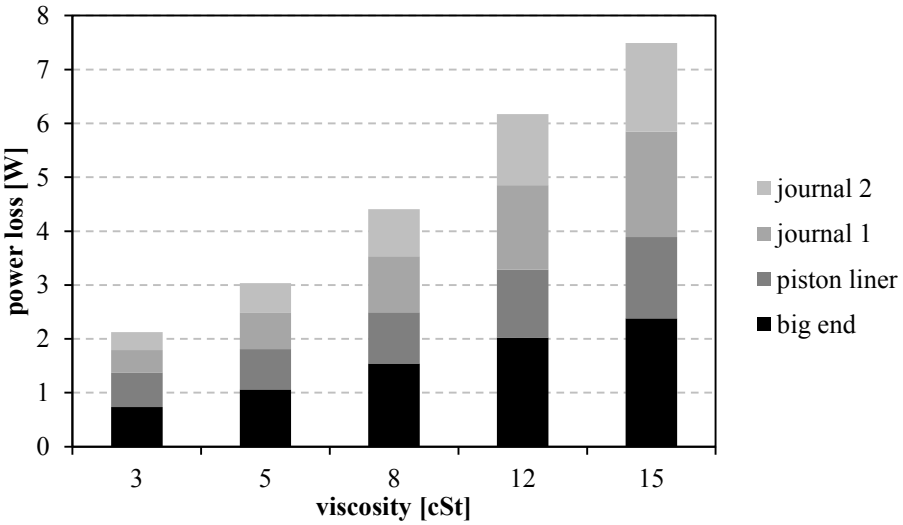

Figure 8. Viscosity influence on the friction power loss.

Similar results are obtained for the variation of the compressor speed (at constant viscosity of 8 cSt). The comparison in Figure 9 shows an almost linear dependence between compressor speed and friction power loss. Another aspect which can be derived from the simulation results is the big influence of the reaction forces on the friction loss compared to the relative speed in the regarded bearing. By comparing the results of the connecting rod big end and the crankshaft journal bearings, the significant influence of the reaction forces can be seen. The share of the power loss in the connecting rod big end joint on the overall power loss is higher compared to the individual crankshaft journal bearings although the relative speed between the bearing gap walls in the connecting rod big end is smaller compared to the relative speed in the crankshaft journal bearings.

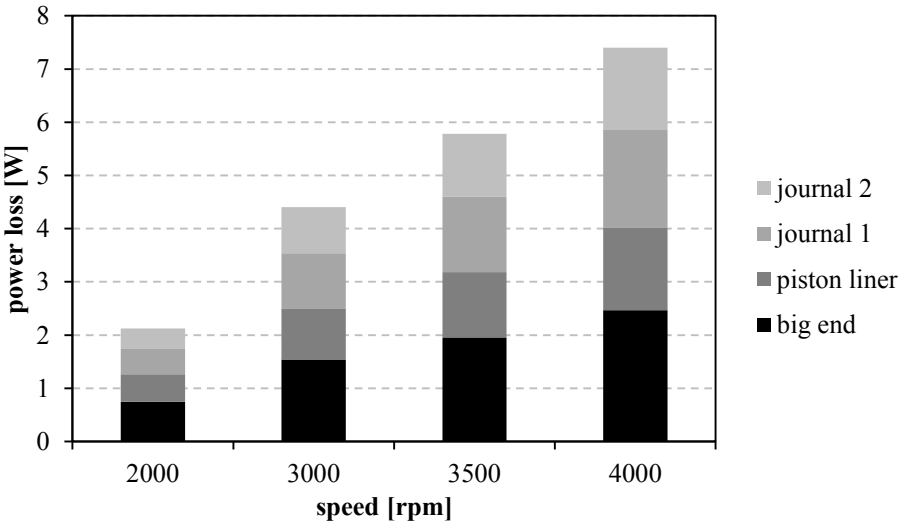

Figure 9. Rotational speed influence on the friction power loss.

Additionally to the investigation of the compressor crank mechanism dynamics and kinematics, the obtained results can be used in thermal modelling of the compressor. The results can serve as input data for modelling approaches like presented in [12]. By taking into account the produced heat due to

friction in the individual joint and considering the heating of the oil, the overall accuracy of such models can be increased.

4. Conclusion

The presented paper deals with the investigation of the friction behaviour of a reciprocating hermetic compressor for refrigeration application. For this purpose a 3d-elastohydrodynamic simulation using the commercial software AVL EXCITE Power Unit was carried out. Focus was laid on the simulation of the connections where the highest friction losses occur which are the two crankshaft journal bearings, the connecting rod big end and the piston liner contact. The simulation model was used to determine the dynamics and kinematic behaviour of the compressor crank mechanism. Furthermore, the influence of the oil viscosity and the compressor speed on the friction power loss was investigated. Based on a predefined standard configuration (3000 rpm, 5 cSt) the friction power loss according to their occurrence and the overall friction power loss of the several configurations were compared. The results show an approximately linear dependency of rotational speed and oil viscosity on the friction loss. It can be pointed out that the connecting rod big end joint produces higher friction losses compared to the other connections due to the high reaction forces although the relative speed between the journal walls is quite small.

The gained results can be used to estimate the usage possibility of the regarded crank mechanism design in a variable speed compressor. According to the presented results, the friction power loss at lower compressor speeds will decrease but this effect can be cancelled out due to the lower temperature in the compressor at lower speeds yielding in higher oil viscosities and therefore in increasing friction losses. This circumstance shows a trade-off in the design of variable speed compressors. The choice of the lubrication oil usually depends on the compressor modes in which the overall compressor temperature is high like in the refrigerator pull-down mode. By linking simulation models of the friction behaviour and thermal compressor models, a holistic approach of modelling the oil influence on the compressor performance can be achieved.

Acknowledgements

This work has been carried out within the framework of ECO-COOL, a research project initiated and funded by the FFG (Austrian Research Promotion Agency). Furthermore the authors particularly acknowledge the technical support by Secop Austria GmbH, formerly ACC Austria GmbH and Liebherr-Hausgeräte Lienz GmbH.

References

[1] Sanvezzo J Jr and Deschamps C J 2012 A Heat Transfer Model Combining Differential and Integral Formulations for Thermal Analysis of Reciprocating Compressors *Proc. Int. Compr. Eng. Conf. at Purdue* **2104**

[2] Lohn S K, Diniz M C and Deschamps C J 2015 A Thermal Model for Analysis of Hermetic Reciprocating Compressors und the On-Off Cycling Operation Condition *Proc. Int. Conf. Compr. and their Sys.(London)* **012068**

[3] Posch S, Hopfgartner J, Heimel M, Berger E, Almbauer R and Stangl S 2016 Thermal Analysis of a Hermetic Reciprocating Compressor using Numerical Methods *Proc. Int. Compr. Eng. Conf. at Purdue* **1215**

[4] Estupinan E A, Santo I F 2009 Modelling Hermetic Compressors Using Different Constraint Equations to Accommodate Multibody Dynamics and Hydrodynamic Lubrication *Journal of the Braz. Soc. of Mech. Science and Eng.* **31** 35-46

[5] Chieh H, Couto P R C and Prat A T 2007 An Integral Analysis and Simulation of the Complete Bearing System in Reciprocating Hermetic Compressors *Proc. Int. Conf. Compr. and their Sys.(London)* **658054**

[6] Patir N and Cheng H S 1978 An average model for determining effects of three-dimensional roughness on partial hydrodynamic lubrication *Journal of Lubr. Tec.* **100** 12-17
[7] Patir N and Cheng H S 1979 Application of average flow model to lubrication between rough sliding surfaces *Journal of Lubr. Tec.* **101** 220-230
[8] Posch S, Hopfgartner J, Heimel M, Berger E, Almbauer R and Schöllauf P 2016 A Numerical Friction Loss Analysis of the Journal Bearings in a Hermetic Reciprocating Compressor *Proc. Int. Compr. Eng. Conf. at Purdue* **1214**
[9] Seifriedsberger J, Wichtl R and Eichlseder H 2016 3d-Elastohydrodynamic Simulation Model for Structure-Borne Noise Analysis of a DI Diesel Engine *SAE Technical Paper* **2016-01-1854**
[10] AVL List GmbH 2011 User Guide – AVL EXCITE Power Unit *AVL List GmbH* **2011.1**
[11] Greenwood J A and Tripp J H 1970 The contact of two nominally flat rough surfaces *Proc. of the Inst. of Mech. Sc. and Eng.* **31** 35-46
[11] Elrod H G 1981 Cavitation Algorithm *Journal of Lubr. Techn.* **103** 350-354
[12] Posch S, Hopfgartner J, Heimel M, Berger E, Almbauer R and Schöllauf S 2016 A Numerical Investigation of the Oil Pump Suction Behaviour in a Hermetic Reciprocating Compressor *Proc. Int. Compr. Eng. Conf. at Purdue* **1215**